VOLUME 87, NO. EM4
AUGUST 1961
PART 1

JOURNAL of the

Engineering Mechanics Division

PROCEEDINGS OF THE
AMERICAN SOCIETY
OF CIVIL ENGINEERS

BASIC REQUIREMENTS FOR MANUSCRIPTS

One of papers and discussions of current papers should be submitted to the Manager of Technical Publications, ASCE. Authors should indicate the technical division to which the paper should be referred. The final date on which a discussion should reach the Society is given as a footnote with each paper. Those who are planning to submit material will expedite the review and publication procedures by complying with the following basic requirements:

1. Titles must have a length not exceeding 50 characters and spaces.

2. An abstract (summary) of the paper should accompany the paper.

3. Manuscripts (1 ribbon copy and two copies) should be double-spaced on one side of the paper by 11-in. paper.

4. The author's full name, Society membership grade, and footnote reference stating present employment should appear on the first page of the paper.

5. Mathematical expressions should be reduced from the copy that is submitted. Because of this, it is necessary that letters be drawn carefully and that special symbols be properly identified.

6. Tables should be typed (ribbon copies) on one side of 8½-in. by 11-in. paper. Specific reference and explanation must be made in the text for each table.

7. Illustrations must be drawn in black ink on paper size of 8½-in. by 11-in. paper. Before final illustrations will be reproduced with a width of between 3-in. and 4-in., the original must be large enough to be legible at this width. Photographs should be submitted as glossy prints. Explanations and descriptions must be made within the text for each illustration.

8. Papers should average about 12,000 words in length and must be no longer than 18,000 words. As an approximation, each full page of typed text, table, or illustration is the equivalent of 500 words.

9. Papers must be written in the third person.

Reprints from this publication may be made on condition that the full title of the paper, name of author, reference, and date of publication by the Society are given. The Society is not responsible for any statement made or opinion expressed in its publications.

This Journal is published monthly by the American Society of Civil Engineers. Publication office is at 2500 South State Street, Ann Arbor, Michigan. Editorial and Executive Offices are at 33 West 39 Street, New York 18, New York. $5.00 of a member's dues are applied as a subscription to this Journal. Second-class postage paid at Ann Arbor, Michigan.

The Index for 1959 was published as ASCE Publication 1960-10 (list price $1.00); indexes for previous years are also available.

LIBRARY OF

Journal of the

ENGINEERING MECHANICS DIVISION

Proceedings of the American Society of Civil Engineers

ENGINEERING MECHANICS DIVISION
EXECUTIVE COMMITTEE
Dan H. Pletta, Chairman; Egor P. Popov, Vice Chairman; Bruce G. Johnston
Merit P. White; Edward Wenk, Jr., Secretary

COMMITTEE ON PUBLICATIONS
Egor P. Popov, Chairman; Hans H. Bleich; Jack E. Cermak;
Albert G. H. Deitz; William J. Hall; John D. Haltiwanger; Ernest F. Masur;
Herbert S. Suer

CONTENTS

August, 1960

Papers

	Page
Stresses in Layered Elastic Solids by M. M. Lemcoe	1
Lateral Stability of Frames by Energy Method by Donald E. Johnson	23
Seepage Losses from Parallel Canal Systems by H. Y. Hammad	43
Vibrations of Structural Systems by Component Mode Synthesis by Walter C. Hurty	51
Irrotational Motion of Two Fluid Strata Towards a Line Sink by D. G. Huber	71
Underground Structures Subject to Air Overpressure by Ernest T. Selig, Keith E. McKee, and Eben Vey	87
Geometry of Moiré Fringes in Strain Analysis by Stanley Morse, August J. Durelli, and Cesar A. Sciammarella	105

(over)

Copyright 1960 by the American Society of Civil Engineers.

Page

Arch Dam Analysis with an Electric Analog Computer
by Richard H. MacNeal 127

Elastic Model Design of the B-58 Airplane
by J. W. Wells and H. B. England 153

DISCUSSION

Shrinkage, Swelling and Creep in Cement, by A. Hrennikoff. (July, 1959. Prior discussion: January, 1960. Discussion closed.)
by A. Hrennikoff (closure) 183

Comparative Study of a Segmental Arch Ring, by O. C. Zienkiewicz. (January, 1960. Prior discussion: None. Discussion closed.)
by J. A. Veltrop 185

White Noise Representation of Earthquakes, by G. N. Bycroft. (April, 1960. Prior discussion: None. Discussion closes September 1, 1960.)
by D. E. Hudson, G. W. Housner and T. K. Caughey 193

Strength and Efficiency Aspects of Plate Structures, by George Gerard. (April, 1960. Prior discussion: None. Discussion closes September 1, 1960.)
by George Pincus and George Winter 197

Errata 201

Journal of the
ENGINEERING MECHANICS DIVISION
Proceedings of the American Society of Civil Engineers

STRESSES IN LAYERED ELASTIC SOLIDS

By M. M. Lemcoe,[1] M. ASCE

SYNOPSIS

In this paper, the general expressions for stress are derived for multi-layer systems which satisfy the conditions of plane strain. To illustrate the procedures involved, expressions for stress are derived for a two-layer system, subjected to a surface line or strip load. Each layer is considered to be an elastic solid. The upper layers are considered to be of finite depth, but of infinite horizontal extent, and the lowest layer of infinite depth and horizontal extent. The general equations developed herein may be used to calculate the stresses in the supporting layered media for embankments, continuous footings, pavement systems, compressor-station foundation mats, canals, etc., if the supporting media can be approximately represented as a two-layer plane strain system. Expressions for stress are developed for conditions at the interface of perfect continuity and zero friction. Such a system permits an analytical solution to many problems of engineering importance. The procedures employed are by no means limited to a two-layer systems. The three and four layer cases may be solved with little additional difficulty with the aid of a digital computer.

The numerical solutions for the two-layer cases were carried out for a value of Poisson's ratio equal to one-quarter, a value which more closely approximates that of most engineering materials than the limiting values of zero and one-half used primarily for convenience by many of the earlier investigators in determining the expressions for stresses and displacements in radially symmetric problems. Any arbitrary values (0 to 1/2) of Poisson's ratio could have been used in view of the generality of the methods which have been developed.

For a given value of Poisson's ratio, and a given condition at the interface, the important parameters of the two-layer system are most conveniently expressed in terms of the non-dimensional ratios a/h and E_2/E_1. Numerical

Note: Discussion open until January 1, 1961. To extend the closing date one month, a written request must be filed with the Executive Secretary, ASCE. This paper is part of the copyrighted Journal of the Engineering Mechanics Division, Proceedings of the American Society of Civil Engineers, Vol. 86, No. EM 4, August, 1960.

[1] Mgr. Strength Analysis Sec., Southwest Research Inst., San Antonio, Texas.

solutions were obtained for $a/h = 0, 1, 2$, and for $E_2/E_1 = 0.02, 0.1$ for the two interface conditions. However, in the interest of brevity, numerical values for stress are tabulated in this paper for $E_2/E_1 = 0.02$ only. Many of the pavement and foundation systems of engineering importance fall within this range. Stresses have been evaluated along the upper surface, interface, and other pertinent locations.

Notation.—The letter symbols adopted for use in this paper are defined where they first appear, in the illustrations or in the text, and are arranged alphabetically, for convenience of reference, in Appendix I.

METHOD OF ANALYSIS FOR TWO-LAYER PLANE STRAIN PROBLEMS

Introduction.—The statical problem concerning an infinite elastic solid bounded by a plane that is subjected to a given distribution of surface forces (or deformation) has attracted the attention of a number of eminent elasticians. The first solution for the problem involving a purely normal load was worked out by G. Lamé and B. P. E. Clapeyron(1)[2] and was published in 1831. Then, in 1884, H. Hertz (2) solved the problem of a loaded slab on a liquid subgrade.

The next important contribution to the subject was made in 1885 by J. Boussinesq, (3) who solved a number of the important cases, including the one of a normal concentrated load acting on the surface of a semi-infinite solid. In 1902, H. Lamb's (4) solution for the case of a symmetrically distributed loading on the surface of a semi-infinite elastic solid was published.

In 1906, A. E. H. Love (5) presented a general solution for the problem of plane strain in a solid of revolution, making use of a stress function, and listed general solutions of the basic differential equations of this function. His development is the basis of most present-day work for layered systems.

During the period 1933 to 1938, K. Marguerre, (6) M. A. Biot, (7) G. Pickett, (8) and W. Passer (9) developed formulas for stress and displacement for the one-layer system, resting on a rigid base, for line or axial loadings.

In 1938, A. H. A. Hogg (10) and D. L. Holl (11) independently solved the problem of a thin slab of infinite size supported by a semi-infinite elastic solid. Their solutions were restricted to symmetrically loaded areas. The solution for an unsymmetrical loading was not worked out until 1947 by E. Volterra. (12)

D. M. Burmister (13) published a paper in 1943 establishing the equations of stress for the two-layer system subjected to a radially symmetric loading, treating each layer as an elastic solid having a value of Poisson's ratio μ of one-half, for conditions of perfect continuity and zero friction at the interface, the upper layer of infinite horizontal extent, the lower layer being of infinite depth. In 1945, he extended his theory to the three-layer system. (14) The

[2] Numerals in parenthesis—thus: (1)—refer to corresponding items in the Bibliography.

computation of stresses from his formulas, for loadings of practical importance, is by no means simple. The determination of the actual numerical values for stress or displacements at points off the axis of loading involves considerable additional computations.

In 1948, L. Fox (15) developed explicit solutions for the two-layer case in the form of integrals for the computation of stresses on the axis of loading, utilizing Burmister's general equations for the two-layer system. The integrals were evaluated by mechanical quadrature. Using R. V. Southwell's (16) relaxation method, he solved the differential equations in such a manner as to also obtain the components of stress off the axis of loading, again using approximate numerical methods.

In 1951, W. E. A. Acum and L. Fox (17) extended this work to the three-layer elastic solid system, again starting with Burmister's equations, to obtain formulas for the horizontal and vertical stresses along the axis of loading. This time they found the application of relaxation methods completely impractical in terms of the labor required for even reasonable accuracy.

The solutions developed by Pickett, Biot, and Marguerre, for the plane strain problem of an elastic solid subjected to this type of loading, as previously mentioned, were restricted to the one-layer system supported on an infinitely rigid base, and as such are mere special cases of the general two-layer solutions developed herein. It should also be noted that the equations for stress developed by Burmister and later modified by Fox are not applicable to the physical systems herein investigated, even though their methods can, by use of the N. M. Newmark (18) charts, be extended to include non-circular loadings.

Assumptions.—The general solution of the two-layer problem derived herein embodied the usual assumptions of the theory of elasticity and further required that certain conditions at the boundaries and interface be satisfied, as follows:

1. The material composing each layer was assumed to be homogeneous, isotropic, and elastic, obeying Hooke's law.

2. The modulus of elasticity, E, and Poisson's ratio, μ, were assumed to be different for each layer, but for convenience in performing the numerical computations, Poisson's ratio was assumed to be the same in both layers.

3. The boundary conditions required that the top of Layer No. 1 be free of shearing stresses, and free of normal stresses everywhere except where the strip or line load was applied, and that the stresses and displacements at infinite depth be zero.

4. The two continuity conditions investigated at the interface required that: (a) perfect continuity exist, that is, the two layers act together with no slippage at the interface, and (b) zero friction exist, that is, the layers are in continuous contact but perfectly free to move horizontally relative to each other. In reality, the actual conditions at the interface are, of course, between these two extremes. For brevity, the conditions (a) and (b) are also referred to as the "rough" and "smooth" cases, respectively.

Theory.

Development of the Basic Equations of Stress for the Two-Layer System with Perfect Continuity at the Interface.—The two-layer system investigated is shown schematically in Figs. 1 and 2. Positive directions for the x and y coordinates and the respective displacements u and v are as indicated. The

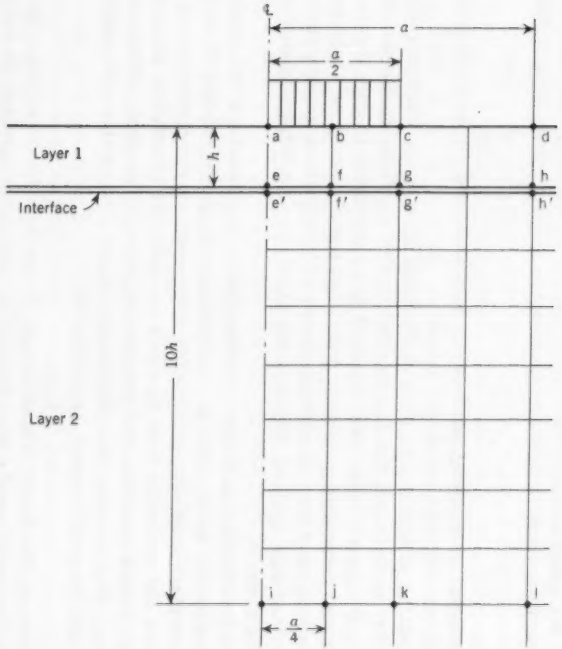

FIG. 1.—TWO-LAYER SYSTEM SHOWING LOCATIONS AT WHICH STRESSES WERE COMPUTED

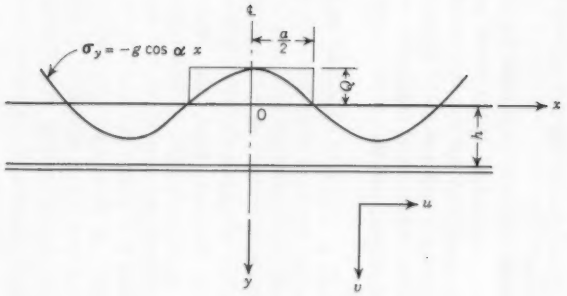

FIG. 2.—SCHEMATIC REPRESENTATION OF TWO-LAYER SYSTEM UNDER SINUSOIDAL LOADING

surface loading is compressive. The solution is carried out for a sinusoidal loading at the surface $\sigma_y = - q \cos \alpha x$, in which σ_y is the incremental normal stress in the y-direction and α is the parameter of loading. It will be shown later that the stresses resulting from a strip load of intensity $Q = q$ and width a, or a line load of equal total force, may be obtained from the solution for the sinusoidal loading by application of the Fourier integral.

Equilibrium Equations.—The basic problem to be solved represents a problem in plane strain. The basic equations for equilibrium, in terms of the displacements are (19)

$$\frac{1}{1 - 2\mu} \frac{\partial e}{\partial x} + \Delta^2 u = 0 \quad \ldots\ldots\ldots\ldots\ldots (1a)$$

$$\frac{1}{1 - 2\mu} \frac{\partial e}{\partial y} + \Delta^2 v = 0 \quad \ldots\ldots\ldots\ldots\ldots (1b)$$

in which $e = \frac{\partial u}{\partial x} + \frac{\partial v}{\partial y}$. Let

$$u = U_y \sin \alpha x \quad \ldots\ldots\ldots\ldots\ldots (2a)$$

$$v = V_y \cos \alpha x \quad \ldots\ldots\ldots\ldots\ldots (2b)$$

in which U is the displacement function for the horizontal displacement u and V is the displacement function for the vertical displacement v. (Hereinafter, for convenience, the subscript y is dropped.) It can be shown that the following displacement functions satisfy the equilibrium and boundary equations.

$$U_1 = A_1 e^{-\alpha y} + A_2 \alpha y e^{-\alpha y} + A_3 e^{\alpha y} + A_4 \alpha y e^{\alpha y} \ldots\ldots (3a)$$

$$V_1 = B_1 e^{-\alpha y} + B_2 \alpha y e^{-\alpha y} + B_3 e^{\alpha y} + B_4 \alpha y e^{\alpha y} \ldots\ldots (3b)$$

$$U_2 = C_1 e^{-\alpha y} + C_2 \alpha y e^{-\alpha y} \quad \ldots\ldots\ldots\ldots\ldots (3c)$$

$$V_2 = D_1 e^{-\alpha y} + D_2 \alpha y e^{-\alpha y} \quad \ldots\ldots\ldots\ldots\ldots (3d)$$

C_3, C_4, D_3, D_4 are zero in Eqs. 3(c) and 3(d), in order to satisfy the condition of zero stress and displacement at $y = + \infty$. A, B, C and D are constants.

Upon rewriting the equations of equilibrium (1) in terms of the partial derivatives of the displacements, we obtain for layer 1,

$$(1 + k_1) \frac{\partial^2 u_1}{\partial x^2} + \frac{\partial^2 u_1}{\partial y^2} + \frac{\partial^2 v_1}{\partial x \partial y} k_1 = 0 \quad \ldots\ldots\ldots\ldots (4a)$$

$$(1 + k_1) \frac{\partial^2 v_1}{\partial y^2} + \frac{\partial^2 v_1}{\partial x^2} + \frac{\partial^2 u_1}{\partial x \partial y} k_1 = 0 \quad \ldots\ldots\ldots\ldots (4b)$$

and, for layer 2

$$(1 + k_2) \frac{\partial^2 u_2}{\partial x^2} + \frac{\partial^2 u_2}{\partial y^2} + \frac{\partial^2 v_2}{\partial x \partial y} k_2 = 0 \quad \ldots\ldots\ldots\ldots (5a)$$

$$(1 + k_2)\ \frac{\partial^2 v_2}{\partial y^2} + \frac{\partial^2 v_2}{\partial x^2} + \frac{\partial^2 u_2}{\partial x\ \partial y}\ k_2 = 0 \quad \ldots\ldots\ldots (5b)$$

in which $k_1 = \frac{1}{1 - 2\ \mu_1}$, and $k_2 = \frac{1}{1 - 2\ \mu_2}$.

Performing the required partial differentiations of the displacement functions, inserting them in Eqs. 5(a) and 5(b), and equating the coefficients of the independent functions $e^{-\alpha y}$, $e^{\alpha y}$, $\alpha\ y\ e^{-\alpha y}$, and $\alpha\ y\ e^{\alpha y}$, in these equations, each separately equal to zero, we obtain

$$-k_1 A_1 - 2 A_2 + k_1 B_1 - k_1 B_2 = 0 \quad \ldots\ldots\ldots\ldots (6)$$

$$-k_1 A_3 + 2 A_4 - k_1 B_3 - k_1 B_4 = 0 \quad \ldots\ldots\ldots\ldots (7)$$

$$-k_1 A_1 + k_1 A_2 + k_1 B_1 - 2(k_1 + 1)B_2 = 0 \quad \ldots\ldots\ldots (8)$$

$$k_1 A_3 + k_1 A_4 + k_1 B_3 + 2(k_1 + 1)B_4 = 0 \quad \ldots\ldots\ldots (9)$$

$$-k_2 C_1 - 2 C_2 + k_2 D_1 - k_2 D_2 = 0 \quad \ldots\ldots\ldots\ldots (10)$$

$$-k_2 C_1 + k_2 C_2 + k_2 D_1 - 2(k_2 + 1)D_2 = 0 \quad \ldots\ldots\ldots (11)$$

Continuity Equations.—(1) Rough Interface - Perfect Continuity of Displacement at the Interface.

For the case of perfect continuity at the interface, we have

$$\left.\begin{aligned} u_1 &= u_2 & (\sigma_y)_1 &= (\sigma_y)_2 \\ v_1 &= v_2 & (\tau_{xy})_1 &= (\tau_{xy})_2 \end{aligned}\right\} \quad \ldots\ldots (12)$$

From Eqs. 2, 12 and Hooke's law, $\sigma_y = \lambda\ e + 2\ G\ \epsilon_y$, we obtain

$$\Big\{G_1\big[(A_1 - A_2 + A_2\ \alpha h) + (B_1 + B_2\ \alpha h)\big] - G_2\big[(C_1 + C_2\ \alpha h - C_2) + (D_1 + D_2\ \alpha h)\big]\Big\}e^{-\alpha h} - G_1\big[A_3 + A_4(\alpha h = 1) - (B_3 + B_4\ \alpha h)\big]e^{\alpha h} = 0 \quad \ldots (13)$$

$$(A_1 + A_2\ \alpha h - C_1 - C_2\ \alpha h)e^{-\alpha h} + (A_3 + A_4\ \alpha h)e^{\alpha h} = 0 \quad \ldots\ldots (14)$$

$$(B_1 + B_2\ \alpha h - D_1 - D_2\ \alpha h)e^{-\alpha h} + (B_3 + B_4\ \alpha h)e^{\alpha h} = 0 \quad \ldots\ldots (15)$$

$$\big[(A_1 + A_2\ \alpha h)\lambda_1 - m_1(B_1 + B_2\ \alpha h) - \lambda_2\ (C_1 + C_2\ \alpha h) + m_2(D_1 - D_2 + D_2\ \alpha h)\big]e^{-\alpha h} + \big[(A_3 + A_4\ \alpha h)\lambda_1 + m_1(B_3 + B_4 + B_4\ \alpha h)\big]e^{\alpha h} = 0 \quad \ldots\ldots\ldots\ldots (16)$$

(2) Smooth Interface (Zero friction)

For the case of zero friction at the interface, we have

$$\left.\begin{aligned} (v)_1 &= (v)_2 & (\tau_{xy})_1 &= 0 \\ (\sigma_y)_1 &= (\sigma_y)_2 & (\tau_{xy})_2 &= 0 \end{aligned}\right\} \quad \ldots\ldots (17)$$

From Eqs. 2 and Eqs. 17, we then obtain

$$(B_1 + B_2\,\alpha h - D_1 - D_2\,\alpha h)e^{-\alpha h} + (B_3 + B_4\,\alpha h)e^{\alpha h} = 0 \ldots\ldots (18)$$

$$\left[(A_1 + A_2\,\alpha h)\lambda_1 - m_1\{B_1 + B_2(\alpha h - 1)\} - \lambda_2(C_1 + C_2\,\alpha h) + m_2\{D_1 + D_2(\alpha h - 1)\}\right]e^{-\alpha h} + \left[\lambda_1(A_3 + A_4\,\alpha h) + m_1\{B_3 + B_4(\alpha h + 1)\}\right]e^{-\alpha h} = 0 \ldots\ldots (19)$$

$$\left[A_1 + A_2(\alpha h - 1) + (B_1 + B_2\,\alpha h)\right]e^{-\alpha h} - \left[A_3 + A_4(\alpha h + 1) - (B_3 + B_4\,\alpha h)\right]e^{\alpha h} = 0 \ldots\ldots (20)$$

$$C_1 - C_2 + C_2\,\alpha h + D_1 + D_2\,\alpha h = 0 \ldots\ldots (21)$$

Boundary Equations.—On the top surfaces, we have $y = 0$, $\sigma_y = -q \cos \alpha x$, and $\tau_{xy} = 0$.

Using these boundary conditions (and the expressions for σ_y and τ_{xy} in each layer), we obtain the remaining equations

$$A_1 - A_2 - A_3 - A_4 + B_1 + B_3 = 0 \ldots\ldots (22)$$

and

$$\lambda_1(A_1 + A_3) - m_1(B_1 - B_2 - B_3 - B_4) = -\frac{q}{\alpha} \ldots\ldots (23)$$

which are applicable to both the rough and smooth interface cases.

Eqs. 6 through 11, 13 through 16, 22 and 23 constitute 12 independent equations for solution to the rough interface problem in terms of the 12 unknown displacement function constants A_1, A_2, A_3, A_4, B_1, B_2, B_3, B_4, C_1, C_2, D_1, D_2, in terms of the loading parameter α. Similarly, Eqs. 6 through 11 and 18 through 23 constitute 12 independent equations for the smooth case. For convenience, these equations are summarized in Tables 1 and 2, for which the parameters are expressed in non-dimensional terms.

The solutions to the two layer systems derived herein, require solving the 12 simultaneous equations for the 12 unknown constants to the displacement functions, in terms of the parameters q, α, a, h, E_1, E_2, μ_1 and μ_2. Obtaining the unknown constants, in terms of these parameters, by formal algebraic solution is impractical. Instead, numerical values, covering a broad range may be assigned to these parameters. Numerical values of the 12 constants were computed for values of α ranging from 0.05 to 10, $E_2/E_1 = 0.02$ and 0.1, $a/h = 0$, 1, and 2, $\mu_1 = \mu_2 = 1/4$ for both the rough and smooth cases. These

TABLE 1.—SUMMARY OF THE BASIC EQUATIONS FOR THE TWO-LAYER SYSTEM - ROUGH INTERFACE

$$-k_2\,\mu_2\,C_1 - 2\,C_2 + k_2\,\mu_2\,D_1 - k_2\,\mu_2\,D_2 = 0 \quad \ldots\ldots (1)$$

$$-k_2\,\mu_2\,C_1 + k_2\,\mu_2\,C_2 + k_2\,\mu_2\,D_1 - 2(k_2\,\mu_2 + 1)D_2 = 0 \quad \ldots\ldots (2)$$

$$-k_1\,\mu_1\,A_1 - 2\,A_2 + k_1\,\mu_1\,B_1 - k_1\,\mu_1\,B_2 = 0 \quad \ldots\ldots (3)$$

$$-k_1\,\mu_1\,A_3 + 2\,A_4 - k_1\,\mu_1\,B_3 - k_1\,\mu_1\,B_4 = 0 \quad \ldots\ldots (4)$$

$$-k_1\,\mu_1\,A_1 + k_1\,\mu_1\,A_2 + k_1\,\mu_1\,B_1 - 2(k_1\,\mu_1 + 1)B_2 = 0 \quad \ldots\ldots (5)$$

$$-k_1\,\mu_1\,A_3 - k_1\,\mu_1\,A_4 - k_1\,\mu_1\,B_3 - 2(k_1\,\mu_1 + 1)B_4 = 0 \quad \ldots\ldots (6)$$

$$(A_1 + \overline{\alpha}\,A_2 - C_1 - \overline{\alpha}\,C_2)e^{-\overline{\alpha}} + (A_3 + \overline{\alpha}\,A_4)e^{\overline{\alpha}} = 0 \quad \ldots\ldots (7)$$

$$(B_1 + \overline{\alpha}\,B_2 - D_1 - \overline{\alpha}\,D_2)e^{-\overline{\alpha}} + (B_3 + \overline{\alpha}\,B_4)e^{\overline{\alpha}} = 0 \quad \ldots\ldots (8)$$

$$\left\{(A_1 + \overline{\alpha}\,A_2)n_1\,\mu_1 - n_1(1 - \mu_1)\left[B_1 + (\overline{\alpha} - 1)B_2\right] - n_2\,\mu_2\left(\frac{E_2}{E_1}\right)(C_1 + \overline{\alpha}\,C_2) + \right.$$
$$\left. + \left(\frac{E_2}{E_1}\right) n_2(1 - \mu_2)\left[D_1 + (\overline{\alpha} - 1)D_2\right]\right\} e^{-\overline{\alpha}}$$
$$+ \left\{(A_3 + \overline{\alpha}\,A_4)n_1\,\mu_1 + n_1(1 - \mu_1)\left[B_3 + B_4(\overline{\alpha} + 1)\right]\right\} e^{\overline{\alpha}} = 0 \quad \ldots\ldots (9)$$

$$\left\{\left[(A_1 + (\overline{\alpha} - 1)A_2 + B_1 + \overline{\alpha}\,B_2\right]\frac{1}{2(1 + \mu_1)} - \left[C_1 + (\overline{\alpha} - 1)C_2 + D_1 + \right.\right.$$
$$\left.\left. + \overline{\alpha}\,D_2\right]\left(\frac{E_2}{E_1}\right)\frac{1}{2(1 + \mu_2)}\right\} e^{-\overline{\alpha}} - \left\{\left[A_3 + (\overline{\alpha} + 1)A_4 - \right.\right.$$
$$\left.\left. - B_3 - \overline{\alpha}\,B_4\right]\frac{1}{2(1 + \mu_1)}\right\} e^{\overline{\alpha}} = 0 \quad \ldots\ldots (10)$$

$$A_1 - A_2 - A_3 - A_4 + B_1 + B_3 = 0 \quad \ldots\ldots (11)$$

$$n_1\,\mu_1(A_1 + A_3) - n_1(1 - \mu_1)(B_1 - B_2 - B_3 - B_4) =$$
$$-2\left(\frac{E_2}{E_1}\right)\frac{\overline{Q}\,h}{\pi\,\overline{\alpha}^2}\sin\frac{\overline{\alpha}}{2}\left(\frac{a}{h}\right)d\overline{\alpha} \quad \ldots\ldots (12)$$

constants were computed by means of a digital computer to eleven digits after the decimal point. Nevertheless, at the high values of a (greater than seven), a lack of precision was noted in the evaluation of C_1, C_2, D_1, D_2 due to increased "round-off" error.

To increase the precision would have required computing the residuals for each solution and adjusting the roots accordingly. Fortunately, however, the methods developed herein for the determination of stresses are such that the contributions of the higher a's to the total value of stress become progressively smaller with the increased α. Thus, a given error in the constants, due to

TABLE 2.—SUMMARY OF THE BASIC EQUATIONS FOR THE TWO-LAYER SYSTEM - SMOOTH INTERFACE

$$-k_2\,\mu_2\,C_1 - 2\,C_2 + k_2\,\mu_2\,D_1 - k_2\,\mu_2\,D_2 = 0 \quad \ldots\ldots (1)$$

$$-k_2\,\mu_2\,C_1 + k_2\,\mu_2\,C_2 + k_2\,\mu_2\,D_1 - 2(k_2\,\mu_2 + 1)D_2 = 0 \quad \ldots\ldots (2)$$

$$-k_1\,\mu_1\,A_1 - 2\,A_2 + k_1\,\mu_1\,B_1 - k_1\,\mu_1\,B_2 = 0 \quad \ldots\ldots (3)$$

$$-k_1\,\mu_1\,A_3 + 2\,A_4 - k_1\,\mu_1\,B_3 - k_1\,\mu_1\,B_4 = 0 \quad \ldots\ldots (4)$$

$$-k_1\,\mu_1\,A_1 + k_1\,\mu_1\,A_2 + k_1\,\mu_1\,B_1 - 2(k_1\,\mu_1 + 1)B_2 = 0 \quad \ldots\ldots (5)$$

$$-k_1\,\mu_1\,A_3 - k_1\,\mu_1\,A_4 - k_1\,\mu_1\,B_3 - 2(k_1\,\mu_1 + 1)B_4 = 0 \quad \ldots\ldots (6)$$

$$(B_1 + \overline{\alpha}\,B_2 - D_1 - \overline{\alpha}\,D_2)e^{-\overline{\alpha}} + (B_3 + \overline{\alpha}\,B_4)e^{\overline{\alpha}} = 0 \quad \ldots\ldots (7)$$

$$\left\{(A_1 + \overline{\alpha}\,A_2)n_1\,\mu_1 - n_1(1-\mu_1)\left[B_1 + (\overline{\alpha}-1)B_2\right] - n_2\,\mu_2\left(\frac{E_2}{E_1}\right)(C_1 + \overline{\alpha}\,C_2) + \right.$$
$$\left. + \left(\frac{E_2}{E_1}\right) n_2(1-\mu_2)\left[D_1 + (\overline{\alpha}-1)D_2\right]\right\} e^{-\overline{\alpha}} +$$
$$+ \left[(A_3 + \overline{\alpha}\,A_4)n_1\,\mu_1 + n_1(1-\mu_1)\left[B_3 + B_4(\overline{\alpha}+1)\right]\right] e^{\overline{\alpha}} = 0 \quad \ldots\ldots (8)$$

$$\left[A_1 + (\overline{\alpha}-1)A_2 + B_1 + \overline{\alpha}\,B_2\right] e^{-\overline{\alpha}} - \left[A_3 + (\overline{\alpha}+1)A_4 - \right.$$
$$\left. - B_3 - \overline{\alpha}\,B_4\right] e^{\overline{\alpha}} = 0 \quad \ldots\ldots (9)$$

$$C_1 + (\overline{\alpha}-1)\,C_2 + D_1 + \overline{\alpha}\,D_2 = 0 \quad \ldots\ldots (10)$$

$$A_1 - A_2 - A_3 - A_4 + B_1 + B_3 = 0 \quad \ldots\ldots (11)$$

$$n_1\,\mu_1(A_1 + A_3) - n_1(1-\mu_1)(B_1 - B_2 - B_3 - B_4) =$$
$$= -2\left(\frac{E_2}{E_1}\right)\frac{\overline{Q}\,h}{\pi\,\overline{\alpha}^2}\,\sin\frac{\overline{\alpha}}{2}\left(\frac{a}{h}\right)d\overline{\alpha} \quad \ldots\ldots (12)$$

the inherent "round-off" at the higher values of α, has little effect, percentage-wise, on the accuracy of the final stresses, even though the percentage of error for the constant itself might be considered significant.

D. Determination of Stresses for Strip or Line Loadings Using the Fourier Integral

Each solution to the 12 simultaneous equations obtained from the digital computer was for a sinusoidal loading of a specific frequency α, and a specific value of the amplitude q, which is a function of α, applied at the top surface of the upper layer. Having obtained the numerical values for the constants to the displacement functions from these solutions, the stress at any point due to the

sinusoidal loading may be obtained from the following general expressions for stress:

$$(\sigma_x)_1' = \alpha \cos \alpha x \Big[m_1 \left\{ A_1 e^{-\alpha y} + A_2 \alpha y e^{-\alpha y} + A_3 e^{\alpha y} + A_4 \alpha y e^{\alpha y} \right\} + \lambda_1 \left\{ - B_1 e^{-\alpha y} - B_2 (\alpha y - 1) e^{-\alpha y} + B_3 e^{\alpha y} + B_4 (\alpha y + 1) e^{\alpha y} \right\} \Big] d\alpha \quad \ldots (24a)$$

$$(\sigma_x)_2' = \alpha \cos \alpha x \Big[m_2 \left(C_1 e^{-\alpha y} + C_2 \alpha y e^{-\alpha y} \right) - \lambda_2 \left\{ D_1 e^{-\alpha y} + D_2 (\alpha y - 1) e^{-\alpha y} \right\} \Big] d\alpha \quad \ldots (24b)$$

$$(\sigma_y)_1' = \alpha \cos \alpha x \Big[\left\{ \lambda_1 A_1 e^{-\alpha y} + A_2 \alpha y e^{-\alpha y} + A_3 e^{\alpha y} + A_4 \alpha y e^{\alpha y} \right\} + m_1 \left\{ - B_1 e^{-\alpha y} - B_2 (\alpha y - 1) e^{-\alpha y} + B_3 e^{\alpha y} + B_4 (\alpha y + 1) e^{\alpha y} \right\} \Big] d\alpha \quad \ldots (24c)$$

$$(\sigma_y)_2' = \alpha \cos \alpha x \Big[\lambda_2 \left(C_1 e^{-\alpha y} + C_2 \alpha y e^{-\alpha y} \right) - m_2 \left\{ D_1 e^{-\alpha y} + D_2 (\alpha y - 1) e^{-\alpha y} \right\} \Big] d\alpha \quad \ldots (24d)$$

$$(T_{xy})_1' = \alpha \sin \alpha x \, G_1 \Big[\left\{ - A_1 e^{-\alpha y} - A_2 (\alpha y - 1) e^{-\alpha y} + A_3 e^{\alpha y} + A_4 (\alpha y + 1) e^{\alpha y} \right\} - \left\{ B_1 e^{-\alpha y} + B_2 \alpha y e^{-\alpha y} + B_3 e^{\alpha y} + B_4 \alpha y e^{\alpha y} \right\} \Big] d\alpha \quad \ldots (24e)$$

$$(T_{xy})_2' = \alpha \sin \alpha x \, G_2 \Big[\left\{ - C_1 e^{-\alpha y} - C_2 (\alpha y - 1) e^{-\alpha y} - D_1 e^{-\alpha y} + D_2 \alpha y e^{-\alpha y} \right\} \Big] d\alpha \quad \ldots (24f)$$

To obtain the stresses for strip or line loading from these solutions, it was then necessary to resort to a procedure which would permit integration over the entire frequency spectrum, with a varying effectively from zero to infinity. This was accomplished by expressing the strip loading in terms of a Fourier integral

$$p(x) = - \frac{2}{\pi} \int_0^\infty \cos \alpha x \, d\alpha \int_0^\infty f(x') \cos \alpha x' \, dx' \quad \ldots (25)$$

where the primes indicate the variable of integration and p(x) is the loading function represented. [For a detailed discussion on the use of the Fourier integral the reader is referred to the work of Churchill (22)]. The numerical values of the integrals were obtained by plotting the integrand and integrating the area under the curve, using Simpson's rule.

Figs. 3 and 4 show the characteristic shapes of typical curves of the incremental stress versus α. Since the stresses σ_x, σ_y, τ_{xy} for each layer are obtained by integrating these curves from zero to infinity, it is evident that the incremental stresses physically represent the changes in stress per unit increase in α, or, mathematically stated, represent the integrands of the final expression for total stress.

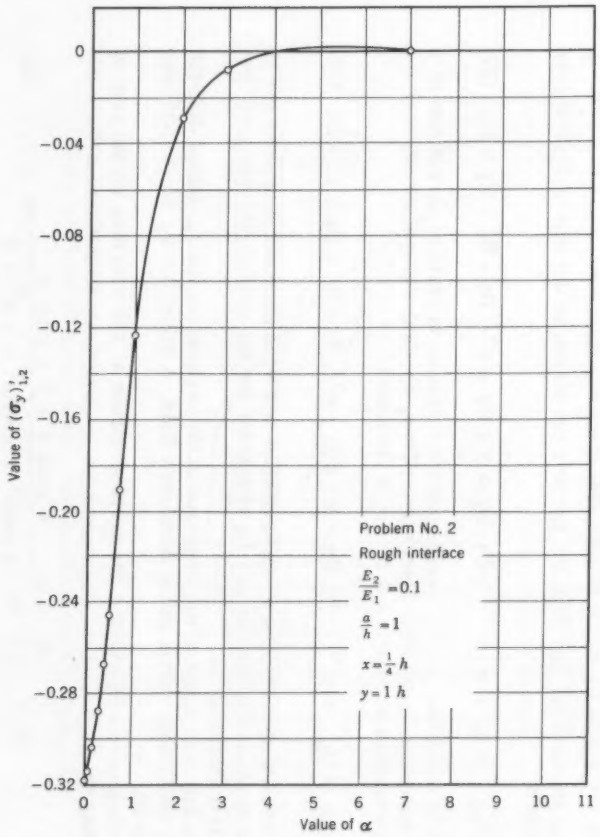

FIG. 3.—SHAPE OF A TYPICAL INTEGRAND OF $(\sigma_y)_1$ AND $(\sigma_y)_2$ FOR TWO-LAYER SYSTEM

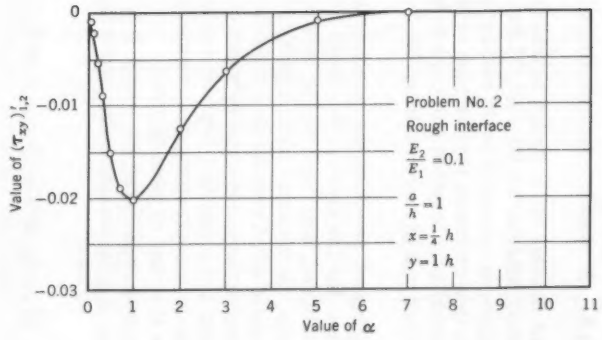

FIG. 4.—SHAPE OF A TYPICAL INTEGRAND OF $(\sigma_{xy})_1$ AND $(\sigma_{xy})_2$ FOR TWO-LAYER SYSTEM

Summaries for the stresses σ_x, σ_y, τ_{xy} for each layer for six problems are found in Tables 3 through 8. A negative sign in these tables indicates compression.

Stresses in an Elastic Solid Resting on a Rough Infinitely Rigid Layer.— Numerous investigators, including Marguerre,(6) Biot,(7) and Pickett(8) have considered the problem of stresses in an elastic solid resting on a rigid layer.

The first correct solution to this problem, for the case of plane strain, was given by Marguerre.(6) Pickett(8) also obtained solutions to this problem for the stresses along the top surface and at the interface, for various values of Poisson's ratio.

In order to provide an independent check on the compactness of the basic equations and methods of solution for the general two-layer system developed herein, a special case was considered, with E_2 equal to infinity. The solution to this problem should, of course, be the same as Marguerre's solution to the problem of the semi-infinite elastic solid resting on a rigid layer.

The comments herein are restricted to the case in which perfect continuity exists at the interface, although the equations derived earlier for the two-layer system, with zero friction at the interface, are completely applicable to the solution of this problem for the case of zero friction.

For convenience, a problem was considered for which P = 1 (a = 0), $\mu = 0$, $E_1 = 1$, and h = 12. The vertical displacements in the upper layer, on the axis of loading, may be expressed

$$v_1 = B_1 e^{-\alpha y} + B_2 \alpha y e^{-\alpha y} + B_3 e^{\alpha y} + B_4 \alpha y e^{\alpha y} \quad \ldots\ldots\ldots (26a)$$

$$\epsilon_y = \frac{\partial v_1}{\partial y} = \alpha\left[e^{-\alpha y}\left(-B_1 - B_2 \alpha y + B_2\right) + e^{\alpha y}\left(B_3 + B_4 + B_4 \alpha y\right)\right] \quad (26b)$$

Also, for $\mu = 0$, $E_1 = 1$, it follows that $\lambda = 0$ and $G_1 = 1/2$.

Using Hooke's law and Eqs. 25, the vertical stress on the axis of loading then becomes

$$(\sigma_y)'_1 = \epsilon_y = \alpha\left[e^{-\alpha y}\left(-B_1 - B_2 \alpha y + B_2 + e^{\alpha y}\left(B_3 + B_4 + B_4 \alpha y\right)\right]\right. \quad (27)$$

It is noted that $(\sigma_y)'_1$ represents the increase in vertical stress due to a unit increase in spectral frequency. Thus, the total vertical stress over the entire spectrum from $\alpha = 0$ to $\alpha = \infty$ becomes

$$\sigma_y = \int_0^\infty \alpha\left[e^{-\alpha y}\left(-B_1 - B_2 \alpha y + B_2\right) + e^{\alpha y}\left(B_3 + B_4 + B_4 \alpha y\right)\right] d\alpha \quad (28)$$

The B's of course, are functions of α and were obtained by solving the 12 general equations for the two-layer system for the arbitrarily assigned numerical values of α.

In Fig. 5 is a plot of the integrand of the vertical stress σ_y. Integrating the area under this curve, using Simpson's Rule, a value for σ_y of -0.0697 was obtained.

Marguerre's (6) solution for vertical stress at the interface on the axis of loading is

$$\sigma_y = -\frac{P}{\pi h} \int_0^\infty \frac{4 \cosh z + 2 z \sinh s}{2 \cosh^2 z + \sinh^2 z + z^2 + 2} \, dz \quad \ldots\ldots (29)$$

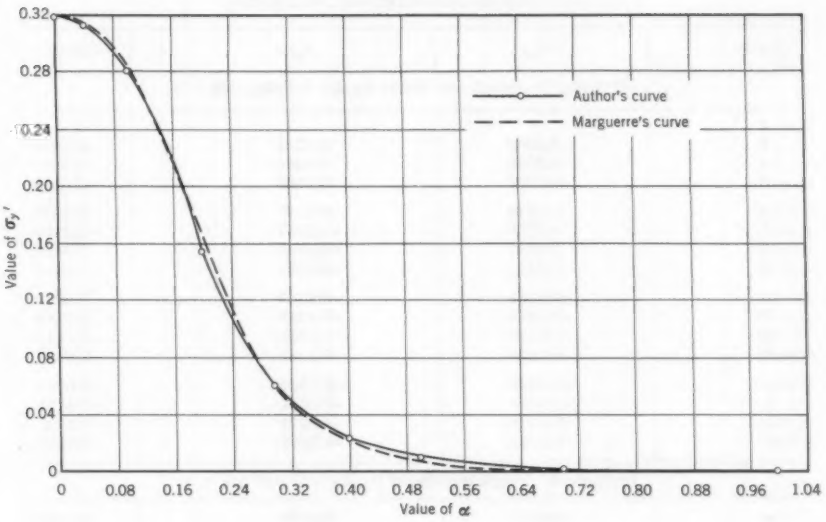

FIG. 5.—COMPARISON OF AUTHOR'S INTEGRAND FOR VERTICAL STRESS, RIGID BASE PROBLEM, WITH MARGUERRE'S INTEGRAND

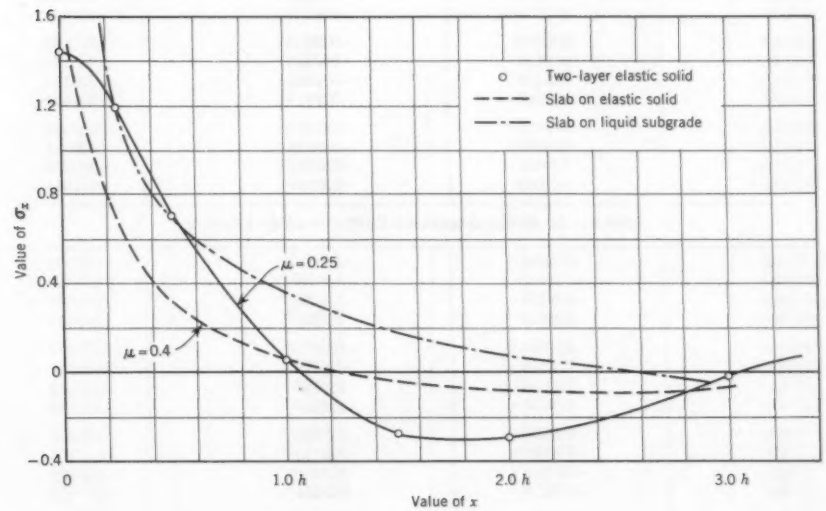

FIG. 6.—COMPARISON OF VALUES OF σ_x AT INTERFACE OF TWO-LAYER ELASTIC SOLID, LAAB ON ELASTIC SOLID, AND SLAB ON LIQUID SUBGRADE

TABLE 3.—SUMMARY OF STRESSES

Point	σ_x	σ_y	τ_{xy}
Problem 1: Rough Interface, $E_2/E_1 = 0.02$, $a/h = 0$			
a			
b	-4.6949	0.0000	0.0000
c	-2.9986	0.0000	0.0000
d	-2.5962	0.0000	0.0000
e	3.2814	-0.2177	0.0000
f	2.9769	-0.2137	-0.0284
g	2.4390	-0.1942	-0.0414
h	1.2242	-0.1483	-0.0994
e'	-0.0056	-0.2177	0.0000
f'	-0.0070	-0.2137	-0.0284
g'	-0.0177	-0.1942	-0.0414
h'	-0.0283	-0.1483	-0.0994
i	+0.0040	-0.0514	0.0000
j	+0.0040	-0.0514	-0.0011
k	+0.0038	-0.0513	-0.0022
l	+0.0035	-0.0508	-0.0044
Problem 2: Rough Interface, $E_2/E_1 = 0.02$, $a/h = 1$			
a	-4.5925	-1.0000	0.0000
b	-4.3034	-1.0000	0.0000
c	-3.6033	-1.0000	0.0000
d	-2.3651	0.0000	0.0000
e	2.8802	-0.2048	0.0000
f	2.7259	-0.2013	-0.0175
g	2.2978	-0.1925	-0.0311
h	1.2979	-0.1612	-0.0448
e'	-0.0078	-0.2048	0.0000
f'	-0.0104	-0.2013	-0.0175
g'	-0.0161	-0.1925	-0.0311
h'	-0.0265	-0.1612	-0.0448
i	0.0040	-0.0514	0.0000
j	0.0040	-0.0514	-0.0011
k	0.0038	-0.0513	-0.0022
l	0.0035	-0.0507	-0.0044
Problem 3: Rough Interface, $E_2/E_1 = 0.02$, $a/h = 2$			
a	-7.4399	-1.0000	0.0000
b	-7.2920	-1.0000	0.0000
c	-6.8221	-1.0000	0.0000
d	-5.2910	0.0000	0.0000
e	4.5790	-0.3800	0.0000
f	4.4883	-0.3715	-0.0218
g	4.1420	-0.3660	-0.0443
h	2.8789	-0.3259	-0.0823
e'	-0.0308	-0.3800	0.0000
f'	-0.0322	-0.3715	-0.0218
g'	-0.0352	-0.3660	-0.0443
h'	-0.0458	-0.3259	-0.0823
i	-0.0303	-0.1025	0.0000
j	-0.0304	-0.1025	-0.0022
k	-0.0308	-0.1022	-0.0044
l	-0.0321	-0.1011	-0.0088

TABLE 3.—SUMMARY OF STRESSES (Continued)

Point	σ_x	σ_y	τ_{xy}
Problem 4: Smooth Interface, $E_2/E_1 = 0.02$, $a/h = 0$			
a			
b	-4.5363	0.0000	0.0000
c	-3.9779	0.0000	0.0000
d	-2.0599	0.0000	0.0000
e	4.3291	-0.2062	0.0000
f	4.1033	-0.1999	0.0000
g	3.3842	-0.1845	0.0000
h	2.1592	-0.1615	0.0000
e'	-0.2062	-0.2062	0.0000
f'	-0.1999	-0.1999	0.0000
g'	-0.1845	-0.1345	0.0000
h'	-0.1615	-0.1615	0.0000
i	-0.0038	-0.0646	0.0000
j	-0.0038	-0.0644	-0.0015
k	-0.0038	-0.0642	-0.0029
l	-0.0042	-0.0634	-0.0059
Problem 5: Smooth Interface, $E_2/E_1 = 0.02$, $a/h = 1$			
a	-4.4377	-1.0000	0.0000
b	-4.1289	-1.0000	0.0000
c	-3.7608	-1.0000	0.0000
d	-1.9367	0.0000	0.0000
e	4.0068	-0.1969	0.0000
f	3.8422	-0.1929	0.0000
g	3.4739	-0.1849	0.0000
h	2.2690	-0.1620	0.0000
e'	-0.1969	-0.1969	0.0000
f'	-0.1929	-0.1929	0.0000
g'	-0.1849	0.1849	0.0000
h'	-0.1620	-0.1620	0.0000
i	-0.0038	-0.0644	0.0000
j	-0.0038	-0.0642	-0.0015
k	-0.0038	-0.0640	-0.0029
l	-0.0042	-0.0632	-0.0059
Problem 6: Smooth Interface, $E_2/E_1 = 0.02$, $a/h = 2$			
a	-6.8201	-1.0000	0.0000
b	-6.7892	-1.0000	0.0000
c	-6.4630	-1.0000	0.0000
d	-5.0046	0.0000	0.0000
e	6.8189	-0.3662	0.0000
f	6.6878	-0.3657	0.0000
g	6.3001	-0.3522	0.0000
h	4.8998	-0.3239	0.0000
e'	-0.3662	-0.3662	0.0000
f'	-0.3657	-0.3657	0.0000
g'	-0.3522	-0.3522	0.0000
h'	-0.3239	-0.3239	0.0000
i	-0.0076	-0.1281	0.0000
j	-0.0077	-0.1280	-0.0030
k	-0.0078	-0.1276	-0.0058
l	-0.0085	-0.1259	-0.0116

The integrand of the above expression is also plotted in Fig. 5 for purposes of comparison. Performing the integration as before, a value for σ_y of -0.0702 was obtained. It should be noted that this value agrees with the writer's values within 0.56%, which is excellent considering the precision with which the numerical integration was performed.

DISCUSSION OF RESULTS AND CONCLUSIONS

Twelve physically distinct problems were solved, covering a fairly broad range in the parameters, in order to study systematically the effect on stress of prescribed changes in values of these parameters, and to illustrate the methods and techniques. However, in the interest of brevity, numerical values of stress are tabulated in this paper for $E_2/E_1 = 0.02$ only (Table 3). Nevertheless, the observations which follow are valid for values of E_2/E_1, ranging from 0.02 to 1.0.

For convenience in performing the numerical calculations it was assumed that $P = Q = E_1 = h = 1$, and $\mu_1 = \mu_2 = 1/4$, unless otherwise noted. However, since the two-layer system is essentially a two-parameter problem, expressible in terms of the non-dimensional ratios a/h and E_2/E_1, it is evident that the stresses obtained from the numerical examples and summarized in Table 3 are directly applicable to the solution of problems for which h and E_1 are other than unity, provided that a/h and E_2/E_1 do not change. For problems involving distributed loading, h and E_1 do not appear explicitly in the final expressions for stress, but appear as non-dimensional ratios x/h, y/h, and E_2/E_1.

For problems involving concentrated line loads ($a/h = 0$) in which h and E_1 are other than unity, the stresses found in the above-mentioned tables still represent the stresses for $P = Q = 1$, provided that they are multiplied by the factor $1/h$. Also, by making plots of the data in these tables, one may obtain stresses for intermediate values of E_2/E_1 and a/h for either line loads or strip loads.

Under G. Pickett's (21) direction, Westergaard's equations for stress in a thin slab resting on a liquid subgrade, and those of Hogg for a thin slab resting on an elastic solid, were solved so as to obtain influence charts and tables from which numerical values for stress may be readily determined. Such charts and tables are found in the above reference, and from them stresses for any general distribution of axial loading may be found.

In Fig. 6 are plotted the horizontal stresses, σ_x, obtained from equations for the layered elastic solid developed herein (with rough interface), along with the flexural stresses obtained from Pickett's numerical solutions for a thin slab resting on either a liquid or an elastic solid subgrade. It should be noted that Pickett's solutions for the slab resting on an elastic solid were for a value of Poisson's ratio equal to 0.4 only. The pertinent data for each system is summarized as follows:

Two-layer elastic solid:

P(concentrated line load) = 1

$h = E_1 = 1$, $E_2 = 0.1$, $\mu = 0.25$.

Slab on elastic solid:

P(concentrated axial load) = 1

$h = E_1 = 1,\ E_2 = 0.1,\ \mu = 0.4.$

Slab on liquid subgrade:[3]

P(concentrated axial load) = 1

$h = E_1 = 1,\ E_2 = 0.1,\ k = 1/360.$

It is noted that the horizontal stresses, σ_x, for the two-layer elastic solid and the slab resting on a liquid subgrade follow the same general trend, and are in fairly close agreement up to $x = 0.5$, except that at the origin, where the slab solution gives an infinite stress. Beyond this point, the two-layer solid values are in closer agreement with those for the slab resting on the elastic solid. It should also be noted that the values of flexural stress obtained for the slab resting on a liquid subgrade are tensile and consistently higher than those obtained from either of the other solutions, at least up to $x = 3$. Since the factor of safety for concrete pavement is usually based on the ratio of the modulus of rupture of the concrete to the maximum computed tensile stress, it appears that a pavement design based on a liquid subgrade would have a somewhat higher factor of safety against cracking than indicated by the computation.

On the basis of the numerical results of this investigation, the following observations regarding the effects of the pertinent parameters on the stresses may be made:

Effects of a/h on stress: σ_x, σ_y, and τ_{xy} increase steadily with increasing a/h at all points when the surface loading is uniformly distributed and of constant intensity, Q. When the loading is a line loading, that is, a/h = 0, the horizontal stresses, σ_x, at y = 0 and at the interface are slightly higher in general (except, of course, at the origin where they are infinite) than the corresponding stresses for a/h = 1. This might be expected, because the total loads for a/h = 0 and 1 are equal, and concentrated loads do cause higher stresses in the vicinity of the load than do distributed loads of the same total value. It is also interesting to note that the stresses for a/h = 0 and a/h = 1 are identical to four decimal places at y = 10h, which is fairly remote from the surface load. This is in accordance with St. Venant's principle.

Effects of friction at the interface on stress: In changing the conditions at the interface from rough to smooth, there is usually a slight decrease in σ_x at the surface (y = 0). At the interface there is a substantial increase in σ_x (tensile stress) in the upper layer, and a considerable increase in σ_x (compressive stress) in the lower layer. At points remote from the surface loading, say y = 10 h, there is only a slight change in σ_x, generally from a slight tension to slight compression. There is only a very slight change in σ_y at all points - usually a small decrease in stress, and a very little change in the value of τ_{xy}, except at the interface, where they all, of course, become zero. This clearly indicates the pronounced effects friction has on the horizontal stresses

[3] An average value of E/36 was used for the modulus of subgrade reaction, k, a value commonly used by the Texas State Highway Dept. The values for k range from approximately E/27 to E/45, depending upon the type of soil and other factors. A theoretical determination of k from the elastic constants, alone, is not possible.

in both layers, and hence the necessity of taking friction into account in the rational analysis or design of any slab or pavement system.

Finally, it should be mentioned that a most interesting characteristic was observed for the smooth cases - almost perfect flexural distribution of the stress σ_x in the upper layers of the system. If a section of the upper layer were considered to be a beam of depth h, point a (Fig. 1) would correspond to a point on the upper surface of the beam, and point e would represent the corresponding point on the lower surface of the beam, each point at a distance h/2 from the neutral axis. For pure bending, the flexural stresses at these two points should, of course, be equal and opposite. Inspection of Table 3, Problem 6, indicates values of -6.8201 and +6.8189, respectively, at points a

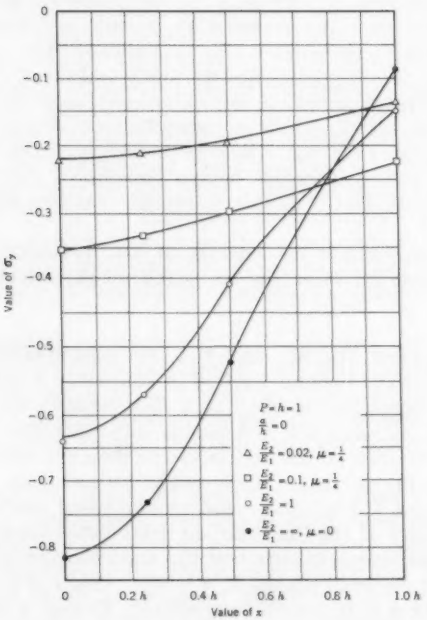

FIG. 7.—COMPARISON OF VALUES OF σ_y AT ROUGH INTERFACE OF TW-LAYER SYSTEM SUBJECTED TO A CONCENTRATED LOAD, FOR VARIOUS STIFFNESS RATIOS

and e, which is in excellent agreement with this requirement. This flexural behavior is most pronounced for low values of E_2/E_1 where the underlying layer is relatively flexible in comparison to the upper layer.

Effects of stiffness ratio: E_2/E_1, on stress: For the smooth cases it was found that increasing the stiffness ratio, E_2/E_1, from 0.02 to 0.1 nearly doubles σ_y at the interface. At the same time, however, σ_x (compressive) at the surface of loading is virtually reduced by a factor of two, as are the horizontal stresses (tensile) at the interface of the upper layer. This would seem

to indicate that increasing the stiffness ratio results in less load being carried in flexure, and more by direct bearing on the supporting layer, as noted previously.

For the rough cases, increasing the stiffness ratio from 0.02 to 0.1 increases σ_y, by approximately one-half, while, at the same time, decreasing σ_x by a factor slightly less than three. The shearing stresses, τ_{xy}, at the interface are, in general, increased by a factor of nearly three.

Fig. 7 shows the effect on σ_y of increasing the stiffness ratio, E_2/E_1, at a rough interface of a two-layer system, subjected to a line load P = 1. It should be noted that the stresses for $E_2/E_1 = \infty$ correspond to the stresses at the interface of an elastic solid for which $\mu = 0$ and h = 1, resting on a rigid base. It is noted that there is less and less spreading of the load with increasing stiffness ratio. For $E_2/E_1 = co$, at x = 0, σ_y at the interface is approximately one-quarter greater than the corresponding stresses for the homogeneous case, $E_2/E_1 = 1$, and nearly three times greater than the stresses corresponding to $E_2/E_1 = 0.02$. This clearly points up the pronounced effect pavement stiffness has on subgrade vertical pressures.

APPENDIX I.—NOTATION

A_1, A_2, A_3, A_4	constants in the displacement functions for horizontal displacement u in the upper layer
B_1, B_2, B_3, B_4	constants in the displacement functions for vertical displacement v in the upper layer
C_1, C_2	constants in the displacement functions for horizontal displacement u in the second layer
D_1, D_2	constants in the displacement functions for vertical displacement v in the second layer
E_i	Young's modulus of elasticity
G_i	modulus of rigidity
P	magnitude of the concentrated line load, P = aQ
Q	amplitude of the uniformly distributed strip loading
$\overline{Q}$	non-dimensional form of Q, $\overline{Q} = Q/E_2$
U_i	displacement function for the horizontal displacement u
V_i	displacement function for the vertical displacement v
a	width of the loaded area
e_i	$\epsilon_x + \epsilon_y + \epsilon_z = \frac{\partial u_i}{\partial x} + \frac{\partial v_i}{\partial y} + \frac{\partial w_i}{\partial z}$ ($\epsilon_z = 0$ for plane strain)
h	depth of Layer 1
k_i	$1/1-2\mu_i$
m_i	$\lambda_i + 2G_i$

n_i	$\frac{1}{(1 + \mu_i)(1 - 2\mu_i)}$
q	amplitude of the sinusoidal loading
u_i, v_i, w_i	components of displacement in the x, y, z directions, respectively
x, y, z	rectangular coordinates
α	parameter of loading, $\alpha = \frac{n\pi}{a}$ (n = 0, 1, 2, etc.)
$\overline{\alpha}$	non-dimensional form of α, $\overline{\alpha} = \alpha h$
Δ^2	$\frac{\partial^2}{\partial x^2} + \frac{\partial^2}{\partial y^2} + \frac{\partial^2}{\partial z^2}$
ϵ_x, ϵ_y, ϵ_z	unit elongations in x, y, and z directions
λ_i	Lamé's constant $\lambda = \frac{\mu_i E_i}{(1 + \mu_i)(1 - 2\mu_i)}$
$(\sigma_x)'_i$, $(\sigma_y)'_i$	incremental normal stresses in x and y directions, respectively
$(\tau_{xy})'_i$	incremental shearing stress in the xy plane
$(\sigma_x)_i$, $(\sigma_y)_i$	normal stresses in x and y directions, respectively
$(\tau_{xy})_i$	shear stress in the xy plane
μ_i	Poisson's ratio

NOTE: Subscripts are used in the text to identify the layer in question; thus u_i, $(\sigma_x)_i$, k_i, μ_i, E_i, etc., refer to the ith layer.

APPENDIX II.—BIBLIOGRAPHY

1. "Mémoire sur l'équilibre intérieur des corps solides homogènes," by G. Lamé and B. P. E. Clapeyron, Crelle's Journal, Vol. 7, 1831, pp. 400-404.
2. "Über das Gleichgewicht schwimmender elastischer Platten," by H. Hertz, Wiedermann's Annalen der Physik und Chemie, Vol. 22, 1884, pp. 449-455.
3. "Applications des potentiels a l'étude de l'équilibre et du mouvement des solides élastiques," by J. Boussinesq, Paris, 1885.
4. "On Boussinesq's Problem," by H. Lamb, London Mathematical Soc. Proceedings, Vol. 34, February 13, 1902, pp. 276-284.
5. "Treatise on the Mathematical Theory of Elasticity," by A. E. H. Love, University Press, Cambridge, England, 1923.

6. "Spannungverteilung und Wellenausbreitung in der kontinuierlich gestuetzten Platte," by K. Marguerre, Ingenieur Archiv., Vol. 4, 1933.

7. "Effect of Certain Discontinuities on Pressure Distribution in a Loaded Soil," by M. A. Biot, Physics, December, 1935, p. 367.

8. "Stress Distribution in a Loaded Soil with Some Rigid Boundaries," by G. Pickett, Proceedings, 18th Annual Meeting Highway Research Bd., Vol. 18, Part II, November, 1938, pp. 35-48.

9. "Druckverteilung durch eine elastische Schict," by W. Passer, Akad der Wissenschaften in Wien, Math-Natur, Klasse Abt. IIa, 144 Band 5 and 6, Heft, Wien, 1935.

10. "Equilibrium of a Thin Slab on an Elastic Foundation of Finite Depth," by A. H. A. Hogg, Philosophical Magazine and Journal of Science, No. 243, London, April, 1944, pp. 265-276.

11. "Thin Plates on Elastic Foundations," by D. L. Holl, Proceedings, 5th Internl. Congress for Applied Mechanics, Cambridge, Mass., 1938, Wiley, 1939, pp. 71-74.

12. "Sul problema generale della piastra poggiata su suolo elastico," by E. Volterra, Pubblicazioni, Dell 'Istituto per le applicazioni del calcolo, N. 201, Consiglio Nazionale Delle Ricerche, Roma, 1947.

13. "The Theory of Stresses and Displacements in Layered Systems and Applications to the Design of Airport Runways," by D. M. Burmister, Proceedings, 23rd Annual Meeting of the Highway Research Bd., November, 1943, pp. 126-144.

14. "The General Theory of Stresses and Displacements in Layered Systems, III," by D. M. Burmister, Journal of Applied Physics, Vol. 16: No. 2, February, pp. 89-96; No. 3, March, pp. 126-267; and No. 5, May, 1945, pp. 296-302.

15. "Computation of Traffic Stresses in a Simple Road Structure," by L. Fox, Road Research Tech. Paper No. 9, London, 1948.

16. "Relaxation Methods Applied to Engineering Problems, IIID. Stress Distributions in Elastic Solids of Revolution," by R. V. Southwell, D. N. Allen, and L. Fox, Philosophical Transactions, Royal Soc., Series A, 1945, pp. 239; 501-537.

17. "Computation of Load Stresses in a Three-Layer Elastic System," by W. E. A. Acum and L. Fox, Geotechnique, Vol. II, No. 4, December, 1951, pp. 293-300.

18. "Influence Charts for Computation of Stresses in Elastic Foundations," by N. M. Newmark, Univ. of Illinois Engrg. Experiment Sta. Bulletin No. 338, 1942.

19. "Theory of Elasticity," by S. Timoshenko and J. N. Goodier, McGraw-Hill, 1951, p. 234.

20. Ibid., p. 87.

21. "Deflections, Moments and Reactive Pressure for Concrete Pavements," by G. Pickett, M. E. Raville, W. C. Janes, and F. J. McCormick, Kansas State College Bulletin No. 65, 1951.

22. "Ruel V Fourier Series and Boundary Value Problems," by R. V. Churchill, McGraw-Hill, 1941.

Journal of the
ENGINEERING MECHANICS DIVISION
Proceedings of the American Society of Civil Engineers

LATERAL STABILITY OF FRAMES BY ENERGY METHOD

By Donald E. Johnson,[1] A.M. ASCE

SYNOPSIS

A method of analyzing the elastic stability of rigid frame structures subject to sidesway is presented. The energy method is applied to an assumed frame deformation compatible with its restraints. The assumed deformations are chosen so that compatibility may be achieved by one standard moment distribution. Formulas describing the energies involved are given and presented in graph form. Two examples are given and compared to results obtained by more rigorous methods.

INTRODUCTION

It is well known that multi-story, rigid frame structures may buckle laterally in sidesway under loads significantly less than those predicted by individual column-buckling formulas. Structures in this category are usually multi-story frames without vertical truss systems. The methods available for a rigorous solution of the lateral stability of such frames involve the task of solving large numbers of transcendental equations in all but the simplest of cases. The purpose of this paper is to present a simplified method that can be easily used to find accurate estimates of the loads under which a given frame will become unstable.

Note: Discussion open until January 1, 1961. To extend the closing date one month, a written request must be filed with the Executive Secretary, ASCE. This paper is part of the copyrighted Journal of the Engineering Mechanics Division, Proceedings of the American Society of Civil Engineers, Vol. 86, No. EM 2, August, 1960.

[1] Graduate Student, Mechanics Department, College of Engineering, Cornell University, Ithaca, N.Y.

Notation.—The letter symbols adopted for use in this paper are defined where they first appear, in the illustration or in the text, and are arranged alphabetically, for convenience of reference, in the Appendix. The symbols used herein (except k, P_O, L_O, I_O, l_O) apply to a particular member which is under consideration. If a member n is being considered, then the subscript n is implied but omitted to simplify the equations. When two or more members are under consideration simultaneously, subscripts are used to avoid ambiguity.

GENERAL ANALYSIS

Assumptions.—Although the method presented could be extended to other cases, the problem limits itself as follows:

1. Frames to be considered consist of horizontal and vertical members only. The configuration is limited to frames of the beam-column or slab-column type such as shown in Fig. 1. Individual column heights need only be identical for a given floor and individual bay spacings need only be identical when located above or below one another. Moments of inertia need not be identical. Bottoms of first floor columns will be considered clamped, although they can be modified easily to allow for various degrees of restraint. All members are assumed to be of uniform cross section.
2. Only loads associated with lateral buckling by sidesway, such as shown in Fig. 1, are considered. Thus, joints on each progressively higher floor undergo progressively greater displacements. Loads on any member are assumed axial but need not be identical. Only frame deformations due to pure bending are considered. It is assumed that direct shortening or lengthening of any column due to axial loads alone may be neglected in describing the buckled shape and computing the critical loads. Although this same assumption is made in the more rigorous methods of analyzing the lateral stability of multi-story frames, it may result in overestimating the buckling loads of very tall and narrow frames that buckle in modes as shown in Fig. 2. Such frames are more accurately analyzed by taking into account the direct shortening or lengthening of columns that occurs during buckling.
3. Instability is assumed to occur in the elastic range and to consist of small deflections. All members are assumed slender enough to allow application of the basic assumptions of simple beam bending theory. All joints are considered rigid.

General Approach.—The energy method as presented by Timoshenko[2] is applied to the entire structure, yielding the equation $\Delta V = \Delta T$. ΔV is the bending energy absorbed by the structure and ΔT is the total work done by the external loads. Both quantities are due to an assumed buckling deformation of the entire structure.

The deformation of each member is assumed to be a third degree polynomial in x, a variable which locates all points along the member's length as shown in Fig. 3. The coefficients defining the polynomial in x for each member are expressed in terms of the end displacements and slopes. The moments and energies related to each member are, in turn, related to the coefficients

2 "Theory of Elastic Stability" by S. Timoshenko, McGraw-Hill Book Co., 1936.

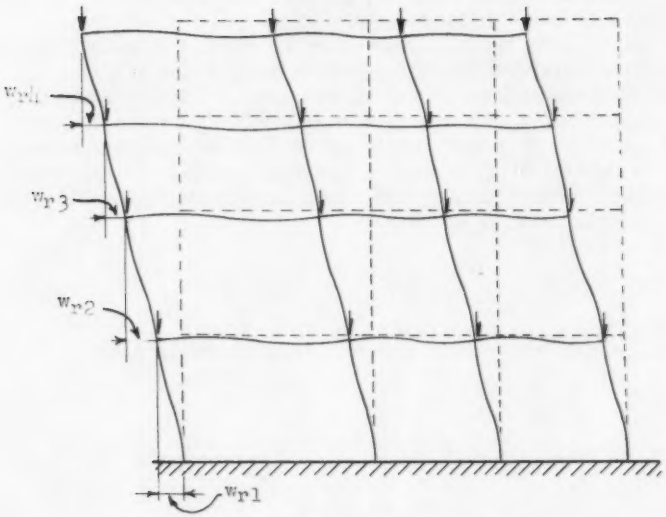

FIG. 1.—TYPE OF BUCKLING CONSIDERED

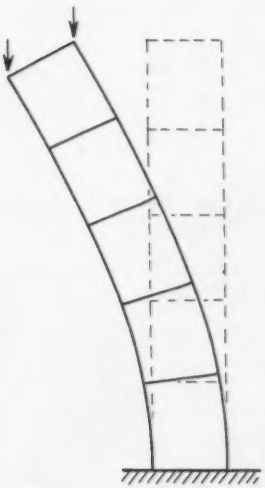

FIG. 2.—TYPE OF BUCKLING NOT CONSIDERED.

of the polynomial. By substitution, general formulas for end moments and energies for any member are derived.

Derivation of Deformation Equations.—The top end of all columns will be considered the right end. Hence the desired deformation of a member (column or beam) is representable, in general, as shown in Fig. 3. Note that the total buckling displacement of a member is w + w(x), in which w is a constant. Since the energies ΔT and ΔV are related only to the first and second derivatives of the displacement, w may be neglected and only the relative displacement w(x) need be considered. The assumed deformation w(x) is chosen as a third degree polynomial in x as

$$w(x) = l\left[A + B\left(\frac{x}{l}\right) + C\left(\frac{x}{l}\right)^2 + D\left(\frac{x}{l}\right)^3\right] \quad \ldots\ldots\ldots \quad (1)$$

From Fig. 3 it can be seen that L differs from 2 l by the amount e. Because

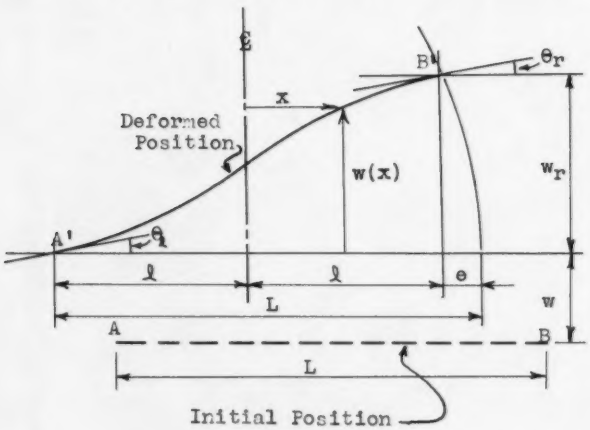

FIG. 3.—BUCKLING DEFORMATION OF A TYPICAL MEMBER AB

very small deflections are assumed, e is negligible relative to l or L. Hence L = 2 l. Introducing y(x) = w(x)/L into Eq. 1 yields

$$2\,y(x) = A + B\left(\frac{x}{l}\right) + C\left(\frac{x}{l}\right)^2 + D\left(\frac{x}{l}\right)^3 \quad \ldots\ldots\ldots \quad (2)$$

differentiating Eq. 1 gives

$$\frac{dw(x)}{dx} = B + 2\,C\left(\frac{x}{l}\right) + 3\,D\left(\frac{x}{l}\right)^2 \quad \ldots\ldots\ldots\ldots \quad (3)$$

similarly

$$\frac{d^2w(x)}{dx^2} = \frac{1}{l}\left(2\,C + 3\,D\left(\frac{x}{l}\right)\right)$$

$$= \frac{1}{L}\left(4\,C + 6\,D\left(\frac{x}{l}\right)\right) \quad \ldots\ldots\ldots\ldots \quad (4)$$

Now we have four unknown coefficients (A, B, C, D) and four boundary conditions:

when $x = +1;\quad y(x) = y_r,\quad \frac{dw(x)}{dx} = \theta_r$ ..... (5a)

$x = -1;\quad y(x) = 0,\quad \frac{dw(x)}{dx} = \theta_l$ ..... (5b)

substituting the boundary conditions of Eqs. 5 into Eqs. 2 and 3 and solving for A, B, C, D yields

$$A = 1/4\ \theta_l + y_r - 1/4\ \theta_r \quad \text{..... (6a)}$$

$$B = -1/4\ \theta_l + 3/2\ y_r - 1/4\ \theta_r \quad \text{..... (6b)}$$

$$C = -1/4\ \theta_l + 1/4\ \theta_r \quad \text{..... (6c)}$$

$$D = 1/4\ \theta_l - 1/2\ y_r + 1/4\ \theta_r \quad \text{..... (6d)}$$

Derivation of Moment and Energy Equations.—Now we have for the moment

$$m(x) = E\ I\ \frac{d^2w(x)}{dx^2} = \frac{E\ I}{L}\left[4\ C + 6\ D\left(\frac{x}{l}\right)\right] \quad \text{..... (7a)}$$

but the dimensionless measure of m(x) is $M(x) = \frac{m(x)\ L_o}{E\ I_o}$ Therefore

$$M(x) = \left(\frac{I}{I_o}\right)\left(\frac{L_o}{L}\right)\left[4\ C + 6\ D\left(\frac{x}{l}\right)\right] \quad \text{..... (7b)}$$

Substituting Eqs. 6(c) and 6(d) into Eq. 7(b) and evaluating for $x = +1$, $x = -1$ yields the following:

$$M_l = \left(\frac{L_o}{L}\right)\left(\frac{I}{I_o}\right)\left(4\ \theta_l - 6\ y_r + 2\ \theta_r\right) \quad \text{..... (8a)}$$

$$M_r = \left(\frac{L_o}{L}\right)\left(\frac{I}{I_o}\right)\left(2\ \theta_l - 6\ y_r + 4\ \theta_r\right) \quad \text{..... (8b)}$$

(Note that the sign has been adapted to moment distribution convention; a clockwise rotation at an end of a member is considered positive.)

For horizontal beam members the relative displacements y_r are neglected in computing end moments from Eqs. 8(a) and 8(b). This is completely consistent with the assumptions made and is explained in the following manner. Consider a frame in its buckling deformation, such as shown in Fig. 1, having lateral joint displacements at each floor of $w_{r1}, w_{r2}, w_{r3}, \ldots$, and slopes for each member of $\theta(x)_1, \theta(x)_2, \theta(x)_3, \ldots$. If we increase the magnitudes of $w_{r1}, w_{r2}, w_{r3}, \ldots$ by a proportion q, then the magnitudes of $\theta(x)_1, \theta(x)_2, \theta(x)_3, \ldots$ are also increased by a proportion q. Associated with the initial displacements $w_{r1}, w_{r2}, w_{r3}, \ldots$, are also displacements $e_1, e_2, e_3, \ldots$ for each member. However, if the magnitudes of $w_{r1}, w_{r2}, w_{r3}, \ldots$ are increased again by

some proportion q, then the displacements e_1, e_2, e_3, . . . are increased by a proportion q^2 by virtue of the equation

$$e = 1/2 \int_0^L [\theta(x)]^2 \, dx \quad \ldots\ldots\ldots\ldots \quad (9)$$

that is applicable to small deflections. Thus if we reduce the proportion q to a very small fraction, e_1, e_2, e_3, . . . become negligible as compared to the slopes $\theta(x)_1$, $\theta(x)_2$, $\theta(x)_3$, ... The relative displacement y_r for a horizontal beam member is composed only of the e displacements of the two adjacent rows of columns below that beam member. Other displacements contributing to y_r are neglected by virtue of assumption number two. Hence y_r is neglected in computing end moments of horizontal beam members. This is often a good approximation even if the w_{r1}, w_{r2}, w_{r3}, . . . are not very small, because in most frames the joints at each floor remain relatively level under buckling deformations.

For beams

$$M_l = - \left(\frac{L_o}{L}\right)\left(\frac{I}{I_o}\right)(4\,\theta_l + 2\,\theta_r) \quad \ldots\ldots\ldots \quad (10a)$$

$$M_r = - \left(\frac{L_o}{L}\right)\left(\frac{I}{I_o}\right)(2\,\theta_l + 4\,\theta_r) \quad \ldots\ldots\ldots \quad (10b)$$

v, the energy absorbed by a member in bending, is representable as

$$v = \frac{1}{2\,E\,I} \int_o^L [m(x)]^2 \, dx \quad \ldots\ldots\ldots\ldots \quad (11a)$$

or expressed in terms of the dimensionless quantities $V = \dfrac{v\,L_o}{E\,I_o}$ and $M(x) = \dfrac{m(x)\,L_o}{E\,I_o}$, yields

$$V = \frac{1}{2\,L_o} \int_o^L [M(x)]^2 \, dx \quad \ldots\ldots\ldots\ldots \quad (11b)$$

substituting into Eq. 11(b) values of C and D from Eqs. 6(c) and 6(d), performing the integration and introducing

$$\beta = \left|\frac{M_l}{m_r}\right| = \left|\frac{M_l}{M_r}\right| \quad \ldots\ldots\ldots\ldots\ldots\ldots \quad (12)$$

yields

$$V = \left(\frac{I_o}{I}\right)\left(\frac{L}{L_o}\right)\left[\frac{\beta^3 + 1}{6(\beta + 1)}\right] M_r^2 \quad \ldots\ldots\ldots\ldots \quad (13a)$$

or introducing $C_1 = \dfrac{\beta^3 + 1}{6(\beta + 1)}$

$$V = \left(\frac{I_o}{I}\right)\left(\frac{L}{L_o}\right) C_1 \, R \, M_r^2 \quad \ldots\ldots\ldots\ldots\ldots \quad (13b)$$

Eq. 12(b) is only applicable for $0 \leqq \beta \leqq \infty$, that is, if the member contains an inflection point. Values of C_1 versus β are presented graphically in Fig. 4 for $0 \leqq \beta \leqq 1.7$. If values are required beyond this range, Eqs. 12 and 13(b) and Fig. 4 can be applied by facing the member from the opposite direction. The value R represents the portion of energy of a member being summed. Usually R is one. If V is expressed in terms of θ_1, θ_r and y_r, the following formula is found:

$$V = \left(\frac{I}{I_o}\right)\left(\frac{L_o}{L}\right)\left(2\,\theta_1^2 + 2\,\theta_r^2 + 6\,y_r^2 + 2\,\theta_1\,\theta_r - 6\,\theta_1\,y_r - 6\,\theta_r\,y_r\right) \quad \ldots \quad (13c)$$

This expression is much more cumbersome than Eq. 13(b) but is applicable if the member contains no inflection point.

The term t is the energy equal to the quantity P e for a given member. The sum of t over all members is the energy released by all of the external loads. t may be expressed as

$$t = \frac{P}{2}\int_o^L \left(\frac{dw(x)}{dx}\right)^2 dx \quad \ldots \quad (14a)$$

for small displacements.

Expressing t in its dimensionless form

$$T = \frac{t}{L_o P_o} \quad \ldots \quad (14b)$$

$$T = \left(\frac{P}{P_o}\right)\left(\frac{1}{2\,L_o}\right)\int_o^L \left(\frac{dw(x)}{dx}\right)^2 dx \quad \ldots \quad (14c)$$

Substituting values of A, B, C, D from Eq. 6 and performing the integration yields

$$T = \left(\frac{P}{P_o}\right)\left(\frac{L}{L_o}\right)\left(\frac{2\,\theta_1^2 + 2\,\theta_r^2 + 18\,y_r^2 - \theta_r\,\theta_1 - 3\,\theta_1\,y_r - 3\,\theta_r\,y_r}{30}\right) \quad \ldots \quad (15a)$$

letting

$$C_2 = \left[\frac{2\left(\frac{\theta_1}{y_r}\right)^2 + 2\left(\frac{\theta_r}{y_r}\right)^2 + 18 - \left(\frac{\theta_r}{y_r}\right)\left(\frac{\theta_1}{y_r}\right) - 3\left(\frac{\theta_1}{y_r}\right) - 3\left(\frac{\theta_r}{y_r}\right)}{30}\right] \quad \ldots \quad (15b)$$

yields

$$T = \left(\frac{P}{P_o}\right)\left(\frac{L}{L_o}\right) C_2\,(y_r)^2 \quad \ldots \quad (16)$$

Values of C_2 for various values of $\left(\frac{\theta_r}{y_r}\right)$ and $\left(\frac{\theta_1}{y_r}\right)$ are presented graphically in Fig. 5. Because C_2 is quite constant for ratios of $\left(\frac{\theta_1}{y_r}\right)$ and $\left(\frac{\theta_r}{y_r}\right)$ used in sidesway, this graph can be used with sufficient accuracy.

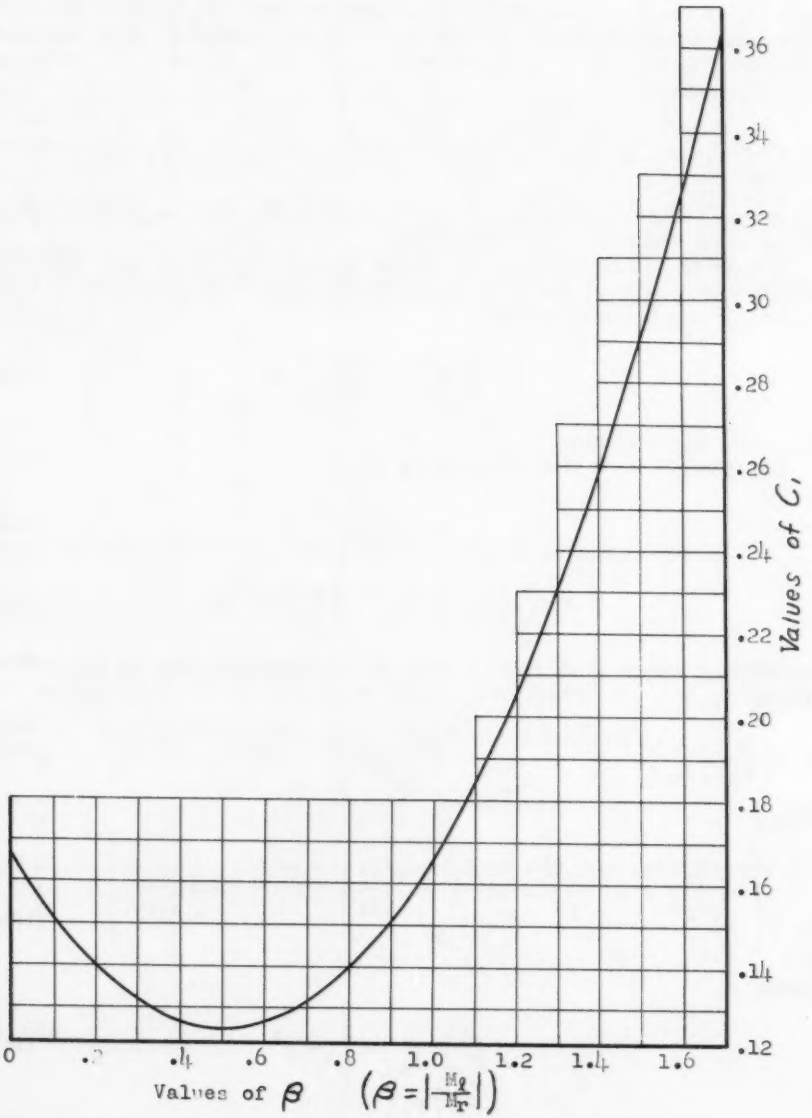

FIG. 4.—PLOT OF C_1 AS A FUNCTION OF β

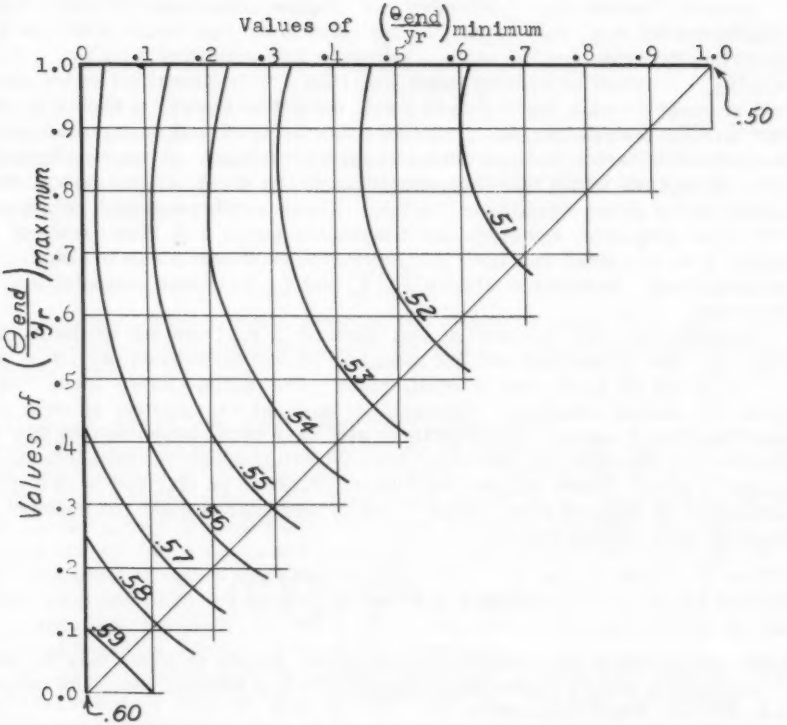

FIG. 5.—PLOT OF C_2 AS A FUNCTION OF END SLOPES AND y_r

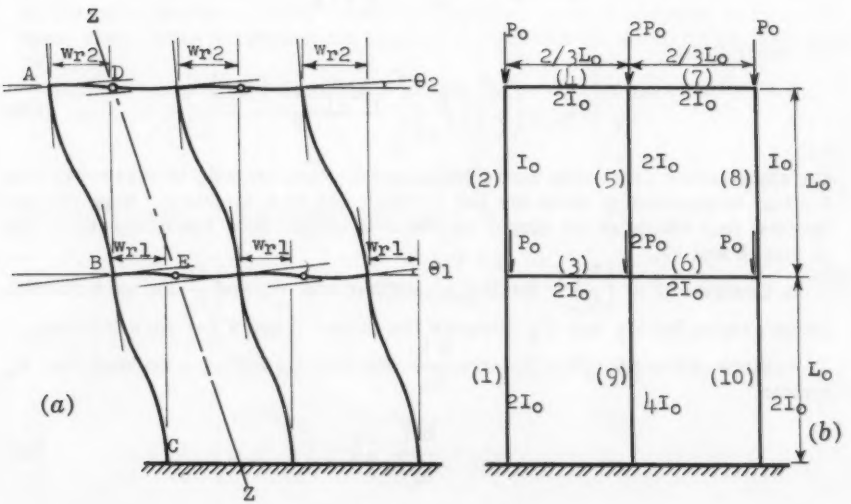

FIG. 6.—EXAMPLE I

General Procedure of Application.—1. Choose convenient arbitrary lateral displacements w_{r1}, w_{r2}, w_{r3}, . . . for each floor that could most probably describe the true buckled shape. Although the quantities w_{r1}/L_1, w_{r2}/L_2, w_{r3}/L_3. . . must be actually much less than 1 to be described by the energy and moment formula applicable to small deflection theory, it should be noted that any convenient series of numbers can be used and interpreted as one magnification factor times a series of small fractions. It can be shown that both ΔT and ΔV would then be proportional to the square of this factor, which would cancel in the equating of the two. These numbers should be selected with good judgment, however, any reasonable guess will give excellent results. It is suggested that floor displacements be chosen so as to simplify the computations. In addition, choose P_o, I_o and L_o to reduce computations to a minimum.

2. Select, for each member n, end slopes θ_{ln}, θ_{rn}, and end moments M_{ln}, M_{rn}, that are compatible with the assumed lateral deflections w_{r1}, w_{r2}, w_{r3}, . . . , so that all joints are in equilibrium. For simple cases these can be found by solving equations representing moment summations at each joint based on Eqs. 8 and 10. The functions w(x) have been chosen so that they are identical to functions that describe beams bending under the influence of end moments only. Hence the desired compatibility can be obtained by use of one application of moment distribution. The dimensionless fixed end moment induced in each column then is

$$FEM = +6\left(\frac{L_o}{L}\right)\left(\frac{I}{I_o}\right)\left(\frac{w_r}{L}\right) \quad \ldots\ldots\ldots\ldots (17)$$

After the moments are completely distributed, slopes at joints may be found by proceeding from a known slope (usually $\theta = 0$ at bottom) using the moment area relation which reduced to

$$\theta_r = \theta_l + \frac{(\beta - 1)}{2}\left(\frac{I_o}{I}\right)\left(\frac{L}{L_o}\right) M_r \quad \ldots\ldots\ldots (18a)$$

or, more simply

$$\theta_r = \theta_l + \left(\frac{I_o}{I}\right)\left(\frac{L}{L_o}\right)\left[\frac{|M_l| - |M_r|}{2}\right] \quad \ldots\ldots\ldots (18b)$$

for any member containing an inflection point. This formula is correct in sign for use in proceeding from the left to the right of a member. It is recommended that values of all slopes be checked against final end moments by use of Eqs. 8 and 10.

3. Compute $\beta = \left|\frac{M_l}{M_r}\right|$ for every member and $\frac{\theta_r}{y_r}$, and $\frac{\theta_l}{y_r}$ for each column. Using graphs for C_1 and C_2 compute the values T and V for each member.

4. Since $\Delta T = \Delta V$, $\Sigma v = \Sigma t$ and $\frac{E\, I_o}{L_o}\Sigma V = P_o\, L_o\, \Sigma T$. Solving for P_o yields:

$$P_o = \frac{E\, I_o}{L_o^2}\frac{\Sigma V}{\Sigma T} \quad \ldots\ldots\ldots\ldots\ldots (19)$$

Hence the buckling coefficient is

$$k = \frac{P_o L_o^2}{E I_o} = \frac{\Sigma V}{\Sigma T} \quad \ldots\ldots\ldots\ldots\ldots\ldots (20)$$

Either Eq. 19 or 20 may be used to determine the cricial load. The energy summation is to be extended over the entire structure or over any representative portion for which it is known that the ratio $\Sigma V/\Sigma T$ is identical to that of the entire structure.

EXAMPLES

Example 1.—This problem involves the frame shown in Figs. 6(a), the assumed buckling shape, and 6(b) the given frame. The solution is obtained as follows

1. L_o, I_o and P_o are chosen according to Fig. 6(b).
2. The assumed deformation is chosen as shown in Fig. 6(a). Notice that all joint rotations at each floor are the same, θ_1 and θ_2, respectively. In addition, the columns above each floor have identical deformed shapes so that all loads on each floor descend the same distance. In other words, $e_1 = e_9 = e_{10}$ and $e_2 = e_5 = e_8$. Each beam deformation is antisymmetric and its inflection point is shown as a hinge in Fig. 6(a). It can be shown by applying Eqs. 13(c) and 15(a), or by similar intuitive reasoning, that, for the deformation assumed, the portion of the frame to the left of section Z-Z has the same ratio of energies $\Sigma V/\Sigma T$ as the entire structure.
3. Choose lateral displacements of each floor $w_{r1}/L_o = 8$, $w_{r2}/L_o = 10$. It is reasonable to assume w_{r2} greater than w_{r1} because the bottom of the structure is clamped.
4. The joint equilibrium of the portion of the frame to the left of section Z-Z can be analyzed as if it contained the hinges shown in Fig. 6(a) because of the antisymmetry. Hence modified stiffness factors are used and the moment distribution is performed only on the portion as shown below (see also Table 2):

For the computation of stiffness factors K we use the general formula

$$K = \frac{I L_o}{I_o L} \quad \ldots\ldots\ldots\ldots\ldots\ldots (21)$$

and the formula for a member with hinged end

$$K = \frac{3}{4} \frac{I L_o}{I_o L} \quad \ldots\ldots\ldots\ldots\ldots\ldots (22)$$

Table 1 is obtained.

For the computation of fixed end moments Eq. 17 is applied to obtain

$$FEM_{AB} = FEM_{BA} = 6(1)\ (10) = +60$$

$$FEM_{BC} = FEM_{CB} = 6(2)\ (8) = +96$$

The deflected slopes at the two joints A and B are determined proceeding from zero slope at the bottom using Eq. 18(b):

$$\theta_1 = 0 + \frac{1}{2}\frac{1}{2}(75.9 - 55.6) = 5.07$$

and

$$\theta_2 = 5.07 + \frac{1}{2}(35.3 - 40.8) = 2.32$$

Checking the beam moments from Eq. 10(a), noting that the deflection is anti-symmetric about Z-Z, yields

$$M_{12} = \frac{1}{2/3} 2 \cdot 6(5.07) = 91.2 \text{ vrs } 90.9 \text{ from moment distribution}$$

and

$$M_{13} = \frac{1}{2/3} 2 \cdot 6(2.32) = 41.7 \text{ vrs } 40.8 \text{ from moment distribution}$$

This accuracy is sufficient because the general method gives results only to within 1% or 2%.

TABLE 1

Member		I/I_o	L_o/L	K	$K/\Sigma K$
Joint A:					
AD	3/4	2	6/2	9/2	.818
AB	1	1	1	2/2	.182
			$\Sigma K =$	11/2	
Joint B:					
BA	1	1	1	2/2	.1335
BE	3/4	2	6/2	9/2	.6000
BC	1	2	1	4/2	.2670
			$\Sigma K =$	15/2	

5. Computations of energies using graphs of Figs. 4 and 5 are presented in Tables 3 and 4.

6. Inserting ΣV and ΣT in Eqs. 19 and 20 yields

$$k = 7.10, \quad P_o = 7.10 \frac{E I_o}{L_o^2}$$

This identical problem has been previously computed by two rigorous methods, one using the method of four moment equations and the other employing the method of slope deflection equations, by Mr. John F. Mullen.[3] These methods both yielded k = 7.09. Hence the error induced by using the

[3] "The Elastic Stability of Rigid Frame Structures Subject to Sidesway" by J. F. Mullen, Master's Thesis, Lehigh University, 1958.

TABLE 2.—MOMENT DISTRIBUTION FOR EXAMPLE ONE

A	D
AB	AD
.182	.818
60.0	
-10.9	-49.1
-10.4	
1.9	8.5
.3	
-.1	-.2
40.8	-40.8

B		E
BA	BC	BE
.1335	.2670	.6000
60.0	96.0	
-20.8	-41.6	-93.6
-5.4		
.7	1.4	3.3
.9		
-.1		
35.3	55.6	-90.9

	CB
	96.0
	-20.8
C	.7
	75.9

TABLE 3.—SUMMATION OF BENDING ENERGY

Member	M_r	$\beta = \left\lvert \frac{M_1}{M_r} \right\rvert$	C_1	M_r^2	$\left(\frac{I_o}{I}\right)$	$\left(\frac{L}{L_o}\right)$	R	V
Energy in dimensionless form, $V = C_1 M_r^2 \left(\frac{I_o}{I}\right) \left(\frac{L}{L_o}\right) R$								
(1)	55.6	.866	.147	3090	1/2	0	1	227
(2)	40.8	1.365	.237	1665	1	0	1	394
(3)	90.9	1.00	.1666	8230	1/2	2/3	1/2[a]	229
(4)	40.8	1.00	.1666	1665	1/2	2/3	1/2[a]	46
							ΣV	896

[a] Only energy to the left of section Z-Z is summed.

TABLE 4.—SUMMATION OF LOAD ENERGY

Member	y_r	θ_1	θ_r	$\frac{\theta_1}{\theta_r}$	$\frac{\theta_r}{y_r}$	C_2	$(y_r)^2$	$\left(\frac{P}{P_o}\right)$	$\left(\frac{L}{L_o}\right)$	T
Energy in dimensionless form, $T = C_2 \ y_r^2 \left(\frac{P}{P_o}\right) \left(\frac{L}{L_o}\right)$										
(1)	8	0	5.07	0	.633	.562	64	2	1	71.8
(2)	10	5.07	2.32	.507	.232	.545	100	1	1	54.5
									ΣT	126.3

energy method in this case is very small. Results obtained from the energy method for assumed lateral joint displacements of $y_{r1} = 6$, $y_{r2} = 10$ and $y_{r1} = 10$, $y_{r2} = 10$, both give $k = 7.17$. Thus, in the three applications of the energy method lateral displacement ratios of y_{r1}/y_{r2} varying as much as 40% from each other, yield critical loads varying less than 1% from each other.

Since these computations involve chart and slide rule accuracies commonly related to errors in the order of 1%, it should be noted that any reasonable selection of y_{r1} and y_{r2} would have given satisfactory results.

Example II.—This example involves a multi-story frame similar to Fig. 1 with the following features:

1. Length of all columns is L_o; of all beams L_b
2. Moments of inertia of a column is I_o; of all beams I_b
3. Total load on all columns is P_o
4. The frame consists of a large number of stories and bays. Thus the problem is analogous to that formulated by Bleich[4] for analysis of tall wide frames.

Solution.—1. In order to avoid the unnecessary work of distributing moments and summing energies over many members, minor modifications in boundary conditions similar to those shown by Bleich will be made. Fig. 7 shows the modifications in boundary conditions made in the present analysis.

The solution presented here is not limited to the size of frame shown in Fig. 7, but applies to any large system with this type of boundary modification. The reductions in moments of inertia and loadings at the top and side edges of the frame, as shown in Fig. 7, can be seen to have little influence on the total critical load of a large sized structure. To further simplify the problem, however, it is necessary to reduce the bottom restraints to that given by a set of beams, also shown in Fig. 7, that renders the loaded structure symmetrical in two directions. With these modifications, if each column and beam are assumed to deflect in the same exact shape, it can be shown that moments at all joints will balance. Furthermore, it can be seen that the energy ratio $\Sigma V/\Sigma T$ for, any representative area, as shown by dotted lines in Fig. 7, is equal to the same ratio for the entire structure. The deformation of this representative area is shown in Fig. 8. Because of the repetition of deformed shapes throughout the frame, the energy summation need only be summed over members AB and BE. Thus the critical load can be determined by considering only the energies in one interior beam and column together.

2. The moments at any internal joint shown in Figs. 8 and 9 are balanced if $M_c + M_b = 0$. (Note that since all interior columns and beams have same deflected shape and I_o, their moments are the same throughout the structure.)

3. Letting $y = w/L_o$, and substituting Eqs. 8 and 10 in the equation $M_c + M_b = 0$ yields:

$$-(6\theta - 6y) - 6\theta\left(\frac{L_o}{L_b}\right)\left(\frac{I_b}{I_o}\right) = 0$$

4. Letting $\left(\frac{L_o}{L_b}\right)\left(\frac{I_b}{I_o}\right) = \alpha$ and simplifying gives $\theta = y/(1 + \alpha)$

[4] "Buckling Strength of Metal Structures" by F. Bleich and H. Bleich, McGraw Hill Book Co., 1952.

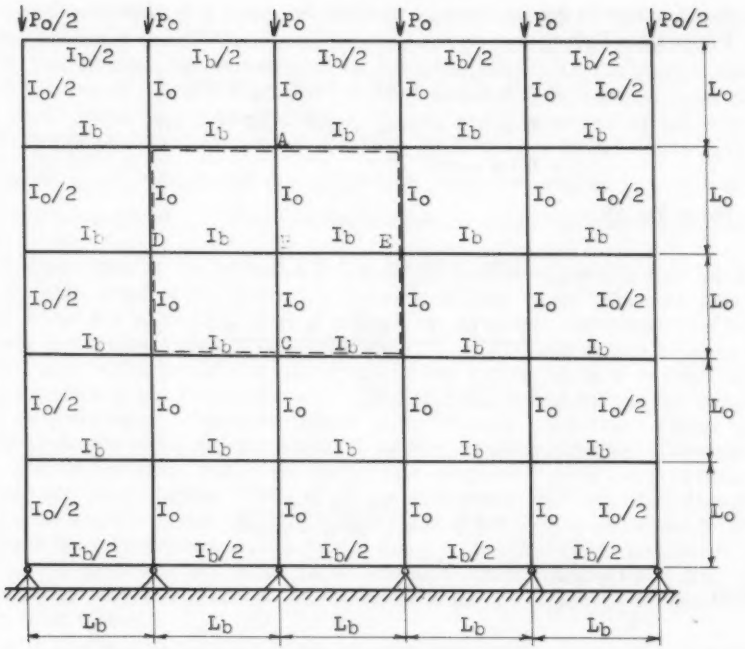

FIG. 7.—SHOWING BOUNDARY MODIFICATIONS FOR EXAMPLE II

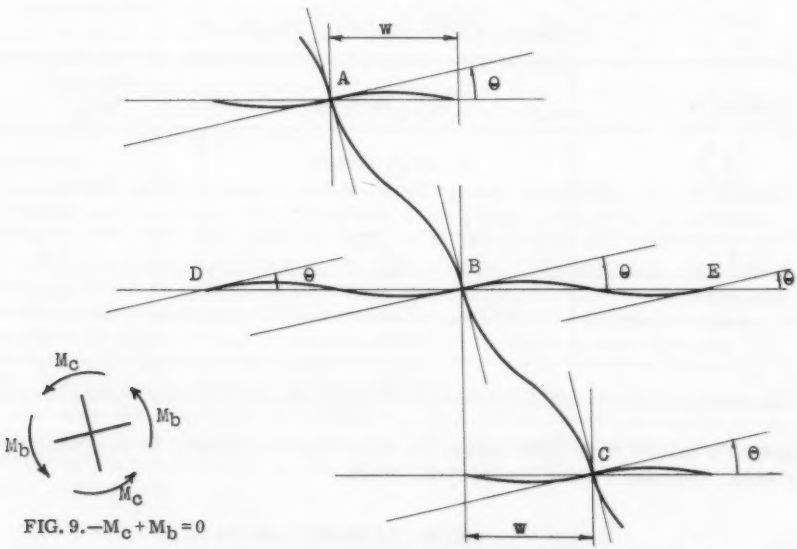

FIG. 8.—ASSUMED BUCKLING DEFORMATION OF REPRESENTATIVE AREA ADCE

FIG. 9.—$M_c + M_b = 0$

5. Since y can be any convenient number, let $y = 1 + \alpha$ then $\theta = 1$.
6. From Eq. 13(c)

$$V = \alpha(6\,\theta^2) + 6\,\theta^2 + 6\,y^2 - 12\,\theta\,y$$
$$= 6\,\alpha + 6 + 6\,(1+\alpha)^2 - 12\,(1+\alpha)$$
$$= 6\,(\alpha + \alpha^2)$$

7. From Eq. 15

$$T = \frac{(3\,\theta^2 + 18\,y^2 - 6\,\theta\,y)}{30}$$
$$= \frac{[3 + 18\,(1+\alpha)^2 - 6\,(1+\alpha)]}{30}$$
$$= \frac{5 + 10\,\alpha + 6\,\alpha^2}{10}$$

8.

$$k = \frac{\Sigma V}{\Sigma T} = \frac{60\,(\alpha + \alpha^2)}{5 + 10\,\alpha + 6\,\alpha^2}$$

in which $\alpha = \left(\frac{L_o}{L_b}\right)\left(\frac{I_b}{I_o}\right)$

Table 5 shows the comparison between values of k computed from Eq. 8 and those given by Bleich for a 10-story building for various values of α.

TABLE 5.—COMPARISON OF VALUES OF l

Value of α	Buckling Coefficient = $k = \frac{P_{cr}\,L_o^2}{E\,I_o}$	
$= \frac{L_o}{L_b}\frac{I_b}{I_o}$	By energy method	From Bleich
1/4	2.39	2.32
1/3	2.97	2.91
1/2	3.91	3.91
1	5.71	5.69
∞	10.00	$9.87\ \pi^2$

Bleich's values have been converted from effective lengths to buckling coefficients. Numbers were scaled from graph.

CONCLUSIONS

In addition to the assumptions described in the section on general analysis, the following limitations, and/or extensions, should be considered:

1. Pin restraints on bottom columns can be described by letting $\beta = 0$. Other boundary conditions can be represented by use of Eqs. 8 and 10.

2. The method can be extended to describe failure in the plastic zone by trial and error. First estimate P_{cr}. Then determine the tangent modulus E_{tn} for each column n for the estimated P_{cr} by use of a stress-strain diagram. The formulas presented herein are then applicable if each column I_n is reduced to $\frac{E_{tn}}{E} I_n$. Apply the energy method using the reduced I_n values to yield a more accurate P_{cr}. Continue the procedure using the more accurate P_{cr} and so on.

3. Inspection of Eq. 16 and the preceding derivation reveals that for a given w_r the values of the factor C_2 are proportional to e. Thus we see from Fig. 5 that the value of e for any column is relatively independent of its end slopes and almost entirely dependent on w_r/L. Although it may be seen from Fig. 5 that variations in end slopes may cause variations in e as high as 20%, this extreme is not realized in many frames. In frames having the most pronounced variation of member sizes in the vertical direction, values of the joint rotations along any particular floor will be quite similar. Consequently the row of columns above any particular floor will have very similar end slopes and very similar values of e. In such a case the total load energy ΣT would be approximately the same regardless of the way in which the total load on each floor is divided among the columns. This fact might be used to allow an investigator to move loads from column to column along each floor so as to simplify the mathematics of the more rigorous methods without a great loss of accuracy.

4. It is always possible to describe a symmetric frame in an antisymmetric buckling mode of deformation that is compatible with the joint equilibrium requirements, even if the loading is not symmetric. Such modes allow the investigator to confine the problem to smaller "representative portions" similar to those used in the given examples and thereby reduce the office work required to distribute moments and to sum energies.

5. The method could be adapted to frames, other than those shown in Fig. 1, that contain only vertical and horizontal members. However, such adaptations are beyond the scope of this paper.

This method is intended for use in checking the lateral stability of frames already designed. Low degree polynomials have been used in the past to solve with accuracies of a few percent many stability problems concerning one member. The method has been developed so that slide rule and well known moment distribution methods can achieve results quickly and easily within the usual required accuracies. This method requires little additional work particularly in designs in which lateral moment distributions have already been made during design for wind, and so forth.

The method can be used on structures with varying column and beam sizes and spacings, varying types of stiffeners, and so on; cases in which more rigorous approaches are often unfeasible. The designer's intuitive knowledge of sidesway buckling modes can be utilized and yet need not be exact in order to yield good results.

ADDITIONAL READING REFERENCES

1. "Method of Split Rigidities and Its Application to Various Buckling Problems" by P. P. Bijlaard, NACA TN 4085, July 1958.

APPENDIX. NOTATION

L	length of a member
l	$= L/2$ half length of a member
L_o	reference length, arbitrarily chosen
l_o	$= L_o/2$ half of reference length
I	moment of inertia of a member
I_o	reference moment of inertia, arbitrarily chosen
P	axial load on a member
P_o	reference axial load, arbitrarily chosen
x	a variable locating points along a member (see Fig. 3)
$w(x)$	a function describing the assumed buckled shape (see Fig. 3)
A,B,C,D	coefficients of a polynomial used to describe $w(x)$
w_r	value of $w(x)$ at right end of a member (see Fig. 3)
y_r	$= w_r/L$ dimensionless measure of w_r
e	relative displacement between ends of a member in axial direction (see Fig. 3)
θ_r	slope of buckled shape at right end of a member
θ_l	slope of buckled shape at left end of a member
m_r	moment at right end of a member
m_l	moment at left end of a member
M_r	$= \frac{m_r L_o}{E I_o}$ dimensionless measure of m_r
M_l	$= \frac{m_l L_o}{E I_o}$ dimensionless measure of m_l
v	energy due to bending of a member
V	$= \frac{v L_o}{E I_o}$ dimensionless measure of v
t	$= P e$ a portion of the load energy assigned to a particular member
T	$= t/L_o P_o$ dimensionless measure of t
k	$= \frac{P_o L_o^2}{E I_o}$ buckling coefficient of the frame
$\lvert\ \rvert$	absolute value of

β $= \left| \frac{M_l}{M_r} \right|$ parameter locating inflection point

R proportion of energy in a member being summed

Journal of the
ENGINEERING MECHANICS DIVISION
Proceedings of the American Society of Civil Engineers

SEEPAGE LOSSES FROM PARALLEL CANAL SYSTEMS

By H. Y. Hammad[1]

SYNOPSIS

This paper deals with the two-dimensional problem of steady seepage flow under gravity from a system of parallel, identical, and equally spaced canals into a semi-pervious clay layer of finite thickness underlain by a freely permeable layer of sand and gravel in which the piezometric head is very near the canal water level. Two steps of conformal mapping are used and an approximation to the canal profile is adopted. In this approximation the specified canal width and depth are not changed.

INTRODUCTION

In most agricultural zones, especially in river valleys, the stratified soil is formed of a top clay layer of finite thickness and medium or low permeability, underlain by highly permeable layers of sand and gravel. The piezometric head in the lower, freely permeable layers is controlled by the river running in the valley.

If, for any reason, the canals running in the top clay cap are run at higher water level than the piezometric level in the lower sand and gravel layers, a steady seepage flow will take place from the canals through the clay layer to the sand and gravel layers beneath.

Note.—Discussion open until January 1, 1961. To extend the closing date one month, a written request must be filed with the Executive Secretary, ASCE. This paper is part of the copyrighted Journal of the Engineering Mechanics Division, Proceedings of the American Society of Civil Engineers, Vol. 86, No. EM 4, August, 1960.

[1] Asst. Prof. of Applied Mech., Faculty of Engrg., Alexandria Univ., Alexandria, Egypt, U. A. R.

In the present treatment, a discharge formula is obtained for the seepage loss from a system of parallel, identical, and equally spaced canals, in which the water level is slightly higher than the piezometric head in the sand and gravel layers beneath. This last condition is in contrast with Wedernikow's problem[2] of deep-lying watertable in the lower sand and gravel aquifer. The same problem, limited to a single canal, has been attempted by the writer.[3] A simple seepage discharge formula is obtained for the present problem, from which the single canal problem derives as a special case when the spacing of the canals is assumed to tend to infinity.

GOVERNING EQUATIONS AND BOUNDARY CONDITIONS

As may be found in texts on flow through porous media,[3] the governing differential equation of the flow is that of Laplace:

$$\nabla^2 \phi = \frac{\partial^2 \phi}{\partial x^2} + \frac{\partial^2 \phi}{\partial y^2} = 0 \quad \ldots\ldots\ldots\ldots\ldots\ldots \quad (1)$$

to be satisfied everywhere in the field of motion, ϕ being the velocity-potential given by

$$\phi = \bar{k}\left(\frac{p}{\rho g} - y\right) + C \quad \ldots\ldots\ldots\ldots\ldots\ldots \quad (2)$$

in which $\bar{k}$ is the permeability of the porous medium, p is the pressure at any point, ρ is the fluid density and g is the acceleration due to gravity.

According to these assumptions, the boundary conditions are:

1. The line of separation between the semi-pervious clay strip and the lower freely permeable layer of sand and gravel is an equipotential line.
2. The canal profiles are also equipotential lines.
3. The vertical lines of symmetry are streamlines, because there can be no flow across them. These lines may, in fact, be replaced by solid boundaries.
4. The pressure vanishes on the free water surface, which is also a streamline.
5. The rise of water by capillarity from the free water surface is neglected.

METHOD OF SOLUTION

Because the piezometric head in the underlying sand is assumed very near the canal water level, the free water surface in the clay layer will, under steady conditions, also be very near the canal water-level. Consequently, the free water surface may be approximated by substituting a horizontal line coinciding with the canal water level. This extra simplification of the problem will cause a slight exaggeration of the seepage discharge obtained by this solution. It may be noted, however, that the deviations of the true free surface from the substituted horizontal line are greatest at points A.B.C..... (Fig. 1) which are

---

2 "Flow of Homogeneous Fluids through Porous Media," by M. Muskat, J. W. Edwards, 1946.

3 "Seepage Losses from Irrigation Canals," by H. Y. Hammad, Proceedings Paper 1991, ASCE, April, 1959.

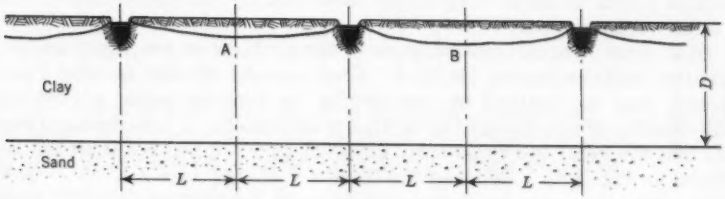

FIG. 1.—GEOLOGICAL SECTION

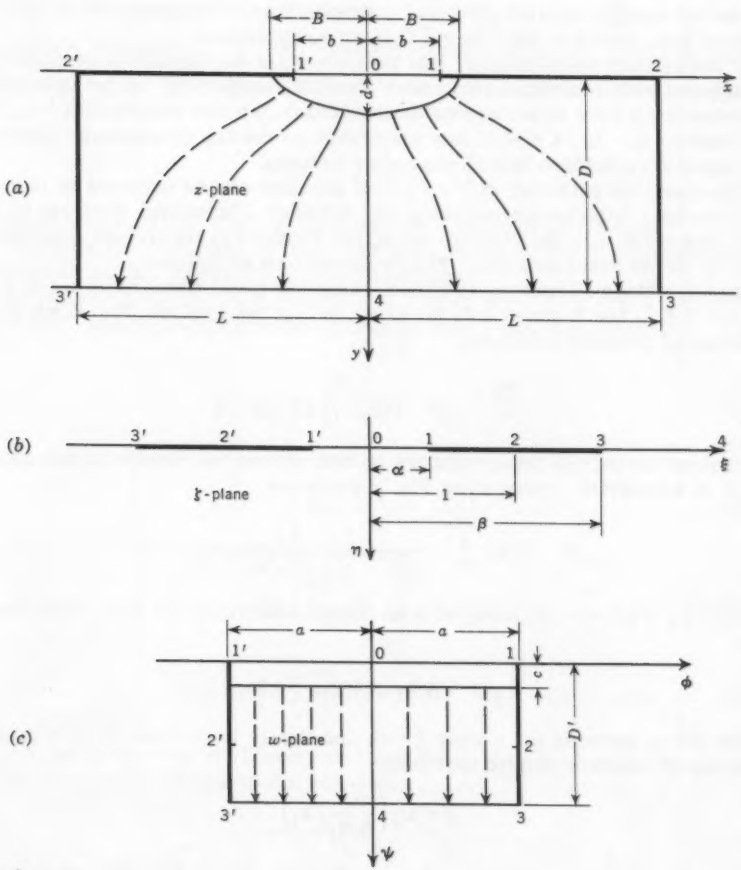

FIG. 2.—STEPS IN CONFORMAL MAPPING

stagnation points in the flow field and, consequently, the approximation will result in no serious error.

A first order approximate solution of the problem of seepage from a series of parallel shallow canals (depth d < semi-breadth B) and spacing 2 L center to center, may be obtained by considering the seepage under gravity from an infinite number of apertures of breadth 2 b and spacing 2 L in the solid boundary y = 0, into the semi-pervious strip bounded by y = 0 and y = D in the Z-plane as shown in Fig. 2(a). Because the lines $x = \pm L, \pm 3\ L, \pm 5\ L, \ldots$ are lines of symmetry, they may be considered as solid boundaries that will divide the field of flow into a series of identical panels. It will then be sufficient to consider the flow in one of these panels, Fig. 2(a).

The line segment (y = 0, $-b < x < +b$) is an equipotential, whereas (y = o, $b < x < L$) and (y = o, $-L < x < -b$ are streamlines. The lines $x = \pm L$ are also streamlines, whereas the line y = D is an equipotential.

It has already been assumed that the free water surface in the seepage layer is high and very near the canal water level. Consequently, as the original assumption for a first order approximate solution, the line segments (y = o, $b < x < L$) and (y = o, $-L < x < -b$) have been taken as the top streamlines instead of the actual free surface that is very near to them.

The complex-potential $w (= \phi + i\,\psi)$ of the flow may be obtained by two steps of conformal transformation using the Schwarz-Christoffel theorem in each step. The term ϕ is the velocity-potential, ψ refers to the stream-function, and $i = \sqrt{-1}$ in the usual notation. The two steps are as follows:

Step 1.—Mapping conformally the rectangular panel bounded by y = o, y = D, and $x = \pm L$ in the Z-plane onto the lower half of the ζ-plane, Fig. 2, we obtain, in terms of complex functions,

$$\frac{dZ}{d\zeta} = \frac{A}{(\zeta^2 - 1)^{1/2}\,(\zeta^2 - \beta^2)^{1/2}} \quad \ldots\ldots\ldots\ldots \quad (3)$$

The points having the same numbers in both planes correspond to one another and A is a constant. Integrating Fig. 3 produces

$$Z = A\,k_1 \int_0^{\zeta} \frac{d\zeta}{\sqrt{(1 - \zeta^2)\,(1 - k_1^2\,\zeta^2)}} + B \quad \ldots\ldots\ldots \quad (4)$$

in which $k_1 = 1/\beta$ and the integral is an elliptic integral of the first kind. Therefore

$$Z = A\,k_1\,F\,(\zeta, k_1) + B \quad \ldots\ldots\ldots\ldots\ldots\ldots \quad (5)$$

But B = o, because z = o when ζ = o, and finally is derived the ζ-Z relation in terms of Jacobi's elliptic functions

$$\zeta = sn\left(\frac{Z}{A\,k_1}, k_1\right) \quad \ldots\ldots\ldots\ldots\ldots\ldots \quad (6)$$

To evaluate the constant A we have at Z = i D, $\zeta = \infty$, Fig. (2), and substitution in Eq. 6 gives $\frac{D}{A\,k_1} = K_1'$, in which K_1 is the complete elliptic integral of the first kind corresponding to the complementary modulus $K_1' = \sqrt{1 - K_1^2}$.

The result of the first step of conformal mapping is then,

$$\zeta = \mathrm{sn}\left(\frac{K_1' Z}{D}, k_1\right) \quad \ldots\ldots\ldots\ldots\ldots\ldots \quad (7)$$

Step 2.—Following the same steps in mapping, conformally, the rectangle bounded by $\phi = \pm a$, $\psi = o$ and $\psi = D'$ in the w-plane onto the lower half of the ζ-plane (Fig. 2) is derived in terms of Jacobi's elliptic functions,

$$\zeta = \alpha\ \mathrm{sn}\left(\frac{\beta}{C} w, k_2\right) \quad \ldots\ldots\ldots\ldots\ldots\ldots \quad (8)$$

in which $k_2 = \alpha/\beta$, and C is an arbitrary constant. To evaluate C there is $\zeta = \infty$ when $w = i\ D$ and substitution in Eq. 8 yields $\frac{\beta D'}{C} = K_2'$, in which K_2' is the complete elliptic integral of the first kind corresponding to the complementary modulus $K_2' = \sqrt{1 - K_2^2}$. The result of the second step of conformal mapping is

$$\zeta = \alpha\ \mathrm{sn}\left(\frac{K_2' w}{D'}, k_2\right) \quad \ldots\ldots\ldots\ldots\ldots\ldots \quad (9)$$

The two relations, Figs. 7 and 9, give the w - Z relation of the flow.

To evaluate the constants α, β, a, and D' in terms of the dimensions of the flow panel D, L, and b (Fig. 2), proceed as follows.

At point 1 (Fig. 2) $Z = b$, $\zeta = \alpha$, $w = a$, and at point 3, $Z = L + i\ D$, $\zeta = \beta$, $w = a + i\ D'$. Substituting these two points in Eqs. 7 and 9 produces

$$\alpha = \mathrm{sn}\left(\frac{K_1' b}{D}, k_1\right) \quad \ldots\ldots\ldots\ldots\ldots\ldots \quad (10a)$$

$$\alpha = \alpha\ \mathrm{sn}\left(\frac{K_2' a}{D'}, k_2\right) \quad \ldots\ldots\ldots\ldots\ldots\ldots \quad (10b)$$

$$\beta = \mathrm{sn}\left(\frac{K_1'}{D}(L + i\ D), k_1\right) \quad \ldots\ldots\ldots\ldots\ldots\ldots \quad (10c)$$

$$\beta = \alpha\ \mathrm{sn}\left[\frac{K_2}{D'}\left(a + i\ D'\right), k_2\right] \quad \ldots\ldots\ldots\ldots\ldots\ldots \quad (10d)$$

Using the properties of elliptic functions Eq. 3, the set of equations 10 may be reduced to the following useful equations:

$$\alpha = \mathrm{sn}\left(K_i \frac{b}{L}, k_1\right) \quad \ldots\ldots\ldots\ldots\ldots\ldots \quad (11a)$$

$$a/D' = K_2/K_2' \quad \ldots\ldots\ldots\ldots\ldots\ldots \quad (11b)$$

$$D/L = K_1'/K_1 \quad \ldots\ldots\ldots\ldots\ldots\ldots \quad (11c)$$

in which $k_1 = 1/\beta$ and $k_2 = \alpha/\beta$ as previously stated.

Because in practice, the clay thickness, D, is small as compared with the canal spacing of 2 L, it follows from Eq. 11(c) that K_1' is small compared with K_1. Consequently, K_1', the modulus of K_2', is small. The complete elliptic functions K_1 and K_1' as expanded in convergent series of K_1' are[4]

$$K_1 = \log_e \frac{4}{k_1'} + \frac{1}{2} k_1' \left(\log_e \frac{4}{k_1'} - 1 \right) \quad \ldots\ldots\ldots (12a)$$

$$K_1' = \frac{\pi}{2} \left(1 + \frac{1}{4} k_1'^2 + \ldots\ldots \right) \quad \ldots\ldots\ldots\ldots (12b)$$

As a first order approximation in K_1' we may put

$$K_1'/K_1 = \frac{\pi}{2} \log_e \frac{4}{k_1'} = \frac{D}{L} \quad \ldots\ldots\ldots\ldots\ldots\ldots (13)$$

From Eq. 13

$$k_1' \simeq 4\, e^{-\frac{\pi L}{2D}}$$

and,

$$k_1 = \sqrt{1 - k_1'^2} \simeq 1 - 8\, e^{-\frac{\pi L}{D}} \quad \ldots\ldots\ldots\ldots (14)$$

The resulting values of k_1 and k_1' may be compared with their more exact values in the mathematical tables of the complete elliptic functions. Computations show that this approximation is quite sufficient for all practical values of D/L.

To introduce the dimensions of canal section represented by the breadth 2 B and maximum depth d we have (Fig. 2) at Z = B, that w = a + i c, and at Z = i d that, w = i c.

Introducing these values into Eqs. 7 and 9,

$$sn\left(\frac{K_1'\ B}{D},\ k_1 \right) = \alpha\ sn\left(\frac{K_2'}{D'}\ (a + i\ c),\ k_2 \right) \quad \ldots\ldots (15a)$$

$$sn\left(\frac{K_1'\ i\ d}{D},\ k_1 \right) = \alpha\ sn\left(\frac{K_2'\ i\ c}{D},\ k_2 \right) \quad \ldots\ldots\ldots (15b)$$

For small values of $\frac{D}{L}$ and $\frac{c}{D}$, Eq. 15 is further reduced, by applying the properties of elliptic functions Eq. 3 to the following simple relations:

$$\alpha \simeq \tanh \left(\frac{\pi}{2} \frac{B}{D} \right) \quad \ldots\ldots\ldots\ldots\ldots (16a)$$

---

4 "Function of a Complex Variable," by Th. M. Macrobert, Macmillan and Co., London, 1925.

$$\frac{c}{D'} \simeq \frac{1}{\alpha K_2'} \tan\left(\frac{\pi}{2}\frac{d}{D}\right) = \frac{\tan\left(\frac{\pi}{2}\frac{d}{D}\right)}{K_2' \tanh\left(\frac{\pi}{2}\frac{B}{D}\right)} \quad \ldots\ldots (16b)$$

in which

$$k_2 = \alpha\, k_1 \simeq \left(1 - 8\, e^{\frac{-\pi L}{D}}\right) \tanh\left(\frac{\pi}{2}\frac{B}{D}\right) \quad \ldots\ldots (17a)$$

and its complementary

$$K_2' = \sqrt{1 = K_2^2} \quad \ldots\ldots (17b)$$

SEEPAGE DISCHARGE FORMULA

Having evaluated the unknowns α, β, $\frac{a}{D}$, $\frac{c}{D}$ in terms of the known values of the flow panel B, d, D and L (Eqs. 11, 14 and 16) one may proceed to obtain a general formula for the seepage loss per unit length of each canal.

From an argument given by Terzaghi,[5] the seepage flux out of each unit length of canal, normal to the plane of motion, (Fig. 2) is, accordingly, given by

$$Q = \bar{k}\, h \frac{2a}{D' - c} \quad \ldots\ldots (18)$$

in which h is the head loss between the canal boundary and the line y = D, or the difference between the canal water level and the piezometric head in the freely permeable sandy layer, and k is the permeability of the clay cap.

Substituting the values for $\frac{a}{D}$ and $\frac{c}{D}$ obtained from Eqs. 11 and 16 into Eq. 18 yields

$$Q = \bar{k}\, h \cdot \frac{2 K_2}{K_2' - \frac{\tan(\pi\, d/2\, D)}{\tanh(\pi\, B/2\, D)}} \quad \ldots\ldots (19)$$

in which K_2 and K_2' are the complete elliptic integrals of the first kind whose moduli are k_2 and k_2' respectively given by Eqs. 17.

It may be worthwhile mentioning that in the case of a drain in which the water level is lower by an amount h than the piezometric head in the sand and gravel aquifer, the seepage flux will be reversed and the drain will be gaining rather than losing the rate given by Eq. 19.

---

5 "Theoretical Soil Mechanics," by K. Terzaghi, John Wiley and Sons, New York, 1946, pp. 246, 247.

SPECIAL CASE

The special case of a single canal attempted by the writer in a separate paper, may be derived from the present result by making the canal spacing 2 L tend to infinity. In that case the moduli of the complete elliptic functions given by Eq. 17 will reduce to

$$k_2 = \tanh\left(\frac{\pi B}{2 D}\right) \quad \ldots\ldots\ldots\ldots\ldots\ldots \quad (20a)$$

$$k_2' = \sqrt{1 - k_2^2} \quad \ldots\ldots\ldots\ldots\ldots\ldots \quad (20b)$$

the discharge formula given by Eq. 19 remains the same in form but the moduli of its complete elliptic functions must be taken from Eq. 20 instead of Eq. 17.

NUMERICAL EXAMPLE

For a parallel canal system of spacing 2 L = 1000 ft, depth of each canal d = 3 ft and breadth a B = 10 ft running in a clay layer of thickness D = 100 ft, and permeability k = 1 ft per day at a level h = 3 ft higher than the piezometric head in the sand and gravel aquifer, the following relation would be true:

$$\frac{\tan\left(\pi \frac{d}{2} D\right)}{\tanh\left(\pi \frac{B}{2} D\right)} = \frac{0.04716}{0.07830} = 0.60230$$

From Fig. 17,

$$k_2 = \left(1 - 8e^{-5\pi}\right) \tanh\left(\frac{\pi 5}{2\ 100}\right) = 0.99999 \times 0.07830 = 0.07829$$

Thus, $K_2^2 = 0.00613$ and the square of its complementary modulus $K_2'^2 = 0.99387$.

From tables of elliptic functions the corresponding complete elliptic integrals of the first kind are $K_2 = 1.5733$ and $K_2' = 3.9385$.

The seepage loss per unit length of each canal may then be computed from Eq. 19 as

$$Q = 1 \times 3 \times \frac{2 \times 1.5733}{3.9385 - 0.6023} = 2.8296 \text{ cu ft per day per ft length of canal}$$

$$= 0.0147 \text{ gpm per ft length of canal.}$$

Journal of the
ENGINEERING MECHANICS DIVISION
Proceedings of the American Society of Civil Engineers

VIBRATIONS OF STRUCTURAL SYSTEMS BY COMPONENT MODE SYNTHESIS

By Walter C. Hurty[1]

SYNOPSIS

Natural modes and frequencies of structural systems are determined by an energy method using mode functions applicable to the complete system, or to a subsystem thereof, that are synthesized from admissible mode functions selected for the component members of the system. The synthesis is accomplished by using equations of constraint that follow from conditions of force equilibrium and deflection compatibility at the junctions.

INTRODUCTION

The analysis of vibration and general dynamical behavior of complex structures has increasingly occupied the attention of analysts during recent years. Methods of analysis applicable to simple structural elements have been known and used for well over a century and these methods have been applied to idealized models of complex structures. Examples are found in analyses of multistory building structures and high aspect-ratio airplane wings in which these structures are dealt with ideally as beams. Such analyses may be quite accurate and useful so long as the bases for the idealizations are valid.

In more recent years methods have been devised by which the behavior of a structure may be predicted in terms of the properties of its elements. These methods of analysis involve, explicitly, every element in the structure, hence they enable one to determine the effects of changes in these elements on the behavior of the entire structure. The method of analysis presented in this

Note.—Discussion open until January 1, 1961. To extend the closing date one month, a written request must be filed with the Executive Secretary, ASCE. This paper is part of the copyrighted Journal of the Engineering Mechanics Division, Proceedings of the American Society of Civil Engineers, Vol. 86, No. EM 4, August, 1960.

[1] Professor of Engineering, University of California at Los Angeles.

paper is in this category and the words "Structural Systems" in the title are used to imply a systems analysis in this sense.

In order to clarify the position of this study relative to other structural systems studies, it is pertinent to refer to some of those that have appeared in the recent literature. A method of analysis of considerable accuracy and versatility has grown out of the well-known methods of Holzer,[2] Myklestad,[3] and Thomson.[4] It has been generalized by Pestel and Associates[5,6] and is described as a method of transfer matrices. As applied to the determination of natural modes and frequencies, it is characterized by the setting up of a frequency determinant that follows as a consequence of satisfying boundary conditions. The computations, which are conveniently carried out in matrix operations, require the insertion of trial values of the frequency into the transfer matrices. Since many such trial values may be necessary in order to identify the frequency spectrum, a great amount of computation is generally involved and it is conceded that high-speed electronic digital computing facilities are required in order that the method be practicable. The versatility of the method lies in the fact that response to static loads as well as steady-state forced vibrations may be handled readily.

Another powerful method of analysis has been applied to frames by Bishop.[7,8,9] Described as a method of receptances, it deals with the forced vibrations of systems in terms of the receptances of its component parts. The convenience of this method lies in the fact that these individual receptances can be catalogued for ready reference. For determining natural modes and frequencies of the structure, those frequencies are sought for which the overall receptance vanishes. This procedure also requires a trial-and-error solution.

Veletsos and Newmark[10,11] have devised a method described as an extension of Holzer's method for continuous beams. It is also applicable to frames without sidesway, that is, frames in which the junctions or corners do not translate. For natural frequency determination, this method seeks those frequencies for which an exciting couple applied to the beam vanishes. This, as in the methods already mentioned, requires repeated trial computations.

---

2 Die Berechung der Drehschwingungen, by H. Holzer, Springer-Verlag, Berlin, 1921.

3 Vibration Analysis, by N. O. Myklestad, McGraw-Hill Book Co., 1944.

4 "Matrix Solution for the Vibration of Nonuniform Beams," by W. T. Thomson, Journal of Applied Mechanics Trans. ASME, Vol. 17, No. 3, Sept. 1950, pp. 337-339.

5 "Ein allgemeines Verfahren zur Berechnung frier underzqungener Schwingungen von Stabwerken," by C. Eduard Pestel, Abhandlungen der Braunschweigischen Wissenchaftlichen Gesellschaft., Vol. VI, 1954, pp. 227-242.

6 "Katalog von Übertragungsmatrizen zur Berechnung Technische Schwingungsprobleme," by E. Pestel, G. Schumpich, and S. Spierig, V.D.I.-Berichte, Vol. 35, 1959, pp. 11-28.

7 "The Analysis and Synthesis of Vibrating Systems," by R. E. D. Bishop, Journal of the Royal Aeronautical Society, Vol. 58, Oct. 1954.

8 "The Analysis of Vibrating Systems which Embody Beams in Flexure," by R. E. D. Bishop, Proceedings of the Institution of Mechanical Engineers, Vol. 169, p. 1031, 1955.

9 "The Vibration of Frames," by R. E. D. Bishop, Proceedings of the Institution of Mechanical Engineers, Vol. 170. p. 955, 1956.

10 "Natural Frequencies of Continuous Flexural Members," by A. S. Veletsos and N. M. Newmark, Proceedings of American Society of Civil Engineers, Vol. 81, 1955, Paper No. 735.

11 Determination of the Natural Frequencies of Continuous Beams on Flexible Supports, by A. S. Veletosos and N. M. Newmark, (to be published).

In contrast with the above methods, the procedure described in this paper leads to the formulation of an eigenvalue problem in terms of generalized coordinates and generalized inertia and stiffness coefficients that are applicable to the complete structure. Once this problem is formulated, a direct solution is obtained by one of several possible techniques that are well-known. The generalized properties are obtained through the application of energy methods using sets of admissible mode functions for the various elements of the system. Best approximations to the true mode shapes are obtained by superposition of a finite number of these functions. This method, as applied to simple structures or to idealized models of complex structures, has been used widely and is often called the Rayleigh-Ritz[12] method. As applied to structural systems, it has often been regarded as inaccurate because of the difficulty in defining suitable mode shapes.[9] However, in the present analysis, mode shapes applicable to the entire system are not defined at the outset. Instead, they are synthesized from mode shapes that are selected for the separate elements of the system. Their synthesis is accomplished by a technique that results from the application of equations of deflection compatibility and force equilibrium at the junctions of these elements. The delineation of this technique is considered to be the principal contribution of this paper. In addition, the technique is extended to enable one to synthesize modes and generalized properties for subsystems that may then be put together to form the complete system. The computations required for each of the subsystems may proceed independently. Points of similarity exist between this analysis and that of Saibel and D'Appolonia[13] in their treatment of continuous beams. In that analysis mode functions are synthesized from the eigen functions of a simple beam obtained by removing the intermediate supports.

Notation.—The letter symbols adopted for use in this paper are defined where they first appear, in the illustrations or in the text, and are arranged alphabetically, for convenience of reference, in the Appendix.

ENERGY ANALYSIS OF THE SYSTEM

For this analysis we shall consider a system of structural members such as beams and rods connected at their ends. These connections may be pins or rigid joints or combinations of these, and the various members may be subjected to bending, torsion, axial loading or combinations of these loadings. We shall restrict the analysis to motions of small amplitude so that free vibrations of the separate elements in longitudinal, transverse and twisting motion are uncoupled. In principle, the geometry of the structure is immaterial and the individual members need not be uniform. The complete structure will be subject to boundary conditions that may be defined at one or more of the junctions.

The first task in the analysis is to select mode functions for each member and to superpose these functions to define longitudinal, transverse and torsional vibrations throughout the system. We write any one of these modes of

---

12 Aeroelasticity, by R. L. Bisplinghoff, Holt Ashley, and R. L. Halfman, Addison-Wesley Publishing Co., Inc., 1955.

13 "Forced Vibrations of Continuous Beams," by Edward Saibel and Elio D'Appolonia, Proceedings of the ASCE, Vol. 77, No. 100, Nov. 1951.

vibration in terms of the selected functions and a set of coordinates as follows:

$$u, w, \theta = \sum_{j=1}^{m} \phi_j(x)\, p_j \quad \ldots\ldots\ldots\ldots\ldots\ldots (1)$$

in which u is the longitudinal displacement, w refers to transverse displacement, θ denotes torsional displacement, $\phi_j(x)$ is the j^{th} mode function, x indicates the independent variable measured along length of member, and p_j is the j^{th} coordinate. Although not explicitly noted, u, w, θ are functions of time as well as of x and the p's are functions of time. As indicated m functions and coordinates are chosen for the structure and these are distributed among the various members. Some of the functions represent longitudinal motion and others transverse and torsional motion.

Although a wide choice exists in the selection of functions several conditions must exist. For example, they must satisfy the boundary conditions on the structure as a whole, that is, if a given element of the structure is subject to such boundary conditions then the functions chosen for that element must satisfy them. Conditions of constraint at the junctions of two or more members are not considered as boundary conditions but will be termed junction conditions. In general, functions must be chosen which admit of displacements at the junctions and also admit the existence of forces at the junctions. For example, if a member enters a junction at x = 1 and if that member may have a transverse displacement at that point, then functions must be chosen for which $w(l) \neq 0$. If a transverse shear force may also exist at that point, then functions must be included for which $w'''(l) \neq 0$, where the prime notation is used to denote differentiation with respect to x. Functions which satisfy the necessary conditions are termed admissible functions in this study.

Limited experience in problem solutions gained thus far indicates that simple functions may be chosen. In the examples included in this paper integral powers of (x/l) are used with good results. Thus, displacements are represented by the series

$$u, w = 1(x)\, p_o + \left(\frac{x}{l}\right) p_1 + \left(\frac{x}{l}\right)^2 p_2 + \ldots + \left(\frac{x}{l}\right)^m p_m \quad \ldots\ldots\ldots (2)$$

In the case of transverse displacement, the functions 1(x) and $\left(\frac{x}{l}\right)$ represent rigid-body modes in translation and rotation, respectively, and the remaining functions represent deformation modes. In longitudinal displacement the function 1(x) represents rigid-body translation. The use of such rigid-body modes permits the inclusion of joint translation in the vibration modes of the complete structure. For example, sidesway in building frames may be handled by this technique.

Consideration of the junction conditions leads to equations of deflection compatibility and force equilibrium which serve as equations of constraint among the m coordinates $p_1, p_2, \ldots, p_m$. Therefore, these are not generalized coordinates in the Lagrangian sense. Application of Hamilton's principle to this problem leads to the equation[14]

$$\int_{t_1}^{t_2} \sum_{i=1}^{m} \left\{ \frac{d}{dt} \frac{\partial T}{\partial \dot{p}_i} - \frac{\partial T}{\partial p_i} + \frac{\partial U}{\partial p_i} \right\} \delta p_i \, dt = 0 \quad \ldots\ldots\ldots (3)$$

14 Methods of Applied Mathematics, F. B. Hildebrand, Prentice-Hall, Inc., 1952.

in which T is the kinetic energy of the system, U refers to the strain energy of the system, δp_i indicates the variation in the coordinates p_i, and t is the time. The dot notation is used to denote differentiation with respect to time. Since the p's are not independent, the variations δp_i cannot be arbitrary, hence, the expressions in the braces in Eq. 3 do not vanish separately. The equations of constraint permit us to express the coordinates p in terms of a set of independent generalized coordinates $q_1, q_2, \ldots, q_n$, thus,

$$p_i = \sum_{k=1}^{n} C_{ik}\, q_k \quad \ldots\ldots\ldots\ldots\ldots\ldots\ldots (4)$$

in which the C_{ik} are coefficients in the linear transformation. Note that if r equations of constraint exist, then

$$n = m - r \quad \ldots\ldots\ldots\ldots\ldots\ldots\ldots (5)$$

From Eq. 4 it is apparent that the variation δp_i is given by

$$\delta p_i = \sum_{k=1}^{n} C_{ik}\, \delta q_k \quad \ldots\ldots\ldots\ldots\ldots\ldots\ldots (6)$$

Substituting this into Eq. 3 and taking account of the independence of the variations δp we obtain

$$\sum_{i=1}^{m} C_{ik} \left\{ \frac{d}{dt} \frac{dT}{\partial \dot{p}_i} - \frac{\partial T}{\partial p_i} + \frac{\partial U}{\partial p_i} \right\} = 0 \quad \ldots\ldots\ldots\ldots (7)$$

Since $k = 1, 2, 3 \ldots, n$ it is clear that n of these equations may be written. For small amplitude vibrations of conservative system, the terms in Eq. 7 are given by the following equations.

$$\left.\begin{aligned} \frac{d}{dt} \frac{\partial T}{\partial \dot{p}_i} &= \sum_{j=1}^{m} m_{ij}\, \ddot{p}_j \\ \frac{\partial T}{\partial p_i} &= 0 \\ \frac{\partial U}{\partial p_i} &= \sum_{j=1}^{m} k_{ij}\, p_j \end{aligned}\right\} \quad \ldots\ldots\ldots\ldots\ldots\ldots (8)$$

In these equations the m_{ij} are inertia coefficients and the k_{ij} are stiffness coefficients associated with the coordinates p. For translation, either in the longitudinal or transverse direction

$$m_{ij} = \int_0^l m\, \phi_i\, \phi_j\, dx \quad \ldots\ldots\ldots\ldots\ldots\ldots\ldots (9)$$

where m is the mass of the element per unit length at point x and the integration is taken over the length l of the member. For transverse bending

$$k_{ij} = \int_0^l E\, I\, \phi_i''\, \phi_j''\, dx \quad \ldots\ldots\ldots\ldots\ldots\ldots\ldots (10)$$

where E I is the modulus of rigidity in flexure. For longitudinal strain and torsional strain, the stiffnesses are given, respectively, by

$$k_{ij} = \int_0^1 E\,A\,\phi_i'\,\phi_j'\,dx \quad \ldots\ldots\ldots\ldots\ldots\ldots (11)$$

and

$$k_{ij} = \int_0^1 G\,J\,\phi_i'\,\phi_j'\,dx \quad \ldots\ldots\ldots\ldots\ldots\ldots (12)$$

The quantities E A and G J are moduli of rigidity in tension-compression and in torsion, respectively.

We may substitute Eq. 8 into Eq. 7 and write the set of n equations in matrix form.

$$[C]^T [m] \{\ddot{p}\} + [C]^T [k] \{p\} = \{0\} \quad \ldots\ldots\ldots\ldots (13)$$

Here, $[C]^T$ is the transpose of the transformation matrix [C]. We now substitute Eq. 4 which, in matrix form is

$$\{p\} = [C] \{q\} \quad \ldots\ldots\ldots\ldots\ldots\ldots (14)$$

and note that for harmonic vibrations

$$\{\ddot{q}\} = -\omega^2 \{q\} \quad \ldots\ldots\ldots\ldots\ldots\ldots (15)$$

where ω is the angular frequency of the vibration. We then obtain the equation

$$\omega^2 [C]^T [m] [C] \{q\} = [C]^T [k] [C] \{q\} \quad \ldots\ldots\ldots\ldots (16)$$

This equation expresses the desired eigenvalue problem whose solution yields the natural modes $\{q^{(1)}\}, \{q^{(2)}\}, \ldots, \{q^{(n)}\}$ and the natural frequencies $\omega_1, \omega_2, \ldots; \omega_n$.

It should be noted that the matrices [m] and [k] are square symmetric matrices of order m × m having as elements the inertia and stiffness coefficients such as obtained from Eqs. 9 through 12. From Eq. 14 it is seen that the transformation or constraint matrix [C] is of order m × n.

In passing, it should be noted that the effects of rotatory inertia and transverse shear strain may be included in the analysis of introducing the appropriate terms in the computation of the m_{ij} and the k_{ij}.

EQUATIONS OF CONSTRAINT

In this section we shall be concerned with the equations of constraint among the coordinates p that lead to the transformation Eq. 14. These equations express the compatibility of displacements and force equilibrium at the junctions. The terms displacement and force are used in the general sense to include rotation as well as translation and moment as well as force.

To clarify the development of these equations let us consider a simple junction of two perpendicular members shown in Fig. 1(a) with forces and displacements only in the plane of the members.

Fig. 1(b) shows a section at the junction with positive axial forces, N, positive shears, V, and positive bending moments, M. In Fig. 1(c) positive displacements u, w, and ψ are shown relative to the positive direction of x for

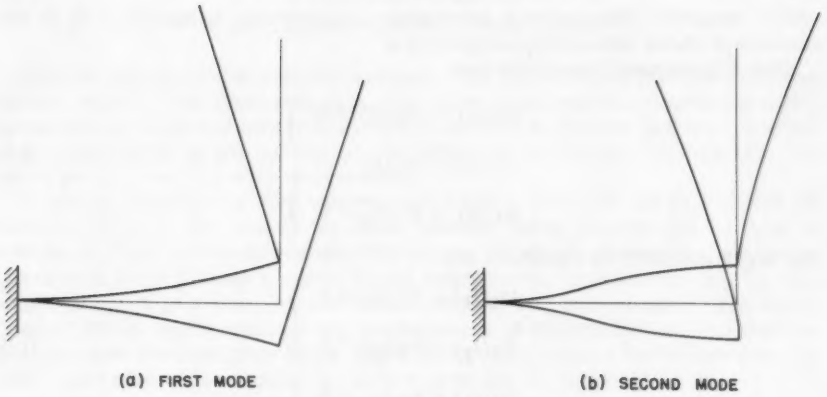

FIG. 1.—A SIMPLE JUNCTION

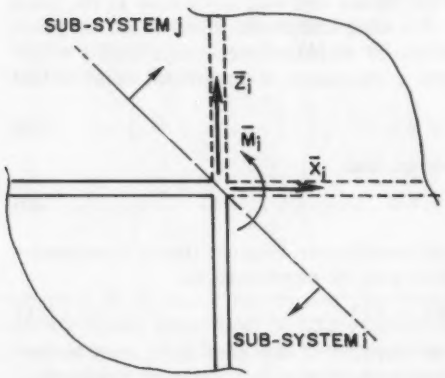

FIG. 2.—TWO SUB-SYSTEMS i & j

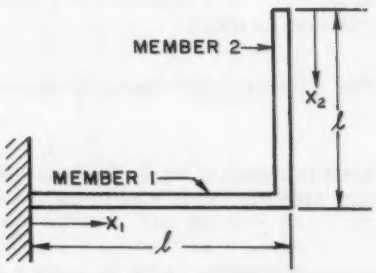

FIG. 3.—BENT CANTILEVER BEAM

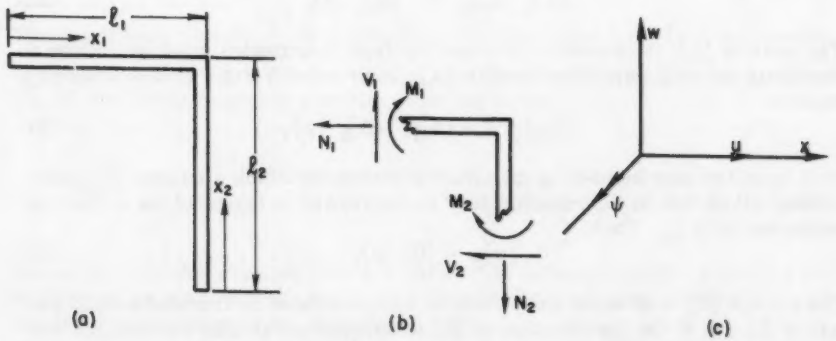

FIG. 4.—FIRST TWO NATURAL MODES OF BENT CANTILEVER BEAM

either member. The angle ψ represents rotation due to bending and, in the absence of shear deflection, is equal to w'.

The displacement equations are

$$\left.\begin{aligned} u_1(l_1) + w_2(l_2) &= 0 \\ w_1(l_1) - u_2(l_2) &= 0 \\ \psi_1(l_1) - \psi_2(l_2) &= 0 \end{aligned}\right\} \quad \ldots\ldots\ldots\ldots\ldots\ldots (17)$$

The force equilibrium equations are

$$\left.\begin{aligned} M_1(l_1) + M_2(l_2) &= 0 \\ V_1(l_1) - N_2(l_2) &= 0 \\ N_1(l_1) + V_2(l_2) &= 0 \end{aligned}\right\} \quad \ldots\ldots\ldots\ldots\ldots\ldots (18)$$

It is clear that comparable equations can be written for members intersecting at other angles. In a plane system with forces and displacements in its plane six equations exist for two members. For each additional member at the junction three additional independent equations of displacement compatibility exist. In general, for s members at a junction, r equations of constraint exist at that junction, in which

$$r = 3\,s \quad \ldots\ldots\ldots\ldots\ldots\ldots\ldots\ldots (19)$$

For a junction in 3-space, it can be shown that

$$r = 6\,s \quad \ldots\ldots\ldots\ldots\ldots\ldots\ldots\ldots (20)$$

Upon introducing Eq. 1, the equations of constraints become linear homogeneous, algebraic equations in the p's which may be expressed as

$$[A]\{p\} = \{0\} \quad \ldots\ldots\ldots\ldots\ldots\ldots\ldots (21)$$

where the matrix [A] is of order r × m. Now, n of the p's, $\{p\}_f$, may be selected as free coordinates in terms of which the remaining r may be expressed. These latter we shall call constrained coordinates, $\{p_r\}_c$. Then Eq. 21 is written as

$$[A]_1 \{p_r\}_c = -[A]_2 \{p\}_f \quad \ldots\ldots\ldots\ldots\ldots\ldots (22)$$

The matrix $[A]_1$ is of order r × r and the free coordinates must be chosen so that it is nonsingular. The matrix $[A]_2$ is of order r × n. Inversion of $[A]_1$ leads to

$$\{p_r\}_c = -[A]_1^{-1} [A]_2 \{p\}_f \quad \ldots\ldots\ldots\ldots\ldots\ldots (23)$$

This equation may be used to construct a matrix by which a column $\{p\}_c$ containing all of the m coordinates may be expressed in terms of the n free coordinates in $\{p\}_f$. Thus,

$$\{p\}_c = [C]\{p\}_f \quad \ldots\ldots\ldots\ldots\ldots\ldots\ldots (24)$$

The matrix [C] is of order m × n and is the constraint or transformation matrix of Eq. 14. If the construction of [C] is carried out in this manner, the column $\{q\}$ in Eq. 14 is identified with column $\{p\}_f$. Matrix [C] is used in Eq. 16 to set up the eigenvalue problem for the complete structure.

PARTITIONING INTO SUB-SYSTEMS

Eqs. 19 and 20 show that for systems with more than a few junctions the number of equations of constraint may be very large and the computations required to multiply and invert large matrices tend to become tedious. Therefore, a variation in the foregoing procedure is offered for constructing [C] which permits dealing with subsystems.

Consider portions of two subsystems i and j that connect at a corner as shown in Fig. 2. For clarity we shall consider these subsystems as lying in a common plane and shall consider only forces and displacements in that plane Interacting forces exist between these subsystems. The forces $\overline{M}_i$, $\overline{Z}_i$, $\overline{X}_i$, shown in Fig. 2 are those imposed on subsystem i by subsystem j. The equations of force equilibrium among the members of subsystem i at this junction are not now homogeneous since these force terms must be included on the right-hand side of the equations. In this case Eq. 21 takes the form

$$[A]\{p\} = \left\{\begin{array}{c} 0 \\ \hline \overline{F} \end{array}\right\} \quad \ldots\ldots\ldots\ldots\ldots\ldots (25)$$

in which the partitioned column on the right consists of (r - 3) zeroes and three force terms (M_i, Z_i, X_i) in the plane case. The subcolumn $\{\overline{F}\}$ may take either of two forms

$$\left(\begin{array}{cc} \frac{l^2}{EI} & \overline{M}_i \\ \frac{l}{EA} & \overline{Z}_i \\ \frac{l}{EA} & \overline{X}_i \end{array}\right) \quad \text{or} \quad \left(\begin{array}{cc} \frac{l^2}{EI} & \overline{M}_i \\ \frac{l^3}{EI} & \overline{Z}_i \\ \frac{l^3}{EI} & \overline{X}_i \end{array}\right)$$

where l, E, A, and I may be any characteristic values. The purpose in introducing these quantities in this manner is to give the elements of $\{\overline{F}\}$ the dimensions of length so that the elements of matrix [A] may be dimensionless.

Eq. 25 is handled in the same manner as Eq. 21 to yield

$$[A]_1 \{p_r\}_c = -[A]_2 \{p\}_f + \left[\frac{0}{I}\right]\{\overline{F}\} \quad \ldots\ldots\ldots\ldots (26)$$

The partitioned matrix $\left[\frac{0}{I}\right]$ is of order $r \times 3$. The upper part is a null matrix of order $(r - 3) \times 3$ and the lower part, the identity matrix. The right side of Eq. 26 may be arranged to give the following form:

$$[A]_1 \{p_r\}_c = \left[\begin{array}{c|c} -A_2 & \begin{array}{c} 0 \\ (r-3)\times 3 \end{array} \\ r \times n_i & \hline \begin{array}{c} I \\ 3 \times 3 \end{array} \end{array}\right] \left\{\begin{array}{c} p_f \\ \hline \overline{F} \end{array}\right\} \quad \ldots\ldots\ldots\ldots (27)$$

The orders of the submatrices are given. As before, matrix A_1 may be inverted and we may express the r constrained p's in terms of the n_i free p's and the forces acting on the subsystem.

$$\{p_r\}_c = [A]_1^{-1} \left[-A_2 \,\vdots\, \frac{0}{I}\right] \left\{\begin{array}{c} p_f \\ \hline \overline{F} \end{array}\right\} \quad \ldots\ldots\ldots\ldots (28)$$

It is now possible to construct the transformation matrix $[C]_i$ using the following arbitrary, but convenient, procedure. First set the top element of $\left\{\begin{matrix} p_f \\ \hline F \end{matrix}\right\}$ equal to unity and all other elements to zero. Using Eq. 28 compute the corresponding elements $\{p_r\}_C$. Thus, we obtain a column $\{p^{(1)}\}_C$ containing all of the constrained p's and the arbitrarily chosen free p's. Next, set the second element in $\left\{\begin{matrix} p_f \\ \hline F \end{matrix}\right\}$ to unity and all others to zero. Thus, a second column $\{p^{(2)}\}_C$ is obtained. When we carry this to completion it is clear that we may obtain $n_i + 3$ such columns. Matrix $[C]_i$ for subsystem i is then constructed from these columns as follows:

$$[C]_i = \left[\{p^{(1)}\}_C \quad \{p^{(2)}\}_C \quad \cdots\cdots \quad \{p^{(n_i+3)}\}_C \right]_i \quad \cdots\cdots\cdots (29)$$

Clearly, $[C]_i$ is of order $m \times (n_i + 3)$ in this case. As stated previously, this procedure is arbitrary since any set of combinations of the elements in $\left\{\begin{matrix} p_f \\ \hline F \end{matrix}\right\}$ may be used to construct the columns of $[C]_i$. However, it must be noted that since any such selection of elements must be linear combinations of those chosen in the suggested procedure, no more than $n_i + 3$ independent columns may be had in any event.

The procedure for constructing $[C]_i$ may be thought of alternately, as a procedure for synthesizing admissible functions for the connected subsystem. These functions are synthesized from the functions $\phi(x)$ chosen for the individual unconnected elements. If Eq. 4 is substituted into Eq. 1, we obtain displacements of the connected system in terms of the free coordinates, q. Thus

$$u, w, \theta = \sum_{j=1}^{m} \phi_j(x) \sum_k C_{jk} q_k = \sum_k \Phi_k q_k \cdots\cdots (30)$$

in which

$$\Phi_k = \sum_{j=1}^{m} C_{jk} \phi_j(x) \quad \cdots\cdots\cdots\cdots (31)$$

is one of the synthesized admissible functions. In the case of the subsystem, i, with three interacting forces at one junction $(n_i + 3)$ of these functions are obtained, three of which serve to admit of the existence of those forces. In the case of the complete system, only n admissible functions are obtained, and, thus, only n degrees of freedom exist for the complete system. Thus, it may seem that we gained three degrees of freedom in the subsystem. Such is not the case, however, since these apparent degrees of freedom are lost in combining subsystems into the complete system.

COMBINING SUBSYSTEMS

Rather than attempting to treat this problem as a complete generality, we shall only consider the problem of combining two subsystems at one junction such as illustrated in Fig. 2. The plane system is again considered. It is believed that this illustrated will serve to indicate procedures to be followed in more general cases.

Again, equations of constraint must be derived that express compatibility of displacement and force equilibrium at the junction of the two subsystems i and j. From the results of the last section, we may determine the forces and displacements in terms of the coordinates q, thus

$$\left\{\frac{\delta}{F}\right\}_i = [B]_i \{q\}_i \quad \ldots\ldots\ldots\ldots\ldots\ldots \quad (32a)$$

and

$$\left\{\frac{\delta}{F}\right\}_j = [B]_j \{q\}_j \quad \ldots\ldots\ldots\ldots\ldots\ldots \quad (32b)$$

in which $\left\{\frac{\delta}{F}\right\}_i$ is a column matrix with six elements in the order

$$\left(\bar{u}, \bar{w}, l\bar{\psi}, \frac{l^2 \bar{M}}{E I}, \frac{l \bar{Z}}{E A}, \frac{l \bar{X}}{E A}\right)$$

For the system shown, the two matrices [B] are of order $6 \times (n_i + 3)$ and $6 \times (n_j + 3)$, respectively. Equating the two deflection-force vectors at the junction ij we are led to a constraining relationship among the elements of the two coordinate vectors

$$[B]_i \{q\}_i = [B]_j \{q\}_j \quad \ldots\ldots\ldots\ldots\ldots\ldots \quad (33)$$

From this we construct a new constraint matrix $[C]_{ij}$ that relates the sets of q's pertaining to both subsystems to a minimum set of free q's. Since in the two sets, we have a total of $n_i + n_j + 6$ coordinates and since we have six equations of constraint it follows that the complete system composed of the two subsystems has $n_i + n_j$ free or generalized coordinates and, hence, that number of degrees of freedom. Generalized inertia and stiffness matrices for the complete system are found by operating on the corresponding matrices for the unconnected subsystems by the constraint matrix $[C]_{ij}$ as shown in Eq. 16.

EXAMPLE

Bent Cantilever Beam.—The first example is a cantilever beam of length 2 l bent through a right angle at its center as shown in Fig. 3. We wish to determine the first two natural modes and frequencies of vibration in the plane of the beam. This simple example is chosen to illustrate the method as applied to a complete system. Bishop worked[9] this problem by the exact method of receptances, hence we shall have a standard against which to check the present method. The boundary conditions are: on member (1); $u_1(0) = 0$, $w_1(0) = w_1'(0) = 0$; on member (2); $w_2''(0) = w_2'''(0) = 0$, $u_2'(0) = 0$.

In order to compare with Bishop's solution, we shall postulate infinite axial rigidity in both members. Therefore, two equations of force equilibrium at the corner are not included in the equations of constraint. The four required equations are

$$w_1(l) + u_2(l) = 0 \quad \ldots\ldots\ldots\ldots\ldots\ldots \quad (34a)$$

$$w_2(l) = 0 \quad \ldots\ldots\ldots\ldots\ldots\ldots \quad (34b)$$

$$w_1'(l) - w_2'(l) = 0 \quad \ldots\ldots\ldots\ldots\ldots\ldots \quad (34c)$$

$$E I\left[w_1''(l) + w_2''(l)\right] = 0 \quad \ldots\ldots\ldots\ldots\ldots\ldots \quad (34d)$$

The functions selected follow. For member (1) the transverse displacement functions are $\phi_1(x_1) = \left(\frac{x}{l}\right)^2$, and $\phi_2(x_1) = \left(\frac{x}{l}\right)^3$. For member (2) the transverse displacement functions are $\phi_3(x_2) = 1$, $\phi_4(x_2) = \left(\frac{x}{l}\right)$, and $\phi_5(x_2) = \left(\frac{x}{l}\right)^4$, and the longitudinal displacement function is $\phi_6(x_2) = 1$. It may be verified readily that these functions satisfy the boundary conditions and that they are admissible functions. The uncoupled inertia and stiffness matrices are obtained by using Eqs. 9 and 10

$$[m] = ml \begin{bmatrix} .20000 & .16667 & 0 & 0 & 0 & 0 \\ .16667 & .14286 & 0 & 0 & 0 & 0 \\ 0 & 0 & 1.00000 & .50000 & .20000 & 0 \\ 0 & 0 & .50000 & .33333 & .16667 & 0 \\ 0 & 0 & .20000 & .16667 & .11111 & 0 \\ 0 & 0 & 0 & 0 & & 1.00000 \end{bmatrix}$$

$$[k] = \frac{E\,I}{l^3} \begin{bmatrix} 4 & 6 & 0 & 0 & 0 & 0 \\ 6 & 12 & 0 & 0 & 0 & 0 \\ 0 & 0 & 0 & 0 & 0 & 0 \\ 0 & 0 & 0 & 0 & 0 & 0 \\ 0 & 0 & 0 & 0 & 28.8 & 0 \\ 0 & 0 & 0 & 0 & 0 & 0 \end{bmatrix}$$

The four equations of constraint are

$$\begin{bmatrix} 1 & 1 & 0 & 0 & 0 & 1 \\ 0 & 0 & 1 & 1 & 1 & 0 \\ 2 & 3 & 0 & -1 & -4 & 0 \\ 2 & 6 & 0 & 0 & 12 & 0 \end{bmatrix} \begin{Bmatrix} p_1 \\ p_2 \\ p_3 \\ p_4 \\ p_5 \\ p_6 \end{Bmatrix} = \begin{Bmatrix} 0 \\ 0 \\ 0 \\ 0 \end{Bmatrix}$$

We select p_1 and p_6 as the free coordinates and determine the matrix [C] to be as follows:

$$[C] = \begin{bmatrix} 1 & 0 \\ -1 & -1 \\ 2 & 4.50 \\ -2.33333 & -5.0 \\ 0.33333 & 0.5 \\ 0 & 1 \end{bmatrix}$$

Following the operations of Eq. 16 the eigenvalue problem becomes

$$\omega^2\, m\, l \begin{bmatrix} 1.17741 & 2.66137 \\ 2.66137 & 7.32062 \end{bmatrix} \begin{Bmatrix} p_1 \\ p_6 \end{Bmatrix} = \frac{E\,I}{l^3} \begin{bmatrix} 7.200 & 10.800 \\ 10.800 & 19.200 \end{bmatrix} \begin{Bmatrix} p_1 \\ p_6 \end{Bmatrix}$$

we obtain $\omega_1 = 1.172\sqrt{\frac{E\,I}{m\,l^4}}$, and $\omega_2 = 3.198\sqrt{\frac{E\,I}{m\,l^4}}$.

Whereas Bishop obtained $\omega_1 = 1.166\sqrt{\frac{E\,I}{m\,l^4}}$, and $\omega_2 = 3.168\sqrt{\frac{E\,I}{m\,l^4}}$. The frequencies in this problem are higher than Bishop's by 0.5% and 1.0% respectively. The two natural modes are shown in Fig. 4.

Two-Story Building Frame—Anti-Symmetrical Modes.—This example is added to illustrate the procedure for handling subsystems. The two-story building frame shown in Fig. 5(a) is divided into two parts. The first story (subsystem 1) is shown in Fig. 5(b) and the second story (subsystem 2) in Fig. 5(c). The structure has a vertical plane of symmetry so that only one-half of it is considered, and only the antisymmetrical modes are determined. For convenience in computation, all members are considered to be identical. The boundary conditions for the antisymmetrical modes are for system 1

$$\begin{aligned} &\text{Member (1):} && w\,(0) = 0 \\ &&& w''(0) = 0 \\ &&& u'\,(0) = 0 \\ &\text{Member (2):} && w\,(0) = 0 \\ &&& w'(0) = 0 \\ &&& u\,(0) = 0 \end{aligned}$$

for system 2

$$\begin{aligned} &\text{Member (1)} && w\,(0) = 0 \\ &&& w''(0) = 0 \\ &&& u'\,(0) = 0 \end{aligned}$$

The equations of displacement compatibility and force equilibrium at the corners of the two subsystems are as follows: for system 1;

$$u_1(1) = -w_2(1) = \bar{u}_1 \quad \ldots\ldots\ldots\ldots\ldots\ldots \quad (35a)$$

$$w_1(1) = u_2(1) = \bar{w}_1 \quad \ldots\ldots\ldots\ldots\ldots\ldots \quad (35b)$$

$$w_1'(1) = w_2'(1) = \bar{\psi}_1 \quad \ldots\ldots\ldots\ldots\ldots\ldots \quad (35c)$$

$$E\,I\,w_1''(1) + E\,I\,w_2''(1) = \bar{M} \quad \ldots\ldots\ldots\ldots\ldots\ldots \quad (35d)$$

$$-E\,I\,w_1'''(1) + E\,A\,u_2'(1) = \bar{Z} \quad \ldots\ldots\ldots\ldots\ldots\ldots \quad (35e)$$

$$E\,A\,u_1'(1) + E\,I\,w_2'''(1) = \bar{X} \quad \ldots\ldots\ldots\ldots\ldots\ldots \quad (35f)$$

for system 2;

$$u_1(1) = -w_2(1) \quad \ldots\ldots\ldots\ldots\ldots\ldots \quad (36a)$$

$$w_1(1) = u_2(1) \quad \ldots\ldots\ldots\ldots\ldots\ldots \quad (36b)$$

$$w_1'(1) = w_2'(1) \quad \ldots\ldots\ldots\ldots\ldots\ldots \quad (36c)$$

$$E\,I\,w_1''(1) + E\,I\,w_2''(1) = 0 \quad \ldots\ldots\ldots\ldots\ldots\ldots \quad (36d)$$

$$-E\,I\,w_1'''(1) + E\,A\,u_2'(1) = 0 \quad \ldots\ldots\ldots\ldots\ldots\ldots \quad (36e)$$

$$E\,A\,u_1'(1) + E\,I\,w_2'''(1) = 0 \quad \ldots\ldots\ldots\ldots\ldots\ldots \quad (36f)$$

Functions selected are listed for the two subsystems separately. Since they are dealt with independently no attempt is made to distinguish between the two

sets in numbering them. For system 1

$\phi_1(x) = 1$ Member 1 - longitudinal

$\phi_2(x) = \left(\frac{x}{l}\right)^2$ Member 1 - longitudinal

$\phi_3(x) = \left(\frac{x}{l}\right)$ Member 1 - transverse

$\phi_4(x) = \left(\frac{x}{l}\right)^3$ Member 1 - transverse

$\phi_5(x) = \left(\frac{x}{l}\right)$ Member 2 - longitudinal

$\phi_6(x) = \left(\frac{x}{l}\right)^2$ Member 2 - transverse

$\phi_7(x) = \left(\frac{x}{l}\right)^3$ Member 2 - transverse

For system 2

$\phi_1(x) = 1$ Member 1 - longitudinal

$\phi_2(x) = \left(\frac{x}{l}\right)^2$ Member 1 - longitudinal

$\phi_3(x) = \left(\frac{x}{l}\right)$ Member 1 - transverse

$\phi_4(x) = \left(\frac{x}{l}\right)^3$ Member 1 - transverse

$\phi_5(x) = \left(\frac{x}{l}\right)$ Member 2 - longitudinal

$\phi_6(x) = \left(\frac{x}{l}\right)^2$ Member 2 - transverse

$\phi_7(x) = \left(\frac{x}{l}\right)^3$ Member 2 - transverse

$\phi_8(x) = 1$ Member 2 - longitudinal

$\phi_9(x) = \left(\frac{x}{l}\right)$ Member 2 - transverse

$\phi_{10}(x) = 1$ Member 2 - transverse

Note that functions ϕ_1 through ϕ_7 are identical for the two systems but that ϕ_8, ϕ_9, and ϕ_{10} are added for system 2 to admit of rigid body motion of that system that cannot occur in the lower frame.

Inertia and stiffness matrices are computed for the uncoupled elements of the two subsystems, using Eqs. 9, 10, and 11. The ratio of axial to transverse stiffness is

$$\frac{\frac{E\,A}{l}}{\frac{E\,I}{l^3}} = \frac{l^2}{\rho^2} = 1600,$$

in which ρ is the section radius of gyration in bending. These matrices are similar to those in the first example. The constraint matrices $[C]_{1,2}$ for the two subsystems are found by the procedure leading to Eq. 29 and will be indicated subsequently in connection with the equations of constraint to show the ordering of the coordinates.

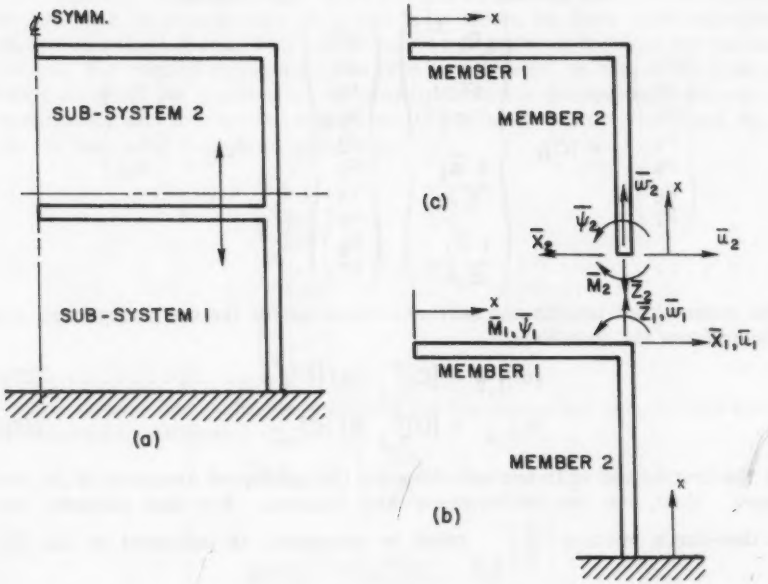

FIG. 5.—TWO-STORY BUILDING FRAME

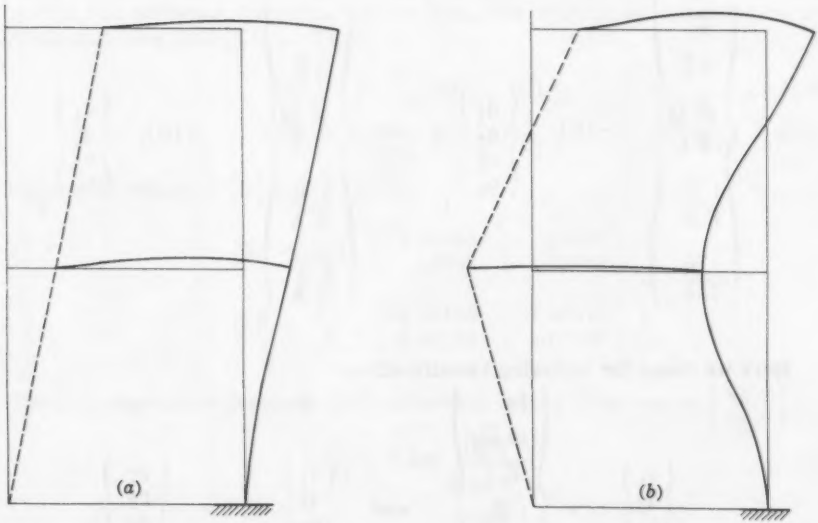

FIG. 6.—NATURAL MODES OF FRAME STRUCTURE

For System 1 For System 2

$$\begin{Bmatrix} p_1 \\ p_2 \\ p_3 \\ p_4 \\ p_5 \\ p_6 \\ p_7 \end{Bmatrix} = [C]_1 \begin{Bmatrix} p_1 \\ \frac{l^2 \bar{M}_1}{EI} \\ \frac{l \bar{Z}_1}{EA} \\ \frac{l \bar{X}_1}{EA} \end{Bmatrix} \qquad \begin{Bmatrix} p_1 \\ p_8 \\ p_9 \\ p_{10} \\ p_2 \\ p_3 \\ p_4 \\ p_5 \\ p_6 \\ p_7 \end{Bmatrix} = [C]_2 \begin{Bmatrix} p_1 \\ p_8 \\ p_9 \\ p_{10} \end{Bmatrix}$$

The generalized inertia and stiffness matrices for the two subsystems are computed from the equations

$$[m]_{1,2} = [C]^T_{1,2} [m] [C]_{1,2} \quad \ldots\ldots\ldots\ldots \quad (37a)$$

$$[k]_{1,2} = [C]^T_{1,2} [k] [C]_{1,2} \quad \ldots\ldots\ldots\ldots \quad (37b)$$

using the inertia and stiffness matrices for the uncoupled elements of the two systems. Next, the two subsystems are coupled. For this purpose, the deflection-force vectors $\left\{ \frac{\delta}{F} \right\}_{1,2}$ must be computed as indicated by Eq. 32.

These are:

$$\begin{Bmatrix} \bar{u} \\ \bar{w} \\ l\bar{\psi} \\ \frac{l^2 \bar{M}}{EI} \\ \frac{l \bar{Z}}{EA} \\ \frac{l \bar{X}}{EA} \end{Bmatrix}_1 = [B]_1 \begin{Bmatrix} q_1 \\ q_2 \\ q_3 \\ q_4 \end{Bmatrix}_1 \quad \text{and} \quad \begin{Bmatrix} \bar{u} \\ \bar{w} \\ l\bar{\psi} \\ \frac{l^2 \bar{M}}{EI} \\ \frac{l \bar{Z}}{EA} \\ \frac{l \bar{X}}{EA} \end{Bmatrix}_2 = [B]_2 \begin{Bmatrix} q_1 \\ q_2 \\ q_3 \\ q_4 \end{Bmatrix}_2$$

Here we make the following identifications

$$\begin{Bmatrix} q_1 \\ q_2 \\ q_3 \\ q_4 \end{Bmatrix}_1 = \begin{Bmatrix} p_1 \\ \frac{l^2 \bar{M}_1}{EI} \\ \frac{l \bar{Z}_1}{EA} \\ \frac{l \bar{X}_1}{EA} \end{Bmatrix} \quad \text{and} \quad \begin{Bmatrix} q_1 \\ q_2 \\ q_3 \\ q_4 \end{Bmatrix}_2 = \begin{Bmatrix} p_1 \\ p_8 \\ p_9 \\ p_{10} \end{Bmatrix}$$

By equating these two vectors, we are led to a constraint matrix connecting the two sets of coordinates $\{q\}_1$ and $\{q\}_2$. Since we have eight coordinates and six equations of constraint there are two degrees of freedom for the entire system. We regard q_{11} and q_{12} as free coordinates, in which the first subscript denotes the position of the coordinate in the subsystem vector and the second subscript denotes the subsystem to which the vector is related. We obtain the following constraining equation

$$\begin{Bmatrix} q_{1,1} \\ q_{2,1} \\ q_{3,1} \\ q_{4,1} \\ q_{1,2} \\ q_{2,2} \\ q_{3,2} \\ q_{4,2} \end{Bmatrix} = [C]_{1,2} \begin{Bmatrix} q_{1,1} \\ q_{1,2} \end{Bmatrix} \quad \ldots\ldots\ldots\ldots (38)$$

The inertia and stiffness matrices for the uncoupled subsystems are next determined as follows:

$$[m]_{1,2} = \left[\begin{array}{c|c} [m]_1 & [O] \\ \hline [O] & [m]_2 \end{array}\right] \quad \ldots\ldots\ldots\ldots (39a)$$

$$[k]_{1,2} = \left[\begin{array}{c|c} [k]_1 & [O] \\ \hline [O] & [k]_2 \end{array}\right] \quad \ldots\ldots\ldots\ldots (39b)$$

where the submatrices have already been computed. We obtain the generalized inertia and stiffness matrices for the complete system by operating on the above matrices with $[C]_{1,2}$. Thus,

$$[\overline{m}] = [C]^T_{1,2}\,[m]_{1,2}\,[C]_{1,2} \quad \ldots\ldots\ldots\ldots (40a)$$

$$[\overline{k}] = [C]^T_{1,2}\,[k]_{1,2}\,[C]_{1,2} \quad \ldots\ldots\ldots\ldots (40b)$$

Numerical values of $[\overline{m}]$ and $[\overline{k}]$ are:

$$[\overline{m}] = m\,l \begin{bmatrix} 1.81355 & .14708 \\ .14708 & 1.33508 \end{bmatrix}$$

$$[k] = \frac{E\,I}{l^3} \begin{bmatrix} 18.50144 & -7.49373 \\ -7.49373 & 5.03150 \end{bmatrix}$$

Thus, an eigenvalue problem is formulated in terms of the vector $\begin{Bmatrix} q_{1,1} \\ q_{1,2} \end{Bmatrix}$.

$$\omega_1 = 1.052\sqrt{\frac{E\,I}{m\,l^4}} \quad \ldots\ldots\ldots\ldots (41a)$$

$$\omega_2 = 3.729\sqrt{\frac{E\,I}{m\,l^4}} \quad \ldots\ldots\ldots\ldots (41b)$$

The corresponding normalized vectors are

$$\begin{Bmatrix} q_{1,1} \\ q_{1,2} \end{Bmatrix}^{(1)} = \begin{Bmatrix} .46419 \\ 1.00000 \end{Bmatrix} \qquad \begin{Bmatrix} q_{1,1} \\ q_{1,2} \end{Bmatrix}^{(2)} = \begin{Bmatrix} -1.41910 \\ 1.00000 \end{Bmatrix}$$

Using the constraint matrix $[C]_{1,2}$ we may find the two vectors $\{q\}_1$ and $\{q\}_2$ for both modes. Then using the constraint matrices $[C]_1$ and $[C]_2$ for the two subsystems we can obtain the values of the p coordinates for both subsystems and for both modes. Using these values and the functions $\phi(x)$ the displacements may be computed. The two natural mode shapes are shown in Fig. 6.

It may be noted that, had we dealt with this problem as a complete system rather than as two subsystems, we again would have had two degrees of freedom. In this case we would have had fifteen equations of constraint at the two junctions and seventeen coordinates, p.

An independent computation of the first mode frequency of the structure was made using the method of transfer matrices.[5] This frequency is

$$\omega_1 = 1.015 \sqrt{\frac{E\,I}{m\,l^4}} \qquad \ldots\ldots\ldots\ldots\ldots\ldots (42)$$

The value obtained herein exceeds this figure by 3.6%.

CONCLUSION

A method of analysis has been presented for the determination of natural modes and frequencies of structural systems using a variation of the Rayleigh-Ritz technique. The method features a procedure for obtaining mode shapes applicable to the connected system by synthesis of admissible mode functions that are defined for the unconnected elements of the system. This procedure eliminates the difficulty that usually attends the conventional Rayleigh analysis of such systems. That is, the difficulty in selecting appropriate mode shapes for the complete system. The method presented here permits the analyst to partition the structure into subsystems that may be treated independently to the point of final synthesis of the generalized properties of the complete system and solution of the eigenvalue problem.

Two problem solutions have been presented and the results compared with other methods of analysis of undisputed accuracy. The results are considered to be quite acceptable for practical engineering analysis.

APPENDIX. NOTATION

C = Transformation matrix

C^T = Transpose of transformation matrix

$E\,I$ = Modulus of rigidity in flexure

$E A$ = Modulus of rigidity in tension-compression

$G J$ = Modulus of rigidity in torsion

M = Bending moments

m = Mass of element per unit length

N = Axial force

p_j = The j-th coordinate

T = Kinetic energy of the system

t = Time

U = Strain energy of the system

u = longitudinal displacement

V = Shear

w = Transverse displacement

x = Independent variable measured along the length of the member

θ = Torsional displacement

ρ = Section radius of gyration in bending

$\phi_j(x)$ = The j-th mode function

ψ = Rotation due to bending

ω = Angular frequency of the vibration

Journal of the
ENGINEERING MECHANICS DIVISION
Proceedings of the American Society of Civil Engineers

IRROTATIONAL MOTION OF TWO FLUID STRATA TOWARDS A LINE SINK

By D. G. Huber,[1] M. ASCE

SYNOPSIS

The flow of two fluids of different density towards a line sink located in the bottom corner of a rectangular configuration with the upstream end extending to infinity, was studied by relaxation techniques. Relationships between the Froude numbers in the two layers were determined and the critical condition, when the lighter fluid begins or ceases to flow, was estimated.

INTRODUCTION

Although much has been published recently on problems involving stratified flow, few papers have dealt with discharge through outlets, orifices, or towards sinks. C. S. Yih has made[2] important contributions in this respect, particularly for continuous density gradients. G. L. Bata studied[3] a thermal-gradient problem involving the flow of cooling water at the inlet to a thermal plant. D. R. F. Harleman has done[4] experimental work on flow under sluice gates. A. Craya analyzed[5] a two-layered system with a sink in a vertical boundary. It

Note.—Discussion open until January 1, 1961. To extend the closing date one month, a written request must be filed with the Executive Secretary, ASCE. This paper is part of the copyrighted Journal of the Engineering Mechanics Division, Proceedings of the American Society of Civil Engineers, Vol. 86, No. EM 4, August, 1960.

[1] Assoc. Prof. of Mech. Engrg., McMaster Univ., Hamilton, Ontario, Canada.

[2] "On the Flow of Stratified Fluid," by C. S. Yih, Proceedings, Third U. S. Natl. Congress of Applied Mech., 1958, pp. 857-861.

[3] "Recirculation of Cooling Water in Rivers and Canals," by G. L. Bata, Proceedings, ASCE, Vol. 83, No. HY 3, June, 1957.

[4] "Submerged Sluice Control of Stratified Flow," by D. R. F. Harleman, R. S. Gooch, and A. T. Ippen, Proceedings, ASCE, Vol. 84, No. HY 2, April, 1958.

[5] "Recherches Théoriques sur l'Ecoulement de Couches Superposées de Fluides de Densités Differentes," by A. Craya, La Houille Blanche, No. 1, 1949.

was this last study, verified experimentally by P. Gariel,[6] that formed the inspiration for the present work.

STATEMENT OF THE PROBLEM

In Fig. 1 a line sink is located at the bottom corner of a rectangular box in which two fluid strata of different densities extend to infinity in the (-x)-direction; $v_{1\infty}$ and $v_{2\infty}$ are the velocity vectors at infinity and are assumed to be oriented in the x-direction and of constant magnitude in their respective layers; and h_1 and h_2 are the depths of each layer far upstream and are considered in this problem to be equal in magnitude. The mass densities of the layers are given symbols of ρ_1 and ρ_2 as shown. Each fluid is considered to be incompressible, inviscid, and homogeneous, and the flow is assumed to be irrotational. It is necessary, therefore, to allow slip to take place at the interface. The pressures are common to each fluid at every point along the interface.

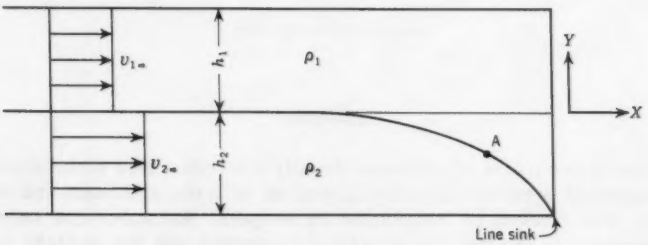

FIG. 1.—DEFINITION SKETCH FOR PROBLEM

If the fluids are at rest, the interface will be horizontal with h_1 equal to h_2. If the strength of the sink is increased from zero, fluid 2 will start to flow and accelerate until, at some critical condition, the interface will be drawn down to the sink and the lighter fluid will begin to take part in the flow. Further increases in the strength of the sink will cause increases in the magnitude of the total discharge and also changes in the proportions of the two fluids in the total flow. It is apparent that two of the factors of paramount importance in the determination of the interfacial shape and the proportions of flow will be inertia and gravity. It might be expected that the Froude number is therefore of considerable value as a parameter and that at large Froude numbers the inertia effect would be predominant, while at low Froude numbers the gravity effects would be particularly important.

Under the foregoing conditions, this problem has as its objective the determination of the relationships between the discharge from each layer, the densities, and the interfacial shape.

---

[6] "Recherches Expérimentales sur l'Ecoulement de Couches Superposées de Fluides de Densités Differentes," by P. Gariel, La Houille Blanche, No. 1, 1949.

ANALYSIS

Because each fluid is considered as incompressible, inviscid, homogeneous, and in irrotational motion, the Laplace equation must be satisfied throughout. Consequently, there must be a stream function in each fluid field that satisfies the Laplace equation at every point in that fluid and also fulfills the boundary conditions imposed by the problem. If such stream functions can be found in each fluid field, the problem of determining the velocities at every point, including those along the interface, is relatively simple. The horizontal and vertical boundaries representing the top, bottom and end of the configuration shown in Fig. 1 are simple boundaries, but the other boundary, the interface, is more complex and must be determined by application of the Bernoulli equation along each side of the interface. In order to derive the interfacial equation, one point is taken at infinity, and the other at some arbitrary position A on the interface (Fig. 1). Then, with symbols referring to the upper fluid given the subscript 1 and those in the lower fluid the subscript 2, the equations become

$$p_{1\infty} + \frac{\rho_1 v_{1\infty}^2}{2} + \gamma_1 y_\infty = p_{1A} + \frac{\rho_1 v_{1A}^2}{2} + \gamma_1 y_A \quad \ldots\ldots\ldots\ldots (1)$$

and

$$p_{2\infty} + \frac{\rho_2 v_{2\infty}^2}{2} + \gamma_2 y_\infty = p_{2A} + \frac{\rho_2 v_{2A}^2}{2} + \gamma_2 y_A \quad \ldots\ldots\ldots\ldots (2)$$

In Eqs. 1 and 2 p is the pressure, γ is the specific weight, y is the vertical distance measured from the horizontal line representing the interface at infinity, ρ is the mass density, and v is the magnitude of the velocity vector. Upon subtraction and use of the relationships $p_{1\infty} = p_{2\infty}$, $p_{1A} = p_{2A}$, and $y_\infty = 0$, the equation of the interface becomes

$$\frac{\rho_1}{2}\left(v_{1A}^2 - v_{1\infty}^2\right) - \frac{\rho_2}{2}\left(v_{2A}^2 - v_{2\infty}^2\right) = y_A \Delta\gamma \quad \ldots\ldots\ldots (3)$$

in which $\Delta\gamma$ is $\gamma_2 - \gamma_1$.

Upon consideration of Eq. 3 as a boundary condition for a potential-flow problem, the possibility of a rigorous mathematical determination of the stream function in each potential field becomes remote, for Eq. 3 is mixed and nonlinear.

Limiting and Critical Conditions.—Two extreme conditions may be studied, a critical one at low discharges when the lighter fluid begins or ceases to flow, and a limiting condition at high discharges when gravity effects become negligible.

The first of these conditions was studied extensively by Craya[5] for his different boundary conditions. He made use of the expression suggested[7] by A. R. Richardson and subsequently discussed[8] by Yih:

$$-\frac{dz}{dw} = \frac{1}{\left\{3g\,G(w)\right\}^{1/3}}\left[\left\{1 - G'^2(w)\right\}^{1/2} + i\,G'(w)\right] \quad \ldots\ldots (4)$$

in which z is the complex variable x + i y, w is the complex potential, g is the gravitational acceleration, primes denote differentiation with respect to w, and

---

[7] "Stationary Waves in Water," by A. R. Richardson, Philosophical Magazine, S6, Vol. 40, No. 235, 1920, pp. 97-110.

[8] "On Stratified Flows in a Gravitational Field," by C. S. Yih, Tellus IX, 1957, pp. 220-228.

G(w) is a function of w such that $G^{1/3}$, G', and $(1 - G'^2)^{1/2}$ are real and finite on the interface. Craya was fortunate in finding a function G(w) for use in this equation that satisfied approximately his boundary conditions, and through a series of transformations he was able to obtain a numerical value for his limiting Froude number. In the present problem the boundary conditions are much more complicated and no corresponding value of G(w) is apparent. Because of the difficulties inherent in this approach, mathematical analysis of the critical condition by this method was not pursued further, in the hope that this relationship might be determined with sufficient accuracy by other methods.

The limiting condition at high discharges may be determined rigorously if it is assumed that the fluids started from rest so that there is no vorticity at the interface. Although this assumption was not stipulated in the statement of the problem, it is reasonable to use it as an intuitive probability to be checked by further analysis. Yih proved[2] that under conditions of high discharge of a stratified fluid in the absence of vorticity and when gravity effects may be neglected, every steady irrotational flow corresponds to a stratified flow the velocity of which is that for the irrotational flow divided by the square root of the density. The streamline pattern for a homogeneous fluid must have a stratified flow counterpart with the interface along a streamline - the central one for the boundary conditions of this problem. Since the velocity at a point on the interface in the homogeneous pattern must be single-valued, in the stratified case the following relationship must result:

$$v_{1\infty}\sqrt{\rho_1} = v_{2\infty}\sqrt{\rho_2} \quad \ldots\ldots\ldots\ldots\ldots\ldots (5)$$

That a similar relationship exists close to the sink may be shown when Eq. 3 is rearranged as

$$\frac{\rho_1 v_{1A}^2}{2} - \frac{\rho_2 v_{2A}^2}{2} = \frac{\rho_1 v_{1\infty}^2}{2} - \frac{\rho_2 v_{2\infty}^2}{2} + y_A \Delta\gamma \quad \ldots\ldots\ldots (6)$$

Multiplying through by $2/v_{2A}^2$ gives

$$\frac{\rho_1 v_{1A}^2}{v_{2A}^2} - \rho_2 = \frac{\rho_1 v_{1\infty}^2 - \rho_2 v_{2\infty}^2}{v_{2A}^2} + \frac{2 y_A \Delta\gamma}{v_{2A}^2} \quad \ldots\ldots\ldots (7)$$

and point A taken close to the sink where v_{2A}^2 becomes very large compared to the other terms in the equation except v_{1A}^2. In the limit the equation

$$\rho_1 v_{1A}^2 = \rho_2 v_{2A}^2 \quad \ldots\ldots\ldots\ldots\ldots\ldots (8)$$

results, which is not based on any of the assumptions necessary for the development of Eq. 5.

If the analysis close to the sink is continued a little further a relationship between the interfacial angle, the velocities, and the densities may be derived. In Fig. 2 the angle that the tangent to the interface at the sink makes with the vertical is θ_1 and with the horizontal, θ_2. If an arc of small radius r is drawn, the discharge through the area $r\theta_1$ is $v_{1A}\, r\theta_1$, and that through the area $r\theta_2$ is $v_{2A}\, r\theta_2$. The ratio of the two discharges is then $v_{1A}\, r\theta_1 / v_{2A}\, r\theta_2$ or $v_{1A}\,\theta_1 / v_{2A}\,\theta_2$. But the discharges may also be written as $v_{1\infty} h_1$ and $v_{2\infty} h_2$, and the ratio becomes $v_{1\infty}/v_{2\infty}$ since h_1 is equal to h_2. When the two expressions for the discharge ratio are equated, and Eq. 8 substituted, the interesting relationship

$$\frac{v_{1\infty}\sqrt{\rho_1}}{v_{2\infty}\sqrt{\rho_2}} = \frac{\theta_1}{\theta_2} \quad \ldots\ldots\ldots\ldots\ldots\ldots (9)$$

results.

It is apparent that at very high discharges, if Eq. 5 is accepted, the interface must make an angle of 45° with the axes close to the sink. This fact also follows from the symmetry of the homogeneous fluid streamline pattern to which this limiting case of stratified flow was assumed equivalent. In addition, for any given interfacial angle at the sink, the velocity and discharge ratios at infinity are known if the densities of the two fluids are given.

Dimensional Analysis.—If a functional relationship is assumed as follows:

$$f(v_{1\infty}, v_{2\infty}, \rho_1, \rho_2, \Delta\gamma, h_1, x, y) = 0 \quad \ldots\ldots\ldots \quad (10)$$

where x and y are the coordinates of the interface, according to the Buckingham π-theorem a different functional relationship involving five dimensionless terms may be written as

$$f_1(\pi_1, \pi_2, \pi_3, \pi_4, \pi_5) = 0 \quad \ldots\ldots\ldots\ldots \quad (11)$$

if only three fundamental units are included in the relationship. When $v_{1\infty}$, ρ_1, and h_1 are combined in turn with the other variables, five dimensionless terms

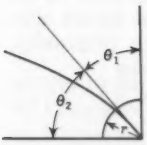

FIG. 2.—INTERFACIAL ANGLE AT THE SINK

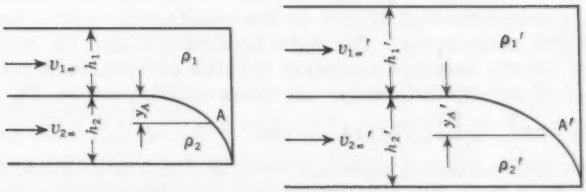

FIG. 3.—DEFINITION SKETCH FOR SIMILARITY CONSIDERATIONS

result: $\pi_1 = v_{1\infty}/v_{2\infty}$, $\pi_2 = \rho_1/\rho_2$, $\pi_3 = \rho_1 v_{1\infty}^2/\Delta\gamma\, h_1$, $\pi_4 = x/h_1$ and $\pi_5 = y/h_1$. By multiplication of π_3 by the inverse of π_1^2, and the product by the inverse of π_2 the equally correct relationship

$$f_2\left(\frac{v_{1\infty}}{v_{2\infty}}, \frac{v_{1\infty}^2}{\frac{\Delta\gamma}{\rho_1} h_1}, \frac{v_{2\infty}^2}{\frac{\Delta\gamma}{\rho_2} h_2}, \frac{y}{h_1}, \frac{x}{h_1}\right) = 0 \quad \ldots\ldots\ldots \quad (12)$$

results since $h_1 = h_2$. The second two terms are Froude numbers, different from the customary Froude numbers because of the inclusion of the density terms in the denominator. Such Froude numbers are used by G. H. Keulegan,[9] Bata,[3] and Craya.[5] From this analysis, a comparison of Froude numbers in the two layers for different velocity ratios and interfaces appears to be useful. It should be remembered, however, that many other similar and possibly equally useful relationships can be found from Eq. 10.

Similarity Considerations.—From similarity considerations two very important results may be obtained. Most important, it may be shown that the in-

[9] "Sixth Progress Report on Model Laws for Density Currents: Effectiveness of Salt Barriers in Rivers," by G. H. Keulegan, Natl. Bur. of Standards, No. 1700, June, 1952.

terfacial shape and the streamline patterns are dependent on the Froude numbers in the two layers and not on the density or velocity alone. In addition, the method of presenting the results of the analysis previously suggested by dimensional considerations is verified.

The two diagrams of Fig. 3 represent situations of geometric and kinematic similarity. Therefore, the interfacial shapes and streamline patterns are similar in each. Eq. 3 written between corresponding interfacial points in each diagram becomes

$$\frac{\rho_1}{2}\left(v_{1A}^2 - v_{1\infty}^2\right) - \frac{\rho_2}{2}\left(v_{2A}^2 - v_{2\infty}^2\right) = y_A\, g\, \Delta\rho \quad \ldots\ldots\ (13)$$

and

$$\frac{\rho'_1}{2}\left(v'^2_{1A} - v'^2_{1\infty}\right) - \frac{\rho'_2}{2}\left(v'^2_{2A} - v'^2_{2\infty}\right) = y'_A\, g'\, \Delta\rho' \quad \ldots\ldots\ (14)$$

If Eq. 13 is divided by Eq. 14, the following equation results:

$$\frac{\rho_1\left(v_{1A}^2 - v_{1\infty}^2\right) - \rho_2\left(v_{2A}^2 - v_{2\infty}^2\right)}{\rho'_1\left(v'^2_{1A} - v'^2_{1\infty}\right) - \rho'_2\left(v'^2_{2A} - v'^2_{2\infty}\right)} = \frac{y_A\, g\, \Delta\rho}{y'_A\, g'\, \Delta\rho'} \quad \ldots\ldots\ (15)$$

Because the assumption of kinematic and geometric similarity requires similar interfacial shapes and similar streamline patterns, and because A and A' are corresponding points on the interfaces, y_A/y'_A may be replaced by the length scale h_1/h'_1. The right-hand side of Eq. 15, which will be called α for simplicity, becomes a product of three scale factors, that of length, of gravity, and of density difference. By cross-multiplication, Eq. 15 becomes

$$\rho_1\left(v_{1A}^2 - v_{1\infty}^2\right) - \rho_2\left(v_{2A}^2 - v_{2\infty}^2\right) = \alpha\rho'_1\left(v'^2_{1A} - v'^2_{1\infty}\right) - \alpha\rho'_2\left(v'^2_{2A} - v'^2_{2\infty}\right) \quad \ldots(16)$$

The corresponding potential fields of Fig. 3 must differ only by a constant factor because of the similar boundary conditions and the geometric and kinematic similarity considerations discussed previously. Therefore, from Eq. 16, the following relationships must hold:

$$\rho_1 v_{1A}^2 = \alpha\rho'_1 v'^2_{1A} \quad \ldots\ldots\ (17)$$

$$\rho_1 v_{1\infty}^2 = \alpha\rho'_1 v'^2_{1\infty} \quad \ldots\ldots\ (18)$$

$$\rho_2 v_{2A}^2 = \alpha\rho'_2 v'^2_{2A} \quad \ldots\ldots\ (19)$$

and

$$\rho_2 v_{2\infty}^2 = \alpha\rho'_2 v'^2_{2\infty} \quad \ldots\ldots\ (20)$$

From these equations, between corresponding points in the similar flow patterns the following general relationship results:

$$v^2 = \alpha\frac{\rho'}{\rho} v'^2 \quad \ldots\ldots\ (21)$$

When the expression for α is substituted, Eq. 21 becomes

$$v^2 = \frac{h\, g\, \Delta\rho}{h' g' \Delta\rho'} v'^2 \quad \ldots\ldots\ (22)$$

By a rearrangement of terms, the necessity for the equality of corresponding Froude numbers becomes apparent:

$$\frac{v^2}{g\, h\, \frac{\Delta\rho}{\rho}} = \frac{v'^2}{g' h' \frac{\Delta\rho'}{\rho'}} = F \quad \ldots\ldots\ (23)$$

The most convenient point in the flow patterns to choose as a reference is at infinity, and the similarity criterion, Eq. 23, becomes

$$\frac{v_{1\infty}^2}{g\, h_1 \frac{\Delta\rho}{\rho_1}} = \frac{v_{1\infty}'^2}{g'\, h_1' \frac{\Delta\rho'}{\rho'}} = \mathbf{F}_1 \quad \ldots\ldots\ldots\ldots \quad (24)$$

and

$$\frac{v_{2\infty}^2}{g\, h_2 \frac{\Delta\rho}{\rho_2}} = \frac{v_{2\infty}'^2}{g'\, h_2' \frac{\Delta\rho'}{\rho_2'}} = \mathbf{F}_2 \quad \ldots\ldots\ldots\ldots \quad (25)$$

A single interfacial shape and corresponding flow pattern must result in a single ratio $\mathbf{F}_1/\mathbf{F}_2$ provided, of course, that the requirements of geometric similarity and of potential flow of both fluids are maintained. As a consequence, the method of comparing the two Froude numbers $\mathbf{F}_1$ and $\mathbf{F}_2$ for various interfacial shapes is again suggested. It is interesting to notice that Eq. 9, which relates the interfacial angle at the sink to the velocity and density ratio, indicates the same conclusion, for if the ratio of the Froude numbers is written for a given system, the quantities $\Delta\rho$, g, and h cancel out, and the ratio becomes

$$\frac{\mathbf{F}_1}{\mathbf{F}_2} = \frac{v_{1\infty}^2\, \rho_1}{v_{2\infty}^2\, \rho_2} \quad \ldots\ldots\ldots\ldots\ldots\ldots \quad (26)$$

which, by Eq. 9 must be equal to θ_1^2/θ_2^2.

Systems of Three or More Layers.—The similarity analysis given for the two-layered system may be extended to systems of three or more layers, but the free choice of density ratios found for the two-layered system is not possible. In the case of two interfaces, equivalent equations corresponding to Eq. 15 and Eq. 16 applied to each interface, in turn, result in two expressions for the velocity in the intermediate layer. If symbols referring to the three layers are given subscripts 1, 2, and 3, where subscript 2 applies to the intermediate layer, the equations equivalent to Eq. 22 are

$$v_2^2 = \frac{h_2\, g\, (\rho_2 - \rho_1)\, \rho_2'}{h_2'\, g'\, (\rho_2' - \rho_1')\, \rho_2}\, v_2'^2 \quad \ldots\ldots\ldots\ldots \quad (27)$$

and

$$v_2^2 = \frac{h_2\, g\, (\rho_3 - \rho_2)\, \rho_2'}{h_2'\, g'\, (\rho_3' - \rho_2')\, \rho_2}\, v_2'^2 \quad \ldots\ldots\ldots\ldots \quad (28)$$

Since the corresponding velocities must be identical for any given flow situation in the same layer, the following relationship between the densities must hold:

$$\frac{\rho_2 - \rho_1}{\rho_2' - \rho_1'} = \frac{\rho_3 - \rho_2}{\rho_3' - \rho_2'} \quad \ldots\ldots\ldots\ldots\ldots\ldots \quad (29)$$

For more than three layers, additional relationships similar to Eq. 29 result. If, then, in a multilayered system some of the densities are given, the others must satisfy relationships between the densities, such as Eq. 29, in order that a certain potential-flow pattern results. The case of the two-layered system is seen to be unique, in that for a simple flow pattern the densities may be chosen at random, provided only that the Froude numbers in the two layers be kept constant.

SOLUTION OF THE PROBLEM

The preceeding analysis indicated the desirability of calculating and plotting the Froude numbers in the upper and lower layers as a solution of the problem. This solution requires the determination of the velocities $v_{1\infty}$ and $v_{2\infty}$ for a number of interfacial shapes and potential field patterns. The difficulty of obtaining a rigorous mathematical solution, because of the complexity of Eq. 3 as a common-boundary equation, was pointed out in the analysis. For this reason the methods of approximate numerical analysis offer the most practicable way of obtaining a solution. The particular technique of relaxation described[10] by J. S. McNown, E. Y. Hsu, and C. S. Yih was followed in the present work.

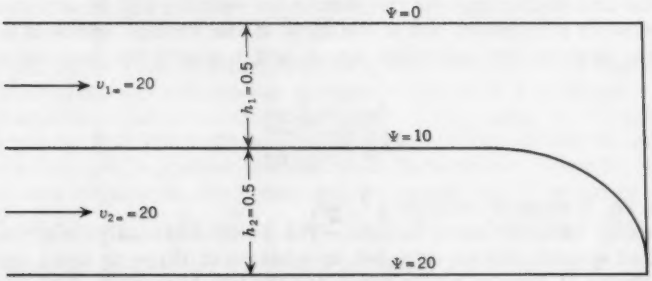

FIG. 4.—DEFINITION SKETCH FOR RELAXATION PROCEDURE

General Method.— The method used for the solution by relaxation procedures necessitated, first, the assumption of an interfacial shape and, second, the estimation of the stream function ψ throughout the two potential fields. By relaxation techniques the assumed values of ψ were altered until they were correct at every point for the assumed boundary conditions. Velocities were calculated at a number of points along the interface and the interfacial equation, Eq. 3, was checked to determine if the boundary condition was satisfied. By the use of constants in the equation it was possible to calculate the two velocities at every point, and thus the Froude number, once the correct interfacial shape was obtained.

Details of the Relaxation Technique.—In Fig. 4 the assumed values of the stream function and velocity are given symbols Ψ, and V, respectively, to distinguish them from the true values ψ and v. The numerical values chosen were as shown for two of the three cases attempted. For the third case the value of Ψ on the lower boundary was 19. The grid pattern used was one of 0.1 unit squares progressively reduced to 0.05 units in the vicinity of the interface, and finally to 0.025 units close to the sink. This pattern is shown in Fig. 5.

---

10 "Applications of the Relaxation Technique in Fluid Mechanics," by J. S. McNown, E. Y. Hsu, and C. S. Yih, Transactions, ASCE, Vol. 120, 1955.

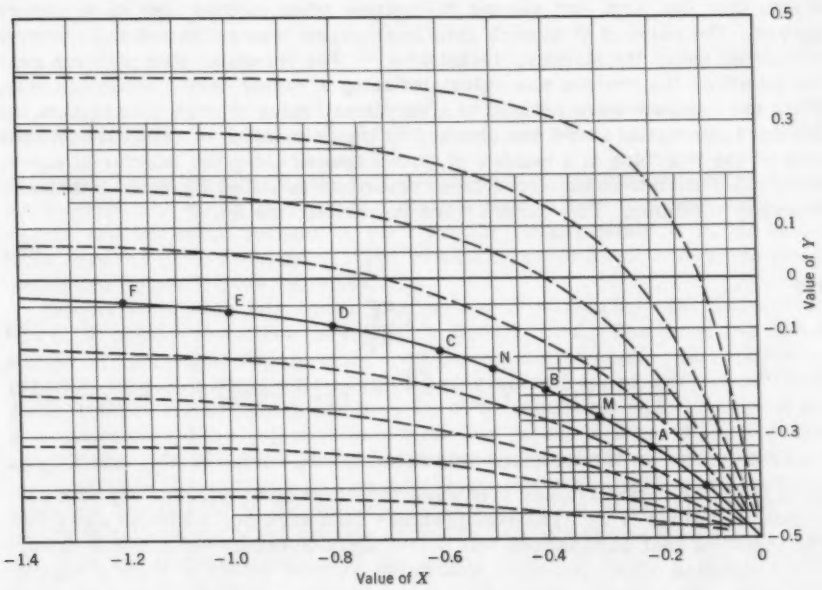

FIG. 5.—RELAXATION GRID AND STREAMLINES, CASE 3

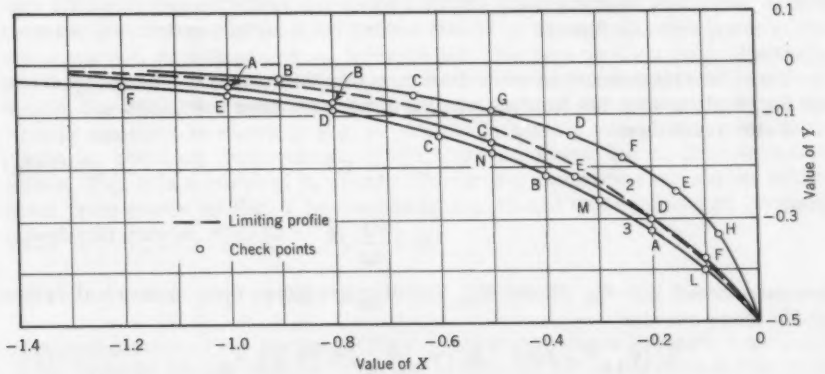

FIG. 6.—COMPARISON OF INTERFACIAL PROFILES

Each case attempted necessitated the assumption of an interfacial curve so drawn that the first and second derivatives when plotted also gave smooth curves. The value of Ψ at each grid intersection was estimated and residues calculated using the standard techniques.[10] For irregular star patterns near the interface, the residue was calculated using a Taylor series expansion of Ψ. When the residues were relaxed to a very small value at each intersection, the assumed interfacial shape was checked by the calculation of velocities on each side of the interface at a number of points spaced along the interfacial curve, and a calculation to determine if these velocities satisfied Eq. 3, the interfacial boundary condition. Two factors were introduced into Eq. 3

$$K = \frac{v_1}{V_1} \quad \ldots\ldots\ldots\ldots\ldots \quad (30a)$$

and

$$J = \frac{v_2}{V_2} \quad \ldots\ldots\ldots\ldots\ldots \quad (30b)$$

to give

$$\frac{\rho_1}{2} K^2 \left(V_{1A}^2 - V_{1\infty}^2\right) - \frac{\rho_2}{2} J^2 \left(V_{2A}^2 - V_{2\infty}^2\right) = y_A \Delta\gamma \quad \ldots \quad (31)$$

A pair of points on the interface was selected and values of V_{1A} and V_{2A} as found from the relaxed values of Ψ were substituted into Eq. 31 along with corresponding values of y_A. The density values used were $\rho_1 = 1.938$ and $\rho_2 = 1.996$. The resulting pair of equations was solved simultaneously for K and J. A correctly assumed interfacial curve would give constant values of K and J regardless of the pair of points selected for the calculation. If K and J were not found reasonably constant by calculation involving successive pairs of points, it was necessary to redraw the interfacial curve and repeat the relaxation procedures.

It was found that K and J were very sensitive to interfacial alterations and it was necessary to make many trials, reduce the grid size and relax the residues to as little as 2 parts in 10,000 before reasonably constant values were obtained.

Three interfacial curves were determined in this manner. These are shown on Fig. 6 along with the limiting profile of homogeneous fluid flow.

If two quantities

$$L = \frac{\rho_1}{\Delta\rho} K^2 \quad \ldots\ldots\ldots\ldots\ldots \quad (32a)$$

and

$$M = \frac{\rho_2}{\Delta\rho} J^2 \quad \ldots\ldots\ldots\ldots\ldots \quad (32b)$$

are introduced into Eq. 31 and $V_{1\infty}$ and $V_{2\infty}$ are given their numerical values of 20, there results

$$L \left(V_{1A}^2 - 400\right) - M \left(V_{2A}^2 - 400\right) = 2 g y_A \quad \ldots\ldots\ldots \quad (33)$$

Eq. 33 can be solved for L and M between successive points without the necessity of introducing numerical values of ρ_1 and ρ_2. The Froude numbers can be calculated directly from L and M using Eqs. 24 and 25

which, when $V_1 = Kv_1$ $V_2 = Jv_2$ $L = \frac{\rho_1}{\Delta\rho} K^2$ and $M = \frac{\rho_2}{\Delta\rho} J^2$ are introduced become

$$F_1 = \frac{L V_{1\infty}^2}{g h_1} \quad \ldots\ldots\ldots\ldots\ldots\ldots \quad (34)$$

and

$$F_2 = \frac{M V_{2\infty}^2}{g h_2} \quad \ldots\ldots\ldots\ldots\ldots\ldots\ldots \quad (35)$$

These expressions verify the result of the similarity considerations developed previously, which indicated that the interfacial shape was a function of the Froude number ratio, because by their use the Froude numbers can be calculated directly from the results of the relaxation procedures without the use of numerical values for the densities.

Results.—The final interfacial location and Ψ-pattern for case 3 are shown in Fig. 5, with streamlines indicated by dashed lines. The three interfacial shapes are plotted in Fig. 6, along with the calculated central streamline for potential flow of a homogeneous fluid, and a table of coordinates is included. Table 1 shows the results of the solution of simultaneous equations for K and J for pairs of points along each interface. The values of K and J are averaged and the maximum deviation from the average values indicated in percent. In the upstream flat portions of the interfaces, numercial difficulties resulted from the small size of the velocity difference terms in Eq. 31, and several points in this region were omitted from the average values of K and J. As a check on the physical meaning of the errors shown in K and J, the pressure difference between pairs of points along each side of the interface was calculated as shown in Table 4. The points on the flat portion of the interface were included in this check, but the maximum errors found were less than 1%. Table 2 gives values of L, M, F_1, F_2, $\sqrt{F_1} + \sqrt{F_2}$ and F_1 / F_2 for each interfacial shape. The values of L and M were calculated from the average values of K and J given in Table 1 by the use of Eq. 32. The curve of Fig. 7 shows the relationship between the two Froude numbers. Because the intercept on the x-axis, where F_1 and $v_{1\infty}$ become zero, is not apparent from this curve, another relationship, that of the ratio of Froude numbers and the sum of the square roots of the Froude numbers, is shown in Fig. 8. This relationship was plotted in order to obtain an abscissa proportional to the total discharge but in dimensionless terms. Fig. 9 is a curve of θ_2 plotted against F_2, comparing the angles calculated from points on Fig. 7 by the use of Eq. 26 and those measured from the interfacial curves, Fig. 6.

DISCUSSION OF RESULTS

A comparison of the curves of Figs. 7 and 8 enables an estimate to be made of the critical Froude number in the lower layer at which the fluid in the upper layer ceases to flow. From Fig. 8 the value of $\sqrt{F_2}$ at this point is seen to be 1.66 by an extension of the curve. The corresponding value of F_2 is 2.76 which, with reference to Fig. 7, appears to be reasonable. Craya obtained[5] a value

TABLE 1.—VALUES OF K AND J

Interface No. 1			Interface No. 2			Interface No. 3		
Points	K	J	Points	K	J	Points	K	J
EH	0.0113	0.0454	AF	0.0247	0.0356	EL	0.0332	0.0334
FH	0.0115	0.0458	BF	0.0267	0.0380	DL	0.0334	0.0336
DH	0.0115	0.0458	CF	0.0259	0.0371	CL	0.0326	0.0329
GH	0.0113	0.0454	DF	0.0250	0.0360	NL	0.0335	0.0337
CH	0.0125	0.0491	EF	0.0257	0.0368	BL	0.0329	0.0332
BH	0.0125	0.0488	AD	0.0246	0.0356	ML	0.0325	0.0328
FE	0.0116	0.0459	BD	0.0271	0.0380	AL	0.0332	0.0334
DE	0.0116	0.0459	CD	0.0262	0.0371	EA	0.0332	0.0334
GE	0.0113	0.0454	ED	0.0261	0.0370	DA	0.0334	0.0336
GR	0.0110	0.0453	AE	0.0239	0.0359	CA	0.0326	0.0329
CE	0.0132	0.0491	BE	0.0276	0.0378	NA	0.0336	0.0337
			CE	0.0264	0.0372	BA	0.0328	0.0331
						MA	0.0320	0.0325
Average without B or C	0.0114	0.0456	Average without A or B	0.0259	0.0369			
Max. % Error without B or C	+1.75 -3.5	+0.7	Max. % Error without A or B	+1.9 -3.5	+0.8 -2.4	Max. % Error	+1.8 -3.0	+1.5 -2.1

TABLE 2.—FROUDE NUMBERS

Interface	L	M	F_1	F_2	F_2/F_2	$\sqrt{F_1}+\sqrt{F_2}$
1	0.004343	0.07150	0.1080	1.778	0.0607	1.663
2	0.02241	0.04683	0.5571	0.9432	0.5906	1.718
3	0.03637	0.03791	0.9042	0.9424	0.9595	1.922

TABLE 3.—INTERFACIAL COORDINATES

-X	No. 1 -Y	No. 2 -Y	No. 3 -Y
0	0	0	0
0.05	0.364	0.434	0.4485
0.10	0.294	0.383	0.4038
0.15	0.247	0.341	0.3639
0.20	0.211	0.305	0.3280
0.25	0.18205	0.2726	0.2955
0.30	0.1581	0.2441	0.2660
0.35	0.13785	0.2184	0.2395
0.40	0.1205	0.1951	0.2154
0.45	0.1055	0.1740	0.1936
0.50	0.09245	0.1550	0.1739
0.55	0.08105	0.1380	0.1561
0.60	0.07105	0.1230	0.1400
0.65	0.0623	0.1095	0.1255
0.70	0.0546	0.0973	0.1125
0.75	0.0478	0.0863	0.1009
0.80	0.04175	0.0764	0.0906
0.85	0.03635	0.0675	0.0815
0.90	0.03145	0.0595	0.0735
0.95	0.02695	0.0523	0.0665
1.00	0.02275	0.0458	0.0604
1.05	0.01875	0.0399	0.0551
1.10	0.01485	0.0345	0.0505
1.15	0.01104	0.0295	0.0465
1.20		0.0248	0.0430
1.25		0.0204	0.0399
1.30		0.0163	0.0371
1.35		0.0124	0.0345
1.40			0.0320

TABLE 4.—PRESSURE DIFFERENCE ALONG INTERFACE

Interface	Pairs of Points	Pressure Fluid 1	Difference Fluid 2	Error	Error %
1	CE	11.070	11.050	0.02	0.18
	BH	16.283	16.272	0.011	0.07
2	AF	16.569	16.573	0.004	0.02
	BE	8.204	8.183	0.021	0.26
3	EL	13.546	13.565	0.019	0.14
	GL	15.327	15.341	0.014	0.09
	AM	2.561	2.581	0.020	0.78

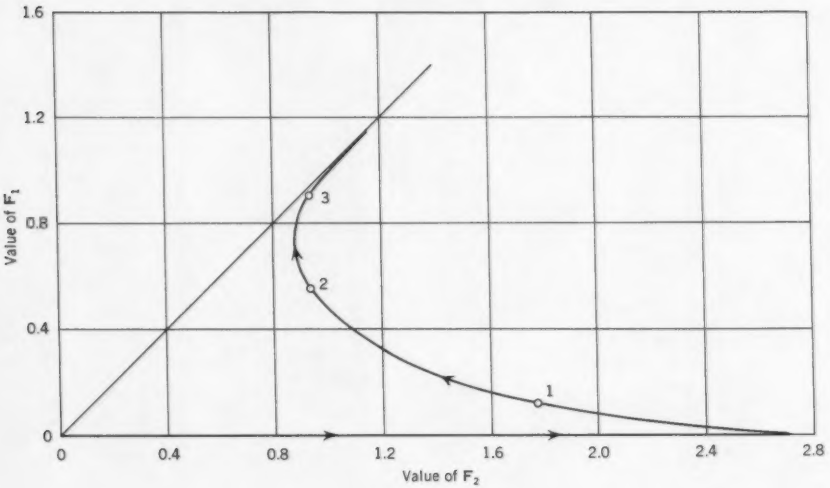

FIG. 7.—FROUDE NUMBER RELATIONSHIP 1

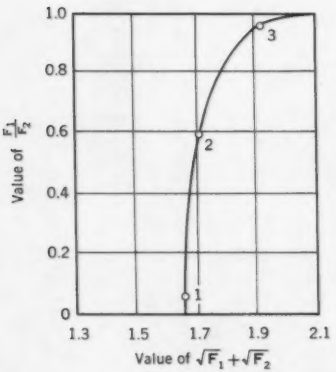

FIG. 8.—FROUDE NUMBER RELATIONSHIP 2

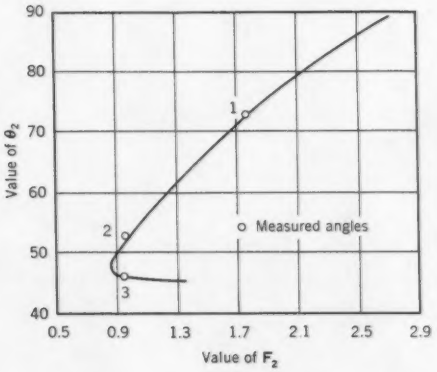

FIG. 9.—INTERFACIAL ANGLE VERSUS FROUDE NUMBER

of 2.283 for this Froude number with his quite different boundary conditions. The significance of this result is that for any pair of fluids in any geometrically similar potential-flow situation, the velocity at infinity of the lower fluid at which the upper fluid either starts or ceases to participate in the flow can be calculated.

The curves as drawn verify the suggested result that at large discharges the inertial effects predominate and the Froude numbers approach each other. In Fig. 7 this asymptote is a 45° line; in Fig. 8 the asymptote is $F_1/F_2 = 1$.

Since, in Fig. 7, the point at which both fluids are at rest is at the origin, it is apparent that the curve drawn must start at this point when the fluid begins to accelerate, and continue along the x-axis until the critical Froude number is reached. Here the upper fluid begins to flow, the total discharge increases slowly (Fig. 8), but the discharge of the heavier fluid decreases as that of the lighter fluid increases. A point is reached, however, when this trend is changed and both discharges increase together as the Froude numbers approach equality. It would be expected that considerable instability would result in the neighborhood of the point of minimum F_2 on the curve of Fig. 7, at a Froude number in the lower fluid of about 0.9. At about this same Froude number a minimum point occurs in the curve of Fig. 9. Below this point the angle approaches its limit of 45° very abruptly as F_2 increases; above this inflection point the angle approaches the critical value of 90° more gradually as F_2 increases to its critical value of 2.76. The values of θ_2 scaled from the interfacial profiles, Fig. 6, agree closely with the curve of Fig. 9, which was plotted from calculated values of Froude number, thereby verifying the relationship between the Froude numbers and the angles as expressed by Eq. 26.

A comparison of the three interfacial profiles as plotted in Fig. 6 and the central streamline calculated for a homogeneous fluid suggests that the interface successively takes flatter shapes as the proportion of the lighter fluid in the flow increases until, at a condition equivalent to the inflection points on Figs. 7 and 9, the trend reverses and the limiting profile is approached.

CONCLUSIONS

The irrotational motion of two fluid strata towards a line sink located within the boundary configurations chosen in this problem has been shown to be governed by the relationship between the Froude numbers in each layer as expressed by the curve of Fig. 7. This relationship indicates a numerical value for the critical Froude number in the lower stratum at which the upper fluid either begins or ceases to flow, and an asymptote representing the equality of Froude numbers at high rates of flow when inertial effects predominate. An interesting feature of this curve is an inflection point at which, for increasing total flow, the rate of flow of the lower fluid begins to increase along with that of the upper rather than decrease.

The shape of the interface and the streamline pattern have been shown to be dependent on the Froude number in the upper layer, since the angle of the interface at the sink is shown to depend on the Froude number ratio, and from Fig. 7 there is only one ratio possible for each value other than zero of the Froude number in the upper stratum.

ACKNOWLEDGMENTS

The writer gratefully acknowledges the direction and help of Hunter Rouse, F. ASCE, of the State University of Iowa, who directed his dissertation, C. S. Yih, of the University of Michigan, under whose direction the work was started, and E. O. Macagno and L. Landweber of Iowa who were generous with their knowledge and advice.

Journal of the
ENGINEERING MECHANICS DIVISION
Proceedings of the American Society of Civil Engineers

UNDERGROUND STRUCTURES SUBJECT TO AIR OVERPRESSURE

By Ernest T. Selig,[1] A.M. ASCE, Keith E. McKee,[2] M. ASCE, and Eben Vey,[3] F. ASCE

SYNOPSIS

An analytical procedure is presented for determining the damage to underground structures induced by pseudo-steady state air overpressure. By introducing appropriate assumptions from the fields of soil mechanics and structural dynamics, it is possible to derive analytical expressions that relate the parameters of the structure, the soil, and the loading as they affect the failure of the structure. The assumptions are stated and the derivation of the analytical procedure is presented. A separate section is devoted to the application of the procedure for the cases of analysis of the vulnerability of an underground structure and the design of an underground structure for any desired level of protection.

INTRODUCTION

This analytical procedure is only concerned with damage induced by the pseudo-steady air overpressure acting on the ground surface above the buried

Note.—Discussion open until January 1, 1961. To extend the closing date one month, a written request must be filed with the Executive Secretary, ASCE. This paper is part of the copyrighted Journal of the Engineering Mechanics Division, Proceedings of the American Society of Civil Engineers, Vol. 86, No. EM 4, August, 1960.

[1] Asst. Research Engr., Struct. Analysis, Armour Research Foundation of Illinois Inst. of Tech., Chicago, Ill.

[2] Research Engr., Struct. Analysis, Armour Research Foundation of Illinois Inst. of Tech., Chicago, Ill.

[3] Prof. of Civ. Engrg., Illinois Inst. of Tech. and Soil Mechanics Cons., Armour Research Foundation, Chicago, Ill.

structure. By "damage" is meant actual structural failure. Stress wave damage is not considered because it is felt that in the locations of interest this agent, in general, causes only minor structural damage.

With sufficiently high overpressure on the ground surface, stresses great enough to fail the structure may be induced in underground structures through the surrounding soil. The structures will tend to deform under the action of these stresses, but failure cannot occur unless large masses of soil can move with the structure in order to maintain the stresses. It will be shown that for a given structure and a given soil the overpressure required to cause failure increases rapidly with the depth of burial.

In order to get movement of the soil it is necessary that the shearing stresses in the soil exceed its ultimate shearing resistance. It is assumed that this shearing resistance is a function of the normal stress on the shear planes, the angle of internal friction and the cohesion of the soil. The shearing resistance in the region of soil surrounding the structure is limited by the strength of the structure. When the structure begins to yield, the soil is shearing resistance is mobilized and increases until the ultimate shearing resistance is reached.

A further increase in overpressure will extend the region in which the shear resistance is exceeded until this region reaches the ground surface. In order to have any movement of the soil, it is necessary that the ultimate shearing resistance be exceeded along some surface extending from the structure to the ground surface.

The general approach to the problem is to select planes within the soil on which the shear stress is equal to the ultimate shear resistance and then to write the equation of motion of the mass of soil which is bounded by these planes, the structure, and the ground surface. This particular volume of soil will be referred to as the "failure mass" and the shear planes as "slip planes." The solution of this equation of motion results in an expression relating the parameters of the structure, the soil and the blast loading as they effect the failure of the structure.

Notation.—The letter symbols used in this paper are defined where they first appear, in the text or by illustration, and are assembled for convenience of reference in the Appendix.

ASSUMPTIONS

Blast Loading.—The uniform air overpressure applied to the ground surfaces, that is, the pseudo-steady state overpressure $p_\sigma(t)$, varies with time. This variation is represented by an initially peaked, linearly decreasing overpressure of duration t_d, given by[4]

$$p_\sigma(t) = p_\sigma(0)\left(1 - \frac{t}{t_d}\right) \quad \ldots\ldots\ldots\ldots\ldots (1)$$

in which $p_\sigma(0)$ is the initial peak overpressure for duration t_d, and t is time. Eq. 1 is shown graphically in Fig. 1. The loading parameters are thus $p_\sigma(0)$

[4] "An Engineering Approach to Blast-Resistant Design," by N. M. Newmark, Transactions, ASCE, Vol. 121, 1956.

and t_d. The actual variation of overpressure with time is of the form[5]

$$p_\sigma(t) = p_\sigma(0)\, e^{-t/t_o} \left(1 - \frac{t}{t_o}\right) \quad \ldots\ldots\ldots\ldots (2)$$

and is shown graphically in Fig. 2. The relationship between the actual and linearized overpressures normally maintains the same peak overpressure and total impulse. Thus t_d is found as a function of t_o, the duration of actual overpressure, by equating the area under the curve in Fig. 1 with that in Fig. 2.

$$t_d = 0.736\, t_o \quad \ldots\ldots\ldots\ldots\ldots\ldots (3)$$

If the actual wave form differs from that given in Eq. 2 then Eq. 3 should be modified accordingly. The parameters $p_\sigma(0)$ and t_o are related to the weapon yield, height of burst, and ground range.[6]

Soil Behavior.—Several fundamental assumptions are made regarding the behavior of the soil under the type of loading previously considered. These are based on conventional static analysis,[7,8,9] and are as follows:

1. The relationship between the vertical and horizontal components of stress at a point in the soil may be expressed by

$$p = K q \quad \ldots\ldots\ldots\ldots\ldots\ldots (4)$$

in which K is the coefficient of earth pressures, p is the horizontal, and q is the vertical soil stress. After the soil has been deposited, whether naturally or artificially, K becomes K_o, the coefficient of earth pressure at rest. If the active Rankine state of plastic equilibrium exists then the coefficient becomes K_A; if the passive then the coefficient becomes K_p.

2. The resistance to failure on the slip planes in the soil is assumed to follow Coulomb's equation

$$s = c + p_n \tan \phi \quad \ldots\ldots\ldots\ldots\ldots\ldots (7)$$

in which s is the ultimate shearing resistance of the soil, c refers to the soil cohesion and ϕ represents the soil's angle of internal friction.

3. For the active Rankine state of plastic equilibrium the slip planes make an angle of $45 + \frac{\phi}{2}$ with the horizontal direction.

4. The compressibility of the soil is negligible.

5. The failure mass can be treated as a rigid body.

6. Because the level of the water table is sufficiently far below the ground surface, no hydrostatic pressures have to be considered. It may reasonably be

---

5 "A Simple Method for Evaluating Blast Effects on Buildings," Review Edition, Armour Research Foundation, July, 1954.

6 "Effects of Nuclear Weapons," U. S. Govt. Printing Office, 1957.

7 "Soil Mecahnics in Engineering Practice," by K. Terzaghi and R. B. Peck Wiley, New York, N. Y., 1956.

8 "Theoretical Soil Mechanics," by K. Terzaghi, Wiley, New York, N. Y., 1956.

9 "Stress Distribution in Dry and in Saturated Sand Above a Yielding Trap Door," K. Terzaghi, Proceedings, Internatl. Conference on Soil Mechanics, Cambridge, Mass., Vol. 1, 1936, pp. 307-311.

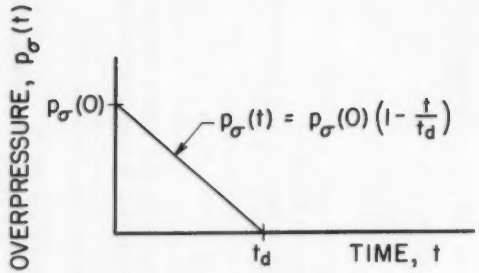

FIG. 1.—ASSUMED OVERPRESSURE-TIME RELATIONSHIP

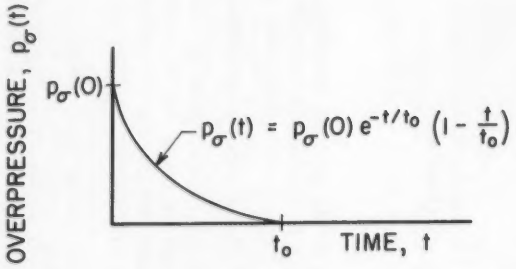

FIG. 2.—ACTUAL OVERPRESSURE-TIME RELATIONSHIP RELATIONSHIP

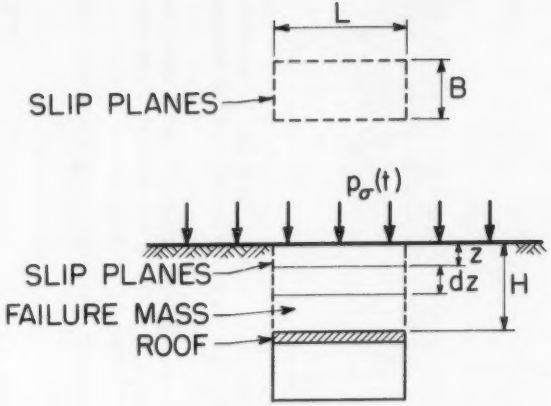

FIG. 3.—ASSUMED SLIP PLANES FOR RECTANGULAR ROOF

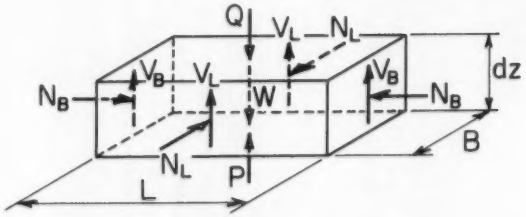

FIG. 4.—FREE-BODY DIAGRAM OF SLICE THROUGH FAILURE MASS FOR RECTANGULAR ROOF

assumed that ground water has no effect if its level is below the structural element being considered. If the water table is above the element it may be assumed that the element is subjected to hydrostatic pressure, that is, the stress will be equal to the overpressure, $p_\sigma(t)$, in the soil in all directions.

Structure.—The mode of failure for a structural element is assumed to be rigid body motion parallel to its initial position. For shear failure this mode is essentially correct while for bending failure it is at best an approximation. Two parameters define the structural elements. These are the ultimate resistance, p_m, and the maximum plastic displacement, x_m.

The ultimate resistance of structural elements, such as walls and roofs, may be determined by standard analytical techniques. A rigid plastic resistance is assumed for these elements and, therefore, it is necessary to consider only the maximum resistance under uniform load. This resistance, p_m, is expressed in units of pressure (pounds per square feet).

It is suggested that x_m be set equal to the maximum allowable displacement for a shear mode of failure and equal to one-half of the maximum displacement for bending failure. This assumption is based on the desire to conserve the displaced volume. It should be pointed out that the maximum displacements being considered are those associated with complete failure, not merely initial signs of failure such as cracking.

ANALYTICAL DEVELOPMENT

Roof Failure.—The dashed lines in Fig. 3 indicate the selected slip planes. The failure mass in this case is that enclosed by the dashed lines, the roof and the ground surface. A free body diagram for a horizontal slice of the failure mass is shown in Fig. 4 and the forces shown are evaluated as follows:

1. Q is the force acting on the top of the slice, σ_v is the vertical stress in soil, L is the length of the wall or roof, and B is a structural dimension.

$$Q = \sigma_v \, L \, B \quad \ldots\ldots\ldots\ldots\ldots\ldots \quad (8)$$

2. P is the force acting on the bottom of the slice and z is the variable soil depth.

$$P = \left[\sigma_v + \frac{\partial \sigma_v}{\partial z} \, dz\right] L \, B \quad \ldots\ldots\ldots\ldots\ldots \quad (9)$$

3. W is the weight of the slice of the failure mass and γ is the unit weight of the soil.

$$W = \gamma \, L \, B \, dz \quad \ldots\ldots\ldots\ldots\ldots\ldots \quad (10)$$

4. The forces V_L and V_B are the shearing forces on the vertical faces of the slice of failure mass. It is assumed that the normal stress on these faces is equal to $K \sigma_v$ according to Eq. 4. Hence

$$V_L = c \, L \, dz + L \, dz \, K \sigma_v \tan \phi \quad \ldots\ldots\ldots\ldots\ldots \quad (11)$$

and

$$V_B = c\ B\ dz + B\ dz\ K\ \sigma_v \tan \phi \quad \ldots\ldots\ldots\ldots (12)$$

5. The forces N_L and N_B are the normal forces on the vertical faces and their effect in resisting motion is included in Eqs. 11 and 12.

The solution of the equation of motion of this slice of the "failure mass" gives the relations between the various parameters that determine the failure of the roof. Using x to represent the vertical motion of the slice this equation of motion is

$$Q + W - P - 2\ V_B - 2\ V_L = \frac{W}{32.2} \frac{d^2x}{dt^2} \quad \ldots\ldots\ldots\ldots\ldots (13)$$

where Q, P, W, V_L, V_B are given by Eqs. 8, 9, 10, 11, and 12 and x is the displacement of the failure mass. Substituting these expressions into Eq. 13 yields

$$\frac{\partial \sigma_v}{\partial z} + \frac{2\ \sigma_v\ K \tan \phi}{L'} = \gamma - \frac{2\ c}{L'} - \frac{d^2x}{dt^2} \frac{\gamma}{g} \quad \ldots\ldots\ldots\ldots (14)$$

in which L' is the structural parameter. Since it is assumed that the failure mass undergoes rigid body motion the parameter x is independent of z. Therefore Eq. 14 becomes an ordinary differential equation in σ_v and z. Solving for σ_v (z,t) and imposing the boundary conditions

$$\sigma_v\ (0, t) = p_\sigma(t)$$

$$\sigma_v\ (H, t) = p_m$$

and rearranging we get

$$144\ p_\sigma(t) = \frac{\gamma H}{r g} \left[e^r - 1\right] \ddot{x}(t) + p_m\ e^r + \frac{H}{r} \left[\frac{2\ c}{L'} - \gamma\right] \left[e^r - 1\right] \quad \ldots\ldots (15)$$

in which

$$L' = \frac{L\ B}{L + B} \quad \ldots\ldots\ldots\ldots\ldots (16a)$$

$$r = \frac{2\ K\ H \tan \phi}{L'} \quad \ldots\ldots\ldots\ldots\ldots (16b)$$

and

$$\ddot{x}(t) = \frac{d^2x}{dt^2} \quad \ldots\ldots\ldots\ldots\ldots (16c)$$

and in which H is the soil depth to the top of the structure, r is a dimensionless parameter, and $\ddot{x}$ is the acceleration of the failure mass of the soil. Eq. 15 is of the form

$$D\ddot{x} + E = F\left(1 - \frac{t}{t_d}\right) \quad \ldots\ldots\ldots\ldots\ldots\ldots (17)$$

in which D, E and F are constants. With the initial conditions $x(0) = \dot{x}(0) = 0$, where $\dot{x}$ is the velocity of the failure mass of the soil. The closed form solution of Eq. 17 is

$$\left[\frac{T'}{t_d}\right]^2 = \frac{1}{4}\left(\frac{F}{E}\right)^2 - \frac{1}{3}\frac{F}{E} \quad \text{for } \frac{F}{E} \geq 2 \quad \ldots\ldots\ldots\ldots (18a)$$

$$\left[\frac{T'}{t_d}\right]^2 = \frac{4}{3}\frac{F}{E}\left[1 - \frac{E}{F}\right)^3 \quad \text{for } 1 \leq \frac{F}{E} \leq 2 \quad \ldots\ldots\ldots\ldots (18b)$$

where the pseudo-period, T', is defined as

$$T' = \sqrt{\frac{2\,D\,x_m}{E}} \quad \ldots\ldots\ldots\ldots\ldots\ldots (19)$$

A comparison of Eq. 15 with Eq. 17 shows that

$$D = \frac{\gamma H}{r g}\left[e^r - 1\right] \quad \ldots\ldots\ldots\ldots\ldots\ldots (20)$$

$$E = p_m e^r + \frac{H}{r}\left[\frac{2c}{L'} - \gamma\right]\left[e^r - 1\right] \quad \ldots\ldots\ldots\ldots (21)$$

and

$$F = 144\, p_\sigma(o) \quad \ldots\ldots\ldots\ldots\ldots\ldots (22)$$

Hence by substituting Eqs. 20, 21, 22 into Eqs. 18 we obtain the solution of Eq. 15. When the duration is infinite the overpressure is constant with time and so the peak overpressure required to cause a failure of the roof is given by

$$144\, \bar{p}_\sigma(o) = E \quad \ldots\ldots\ldots\ldots\ldots\ldots (23)$$

For convenience the closed form solution given by Eqs. 18 has been shown graphically in Fig. 5 with the substitution of $\frac{p_\sigma(o)}{\bar{p}_\sigma(o)}$ for $\frac{E}{F}$, in which $\bar{p}_\sigma(o)$ is the initial overpressure for infinite duration. Using Eq. 19 for T' and Eq. 23 for $\bar{p}_\sigma(o)$ then the peak overpressure $p_\sigma(o)$ of the overpressure-time history required to fail the structure for any duration t_d may be determined from Fig. 5.

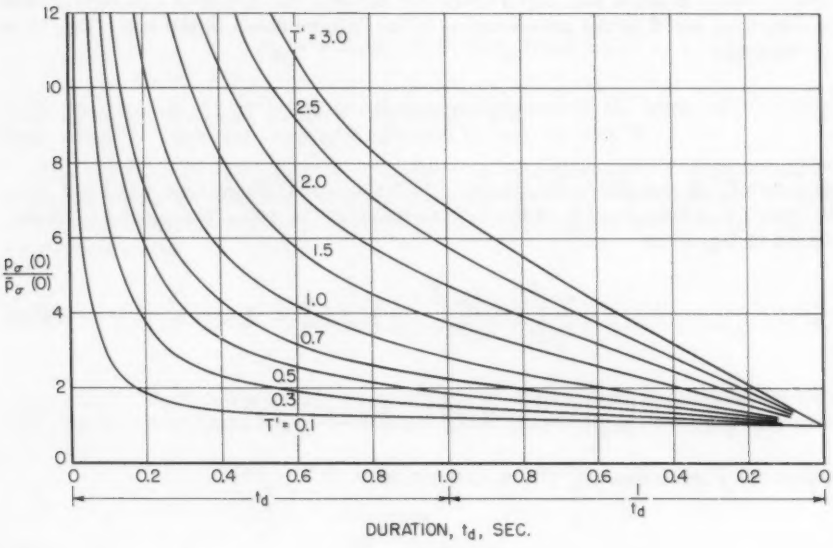

FIG. 5.—EFFECT OF DURATION ON PEAK OVERPRESSURE REQUIRED TO FAIL STRUCTURE

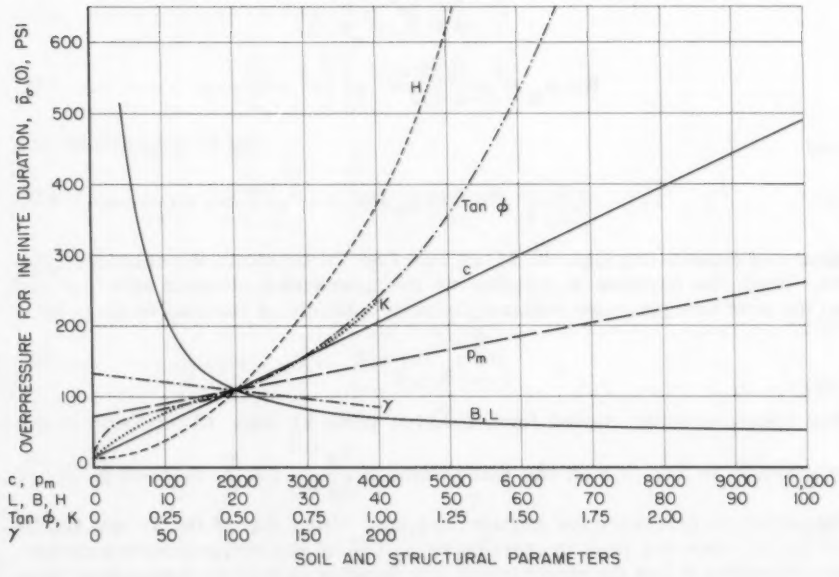

FIG. 6.—ROOF FAILURE-VARIATIONS OF OVERPRESSURE, $\bar{p}$ (0), WITH SOIL AND STRUCTURAL PARAMETERS

In order to demonstrate the effects of each of the parameters on $\overline{p}_\sigma(o)$ and T', Figs. 6 and 7 have been prepared. Representative values of each of the parameters were selected. These values are as follows: c = 2000 psf; tan ϕ = 0.5; K = 1/2; γ = 100 pcf; p_m = 2000 psf; x_m = 1 ft; and H = B = L = 20 ft.

The curves in Figs. 6 and 7 were obtained by varying the parameters one at a time while holding the others fixed at the selected representative values previously listed.

Wall Failure.—The dashed lines in Fig. 8 indicate the selected slip planes. The failure mass in this case is that enclosed by the dashed lines, the wall, and the ground surface. In deriving the equation of motion the failure mass is divided into two parts, the upper mass M_1 and the lower mass M_2.

The equation of motion of M_1 is exactly the same as that of the failure mass associated with roof failure, Eq. 15, with B replaced by $H_1 \tan (45 - \phi/2)$ and p_m replaced by p_t, the normal stress between failure masses M_1 and M_2.

The equation of motion of M_2 is determined with the following assumptions (Fig. 9).

1. The mass M_2 may be treated as a rigid body.
2. The direction of motion is parallel to the inclined face of M_2.
3. The vertical component of motion is equal to that of M_1.
4. There are no shear forces induced on the common surface between M_1 and M_2.
5. The vertical stress and hence the horizontal stress is constant throughout the failure mass M_2. The value of the vertical stress is assumed to be equal to the stress acting on the top surface of the failure mass.
6. The normal force Q is given by

$$Q = p_t L H_1 \tan (45 - \phi/2) \quad \ldots\ldots\ldots\ldots\ldots\ldots (24)$$

in which H_1 is the height of the wall.

7. The normal force N_2 is given by

$$N_2 = K p_t \left[\frac{1}{2} H_1^2 \tan (45 - \phi/2)\right] \quad \ldots\ldots\ldots\ldots (25)$$

8. The induced shear forve V_2 parallels the direction of motion and is given by

$$V_2 = (c + K p_t \tan \phi) \left[\frac{1}{2} H_1^2 \tan (45 - \phi/2)\right] \quad \ldots\ldots\ldots (26)$$

9. The resistance of the wall p_m acts normal to the wall, which means that there are no shear forces along the surface of the wall. The force R, the wall resistance, is related to p_m by

$$R = p_m (L H_1) \quad \ldots\ldots\ldots\ldots\ldots\ldots (27)$$

10. The force V_1 is related to the force N_1 by Coulomb's equation (Eg. 7). The magnitude of these forces are selected so as to satisfy the equilibrium requirements of M_2.

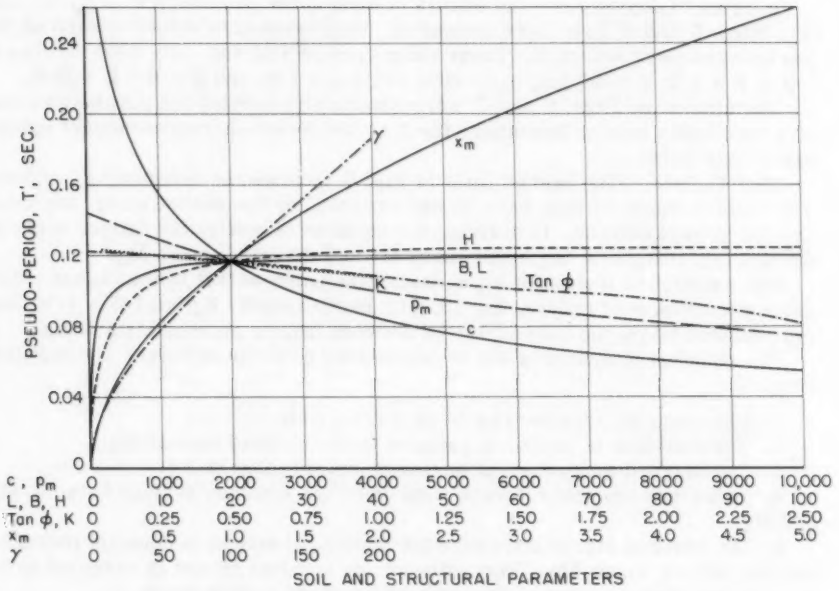

FIG. 7.—ROOF FAILURE-VARIATIONS OF PSEUDO PERIOD, T', WITH SOIL AND STRUCTURAL PARAMETERS

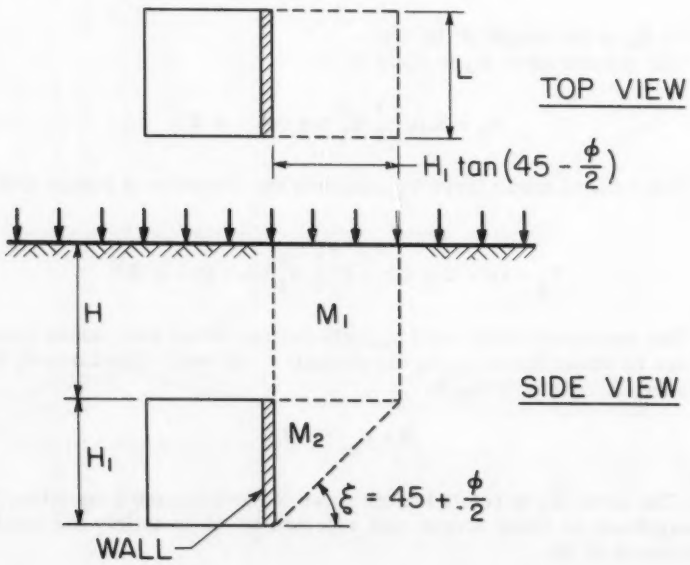

FIG. 8.—ASSUMED SLIP PLANES FOR RECTANGULAR WALL

On the basis of these assumptions an equation of motion for M_1 and M_2 may be written that relates the resistance of the wall p_m to the overpressure $p_\sigma(t)$. This equation is

$$144\, p_\sigma(t) = \frac{L'}{2\, K\, m}\left[\gamma - \frac{2\,c}{L'} - \frac{\gamma}{g}\,\ddot{x}\,(t)\right]\left[e^r - 1\right]\left[\frac{\cos\,(45 - \phi/2)}{\tan\,\phi} - \frac{K\,H_1}{L}\right.$$

$$\left. - \sin\,(45 - \phi/2)\right] - \frac{c\,e^r}{m}\left[\frac{1}{\sin\,(45 - \phi/2)} + \frac{H_1}{L}\right] + \frac{\cos\,(45 - \phi/2)\,e^r}{m}\left\{\frac{\gamma\,H_1}{2} - p_m\right.$$

$$\left.\left[1 + \frac{\tan\,\phi}{\tan\,(45 - \phi/2)}\right] - \frac{\gamma\,H_1\,\ddot{x}\,(t)}{2\,g\cos\,(45 - \phi/2)} - \frac{1}{2}\gamma\,H_1\tan\,\phi\,(45 - \phi/2)\right\} \quad ..(28)$$

where

$$L' = \frac{L\,H_1\tan\,(45 - \phi/2)}{L + H_1\tan\,(45 - \phi/2)} \quad \ldots\ldots\ldots\ldots (29a)$$

$$r = \frac{2\,K\,H\tan\,\phi}{L'} \quad \ldots\ldots\ldots\ldots\ldots\ldots (29b)$$

and

$$m = \frac{K\,H_1\tan\,\phi}{L} - \cos\,(45 - \phi/2) + \tan\,\phi\,\sin\,(45 - \phi/2) \quad \ldots (29c)$$

and in which m is a dimensionless parameter.

For a triangular overpressure-time history this equation can be written in the form given by Eq. 17 where

$$D = \frac{L'\,\gamma}{2\,K\,g\,m}\left[e^r - 1\right]\left[\frac{K\,H_1}{L} - \frac{\cos\,(45 - \phi/2)}{\tan\,\phi} + \sin\,(45 - \phi/2)\right]$$

$$- \frac{e^r}{m}\left[\frac{\gamma\,H_1}{2\,g}\right] \quad \ldots\ldots\ldots\ldots\ldots\ldots\ldots\ldots\ldots\ldots\ldots\ldots\ldots\ldots\ldots\ldots\ldots\ldots (30)$$

and

$$E = \frac{L'}{2\,K\,m}\left[\gamma - \frac{2\,c}{L'}\right]\left[e^r - 1\right]\left[\frac{\cos\,(45 - \phi/2)}{\tan\,\phi} - \frac{K\,H_1}{L} - \sin\,(45 - \phi/2)\right]$$

$$- \frac{c\,e^r}{m}\left[\frac{1}{\sin\,(45 - \phi/2)} + \frac{H_1}{L}\right] + \frac{\cos\,(45 - \phi/2)\,e^r}{m}\left\{\frac{\gamma\,H_1}{2} - p_m\right.$$

$$\left.\left[1 + \frac{\tan\,\phi}{\tan\,(45 - \phi/2)}\right] - \frac{1}{2}\gamma\,H_1\tan\,\phi\,\tan\,(45 - \phi/2)\right\} \quad \ldots\ldots\ldots\ldots\ldots (31)$$

in which L', r and m are as previously defined

$$F = 144\, p_\sigma(o) \quad \ldots\ldots\ldots\ldots\ldots\ldots (32)$$

When the duration is infinite the overpressure is constant with time and so the peak overpressure required to fail the wall is given by:

$$144\, \bar{p}_\sigma(o) = E \quad \ldots\ldots\ldots\ldots\ldots\ldots (33)$$

As for the roof analysis, Fig. 5 presents the ratio $\frac{p_\sigma(o)}{\bar{p}_\sigma(o)}$ as a function of the duration, t_d, and pseudo-period, T', in which T' is defined by Eq. 19, using Eqs. 30 and 31 for D and E.

In order to demonstrate the effects of each of the parameters on $\bar{p}g(o)$ and T', Figs. 10 and 11 have been prepared. The following representative values

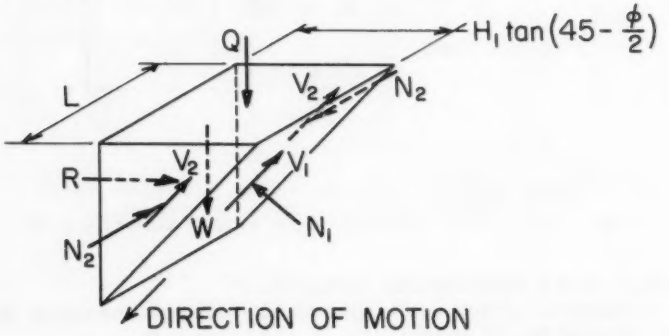

FIG. 9.—FREE-BODY DIAGRAM OF LOWER FAILURE MASS, M_2

of each of the parameters were selected: c = 2000 psf; ϕ = 20°; K = 1/2; γ = 100 pcf; p_m = 2000 psf; x_m = 1 ft; H = 5 ft; H_1 = 20 ft; and L = 20 ft.

The curves in Figs. 10 and 11 were obtained by varying the parameters one at a time while holding the others fixed at the selected representative values listed above.

APPLICATIONS

There are two major applications of the analysis presented in the preceding sections. One is the analysis of a given structure, that is the determination of the overpressure-time history required to fail a particular underground structure in a given location. It should be noted that the overpressure-time history is completely described by the peak overpressure and the duration. The other application is to design an underground structure to withstand a prescribed overpressure-time history.

Analysis.—Where a structure has more than one element to be analyzed, for example, a roof and two dissimilar walls, each element should be analyzed independently. In this case the lowest peak overpressure for a given duration, obtained considering failure of each of the structural elements, is considered to

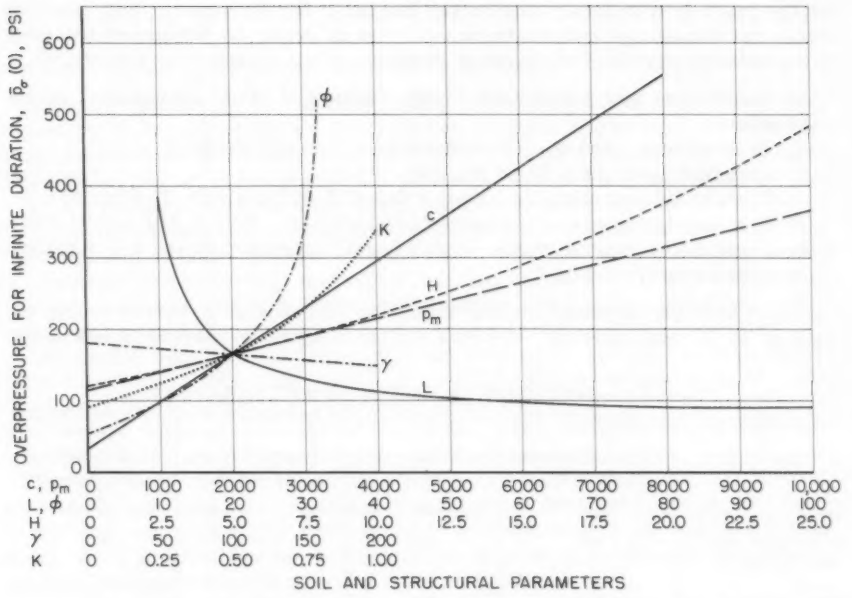

FIG. 10.—WALL FAILURE-VARIATIONS OF OVERPRESSURE, $\bar{p}$ (0), WITH SOIL AND STRUCTURAL PARAMETERS

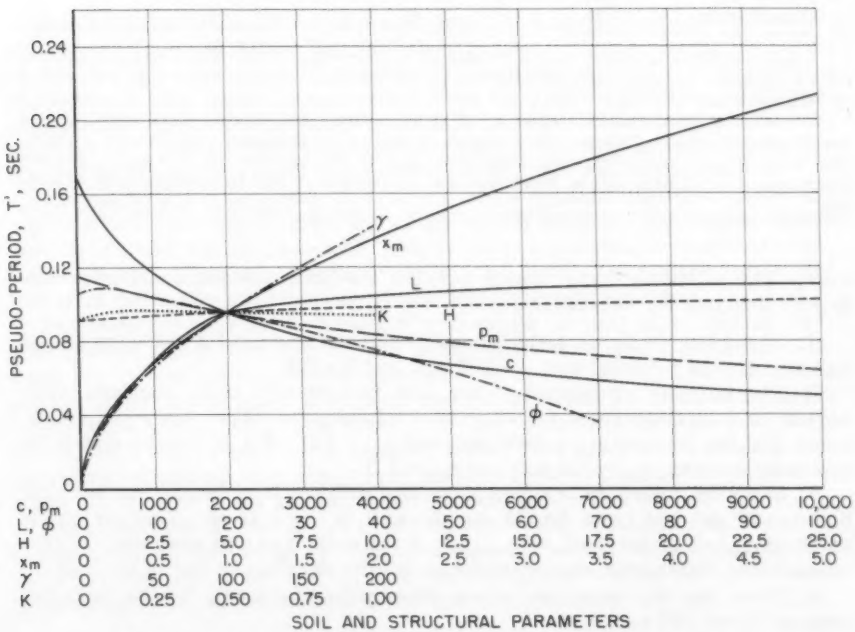

FIG. 11.—WALL FAILURE-VARIATIONS OF PSEUDO PERIOD, T', WITH SOIL AND STRUCTURAL PARAMETERS

be the peak overpressure that causes failure of the structure. The following steps outline the procedure to be followed in order to determine the peak overpressure-duration relationship required to fail a particular structure.

1. Select the soil properties (from Table 1 if other information is not available).
2. Determine p_m and x_m for each element being considered.
3. Compute $\bar{p}_\sigma(o)$ (Eq. 23 or Eq. 33)
4. For the element with the lowest value of $\bar{p}_\sigma(o)$ compute T' (Eq. 19).
5. For any t_o, t_d may be computed from Eq. 3. With $\bar{p}_\sigma(o)$ and T' from steps 3 and 4, the overpressure needed to fail the structure for any duration, t_o, may be found from Fig. 5.

As an example, consider a cubic structure 10 ft on a side, buried so that the roof is 15 ft underground. The soil surrounding the structure is soft moist

TABLE 1.—APPROXIMATE VALUES OF SOIL PARAMETERS

Type of Soil	Angle of internal friction, ϕ in degrees	Soil cohesion, c in psf	Density,[a] in lbs per cu ft	Coefficient of earth pressure K[b]
Soft moist clay	10	400	100	0.7
Medium moist clay	10	800	100	0.7
Stiff moist clay	10	1500	100	0.7
Hard clay	10	4000	100	0.7
Sandy loam	25	400	100	0.6
Dry loose sand	30	0	100	0.5
Dry dense sand	35	0	100	0.6

[a] Soil densities normally have a relatively narrow range. For this reason, and since this parameter has only limited influence on the results, a single value of 100 lb per cu ft was selected.

[b] It will be noted that the values for K given in this table are less than unity. Based on Terzaghi's paper, "Stress Distribution in Dry and in Saturated Sand Above a Yielding Trap Door," one might expect the value of K to exceed unity for dry sand. For the purposes of this table, values which would be conservative for design have been selected.

clay. The following steps, which parallel the previous sequence, show the failure analysis for this example.

1. According to Table 1 the values of soil parameters for soft clay are as follows: $\phi = 10°$; c = 400 psf; $\gamma = 100$ pcf; and K = 0.6.
2. The ultimate resistance of the roof is computed from standard techniques or estimated from known design information. For this example assume that for the roof $p_m = 1400$ psf, and $x_m = 1$ ft. For the wall assume the following values: $p_m = 800$ psf; and $x_m = 1$ ft.
3. Using the values determined above one obtains, from Eq. 23, for the roof $\bar{p}_\sigma(o) = 27$ psi and from Eq. 33, for the wall, $\bar{p}_\sigma(o) = 48$ psi. Comparing the value of $\bar{p}_\sigma(o)$ of the roof with $\bar{p}_\sigma(o)$ of the wall, it can be seen that for this example the lower peak overpressure at infinite duration is that of the roof.
4. From Eq. 19, using the values determined previously for the roof, one obtains T' = 0.183 sec.

5. Assume the duration is t_o equals 2 sec. Then from Eq. 3, t_d equals 1.47 sec and from Fig. 5, $p_\sigma(o)$ = 34 psi. This step can be repeated as often as possible to obtain other combinations of duration and overpressure.

Design.—Application of the analytical procedure to design is probably best treated by an iterative process. The first trial design may be made by conventional methods based on cost, use, etc. This structure may then be subjected to the method of analysis previously outlined. If the analysis shows that the structure does not have the desired resistance the design can be modified and the analysis repeated until a design is obtained that satisfied the requirements. The preceding example problem can thus serve as an example of design. Based on assumed values for p_m and x_m, a relationship between overpressure and duration can be established. If this overpressure and duration satisfies the design requirements then the assumed values of p_m and x_m are satisfactory.

One useful simplification results if the loading is considered to be of infinite duration. Under this condition inertial effects, as given by T', are eliminated, the arithmetic is simplified, and the results are conservative. In other words, a structure designed for 50 psi by this method could be expected to withstand well over 50 psi for any real condition.

Extensions of the theory have been made to non-flat roof or wall surfaces, such as arches, domes and cylinder. The approach used for these shapes was to define an equivalent flat surface and to proceed exactly as indicated in this paper. Such applications can be considered, at best, to be suitable for interim use until further research provides a better solution.

CONCLUSIONS

The methods outlined in this paper are based on the assumption that the soil parameters are known and that they remain constant during the entire loading process. No account is taken of non-uniformity of soil or possible variations in soil shear parameters during the yielding process. It is quite possible that stress distributions in the soil may vary continuously as yielding takes place. In cases where any of these effects are very pronounced the analytical methods given might not be expected to give sensible results.

The analytical approaches in this paper are dynamic modifications of accepted static analyses.[8] Even for static conditions these approaches represent simplifications introduced in order to make it possible to arrive at a solution. Certainly questions arise regarding the location of failure planes, behavior of the failing structural elements, and behavior of the soil.

The work reported by K. Terzaghi[9] represents the only experimental study known to the authors for the static conditions. These experiments form the basis for Terzaghi's theoretical approach, which was modified for use in this paper. Based on this paper one might also conclude that the value of K for dry sand should excess unity. Application of this value for K is questionable and the values recommended in this paper (Table 1) were selected so as to be conservative for design. The uncertainty in these values should be noted however since the value of K has an important influence on the results.

Therefore, the method of this paper should only be considered as a first approximation for the design or analysis of underground structures subjected to air overpressure. Future work, both theoretical and experimental can be expected to provide improvements in the analysis presented herein.

ACKNOWLEDGMENTS

The research reported on in this paper is a modification of work originally conducted at The Armour Research Foundation under contract with the United States Air Force, Dept. of Defense. The authors wish to express their appreciation to the Air Force for permission to publish this paper.

APPENDIX.—NOTATION

The following is a list of symbols and units used in the analysis.

B	= structural dimension, in feet
c	= soil cohesion, in pounds per square feet
D, E, F	= constants
g	= acceleration of gravity, in feet per square second
H	= soil depth to top of structure, in feet
H_1	= height of wall, in feet
K	= coefficient of earth pressure
K_A	= coefficient of active earth pressure
K_O	= coefficient of earth pressure at rest
K_p	= coefficient of passive earth pressure
L	= length of wall or roof, in feet
L'	= structural parameter, in feet
m	= dimensionless parameter
M_1, M_2	= soil failure masses
N_1, N_2, N_L, N_B	= normal forces on slip planes, in pounds
P	= force on bottom of horizontal soil slice, in pounds
p	= horizontal soil stress, in pounds per square foot
p_m	= resistance of structural element, in pounds per square foot
p_t	= normal stress between failure masses M_1 and M_2, in pounds per square foot
$p_\sigma(t)$	= time varying overpressure, in pounds per square inch
$p_\sigma(o)$	= initial peak overpressure for duration, t_d, in pounds per square inch
$\bar{p}_\sigma(o)$	= initial overpressure for infinite duration, in pounds per square inch
q	= vertical soil stress, in pounds per square foot

Q	= force on top of horizontal soil slice, in pounds
R	= wall resistance, in pounds
r	= dimensionless parameter
s	= ultimate shearing resistance of soil, in pounds per square foot
t	= time, in seconds
t_o	= duration of actual overpressure, in seconds
t_d	= duration of linearized overpressure, in seconds
T'	= pseudo-period, in seconds
V_1, V_2, V_L, V_B	= shearing forces on the failure masses, in pounds
W	= weight of horizontal soil slice, in pounds
x	= displacement of failure mass, in feet
x_m	= maximum plastic displacement of structural element, in feet
$\dot{x}$	= velocity of failure mass of soil, in feet per second
$\ddot{x}$	= acceleration of failure mass of soil, in feet per square second
z	= variable soil depth, in feet
γ	= unit weight of soil, pounds per cubic foot
σ_v	= vertical stress in soil, in pounds per square foot
ϕ	= angle of internal friction of soil, in degrees

Journal of the
ENGINEERING MECHANICS DIVISION
Proceedings of the American Society of Civil Engineers

GEOMETRY OF MOIRÉ FRINGES IN STRAIN ANALYSIS

by Stanley Morse,[1] August J. Durelli,[2] and Cesar A. Sciammarella[3]

SYNOPSIS

This paper shows how moiré fringes can be used in the two-dimensional analysis of strains. The fundamental equations of the moiré method are derived and are presented in the form of graphs by means of which strains and rotations can be obtained from simple measurements with a minimum of computation.

INTRODUCTION

The moiré or watered-silk effect is an optical phenomenon produced when two somewhat similar arrays of dots or lines are superimposed, resulting in the formation of alternating light and dark fringes. It is an effect common in everyday life, being seen in mismatched window screens, as the "Venetian-blind" defect in television, and so forth.

Note.—Discussion open until January 1, 1961. To extend the closing date one month, a written request must be filed with the Executive Secretary, ASCE. This paper is part of the copyrighted Journal of the Engineering Mechanics Division, Proceedings of the American Society of Civil Engineers, Vol. 86, No. EM 4, August, 1960.

[1] Associate Engineer, Mechanics Research Div., Armour Research Foundation, Chicago, Illinois.

[2] Professor in Civil Engineering, Illinois Institute of Technology and Supervisor, Stress Analysis, Armour Research Foundation, Chicago, Illinois.

[3] Associate Research Engineer, Illinois Institute of Technology, Chicago, Illinois.

Because the fringes are the result of displacement of the elements of the two arrays with respect to each other, the moiré effect is obviously a tool by which strain measurements can be made. If, for example, one begins with two identical sets of straight, parallel lines, fringes are produced by either rotation (Fig. 1(a)) or elongation (Fig. 1(b)) of one set with respect to the other.

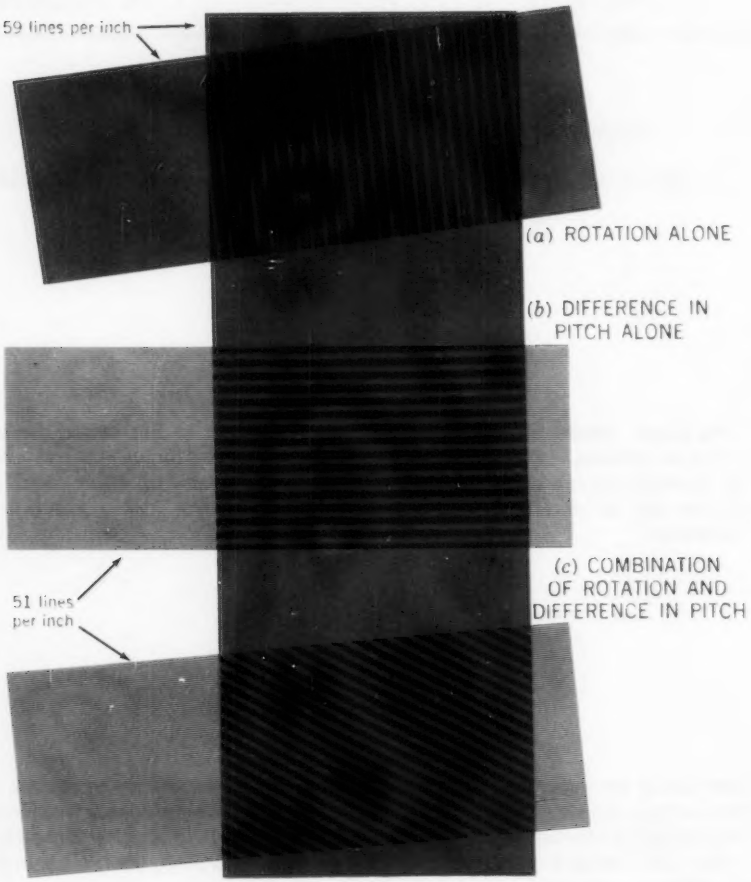
59 lines per inch
(a) ROTATION ALONE
(b) DIFFERENCE IN PITCH ALONE
51 lines per inch
(c) COMBINATION OF ROTATION AND DIFFERENCE IN PITCH

FIG. 1.—MECHANISM OF FORMATION OF MOIRÉ FRINGES

Simple equations govern the interpretation of pure rotations and elongations. Within the limits of small deformations, these effects can be considered to be linear and capable of being superimposed. A number of papers have been published under these assumptions, notably by R. Weller and M. Shepard[4] and by P. Dantu.[5]

[4] "Displacement Measurements by Technical Interferometry," by R. Weller and B. M. Shepard, Proc. S.E.S.A., No. 1, 1948.

[5] "Utilization des Reseau pour l'etude des Deformations," by P. Dantu, Laboratoire Central des Ponts et Chaussees, Paris, Publication 57-6, 1957.

Actually, the moiré effect is not limited in any way to separate rotations and elongations nor to infinitesimal deformations. Neither is it necessary that the arrays be originally identical in either spacing or orientation.

In this paper only sets of straight, parallel, nondiffracting lines will be considered. However, moiré fringes that can be analyzed could be obtained from circular, radial, or other nonparallel arrays, and diffraction gratings could be used under suitable conditions.

Fig. 1(c) shows the effect of combined rotation and differences in pitch of straight, parallel sets of lines representing a homogeneous field for which equations will be derived. The relationships so obtained can also be applied to sufficiently small elements of a nonhomogeneous field such as would be presented in a general two-dimensional strain problem.

The moiré method can certainly be used for the analysis of large strains and rotations, but such application is beyond the scope of this paper. However, the equations will be derived in the most general terms before being related to such specific quantities as strain. Approximations for the case of infinitesimal deformations will also be developed.

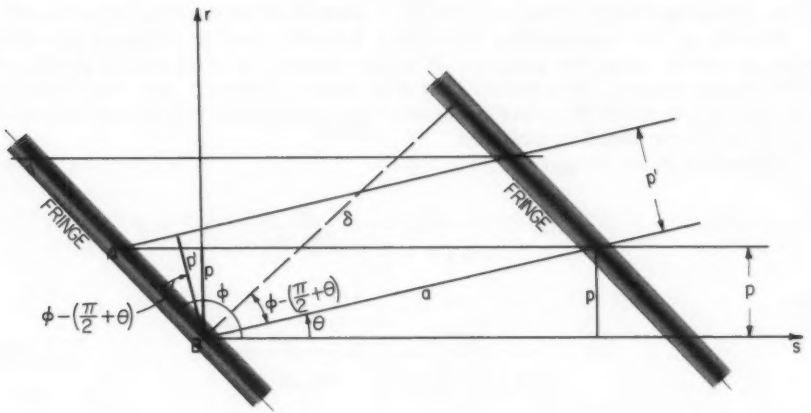

FIG. 2.—GEOMETRY OF MOIRÉ FRINGES

BASIC PROPERTIES AND DEFINITIONS

In the subsequent derivations, a fixed array of straight, parallel lines called the "master grid" is used as a reference both for analysis of the properties of the moiré and for establishment of coordinate directions. The center-to-center distance between the master grid lines is defined as the master pitch, p, and the directions perpendicular and parallel to these lines are designated as r and s, respectively.

The model also bears a similar array of lines which in the undistorted state are not necessarily of the same pitch as the master grid. The pitch of this grid at any particular point in any state of distortion is called the "model pitch" and is designated by p'.

The angle θ is defined as the acute angle at any point and in any given state of deformation measured from the fixed master grid lines to the model grid lines. The angle from the fixed master grid lines to a fringe at a point measured in the same direction as θ is designated as ϕ and may be either acute or obtuse. Fig. 2 shows how to obtain the inclination ϕ of the moiré fringes and their distances δ as functions of the master grid pitch p, the model grid pitch p', and the rotation θ of both grids at a point.

Let us assume either the case of a homogeneous deformation and rotation (which may be accompanied by translation) or of a sufficiently small element of a nonhomogeneous field. Equations relating any desired sets of parameters for the moiré phenomenon are easily derived from the simple geometry of fringe formation. Those for the normal fringe spacing, δ, and the fringe angle, ϕ, are perhaps the most fundamental. However, the information available for the analysis will usually be in the form of photographs on which δ and ϕ and the coordinate fringe spacings δ_r and δ_s can be measured, and the purpose of the analysis will be the determination of θ and p' at the desired points. Obviously, the master grid pitch, p , and the direction of its lines must be known.

Several of the expressions developed herewith can be obtained in other ways, some by using the property of moiré fringes of being loci of points of equal displacement. The derivations that follow, however, are very simple and general. Some of the curves representing relationship between parameters may prove to be useful in practice.

Inclination of the Fringes.

$$\overline{AB} = \frac{P}{\cos\left(\phi - \frac{\pi}{2}\right)} = \frac{P}{\sin \phi} \quad \ldots\ldots\ldots\ldots\ldots\ldots (1)$$

and

$$\overline{AB} = \frac{p'}{\cos\left(\phi - \frac{\pi}{2} - \theta\right)} = \frac{p'}{\sin (\phi - \theta)} \quad \ldots\ldots\ldots\ldots (2)$$

therefore

$$p' = p \frac{\sin (\phi - \theta)}{\sin \phi} \quad \ldots\ldots\ldots\ldots\ldots\ldots (3)$$

Because

$$p (\sin \phi \cos \theta - \sin \theta \cos \phi) = p' \sin \phi \quad \ldots\ldots\ldots (4)$$

then

$$\tan \phi = \frac{p \sin \theta}{p \cos \theta - p'} \quad \ldots\ldots\ldots\ldots\ldots\ldots (5)$$

Distance between Fringes.—Also from Fig. 2 and the foregoing:

$$a = \frac{p}{\sin \theta} \quad \ldots\ldots\ldots\ldots\ldots\ldots\ldots (6)$$

and

$$\delta = a \cos\left(\phi - \frac{\pi}{2} - \theta\right) = \frac{p \sin (\phi - \theta)}{\sin \theta} = \frac{p' \sin \phi}{\sin \theta} \quad \ldots\ldots\ldots (7)$$

From Eq. 5:

$$\sin \phi = \frac{p \sin \theta}{\sqrt{p^2 \sin^2 \theta + (p \cos \theta - p')^2}} \quad \ldots\ldots\ldots (8)$$

and

$$\delta = \frac{p\, p'}{\sqrt{p^2 \sin^2 \theta + (p \cos \theta - p')^2}} \quad \ldots\ldots\ldots (9)$$

Rotation in Terms of the Inclination of the Fringes and their Spacing.— From Eq. 7:

$$\frac{\delta}{p} \sin \theta = \sin (\phi - \theta) = \sin \phi \cos \theta - \cos \phi \sin \theta \quad \ldots\ldots (10)$$

and

$$\tan \theta = \frac{\sin \phi}{\frac{\delta}{p} + \cos \phi} \quad \ldots\ldots\ldots\ldots\ldots (11)$$

To represent graphically the relationship between θ and ϕ it is convenient to introduce the following definitions:

$$\alpha_\delta = \frac{\delta}{p} \tan \theta = \frac{\delta}{p}\left[\frac{\sin \phi}{\frac{\delta}{p} + \cos \phi}\right] = \frac{\sin \phi}{1 + \frac{p}{\delta} \cos \phi} \quad \ldots\ldots\ldots (12)$$

and

$$\tan \theta = \alpha_\delta \frac{p}{\delta} \quad \ldots\ldots\ldots\ldots\ldots\ldots (13)$$

Values of α_δ for the entire possible range of ϕ (0° to 180°) and for various values of δ/p are plotted in Fig. 3, permitting easy determination of the model rotation at a point without knowledge of p', the model pitch.

Model Pitch in Terms of ϕ and δ.—Again, from Eq. 7:

$$p' = \frac{\delta \sin \theta}{\sin \phi} \quad \ldots\ldots\ldots\ldots\ldots\ldots (14)$$

From Eq. 11:

$$\sin \theta = \frac{\sin \phi}{\sqrt{\sin^2 \phi + \left(\frac{\delta}{p} + \cos \phi\right)^2}} \quad \ldots\ldots\ldots (15)$$

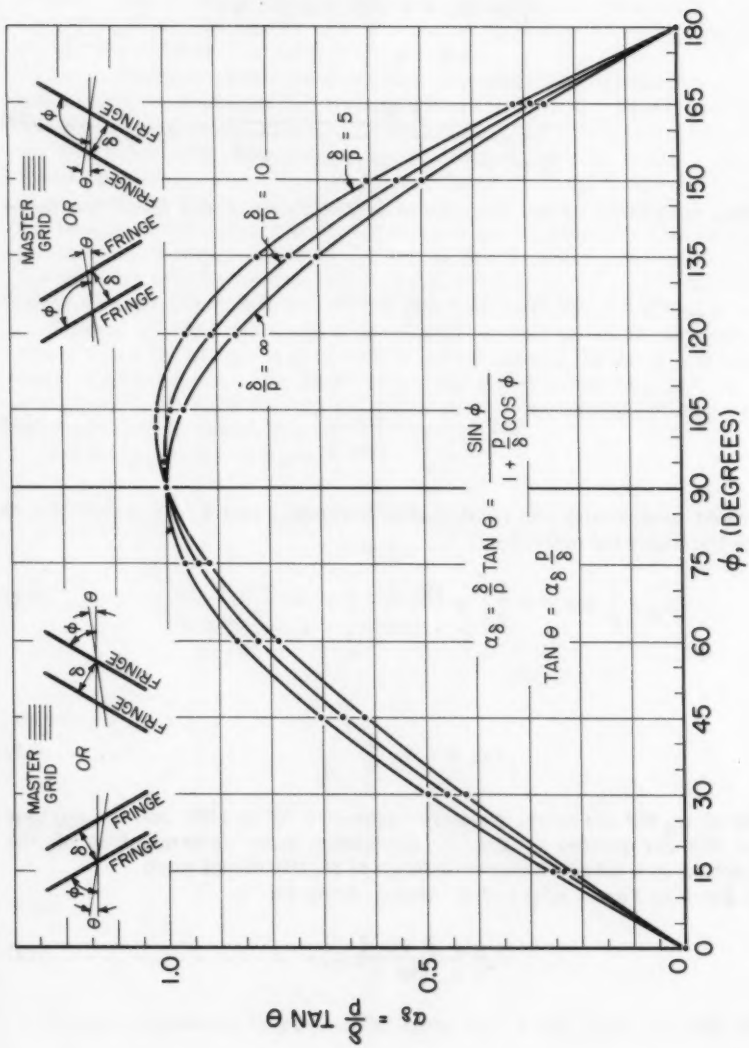

FIG. 3.—ROTATION AS A FUNCTION OF FRINGE ANGLE AND NORMAL FRINGE SPACING

$$p' = \frac{\delta}{\sqrt{1 + \left(\frac{\delta}{p}\right)^2 + 2\left(\frac{\delta}{p}\right)\cos\phi}} \quad \ldots\ldots\ldots\ldots (16)$$

and

$$\frac{p}{p'} = \sqrt{\left(\frac{p}{\delta}\right)^2 + 2\left(\frac{p}{\delta}\right)\cos\phi + 1} \quad \ldots\ldots\ldots\ldots (17)$$

Determination of "True" and "Conventional" Strains.—To compute the value of the strain using the measured quantities δ and ϕ, a graphical construction can be utilized. For this construction it is convenient to introduce the following definitions:

$$\beta_\delta = \frac{\delta}{p}\left(1 - \frac{p}{p'}\right) = \frac{\delta}{p}\left[1 - \sqrt{\left(\frac{p}{\delta}\right)^2 + 2\left(\frac{p}{\delta}\right)\cos\phi + 1}\right] \ldots\ldots (18)$$

and

$$\epsilon_{r\ true} = 1 - \frac{p}{p'} = \frac{p' - p}{p'} = \beta_\delta\left(\frac{p}{\delta}\right) \ldots\ldots\ldots\ldots (19)$$

Values of β_δ for all possible values of ϕ and for various values of δ/p have been plotted in Fig. 4, permitting easy determination of the model pitch, pitch ratio, or the quantity $1 - (p/p')$ free from the influence of rotation. It should be noted that $1 - (p/p')$ is the "true" strain perpendicular to the direction of the master grid lines if p and p' were originally equal before distortion of the model.

If Eq. 19 is converted to the form:

$$\epsilon_r = \frac{p'}{p} - 1 = \frac{p' - p}{p} = \frac{\frac{\beta_\delta\, p}{\delta}}{1 - \frac{\beta_\delta\, p}{\delta}} \quad \ldots\ldots\ldots\ldots (20)$$

we obtain the "conventional" or "nominal" strain perpendicular to the direction of the master grid lines.

Rotation in Terms of ϕ and Distance between Fringes along the Coordinate Directions.—In many cases it may be preferred to measure the fringe spacing along the coordinate directions or it may be desirable to have a second method for checking the model rotations. From Fig. 5 we have, for the two cases (a) ϕ acute, and (b) ϕ obtuse, respectively:

$$\delta = \delta_s \sin\phi \quad \ldots\ldots\ldots\ldots (21a)$$

and

$$\delta = \delta_s \sin(\pi - \phi) = \delta_s \sin\phi \quad \ldots\ldots\ldots\ldots (21b)$$

Substituting Eqs. 21 into Eq. 11 and extracting $\sin\theta$ by trigonometric transformation, we obtain:

$$\sin\theta = \frac{1}{\sqrt{1 + \left(\frac{\delta_s}{p} + \cot\phi\right)^2}} \quad \ldots\ldots\ldots\ldots (22)$$

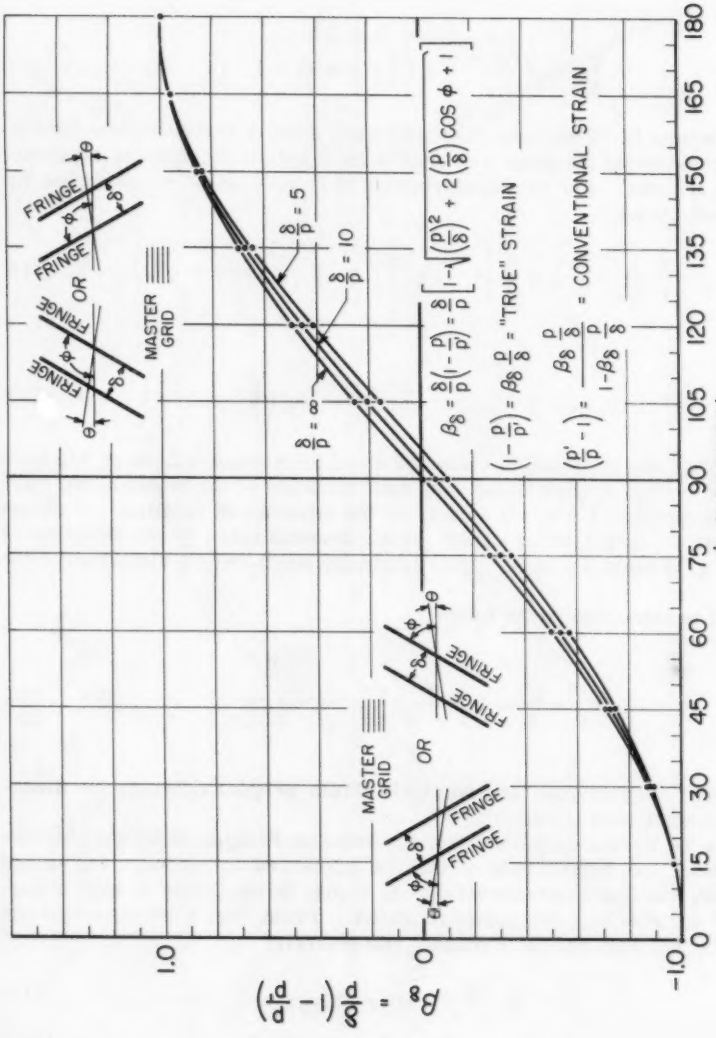

FIG. 4.—MODEL PITCH AS A FUNCTION OF FRINGE ANGLE AND NORMAL FRINGE SPACING

Similarly, from Fig. 5:

$$\delta = \delta_r \cos \phi \quad \ldots\ldots\ldots\ldots\ldots\ldots\ldots\ldots \quad (23a)$$

$$\delta = \delta_r \cos (\pi - \phi) = \delta_r (- \cos \phi) \quad \ldots\ldots\ldots\ldots \quad (23b)$$

To avoid having to give a negative sign to δ_r, a measured distance, these equations can be combined as:

$$\delta = \delta_r \mid \cos \phi \mid \quad \ldots\ldots\ldots\ldots\ldots\ldots\ldots \quad (24)$$

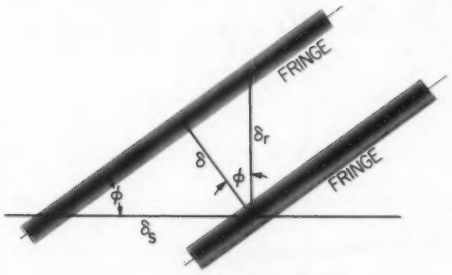

CASE (a), ϕ AN ACUTE ANGLE

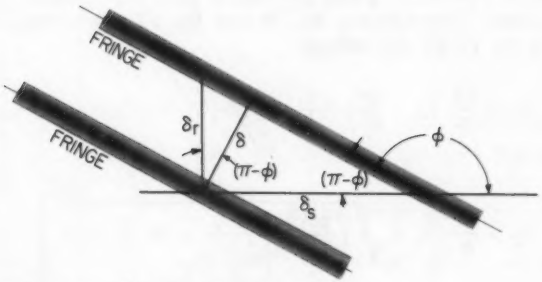

CASE (b), ϕ AN OBTUSE ANGLE

FIG. 5.—SKETCHES TO DERIVE THE FRINGE SPACING IN THE COORDINATE DIRECTIONS

Again substituting in Eq. 11 and extracting sin θ:

$$\sin \theta = \frac{1}{\sqrt{1 + \left(1 + c \frac{\delta_r}{p}\right)^2 \cot^2 \phi}} \quad \ldots\ldots\ldots\ldots \quad (25)$$

where $c = +1, 0 < \phi < \frac{\pi}{2}$ and $c = -1, \frac{\pi}{2} < \phi < \pi$.

Following the same method used previously we can define α_s and α_r as follows:

$$\alpha_s = \frac{\delta_s}{p} \sin\theta = \frac{\frac{\delta_s}{p}}{\sqrt{1 + \left(\frac{\delta_s}{p} + \cot\phi\right)^2}} \quad \ldots\ldots\ldots (26)$$

and

$$\alpha_r = \frac{\delta_r}{p} \sin\theta = \frac{\frac{\delta_r}{p}}{\sqrt{1 + \left(1 + c\,\frac{\delta_r}{p}\right)^2 \cot^2\phi}} \quad \ldots\ldots\ldots (27)$$

Then

$$\sin\theta = \alpha_s \frac{p}{\delta_s} \quad \ldots\ldots\ldots\ldots\ldots (28)$$

and

$$\sin\theta = \alpha_r \frac{p}{\delta_r} \quad \ldots\ldots\ldots\ldots\ldots (29)$$

Values of α_s and α_r are plotted in Figs. 6 and 7, respectively. Their combined usable ranges cover all possible values of ϕ.

Model Pitch in Terms of ϕ and Distances between Fringes along the Coordinate Directions.—Substituting Eq. 24 into Eq. 17 and setting up a relationship similar to Eq. 18 we can define:

$$\beta_r = \frac{\delta_r}{p}\left(1 - \frac{p}{p'}\right) \quad \ldots\ldots\ldots\ldots\ldots (30a)$$

and

$$\beta_r = \frac{\delta_r}{p}\left[1 - \sqrt{\left(\frac{p}{\delta_r}\right)^2 \frac{1}{\cos^2\phi} + 2c\,\frac{p}{\delta_r} + 1}\,\right] \quad \ldots\ldots (30b)$$

in which $c = +1$, $0 < \phi < \pi/2$ and $c = -1$, $\pi/2 < \phi < \pi$.

Similarly, substituting Eqs. 21 into Eq. 17:

$$\beta_s = \frac{\delta_s}{p}\left(1 - \frac{p}{p'}\right) \quad \ldots\ldots\ldots\ldots\ldots (31a)$$

and

$$\beta_s = \frac{\delta_s}{p}\left[1 - \frac{1}{\sin\phi}\sqrt{\left(\frac{p}{\delta_s}\right)^2 + \frac{p}{\delta_s}\sin 2\phi + \sin^2\phi}\,\right] \quad \ldots\ldots (31b)$$

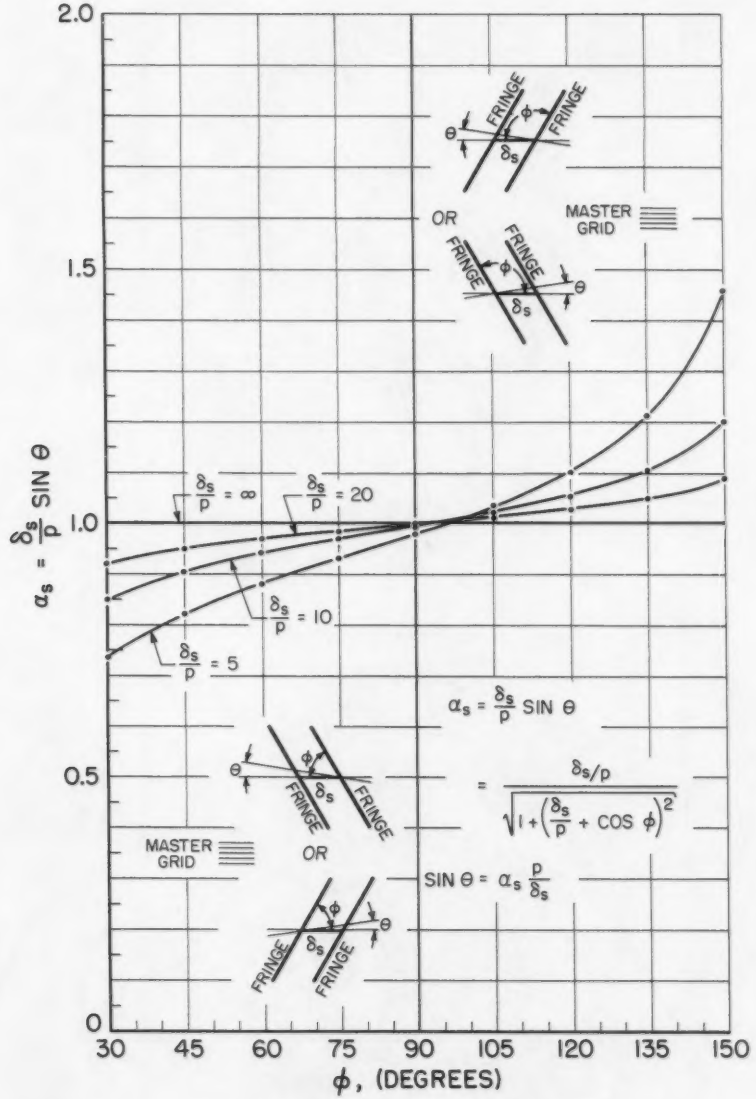

FIG. 6.—ROTATION AS A FUNCTION OF FRINGE ANGLE AND FRINGE SPACING IN THE DIRECTION OF THE MASTER GRID LINES

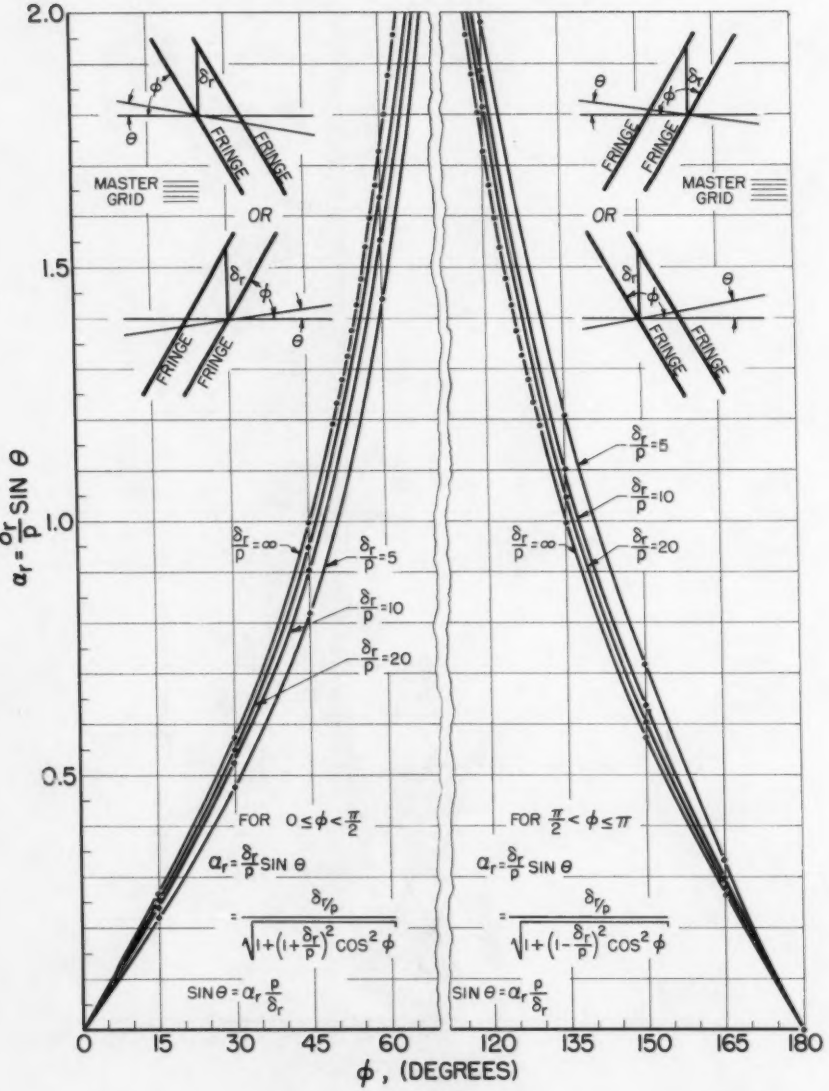

FIG. 7.—ROTATION AS A FUNCTION OF FRINGE ANGLE AND FRINGE SPACING NORMAL TO THE DIRECTION OF THE MASTER GRID LINES

Then:

$$\epsilon_{r\ true} = 1 - \frac{p}{p'} = \frac{p' - p}{p'} = \beta_r \left(\frac{p}{\delta_r}\right) \quad \ldots\ldots\ldots\ldots (32)$$

and

$$1 - \frac{p}{p'} = \beta_s \left(\frac{p}{\delta_s}\right) \quad \ldots\ldots\ldots\ldots\ldots\ldots (33)$$

Values of β_r and β_s are plotted in Figs. 8 and 9, respectively. Their combined usable ranges cover all possible values of ϕ.

Simplified Equations for Small Deformations and Rotations.—It is apparent from Fig. 8 that if ϕ is sufficiently close to 0° or 180° (depending also on the value of δ_r/p), the value of β_r is close to -1.0 or 1.0. This means that rotations θ are very small (Eq. 11). In many problems, sufficient accuracy may result from taking $\beta_r = \pm 1$ and reducing Eq. 32 to:

$$\epsilon_{true} = \frac{p' - p}{p'} = \pm \frac{p}{\delta_r} \quad \ldots\ldots\ldots\ldots\ldots (34)$$

By simple transformation

$$\epsilon_{nom} = \frac{p' - p}{p} = \frac{\pm \frac{p}{\delta_r}}{1 \mp \frac{p}{\delta_r}} \quad \ldots\ldots\ldots\ldots\ldots (35)$$

If, furthermore, p/δ_r is sufficiently small in comparison with unity (that is if strains are very small), Eqs. 34 and 35 both reduce to:

$$\epsilon = \pm \frac{p}{\delta_r} \quad \ldots\ldots\ldots\ldots\ldots\ldots (36)$$

On the other hand, in Fig. 6, if ϕ is sufficiently close to 90° (depending on the value of δ_s/p) the value of α_s is close to 1.0, and sufficient accuracy may result from a reduction of Eq. 29 to

$$\sin \theta = \frac{p}{\delta_s} \quad \ldots\ldots\ldots\ldots\ldots\ldots (37)$$

Determination of the Direction of the Fringe Angle.—In order to determine the direction in which the fringe angle, ϕ, is to be measured in the foregoing equations and graphs, a small amount of information is needed in addition to a photograph of the fringe pattern. For example, the direction of rotation may often be deduced from the loading conditions or could always be found by means of a coarse set of lines or dots on the model in addition to the closely-spaced array which produces the moiré. Once the direction of θ is known, the direction of ϕ is determined by its definition and all ambiguity disappears.

Alternatively, all ambiguity is removed if the sign of the quantity $1-(p/p')$ is known, that is, whether p/p' is greater or less than unity. This can usually

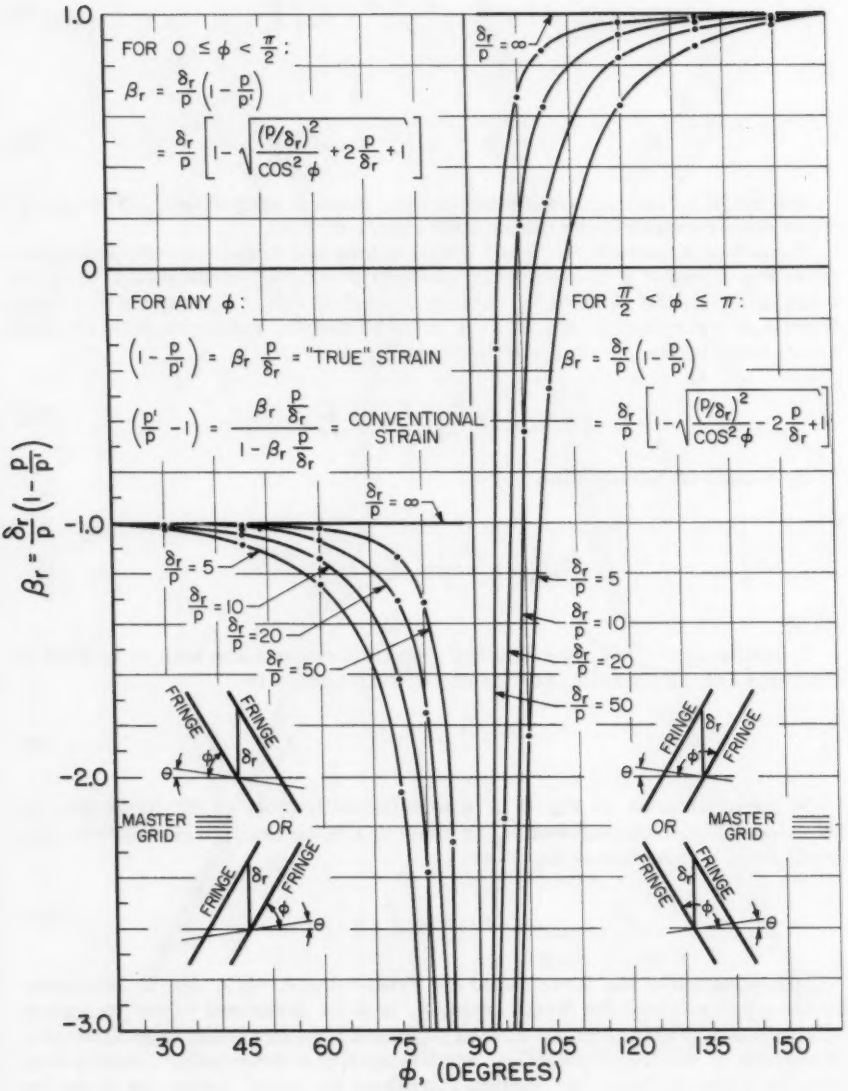

FIG. 8.—MODEL PITCH AS A FUNCTION OF FRINGE ANGLE AND FRINGE SPACING PERPENDICULAR TO THE DIRECTION OF THE MASTER GRID LINES

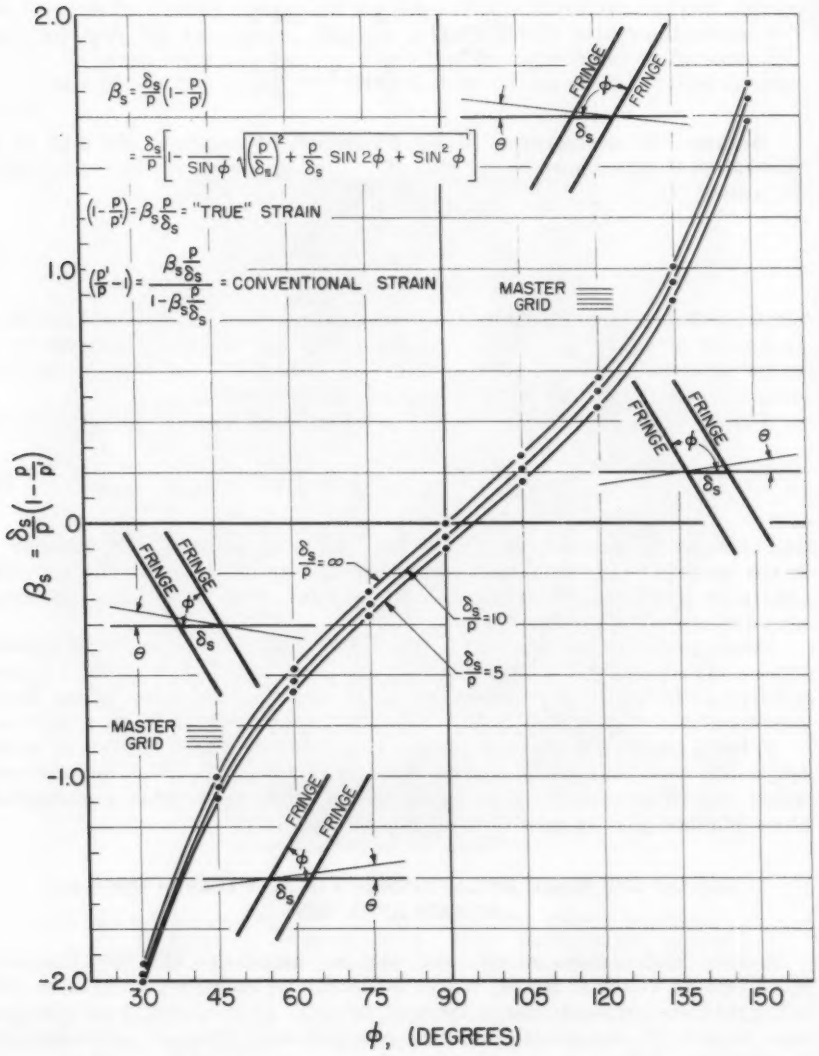

FIG. 9.—MODEL PITCH AS A FUNCTION OF THE FRINGE ANGLE AND FRINGE SPACING IN THE DIRECTION OF THE MASTER GRID LINES

be determined from the moiré pattern if the actual loaded model and master grid are available. Differentiating Eq. 1 leads to

$$\frac{d(\tan \phi)}{d\theta} = \frac{1 - \frac{p'}{p} \cos \theta}{\left(\cos \theta - \frac{p'}{p}\right)^2} \quad \ldots\ldots\ldots\ldots (38)$$

Because the denominator of Eq. 38 cannot be negative, the sign of the derivaties is determined by the sign of $1 - [(p'/p) \cos \theta]$. If this expression is negative,

$$\frac{p'}{p} > \sec \theta \geq 1 \quad \ldots\ldots\ldots\ldots\ldots\ldots (39)$$

meaning that ϕ decreases for an increase in θ. If the master grid is rotated in a given direction with respect to the model and the fringes rotate in the same direction, this condition is satisfied and $p'/p > 1$. If the grids were originally identical, this positively indicates tensile strain.

For $1 - [(p'/p) \cos \theta]$ negative the situation is not quite so definite because

$$\frac{p'}{p} < \sec \theta \geq 1 \quad \ldots\ldots\ldots\ldots\ldots\ldots (40)$$

can be satisfied in a number of ways when θ is a large angle. If, however, ϕ is not near 90° and the fringes rotate opposite to the rotation of the master grid p'/p may ordinarily be considered to be less than 1, indicating compression for originally identical grids.

Other guides to the sign of $1 - (p/p')$ are sometimes available directly from a moiré photograph. If ϕ is 90° at any point, $p/p' > 1$ from Eq. 17. Once a fringe is known to represent $p/p' > 1$ at any point, the same fringe cannot represent $p/p' < 1$ without going beyond 90°, actually through $\phi = \pi/2 + \theta/2$.

Fringes parallel to the master grid lines represent the condition of no rotation (Eq. 11). Unless they are continuations from areas where the p/p' condition can be evaluated, it is impossible to distinguish from a photograph alone whether p/p' is greater than or less than unity.

USE OF THE BASIC RELATIONSHIPS IN A TWO-DIMENSIONAL STRAIN ANALYSIS

In order to determine strains and rotations associated with two coordinate directions in an actual model, it will obviously be necessary to have models with grid lines perpendicular to these directions. If the model is not identical when turned 90°, two models must be equipped with grids, or, alternatively, two sets of grid lines can be placed on the same model and analyzed separately with a one-way master grid.

Individual measurements of the distance between two fringes cannot be very accurate, as will be apparent from an examination of Figs. 10 and 11. Also, the point being examined may not be exactly on a fringe centered between two fringes.

It is much more convenient and accurate to measure across a series of fringes along a line including the point of interest and plot the accumulated fringe distances from any convenient point as in Fig. 12. A smooth curve is drawn through the plotted points, and the slope of this curve at any point gives fringes per inch, the reciprocal of which is the value in inches per fringe of δ, δ_r, or δ_s as the case may be. In Fig. 12(b) because there is no rotation along an axis of symmetry, the process of differentiation gives the true strain directly.

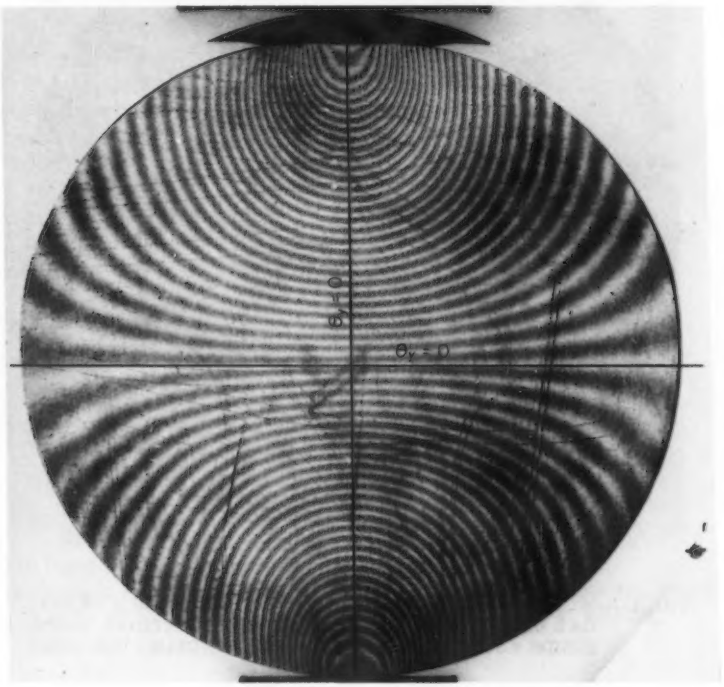

FIG. 10.—MOIRÉ FRINGES ON DISK OF HYSOL 8705 UNDER VERTICAL DIAMETRAL COMPRESSION WITH HORIZONTAL GRIDS (GRIDS = 300 LINES PER INCH ON 4-IN.-DIAMETER DISK)

As will be apparent from Figs. 10 and 11, even in a simplified case such as a disk, it will not usually be possible to measure both δ_r and δ_s at the same point with anything approaching accuracy, and at some points neither can be measured. However, δ can always be measured and values of $1-(p/p')$ and θ from measurements of δ can supplement or check those from measurements of δ_r and δ_s.

The measurements of ϕ will, in general, not be very accurate. However, since one can usually make a choice from among the measurements of δ, δ_r,

and δ_s at any given point of interest, the sensitivity to errors in measurements of ϕ can be kept at a fairly low level for most fringe configurations.

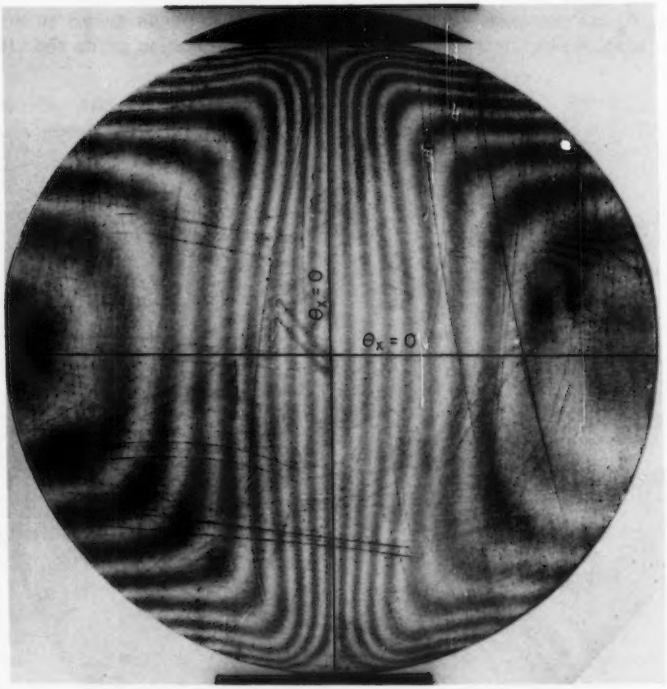

FIG. 11.—MOIRÉ FRINGES ON DISK OF HYSOL 8705 UNDER VERTICAL DIAMETRAL COMPRESSION WITH VERTICAL GRIDS (GRIDS = 300 LINES PER INCH ON 4-IN.-DIAMETER DISK)

The values of $1 - (p/p')$ and θ found with grids in each of the two directions comprise all the information needed to solve the general strain problem. In addition to the normal true strains:

$$\epsilon_{x\ true} = \beta_i \frac{p}{\delta_i} \quad \ldots\ldots\ldots\ldots\ldots\ldots \quad (41a)$$

with grid lines in the y-direction, and

$$\epsilon_{y\ true} = \beta_i \frac{p}{\delta_i} \quad \ldots\ldots\ldots\ldots\ldots\ldots \quad (41b)$$

with grid lines in the x-direction.

Their nominal (conventional) strain counterparts are

$$\epsilon_{x\ nom} = \frac{\beta_i \frac{p}{\delta_i}}{1 - \beta_i \frac{p}{\delta_i}} \quad \ldots\ldots\ldots\ldots (42a)$$

with grid lines in the y-direction, and

$$\epsilon_{y\ nom} = \frac{\beta_i \frac{b}{\delta_i}}{1 - \beta_i \frac{p}{\delta_i}} \quad \ldots\ldots\ldots\ldots (42b)$$

with grid lines in the x-direction. In the foregoing β_i refers to β_δ, β_r or β_s and δ_i refers to the corresponding δ, δ_r, or δ_s.

We have also the rotations

$$\theta_y = \text{arc tan } \frac{\alpha_\delta\ p}{\delta} \quad \ldots\ldots\ldots\ldots\ldots\ldots (43a)$$

$$\theta_y = \text{arc sin } \frac{\alpha_r\ p}{\delta_r} = \text{arc sin } \frac{\alpha_s\ p}{\delta_s} \quad \ldots\ldots\ldots (43b)$$

with grid lines in the y-direction, and

$$\theta_x = \text{arc tan } \frac{\alpha_\delta\ p}{\delta} \quad \ldots\ldots\ldots\ldots\ldots\ldots (44a)$$

$$\theta_x = \text{arc sin } \frac{\alpha_r\ p}{\delta_r} = \text{arc sin } \frac{\alpha_s\ p}{\delta_s} \quad \ldots\ldots\ldots (44b)$$

with grid lines in the x-direction.

In general, there will be a rigid body rotation, and if signs are given to θ_x and θ_y (say + for counterclockwise), the rigid rotation ψ will be:

$$\psi = \frac{1}{2}\left(\theta_x + \theta_y\right) \quad \ldots\ldots\ldots\ldots\ldots\ldots (45)$$

and the shear strain γ will be:

$$\gamma = \frac{1}{2}\left(\theta_x - \theta_y\right) \quad \ldots\ldots\ldots\ldots\ldots\ldots (46)$$

APPLICATION OF THE METHOD TO AN ACTUAL PROBLEM

The moiré method has been applied to the familiar case of a circular disk under diametral compression. In order to obtain a satisfactory level of response with the 300-lines per in. grid available, a sheet was made of urethane rubber (Hysol 8705) on which the grid was photoprinted using the sensitized resist marketed as Gaco. After printing, a 4-in. disk was machined from the 1/2-in.-thick sheet.

The disk was loaded between flat plates, first with grid lines perpendicular to the loading directions (Fig. 10), then with the grid lines parallel to the loading direction (Fig. 11). Photography was by the double-exposure method, the unloaded and loaded conditions being successively exposed on the same sheet of Kodalith film with no intermediate change except for application of the load. (In this method of fringe formation the film-and-lens system must be capable of clearly resolving the individual grid lines at high contrast.)

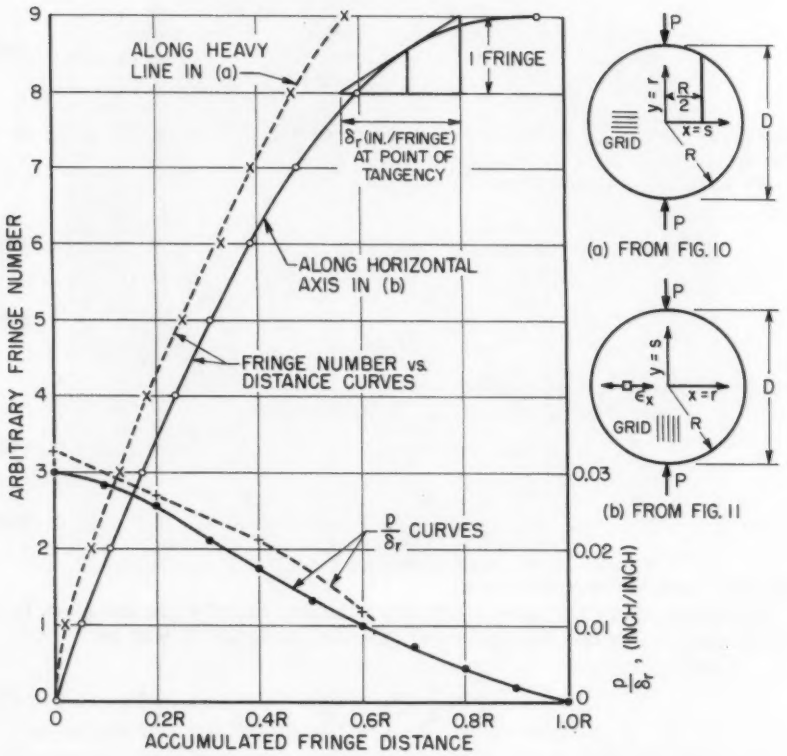

FIG. 12.—DETERMINATION OF δ_r AT ALL POINTS ALONG LINES BY MEANS OF A PLOT OF ACCUMULATED FRINGE DISTANCE FROM ANY ARBITRARY BEGINNING

Fig. 12 is a plot of the measured positions of successive fringes along two representative lines where δ_r could be successfully measured in Figs. 10 and 11. On a separate scale in Fig. 12 are also plotted the values of the quantity p/δ_r determined by differentiation of the fringe-position curves. From the values of p/δ_r (also p/δ_s and p/δ from separate measurements in appropriate directions), the strains can be found as previously described.

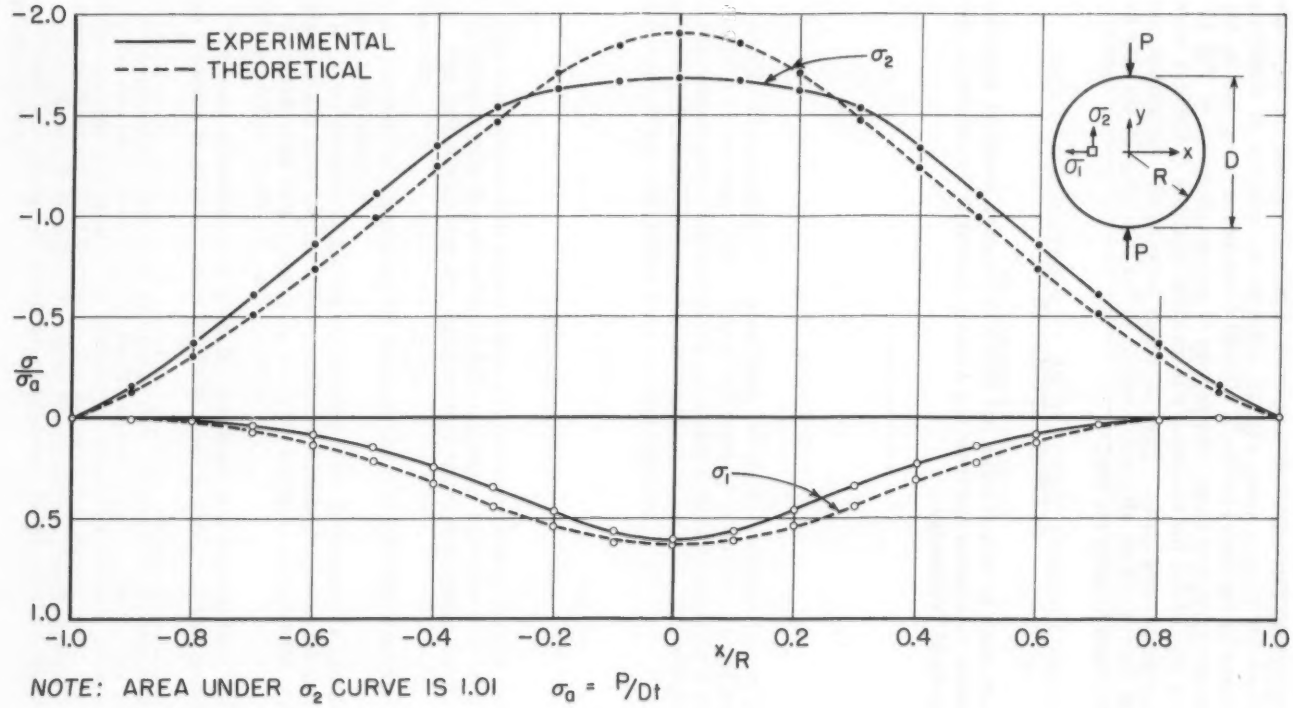

FIG. 13.—PRINCIPAL STRESSES ON THE HORIZONTAL AXIS OF A DISK (HYSOL 8705) UNDER DIAMETRAL COMPRESSION, OBTAINED USING THE MOIRÉ METHOD

From a series of measurements across the horizontal axis of Fig. 10, the value of $\epsilon_{y\,true}$ was determined at a number of points. These values, combined with those for $\epsilon_{x\,true}$ from Fig. 12 and with the modulus of elasticity (also determined by the moiré method), allowed computation of σ_x and σ_y (σ_1 and σ_2 respectively in this case), the results of which are shown in Fig. 13. Also shown in Fig. 13 are the results of a theoretical analysis of the disk when subjected to concentrated loads. The difference between the theoretical and experimental curves can be attributed mainly to the flattening of the disk by the flat plates used to apply the load.

ACKNOWLEDGMENTS

The writers wish to acknowledge the financial support received from the National Science Foundation and from the Armour Research Foundation of the Illinois Institute of Technology.

Journal of the
ENGINEERING MECHANICS DIVISION
Proceedings of the American Society of Civil Engineers

ARCH DAM ANALYSIS WITH AN ELECTRIC ANALOG COMPUTER

By Richard H. MacNeal[1]

SYNOPSIS

An electrical analogy that simulates the elastic deformations of arch dams is described herein. This analogy consists of resistors, transformers, and current generators. The results of an analog computer analysis of the Stevenson Creek Dam are compared with field measurements. The results of a design study of the Blue Ridge Dam are summarized.

INTRODUCTION

The determination of the stresses and deformations of an arch dam has long been recognized as one of the most difficult analysis problems in civil engineering. The difficulties that are encountered arise principally for the following reasons:

1. Elastic deformations play an important role in the determination of stresses in arch dams.
2. Many structural degrees of freedom must be included in a realistic analysis in order to account for several different kinds of elastic deformation.
3. Each arch dam requires a separate analysis due to wide variations in canyon profile, thickness, and so forth.

The most elaborate and probably the most accurate method for analyzing the stresses in an arch dam is the Trial Load Method.[2] In this method the dam

Note.—Discussion open until January 1, 1961. To extend the closing date one month, a written request must be filed with the Executive Secretary, ASCE. This paper is part of the copyrighted Journal of the Engineering Mechanics Division, Proceedings of the American Society of Civil Engineers, Vol. 86, No. EM 4, August, 1960.

[1] Mgr., Engrg. Service Div., Computer Engrg. Assoc., Pasadena, Calif.

[2] "Trail Load Method of Analyzing Arch Dams," Boulder Canyon Reports, Part V, Bulletin 1, 1938.

is replaced by an intersecting gridwork of horizontal arches and vertical cantilevers each of which resists extension, bending, shear, and twisting. The solution is obtained by adjusting the forces of interaction between arches and cantilevers so as to equalize radial, tangential, and rotational displacements. Because of the large number of equations required in a trial load analysis, computations employing desk calculators have proven to be extremely time consuming.[3] Adaptations of the method for solution by electronic digital computers should greatly increase its speed and general utility.

Since presently available metheds of analyzing arch dams are either quite laborious or over-simplified, many designers prefer the use of scale models instrumented with strain gages. Considerable success has been achieved in Europe with this method.[4]

The method described in this paper makes use of an electrical analogy in which passive electrical elements (resistors and transformers) simulate the elastic and load transforming properties of the structure. Such analogies have been successfully employed for solving many other types of structural problems. Perhaps the earliest practical application of electrical analogies to structural problems was the solution of truss and framework problems by Vannevar Bush in 1933.[5] In the last decade the method has been extended to the static and dynamic analysis of beams,[6,7,8,9] plates,[10,11] and shells.[12] Much use has been made of these analogies in aircraft structural analysis.[13,14,15]

When regarded as tools for engineering computations, physical analogies are hybrid forms that have some of the characteristics of scale models and some of the characteristics of conventional mathematical analysis. As in model testing, the answers are obtained from physical measurements, the essential distinction being that the quantities measured in an analogy are of a different physical type than those in the prototype system. The techniques of measurement and the problems associated with measurement are similar. An important difference between scale models and physical analogies is that a scale

---

[3] Discussion of Reference 4, below, by F. A. Houck.

[4] "Arch Dams: Design and Observation of Arch Dams in Portugal," by Rocha, Serafim, and da Silveira, Proceedings, ASCE, Vol. 82, No. PO 3, June, 1956.

[5] "Structural Analysis by Electric Circuit Analogies," by V. Bush, Journal of Franklin Inst., Vol. 217, March, 1934, p. 289.

[6] "Beam Vibration Analysis with the Electric Analog Computer," by G. D. McCann and R. H. MacNeal, Journal of Applied Mecahnics, Transactions, ASME, Vol. 72, 1950, p. 13.

[7] "An Equivalent Circuit for a Vibrating Beam which Includes Shear Motions," by H. M. Trent, Journal of Accoustical Soc. of America, Vol. 22, 1950, p. 355.

[8] "An Improved Electrical Analogy for the Analysis of Beams in Bending," by W. T. Russell and R. H. MacNeal, Journal of Applied Mechanics, Vol. 20, 1953, p. 349.

[9] "Electrical Analogies of Statically Loaded Structures," by F. Ryder, Transactions, ASCE, Vol. 119, 1954.

[10] "The Solution of Elastic Plate Problems by Electrical Analogies," by R. H. MacNeal, Journal of Applied Mechanics, Transactions, ASME, Vol. 73, 1951, p. 59.

[11] "Equivalent Plate Theory for a Straight Multicell Wing," by S. U. Benscoter and R. H. MacNeal, NACA TN 2786, September, 1952.

[12] "Electrical Analogies for Stiffened Shells with Flexible Rings," by R. H. MacNeal, NACA TN 3280, December, 1954.

[13] "The Solution of Aeroelastic Problems by Means of Electrical Analogies," by R. H. MacNeal, G. D. McCann, and C. H. Wilts, Journal of Aero. Science, December, 1951.

[14] "Analysis of Multicell Delta Wings on Caltech Analog Computer," by R. H. MacNeal and S. U. Benscoter, NACA TN 3114, January, 1954.

[15] "The Integrated Use of Analog and Digital Computing Machines for Aircraft Dynamic Load Problems," by B. Mazelsky and R. F. O'Connell, Journal of Aero. Science, Vol. 23, August, 1956, pp. 721-740.

model can be constructed even when knowledge of the processes involved in the prototype structure is incomplete, whereas the construction of an analogy requires a complete description of the physical laws and properties of the prototype. Thus, in a scale model, it is usually sufficient to use similar materials and to produce dimensions and applied loads whose ratios are in accordance with principles of dimensional analysis. A physical analogy, on the other hand, is an analogy only by virtue of similarities in its physical laws with those of the prototype system. In fact it must be possible to describe the behavior of the analogy by a set of mathematical equations that is essentially identical to the set satisfied by the prototype system. In this respect, computation by physical analogy is similar to computation by mathematical analysis.

Thus, if a problem can be solved by physical analogy, it can also be solved by direct mathematical analysis. For this reason an analog computer is more frequently regarded as an aid to mathematical computation than as a form of model testing. While this view expresses an intrinsic truth, it should be realized that the operation of an analog computer is more closely related to model testing than it is to the operation of a digital computer.

Computation with an electric analog computer has certain advantages over both model testing and conventional mathematical analysis. The recording of results is more rapid and usually more accurate than in model testing due to special measuring equipment built into the computer. The elements from which the analogy is constructed are permanent and re-usable and can be easily adjusted to any desired value. The main advantages over digital computation are the speed of obtaining results and the fact that a great deal less algebraic manipulations are required in the preparation of a problem.

Along with these advantages, analog computing has its own special difficulties. Unlike a general purpose digital computer, a given analog computer is restricted as to the kinds of problems that it can be used to solve. The type of computer described in this paper is mainly useful for determining the static and dynamic response of structures and for the solution of related mechanical problems. Other analog computers are designed to solve heat flow problems or control system problems.

Accuracy limitations are often considered a disadvantage of analog computers. While it is true that precision comparable to digital computation cannot be achieved, the degree of accuracy is usually sufficient for most engineering applications. Another important disadvantage of the analog computer, with respect to digital computation, is that it must be re-assembled for each problem that is analyzed. Although the use of removable patch boards can reduce this operation to a few hours, the set-up time is incomparably greater than that of a card- or tape-programmed digital computer.

The advantages claimed for analog computers should be particularly significant for the analysis of arch dams. Since the numerical computations are lengthy and the construction and testing of an accurate model is a painstaking operation, the analog computer should enjoy a speed advantage. Since many design changes are required to achieve an efficient design, the flexibility of the analog computer with regard to parameter changes should be a very useful feature.

ELECTRICAL ANALOGIES FOR THE STATIC ANALYSIS OF ELASTIC STRUCTURES

In the type of electrical analogy described herein, current is proportional to force and voltage is proportional to displacement. Since flexibility is the ratio of displacement to force, and resistance is the ratio of voltage to current, it follows that electrical resistance is analogous to elastic flexibility, as illustrated in Fig. 1.

A very important component in the electrical analogies of elastic structures is the ideal transformer. Although this element has many uses, it is commonly considered to be the analogy of an ideal, weightless lever, as illustrated in Fig. 2. There are two fundamental relationships for an ideal transformer. The first is that, for different coils wound on the same magnetic core, the voltage across each coil is proportional to the number of turns in the coil. The second is that, when the current flowing in each coil is multiplied by the number of turns, the sum of such products is zero. These relationships are illustrated in Fig. 2(b). The winding sense of each coil is indicated by plus and minus signs. The positive direction of current flow is from the positive toward the negative terminal of the winding so that, in the figure, the current in the winding with n_2 turns is I_3 while the current in the winding with n_1 turns is $-I_1$. The relationship $I_1 + I_2 + I_3 = 0$ expresses the fact that the sum of currents flowing into the junction with voltage e_2 is zero.

From the relationships given in Fig. 2, it is seen that the transformer-turns ratio n_1/n_2 is analogous to the lever ratio l_1/l_2.

The relationships for the ideal lever may be combined to show that the mechanical work done by the external forces is zero. Similarly the relationships for the ideal transformer may be combined to show that the electrical power consumed by the transformer is zero. These statements express the intrinsic meanings of the terms ideal lever and ideal transformer. Practical levers and practical transformers are not ideal. A major portion of the expense of an analog computer of the type considered here is involved in the construction of transformers that satisfy the relationships of ideal transformers with sufficient accuracy. These relationships are not even approximately satisfied at very low frequencies or at very high frequencies. For this reason the computer is usually operated at frequencies in the medium audio range (100-500 cps). Since resistors are the only impedance elements, direct current concepts may be used in connection with the circuits.

In addition to resistors and transformers, electrical analogies for static structural analysis must include devices that simulate applied loads. Since current is analogous to force, the analogy for a constant load is a constant current generator. Such a device may be approximated by a very high voltage source feeding through a very large resistance.

Resistors, transformers, and constant current generators are the only elements required in the analogy for a statically loaded structure. The manner in which these elements are interconnected to form the analogy for a complete system is illustrated in Fig. 3. A good method for constructing an analogy of a complete system consists of the following steps:

1. Subdivide the mechanical system into simple elements.
2. Construct electrical analogies for these elements from a standard list of analogies. If the list does not contain an analogy for an element, write the relationships satisfied by the element and devise an electrical circuit that satisfies these relationships.

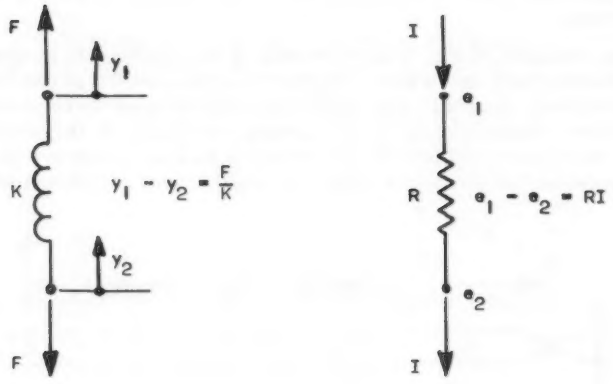

FIG. 1.—ANALOGY BETWEEN FLEXIBILITY AND RESISTANCE

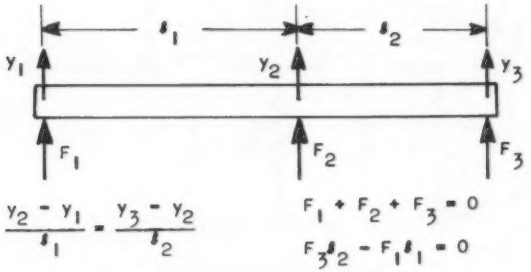

(a) IDEAL LEVER

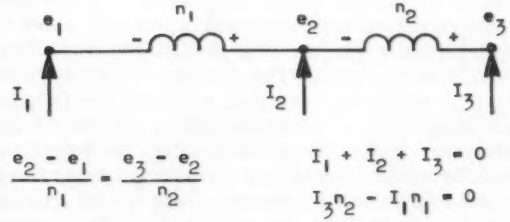

(b) IDEAL TRANSFORMER

FIG. 2.—ANALOGY BETWEEN IDEAL TRANSFORMER AND IDEAL LEVER

3. Interconnect the elemental electrical analogies to satisfy continuity relationships.

In the example of Fig. 3 the elements of the mechanical system are a rigid lever, two springs and a load. Electrical analogies for these elements have been previously derived. The continuity relationships to be satisfied are that the relative displacements of the elements are zero at the points where they are joined together and that the forces acting on these joints are in equilibrium. The displacement conditions imply the equilibrium conditions and vice versa

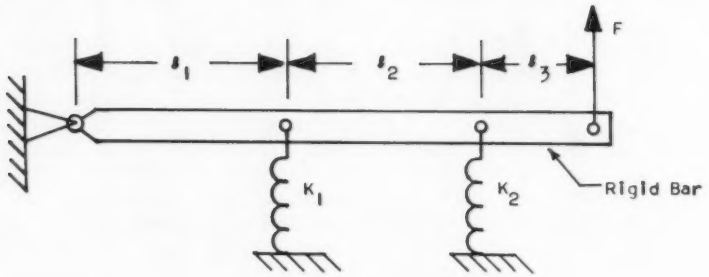

(a) MECHANICAL SYSTEM

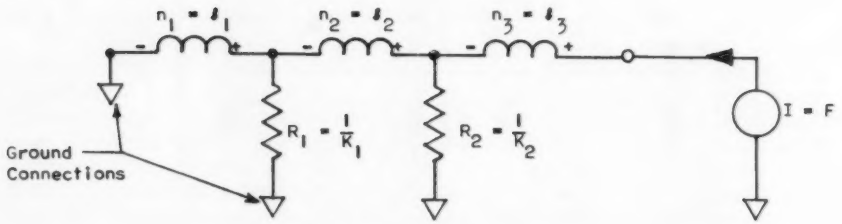

(b) ELECTRICAL ANALOGY

FIG. 3.—ELECTRICAL ANALOGY FOR A SIMPLE MECHANICAL SYSTEM

since no work is done on the joints. Thus, since an electrical connection consumes no power, either condition may be used as a basis by which to interconnect the elementary electrical analogies. The displacement condition is somewhat easier to apply in the example of Fig. 3 since it merely states that the voltages of the electrical elements are equal at points corresponding to the joints of the mechanical system. In examples where the forces at a joint are not co-linear, transformers may be required to affect the interconnection and in such cases the equilibrium conditions are frequently easier to apply.

The bending of a beam provides a somewhat less trivial example. In this example, illustrated in Fig. 4, the first step is to replace the continuously elastic beam by a set of lumped springs, concentrated loads and simple rigid bars. The only new element occurring in this idealized lumped structure is the rigid bar for which an electrical analogy is derived in Fig. 5. With this new elementary analogy, the principles outlined above easily lead to the complete electrical analogy shown in Fig. 4(c). In this circuit, mechanical symbols are used to

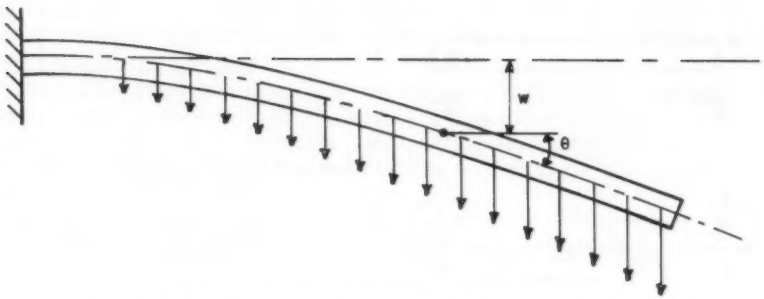

(a) UNIFORM CANTILEVER BEAM WITH DISTRIBUTED LOAD

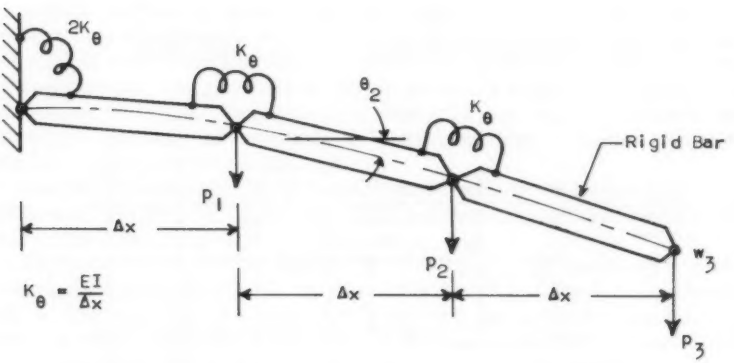

(b) EQUIVALENT LUMPED MODEL

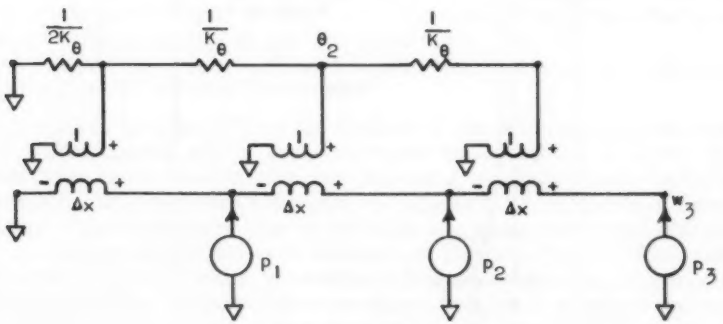

(c) ELECTRICAL ANALOGY

FIG. 4.—ELECTRICAL ANALOGY FOR A CANTILEVER BEAM

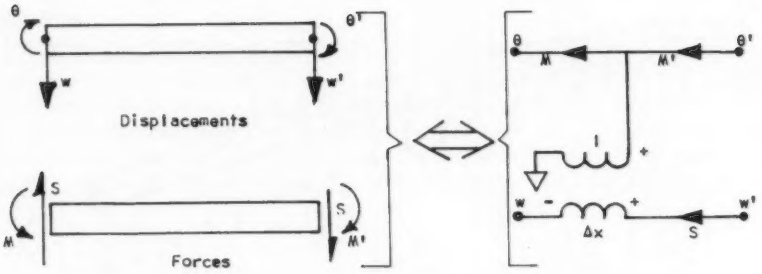

Equations Satisfied: $\theta = \theta' = \frac{w' - w}{\Delta x}$

$$S\,\Delta x + M' - M = 0$$

FIG. 5.—ELECTRICAL ANALOGY FOR A RIGID BAR

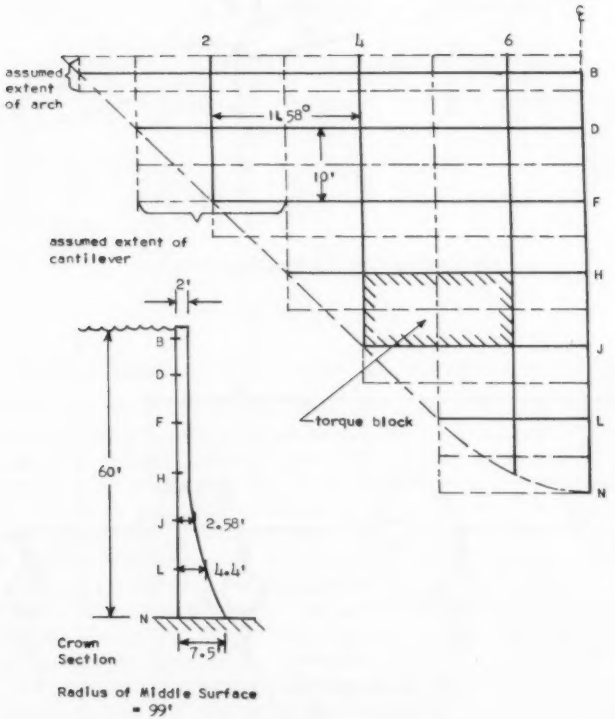

FIG. 6.—IDEALIZED MODEL OF STEVENSON CREEK DAM

designate the values of electrical elements as an economy measure. The actual electrical values will be equal to the mechanical values multiplied by scale factors.

The subsequent development of the theory of electrical analogies for statically loaded elastic structures consists mainly of an elaboration of the techniques previously described with more complex structural elements. The elementary analogies required in the analysis of arch dams will be derived subsequently.

STRUCTURAL MODEL USED IN THE ANALYSIS OF A CYLINDRICAL ARCH DAM

The arch dam may be characterized as a relatively thick shell of homogeneous elastic material. It will be assumed that displacements vary linearly across the thickness of the dam, which is assumed to be sufficiently thin for the middle surface to be taken as the neutral surface for bending, but not so thin that any components of shearing strain may be neglected. Because there are a finite number of lumped circuit elements in the computer, finite difference approximations are required in the analysis. Furthermore, since resistors are linear elements, assumptions of linearity are required unless expensive nonlinear elements are available in large quantities or unless iterative solution techniques are employed.

In order to simplify the presentation, it will be assumed that the middle surface of the dam is a cylinder. This assumption was not made in the analysis of the Blue Ridge Dam.

The first step in the idealization of the structure is to lay out a gridwork of horizontal and vertical lines in the middle surface of the dam as illustrated in Fig. 6. The dimensions shown in this figure refer to the Stevenson Creek Dam. The dam is then replaced by an idealized structure with three kinds of elements. These elements are:

1. Horizontal arch elements, that resist axial thrust, bending about a vertical axis, and shear in a horizontal plane.
2. Vertical cantilever elements, that resist vertical thrust, bending about a horizontal axis tangent to the neutral surface, shear in a radial plane, and shear in a plane tangent to the neutral surface.
3. Torque blocks, that occupy the panels between arch elements and cantilever elements, and that resist twist.

The loads distributed over the surface of the dam are replaced by concentrated loads acting at the arch-cantilever intersections. In order that such loads may be resisted without inducing local bending stresses in the arches, the curved arch elements are replaced by straight chords between intersection points. This substitution may be justified by a finite-difference analysis.

The lumped model for arch elements is shown in Fig. 7, which also illustrates the manner in which a variable radius of curvature may be treated. The bending stiffness of the arch is represented by a set of rotational springs. The flexibility of each spring is computed by the formula

$$\frac{1}{K_e} = \int \frac{ds}{E\,I} \quad \ldots\ldots\ldots\ldots\ldots\ldots \quad (1)$$

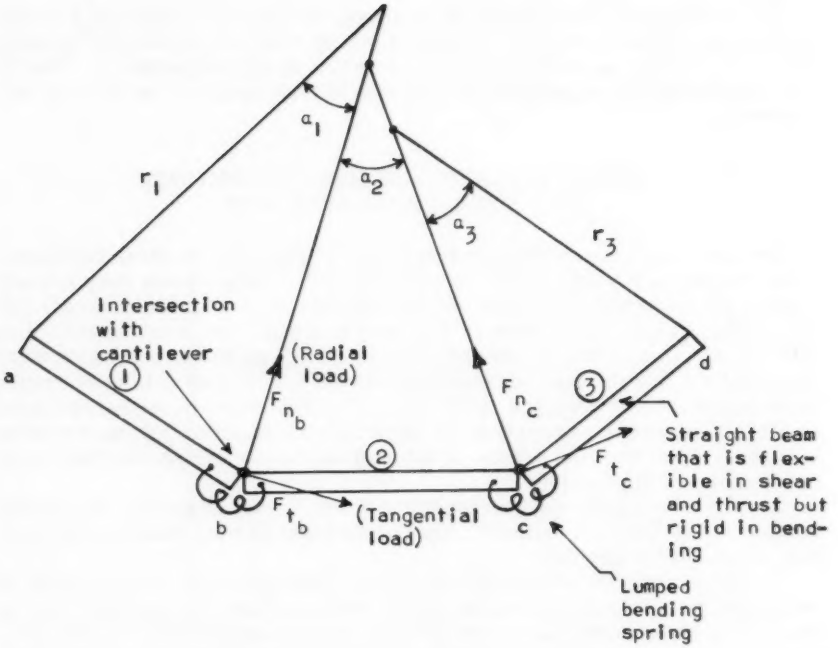

FIG. 7.—LUMPED MODEL FOR ARCH ELEMENTS

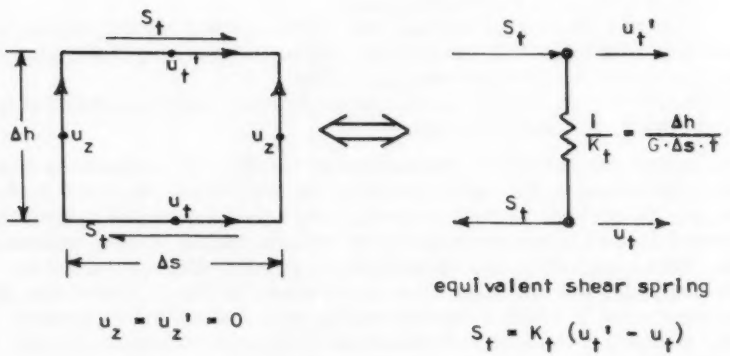

FIG. 8.—ELEMENT RESISTING TANGENTIAL SHEAR IN THE NEUTRAL SURFACE

The limits of integration are from the center of one arch element to the center of the next arch element. I is the moment of inertia of the arch cross section and is equal to $1/12\ t^3\ \Delta h$, where t is the thickness of the dam and Δh is the vertical dimension of the arch. The thrust and shear flexibilities respectively of an arch element are given by the formulas

$$\frac{1}{K_T} = \int \frac{ds}{E\ A} \quad \ldots\ldots\ldots\ldots\ldots\ldots (2)$$

and,

$$\frac{1}{K_S} = \int \frac{ds}{K'\ G\ A} \quad \ldots\ldots\ldots\ldots\ldots\ldots (3)$$

K' is a shear correction factor, approximately equal to 0.8, and A is the cross sectional area of the arch.

With regard to vertical cantilever elements, the usual assumption of the trial load method, that the cantilevers are inextensional for vertical thrust, will be made. This assumption has the effect of decoupling the effects of vertical and horizontal loads so that only horizontal loads need be included in the analysis considered here. The assumption also has the effect of making shear stresses in the neutral surface functions only of the relative tangential motions of adjacent arches. Thus, the resistance to tangential shear deformation may be represented by simple shear springs connected between adjacent arch-cantilever intersections as shown in Fig. 8.

The resistance to bending and shear in a radial plane is provided by a lumped beam model similar to that shown in Fig. 4(b).

Neither the arch elements nor the cantilever elements resist twist. Resistance to twist is provided by a third type of element, referred to as a torque block, which occupies the panel defined by arch and cantilever centerlines. Twisting of the dam may be regarded as a warping of the plane connecting the four corners of such a panel caused by concentrated loads acting at the corners. These corner loads may be replaced by couples acting on the top and bottom faces of the torque block as shown in Fig. 9. The block is then replaced by a torsional spring with flexibility

$$\frac{1}{K_{T_\theta}} = \frac{\Delta h}{GJ} \quad \ldots\ldots\ldots\ldots\ldots\ldots (4)$$

where $J = \frac{1}{3}\ \Delta s\ t^3$.

This spring is joined to adjacent arch elements at their centers. It is unnecessary to add additional springs connecting adjacent cantilevers since the twisting deformation of the dam is completely defined by the relative rotation of adjacent arches. Although the method of treating twist described here correctly accounts for the strain energy of twist and leads to a simple electrical analogy, it introduces ficticious components of radial shear into the arch and cantilever elements that should be subtracted from the radial shears measured in the analog computer.

The structural model that has been described is more-or-less equivalent to that employed in conventional trial load analysis. The principal differences are in the manner of treating twist and in the substitution of concentrated loads for loads continuously distributed along the arches. From the viewpoint of shell theory, the main objections to the model are the elimination of thrust deformation in the cantilevers and the omission of Poisson's ratio coupling. Both of these effects can be included at the expense of additional elements in the model.

Since the number of electrical elements available in an analog computer is limited, the inclusion of these relatively unimportant effects would decrease the number of grid points that could be represented.

The concentrated loads applied at arch-cantilever intersections require special attention. Due to the uniform character of the loads sustained by an arch dam, a small percentage of change in the load at a given point may produce a disproportionately large change in the local bending moment. For most load effects the lateral load applied at a given point may be regarded as the product of a pressure and a surface area. The value of surface area at a given arch-cantilever intersection should be chosen such that, in an idealized circular arch model consisting of chord members, a uniform radial pressure gives a uniform

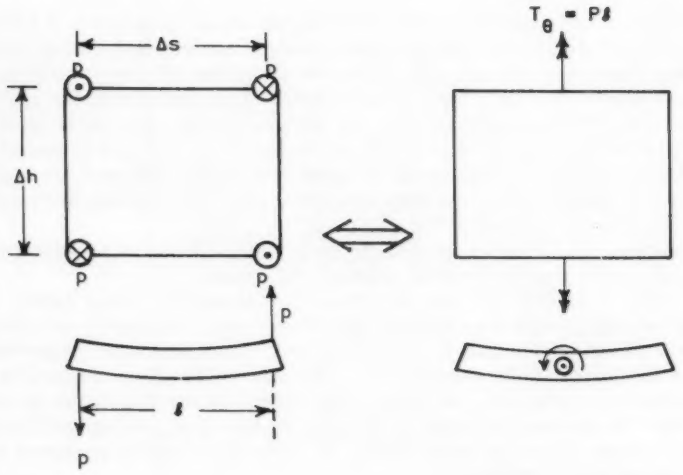

(a) ELEMENT WITH CORNER LOADS

(b) ELEMENT WITH COUPLES ON HORIZONTAL FACES

FIG. 9.—TORQUE BLOCK

stress equal to p r/t in the absence of rib shortening. This condition is satisfied at point b in the model of Fig. 7 if the radial load is equal to:

$$F_n = p\,\Delta h \left[r_1 \tan\frac{\alpha_1}{2} + r_2 \tan\frac{\alpha_2}{2} \right] \quad \ldots\ldots\ldots\ldots (5)$$

Δh must be equal for all points on the same arch.

The effects of thermal strain due to a temperature rise, ΔT, uniform across the thickness of the dam, may be simulated by equivalent radial and tangental loads. The basis of this equivalence is the fact that the total strain in the circumferential direction, γ may be written as

$$\gamma = \frac{1}{E} \left(\sigma + \alpha E\, \Delta T \right) \quad \ldots\ldots\ldots\ldots\ldots (6)$$

where σ is the actual tensile stress and α is the coefficient of thermal expansion. The term $\alpha E \Delta T$ may be regarded as an applied thermal stress. For a constant thickness, constant radius arch, this applied stress may be produced by a radial pressure equal to $-\alpha E \Delta T\, t/r$. In more general cases the equivalent thermal loads to be applied at point b of Fig. 7 are:

$$F_n = -\alpha E \Delta T \Delta h \left[t_1 \sin \frac{\alpha_1}{2} + t_2 \sin \frac{\alpha_2}{2} \right] \quad \ldots\ldots\ldots (7)$$

$$F_t = -\alpha E \Delta T \Delta h \left[t_1 \cos \frac{\alpha_1}{2} - t_2 \cos \frac{\alpha_2}{2} \right] \quad \ldots\ldots\ldots (8)$$

After the deformations and stresses due to this loading are measured, or computed, the quantity $\alpha E \Delta T$ must be subtracted from the resulting tensile stress in the circumferential direction.

The effects of a uniform temperature gradient through the thickness of the dam may be simulated by applied moments about a vertical axis which may, in turn, be replaced by a distribution of point loads with predominating tangential components.

ELECTRICAL ANALOGY FOR A CYLINDRICAL ARCH DAM

The remaining steps in the construction of an electrical analogy are to draw electrical circuit analogies for these elements and then to connect the circuits together so as to satisfy the conditions of continuity.

The elements of the arch dam and their corresponding electrical analogies are shown in Fig. 10. The analogy for an arch chord element contains a resistor simulating the thrust flexibility and a separate circuit simulating the shear and rotational properties of the element. This latter circuit is similar to the circuit for a rigid bar shown in Fig. 5 except for the addition of a resistor simulating the shear flexibility given by Eq. 3.

The special circuit of Fig. 10(c) is required to satisfy the relationships existing at a joint between arch elements such as joint b in Fig. 7. Since no work is done on the joint, either the displacement conditions or the equilibrium conditions may be used in the derivation of the analogy. The displacement conditions will be used. Transformed displacements are defined as follows:

$$\left.\begin{aligned} \bar{u}_{n_1} &= \frac{u_{n_1}}{\cos \frac{\alpha_1}{2}} & \bar{u}_{n_2} &= \frac{u_{n_2}}{\cos \frac{\alpha_2}{2}} \\ \bar{u}_{t_1} &= \frac{u_{t_1}}{\cos \frac{\alpha_1}{2}} & \bar{u}_{t_2} &= \frac{u_{t_2}}{\cos \frac{\alpha_2}{2}} \end{aligned}\right\} \quad \ldots\ldots\ldots (9)$$

Then the displacement conditions are

$$\bar{u}_{n_1} = u_{n_b} + u_{t_b} \tan \frac{\alpha_1}{2} \quad \ldots\ldots\ldots\ldots\ldots (10)$$

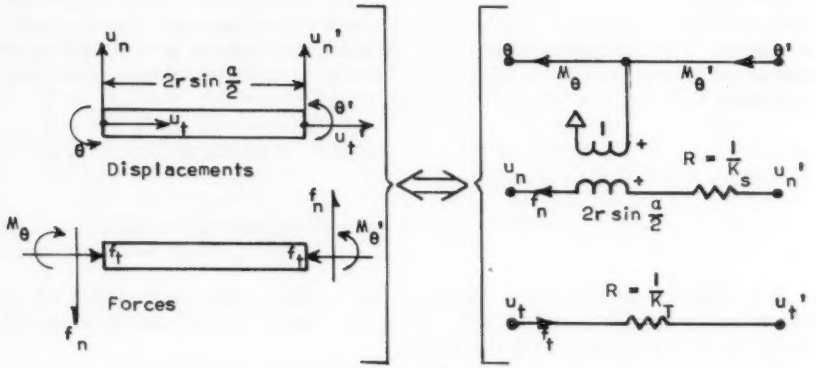

(a) ARCH CHORD ELEMENT

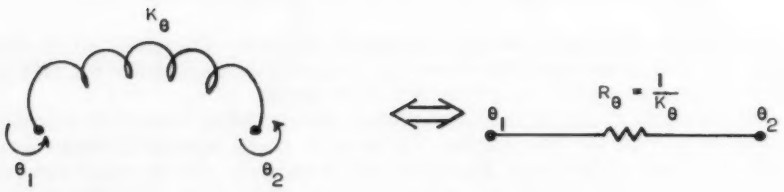

(b) ARCH BENDING SPRING

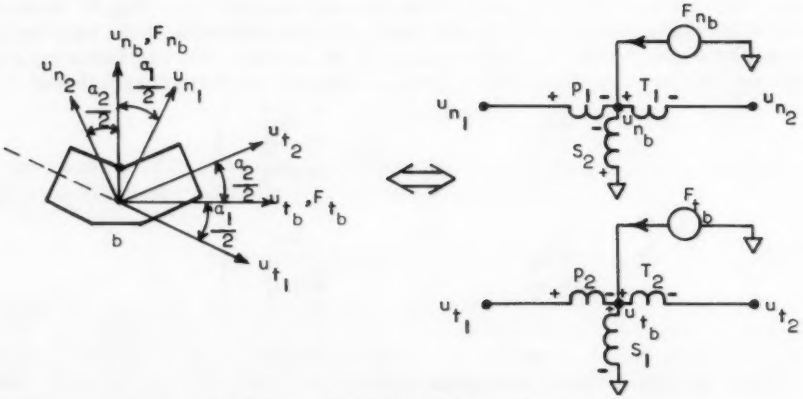

(c) JOINT BETWEEN ARCH ELEMENTS

FIG. 10.—ANALOGIES FOR THE ELEMENTS OF AN ARCH DAM

$$\bar{u}_{n_2} = u_{n_b} - u_{t_b} \tan\frac{\alpha_2}{2} \quad \ldots\ldots\ldots\ldots\ldots\ldots (11)$$

$$\bar{u}_{t_1} = u_{t_b} - u_{n_b} \tan\frac{\alpha_1}{2} \quad \ldots\ldots\ldots\ldots\ldots\ldots (12)$$

and,

$$\bar{u}_{t_2} = u_{t_b} + u_{n_b} \tan\frac{\alpha_2}{2} \quad \ldots\ldots\ldots\ldots\ldots\ldots (13)$$

These relationships are satisfied by the circuit of Fig. 10(c), provided that the transformer turns ratios are set to the following values for transformer 1:

$$\frac{P_1}{s_1} = \tan\frac{\alpha_1}{2} \qquad \frac{T_1}{s_1} = \tan\frac{\alpha_2}{2} \quad \ldots\ldots\ldots\ldots\ldots (14a)$$

and for transformer 2;

$$\frac{P_2}{s_2} = \tan\frac{\alpha_1}{2} \qquad \frac{T_2}{s_2} = \tan\frac{\alpha_2}{2} \quad \ldots\ldots\ldots\ldots\ldots (14b)$$

The scale transformation of Eq. 9 must also be applied to the arch chord elements.

The current generators simulating radial and tangential loads are connected to nodes where the voltages are proportional to u_{n_b} and u_{t_b}. The circuits for the other elements in Fig. 10 make use of previously derived analogies.

The manner in which the elements are connected together is illustrated in Fig. 11, which shows the complete analogy for a very simple model consisting of two arches and one cantilever. The foundation is assumed to be infinetely rigid so that all components of displacement are zero at the abutments. This condition is simulated by grounding all electrical elements at points on the abutments. The circuit is shown in four separate diagrams, one diagram for each type of coordinate represented in the analysis. Expressed in electrical terms, the conditions of displacement continuity are that, at points where elements are connected together, voltages corresponding to the same type of coordinate are equal. These conditions are satisfied by solid electrical connections between corresponding nodes.

The electrical analogy for an arch dam model containing many arches and many cantilevers is similar in form to Fig. 11, but contains many more electrical elements. Special problems encountered in practical analyses will be discussed subsequently.

ANALYSIS OF THE STEVENSON CREEK DAM

The Stevenson Creek Dam is a small test dam built in 1926 specifically for the purpose of obtaining field measurements of the stresses and deformations of an arch dam. A complete account of the construction and testing is given elsewhere.[16] The dimensions of the dam are shown in Fig. 6, where it may be seen that the abutment profile is an almost exactly symmetrical 45° V. The dam was instrumented on the downstream face with gages that measured the horizontal and vertical components of strain. The small reservoir could be emptied or filled in a few hours so that fairly reliable measurements of the

[16] "Arch Dam Investigation," Report by ASCE Committee, Vol. 1, November, 1927.

FIG. 11.—ANALOGY FOR ARCH DAM

strains due to water load were obtained. The dam was filled to progressively higher levels as the tests proceeded. Large vertical cracks appeared at the top and bottom of the crown section when the water level reached 40 ft, the cracks extending about 15 ft up from the bottom and 15 ft down from the crest. The cracks did not appear to grow when the water level was raised to the crest of the dam (60 ft).

The Stevenson Creek Dam was selected for investigation on the analog computer because of the availability of carefully recorded field measurements, the simplicity of the cylindrical structure, and the general interest in the dam as a test structure. The crown section was considered to be a plane of symmetry so that a representation of only one half of the dam was required in the analysis. As shown in Fig. 6, the idealized model of the half-dam contained six arches and three vertical cantilevers. The number of cantilevers was made purposely small in order to examine the effects of finite-difference approximations under conditions where these effects would be large.

A complete description of the analog computer investigation is given elsewhere.[17] The electrical analogy contained a total of 48 transformers and 140 resistors. A large number of cases were analyzed corresponding to different water levels, different temperature conditions, different elastic moduli for the foundation material, and different conditions of cracking along the abutments and along the crown section.

The effects of a uniform temperature change were examined by the equivalent load method discussed previously. The presence of the foundation was simulated by shear, bending and thrust springs computed by the method of F. Vogt.[18] These springs were replaced by electrical resistors which were added in series with corresponding adjacent elements of the dam.

The effects of cracks could only be guessed. In the case of the crack at the top of the crown section, it was reported[16] that this crack did not close until the dam was nearly filled with water. For this reason the thrust stiffness of the top arch (B) at the centerline was made zero and the thrust stiffness at the centerline of arch D was given a reduced value. Arches B, D, and L were given zero bending stiffness at the centerline.

Results of the cracked dam simulation with a full head (60 ft) of water and no temperature change are shown in Figs. 12, 13, and 14, where they are compared with stresses derived from field measurements. For this comparison it was assumed that the elastic modulus of the concrete used in the dam is 2.9×10^6 psi, that the elastic modulus of the foundation, E, is 1.6×10^6 psi and that Poisson's ratio, μ, for the dam is 0.15. Since strains rather than stresses were measured in the field, values of E and μ are required for the reduction of stresses from field measurements.

In Fig. 12 it will be observed that the peak horizontal stress on the downstream face obtained on the analog computer is about 100 psi less than the peak stress obtained from field measurements. There is reason to believe that part of this discrepancy is due to finite difference approximation in the arch bending model which increases twisting moments at the expense of arch bending moments. This approximation can be greatly reduced by a refinement of the arch bending model.

---

17 "Analysis of Stevenson Creek Arch Dam," by R. H. MacNeal and J. H. Hill, Computer Engrg. Assocs. report on project REE 148, March, 1959.

18 "Uber die Berechnung der Fundament deformation," by F. Vogt, Anhandlinger det Norske Videnskaps-Academi, Oslo, 1925.

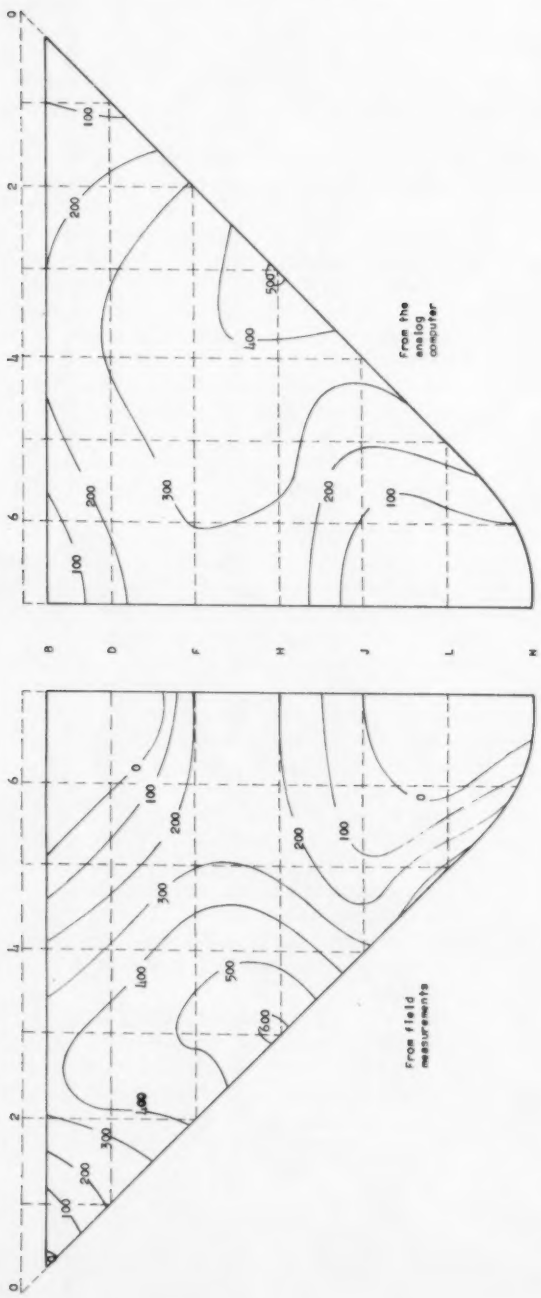

FIG. 12.—LINES OF CONSTANT HORIZONTAL STRESS (psi)

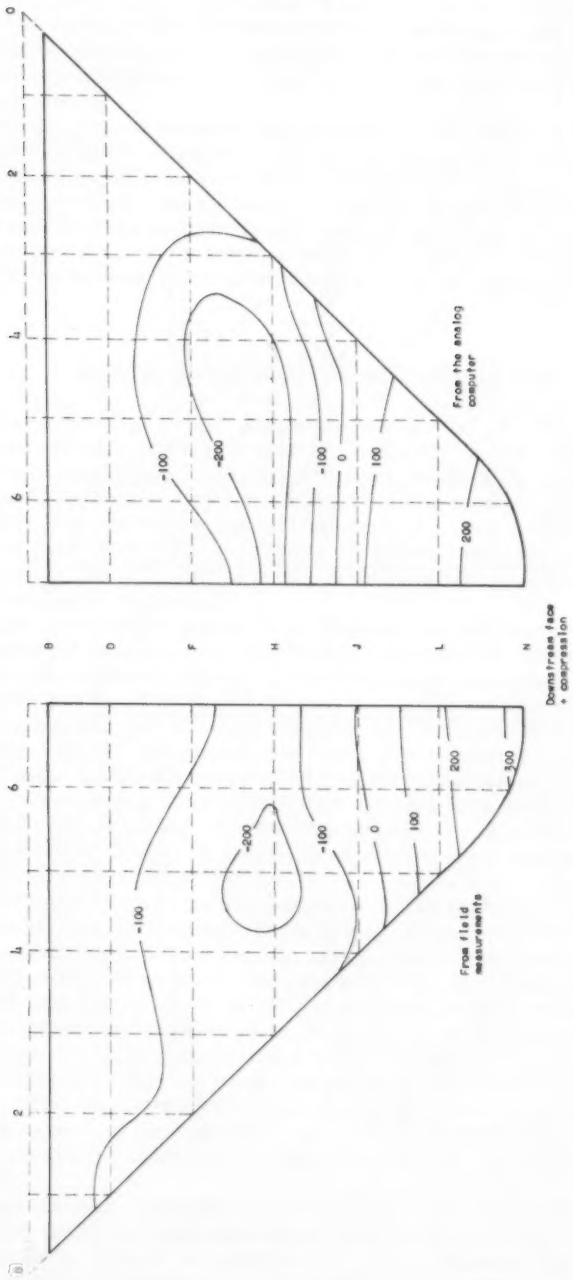

FIG. 13.—LINES OF CONSTANT VERTICAL STRESS (psi)

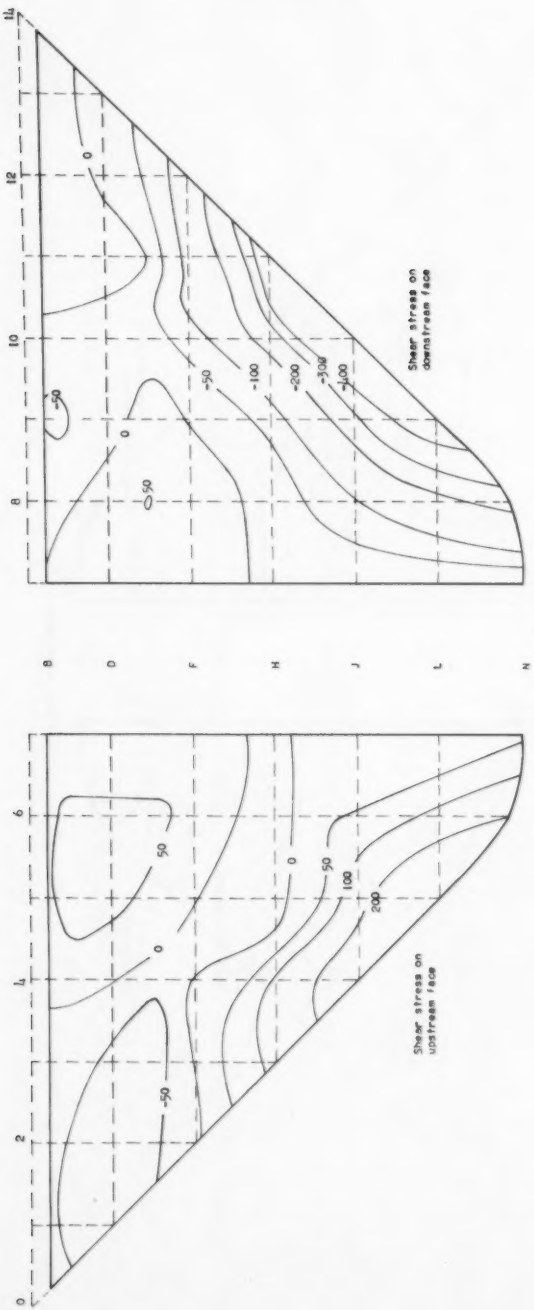

FIG. 14.—LINES OF CONSTANT SHEAR STRESS (psi)

No field measurements were made of shear strains. The analog computer results given in Fig. 14 show a concentration of shear stresses along the abutments. These shear stresses measured in a horizontal-vertical coordinate system indicate a tendency of the dam to bend about axes that were coincident with the abutments.

The contour plots of stresses were obtained from analog computer results by the following steps. Electrical currents were converted into internal loads and moments of the idealized model. These loads and moments were converted into stress components on the faces of the dam at specific points. Contributions to a stress component from different sources, such as horizontal stress due to arch thrust and arch bending, were interpolated to the same points and added. Finally contour lines were drawn with these values as bench marks.

DESIGN STUDY FOR THE BLUE RIDGE DAM

Sketches of the Blue Ridge Dam are shown in Fig. 15. The canyon profile is distinctly unsymmetrical with a fairly steep slope on the right abutment and a relatively gentle slope on the left abutment terminating in a thrust block. The radius of curvature varies from 223 ft at the crest to less than 100 ft at stream bed. The arch barrel is exceptionally thin with a ratio of base width to height of less than 10%. In order to eliminate extensive undercutting due to change of radius with elevation, the crown section is inclined downstream at an average angle of about 15°.

The distortions of the geometrical shape of the dam from a true cylinder create problems in analysis not previously mentioned in this paper. The first problem is the matter of defining the centerlines of cantilevers in the idealized model. This problem was solved by passing planes through a vertical reference axis arbitrarily located near the "average" center of curvature of the dam as shown in Fig. 15. Intersections of these planes with the arch centerlines define the arch-cantilever intersection points. An elevation diagram was then prepared by projecting these points on a cylinder with the reference axis as center, as shown in Fig. 15. In this diagram arches and cantilevers are horizontal and vertical lines. As may be seen, a total of six arches and nine cantilevers were used in the analysis.

The second problem is the determination of the principal planes of bending of a cantilever. In the model of a cylindrical dam, a cantilever is assumed to have infinite bending stiffness about an axis perpendicular to the face of the dam and infinite stiffness about an axis tangent to the face of the dam. In a noncylindrical dam the direction of the normal changes along each cantilever so that the principal planes of bending are rotated as the elevation is changed. This problem was solved by changing the directions of the principal planes at arch-cantilever intersection points, so that each cantilever element remained untwisted. The tangential and radial displacements of a cantilever element were then related to the tangential and radial displacements of the adjacent arches in the electrical analogy by means of additional taps on the transformers in Fig. 10(c).

Perhaps the most important problem is the resolution of applied loads into components. Since the cantilevers are inclined they cannot resist vertical loads without bending. The crown section is, in fact, statically unstable under the action of gravity. This problem was handled by resolving applied loads into

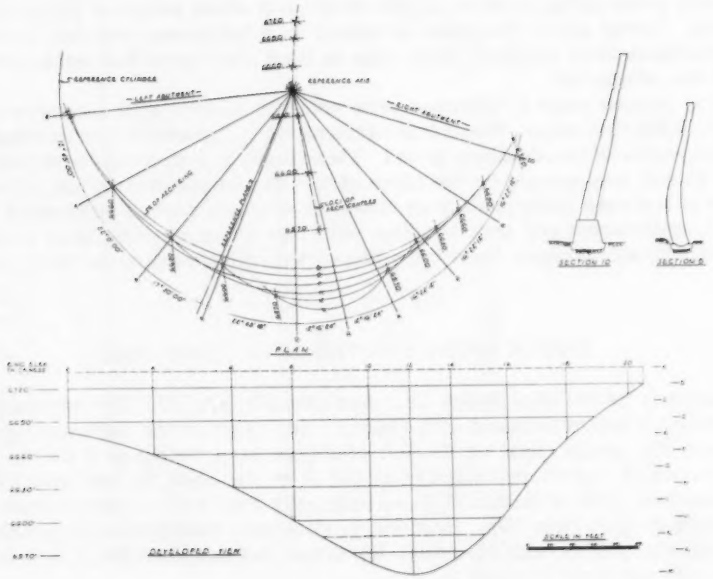

FIG. 15.—BLUE RIDGE DAM

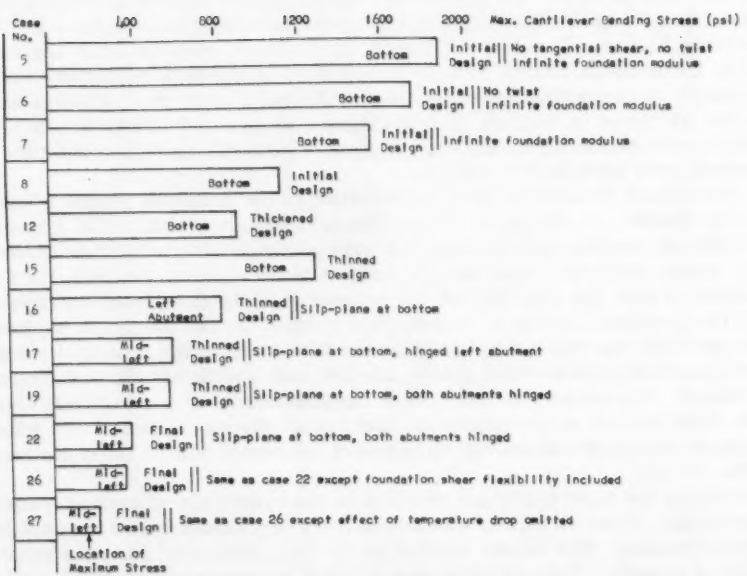
Case No.
400
800
1200
1600
2000
Max. Cantilever Bending Stress (psi)
5 Bottom Initial Design || No tangential shear, no twist infinite foundation modulus
6 Bottom Initial Design || No twist infinite foundation modulus
7 Bottom Initial Design || Infinite foundation modulus
8 Bottom Initial Design
12 Bottom Thickened Design
15 Bottom Thinned Design
16 Left Abutment Thinned Design || Slip-plane at bottom
17 Mid-left Thinned Design || Slip-plane at bottom, hinged left abutment
19 Mid-left Thinned Design || Slip-plane at bottom, both abutments hinged
22 Mid-left Final Design || Slip-plane at bottom, both abutments hinged
26 Mid-left Final Design || Same as case 22 except foundation shear flexibility included
27 Mid-left Final Design || Same as case 26 except effect of temperature drop omitted
Location of Maximum Stress

FIG. 16.—CASE HISTORY OF MAXIMUM CANTILEVER BENDING STRESS

horizontal components and components tangent to the axes of the cantilevers. The horizontal components so defined were assumed to be resisted by the lateral load-carrying capacity of the dam as a whole, including arch bending, cantilever bending, and so on.

The components tangent to the axes of cantilevers were assumed to be carried by cantilever thrust without bending. These assumptions appear reasonable so long as the radius of curvature in a vertical plane is large compared to the radius of curvature in a horizontal plane.

The electrical circuit analogy for the dam was similar in form to that of Fig. 11 and employed approximately 140 transformers, 250 resistors, and 70 current generators. As in the analysis of the Stevenson Creek Dam foundation flexibility was simulated by the method indicated by Vogt.[18] The foundation modulus for thrust was made less than the foundation modulus for bending in order to approximate the effect of plastic deformation.

The primary objective of the study was to find a satisfactory design in which allowable stresses were not exceeded. Subsidiary objectives were to investigate the mechanisms of load distribution and to analyze the final design configuration for a variety of loading conditions. Complete sets of stresses and deflections were obtained for a total of 36 cases.

In the first seven cases the elastic model of the dam was built up by adding an additional class of elements in each successive case. Thus arch thrust flexibility, cantilever bending stiffness, tangential shear stiffness, twisting stiffness, and foundation flexibility were successively added. Besides providing simplified models that could be easily checked, these cases gave valuable insight into the importance of each type of element and the mechanisms of load transfer generally.

The next twenty cases were used in the investigation of design modifications. In the initial design, extremely high cantilever bending stresses were observed at the base of the dam. It was soon realized that these high stresses could not be eliminated either by reasonable changes in the thickness of the dam or by minor changes in its shape. Major improvements were obtained by introducing a slip plane midway between arches J and L (Fig. 17) and by hinging the dam along the abutments. After these changes were made, the region of maximum cantilever bending stresses was shifted to the neighborhood of the intersection of arch F and cantilever No. 8. These stresses were further reduced by changing the thickness distribution in the top half of the dam. Satisfactory stress levels were finally achieved by eliminating the effects of temperature drop. The progress made in reducing cantilever bending stresses is indicated by the bar chart in Fig. 16.

The last nine cases were used for the investigation of minor design alternatives and for the analysis of additional loading conditions such as water loads for a partly filled reservoir and equivalent earthquake loads. The principal stresses on the upstream and downstream faces of the final dam design are shown in Fig. 17. The radial deflections for this case are shown in Fig. 18. The design study of the Blue Ridge Dam occupied the analog computer for a total time of ten days.

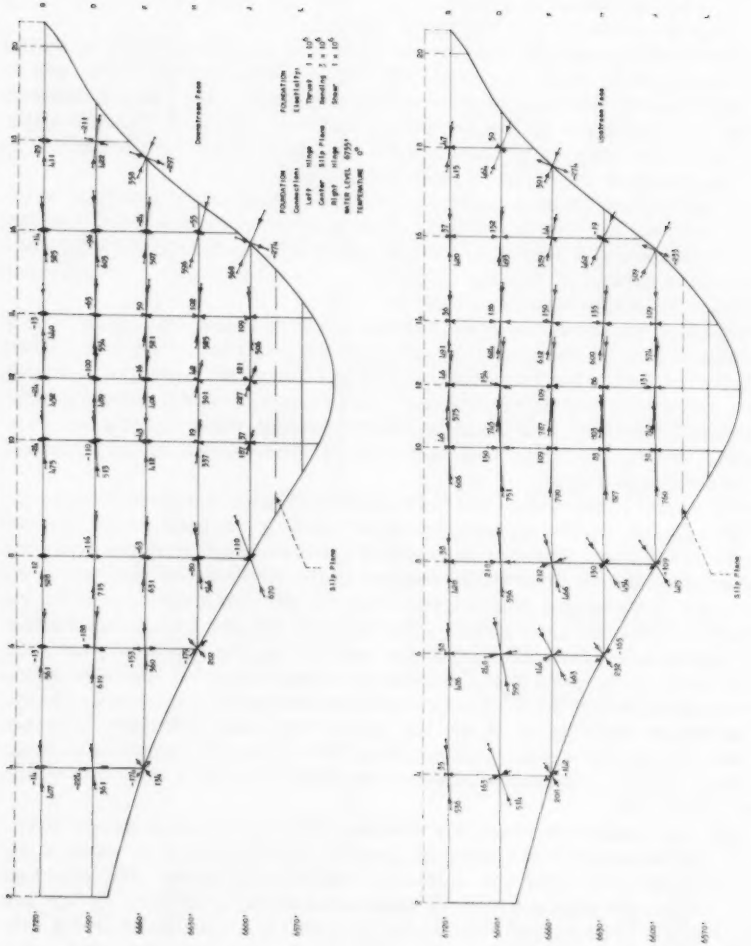

FIG. 17.—PRINCIPAL STRESSES FOR FINAL DESIGN OF THE BLUD RIDGE DAM

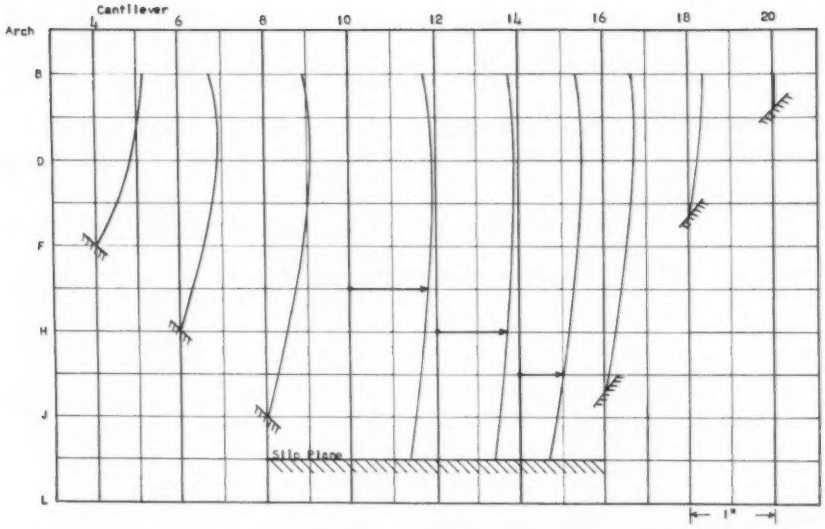

FIG. 18.—RADIAL DEFLECTIONS FOR THE FINAL DESIGN OF THE BLUE RIDGE DAM

ACKNOWLEDGMENTS

The arch dam design study for the Blue Ridge Dam was performed for the firm of Leeds, Hill and Jewett of Los Angeles, Calif. A complete report of the results of this study is given elsewhere.[19]

19 "Design Study of the Blue Ridge Dam," by R. H. MacNeal and J. H. Hill, Computer Engrg. Assocs. report on project ESS 143, March, 1959.

Journal of the
ENGINEERING MECHANICS DIVISION
Proceedings of the American Society of Civil Engineers

ELASTIC MODEL DESIGN OF THE B-58 AIRPLANE

By J. W. Wells[1] and H. B. England[2]

SYNOPSIS

This paper outlines the extensive elastic model test program used in the design of highly redundant structure on the B-58 airplane. Considerations in the design of the various models on the program are listed and several unique methods of obtaining and presenting test data are shown. Scale factors for both structure and loadings are developed in detail in the Appendix.

INTRODUCTION

The elastic model program used in the stress analysis of the B-58 bomber at Convair-Fort Worth, A Division of General Dynamics Corporation, represents one of the most extensive programs of its kind ever attempted. It was started at a time when other available methods for analyzing highly redundant structures had failed completely in producing the degree of accuracy required by this radical, long range weapons system with its minimum structural weight requirements (Figs. 1 and 2).

The latest model in this program is now being used in the evaluating of a number of design improvements on the production B-58 airplane. This model represents the last of four distinct model configurations used, since 1952, in evaluating more than 300 full airplane loading conditions (Fig. 3).

Note.—Discussion open until January 1, 1961. To extend the closing date one month, a written request must be filed with the Executive Secretary, ASCE. This paper is part of the copyrighted Journal of the Engineering Mechanics Division, Proceedings of the American Society of Civil Engineers, Vol. 86, No. EM 4, August, 1960.

[1] Sr. Struct. Engr., Convair-Ft. Worth, A Division of General Dynamics Corporation.
[2] Sr. Struct. Engr., Convair-Ft. Worth, A Division of General Dynamics Corporation.

FIG. 1

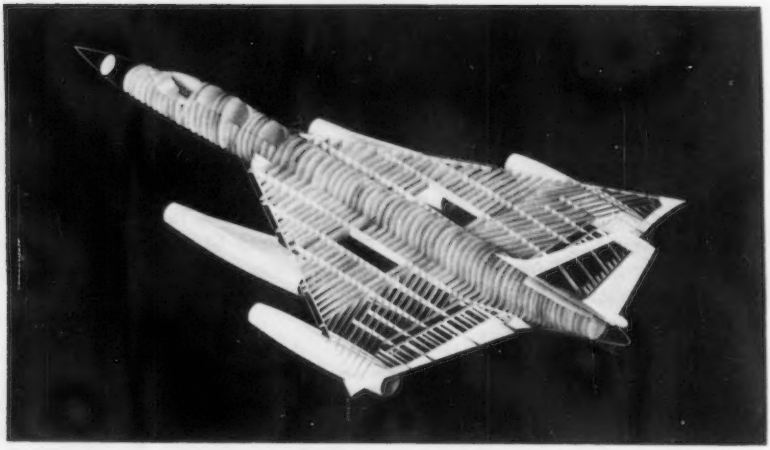

FIG. 2

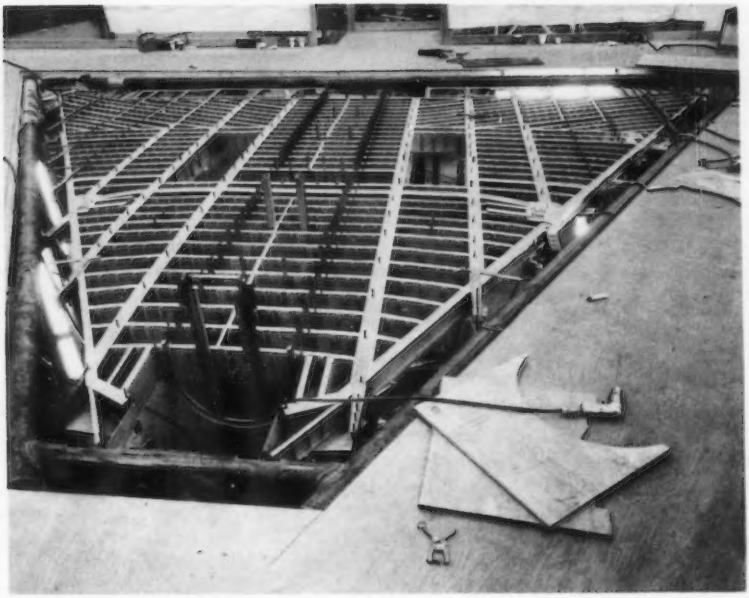

FIG. 3

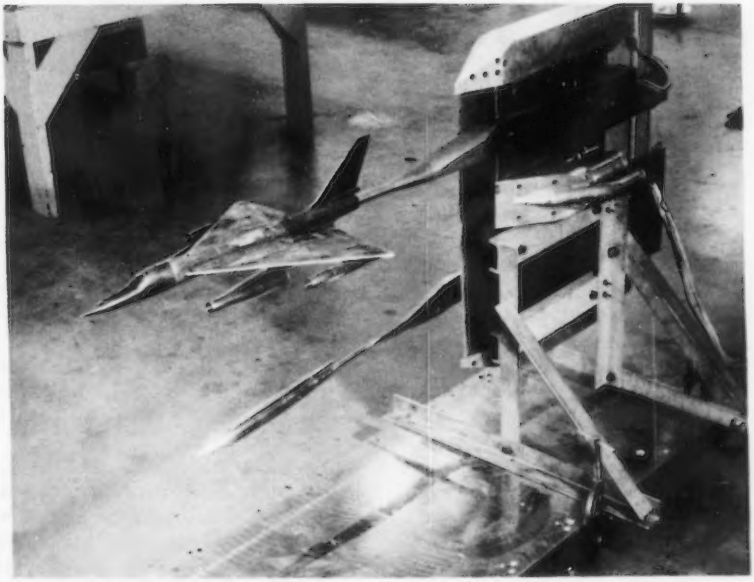

FIG. 4

DEFINITION OF AN ELASTIC MODEL

An elastic model is a representation that structurally simulates its prototype in one or more important respects, and has the necessary provisions included for simulating predicted loadings, usually by hydraulic rams or lead weights. Additional provisions are commonly made in the form of strain and dial gages for determining stresses and deflections at significant points during test loadings.

The size of the model, degree of simulation, extent of instrumentation and number of conditions to be tested are strictly a function of the accuracy needed and time and money available for the program. Scale models range in size from as small as 1/100 for small plastic models up to full size as is the case for static test airplanes.

OTHER TYPES OF SCALE MODELS

A number of other types of models are used in the developmental phases of an airplane. Several of these are the force model, pressure model, and flutter model. Each of these is a true aerodynamic model and represents the outside configuration of its prototype to a high degree. While the force model (Fig. 4) determines only a value of total net airload for a given attitude, the pressure model yields a refined pressure distribution over its surface. The flutter model simulates the external airplane contour, its elastic properties, and its internal mass distribution in the evaluation of certain aeroelastic phenomena (Fig. 5).

NEED FOR THE ELASTIC MODEL PROGRAM

At the initiation of the elastic model program in 1952, the most advanced analytical method available for the analysis of redundant structures consisted of attempted hand solutions of structural matrices near order 30. Later, the IBM-701 high speed digital computer became available for use on this project. The largest passive analog computer available was the SES Analog installation at the California Institute of Technology. However, all attempts at using both these techniques in an over-all analysis of the wing proved futile. Where certain simplifying and overlapping assumptions would have been possible for a different type of weapons system, the B-58 with its maximum range concept demanded an absolute, unyielding loyalty to the task of eliminating all unnecessary structural weight. This could only be attained by devising a more rigorous and extensive analysis technique for redundant structures than had previously been attempted.

Because of the success achieved using experimental methods on other problems which had defied analytical solution, it was decided to attempt an experimental technique on this program. Therefore, a feasibility study was started to outline the requirements of the initial model configuration.

This experimental model technique has proved so successful that the first crudely designed 1/4 scale model has been succeeded by three others, each incorporating extensive improvements in both degree of simulation and amount of instrumentation. The last model, the 3/8 scale, has provisions for reading strains at 1,826 locations and deflections at 170 locations during a given test. Virtually all extensive data reduction, such as principal stress determinations

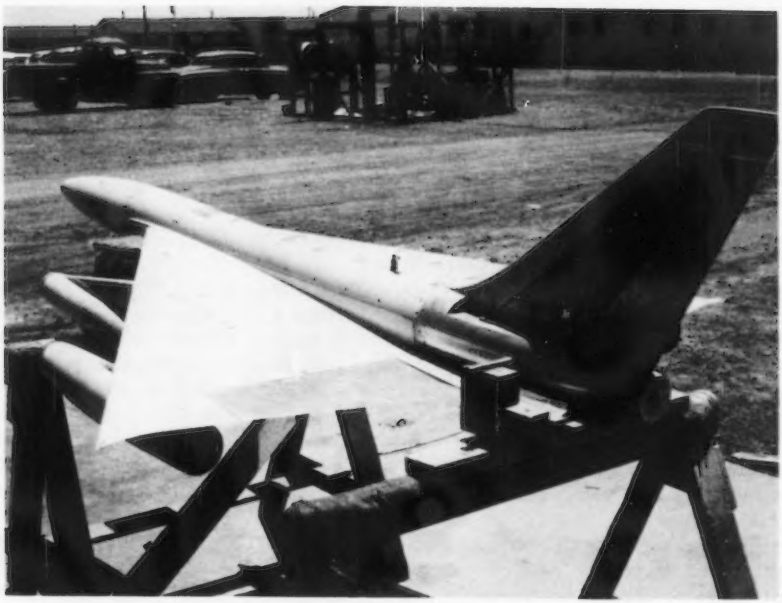

FIG. 5

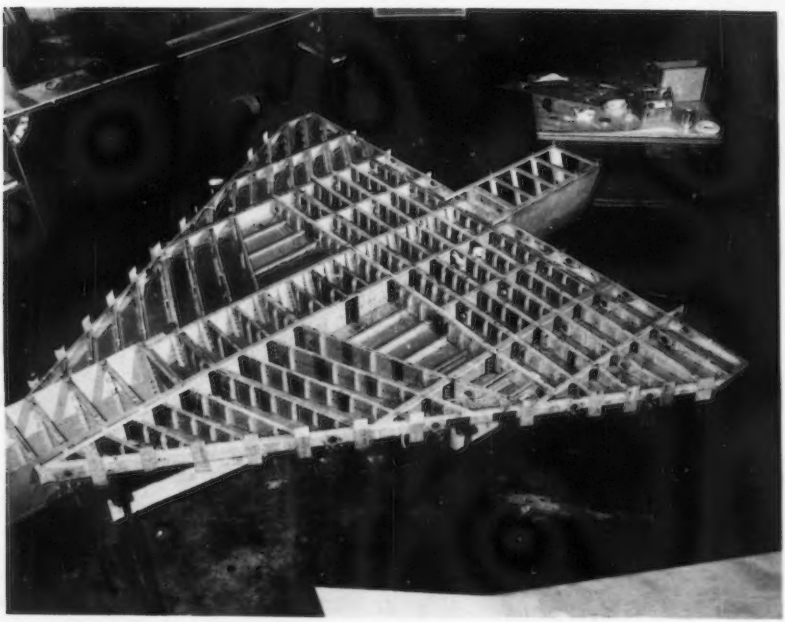

FIG. 6

and internal station balances, are coded for solution on the computer installation.

Because this latest model incorporates all the refinements of its predecessors, the balance of this paper will be concerned with explaining only the details of the 3/8 scale elastic model program.

DESIGN AND INSTRUMENTATION

Design Of 3/8 Scale Elastic Model.—The unusual 3/8 scale of this final elastic model was selected as a compromise between two of the earlier models having scales of 1/4 and 1/2 respectively. After two of the earlier 1/4 scale models had been built it became apparent that they were too small to provide space for refined representation of small fittings and installation of necessary strain gages. Because the 1/2 scale model, built to represent only the outer portion of the wing, had proved to be more than adequate in size and costly in construction it was decided to proceed with a 3/8 scale representation. After more than three years of testing on this model, its scale selection has been fully justified. One consideration in keeping a model's scale as small as possible is the reduction in the amount of simulated load that must be applied for each test condition. It should be noted that by keeping all other considerations equal, an increase in model scale by a factor of 2.0 increases the amount of applied load for a given condition by a factor of 4.0. The necessity of applying additional load of this magnitude during a test can be very time consuming and costly. Therefore, any increase in model scale should be fully justified before being approved.

Model Scaling Factors.—Requirements and assumptions that must be considered in any general scaled prototype representation and those considered in the 3/8 scale elastic model program are included in detail in the Appendix.

Structure Simulated On The Model.—Because the elastic model program was started primarily for use as a tool in wing stress analysis, no great degree of refinement was included in the simulation of other airplane components. Photographs of the earlier models show no nacelle or vertical tail representation and show only a crude box structure used to simulate fuselage stiffness (Figs. 6 and 7).

However, it became evident early in the program that some refined simulation of other components would be justified because their elastic properties affected wing internal loads and the model presented an economical method of obtaining their design stresses as well as those for the wing. Again, a study of the four models on the program indicates a successive increase in the degree of component simulations on each.

The 3/8 scale model shows the greatest development of this concept of all component representation. In it is found a model that simulates virtually all the wing, fuselage, and nacelle structure. Even the vertical tail is simulated near its root to insure proper load introductions to the aft fuselage structure (Figs. 8, 9, and 10). The only remaining components not simulated are the landing gear and elevous. However, the computed loads on these components are introduced as concentrated loads at their simulated points of attachment on the model.

Although the earlier models simulated the stiffness of several structural members by only one model member, this lumping has been almost completely eliminated on the latest design. Although lumping stiffnesses of members and

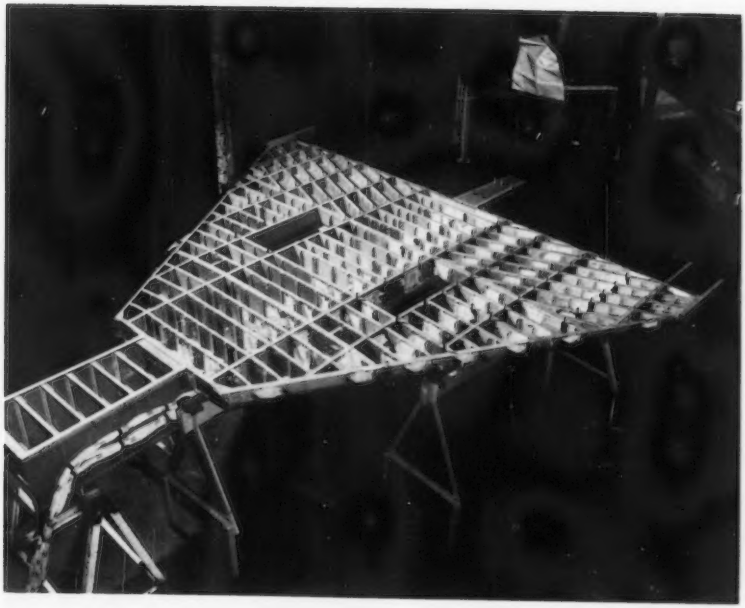

FIG. 7

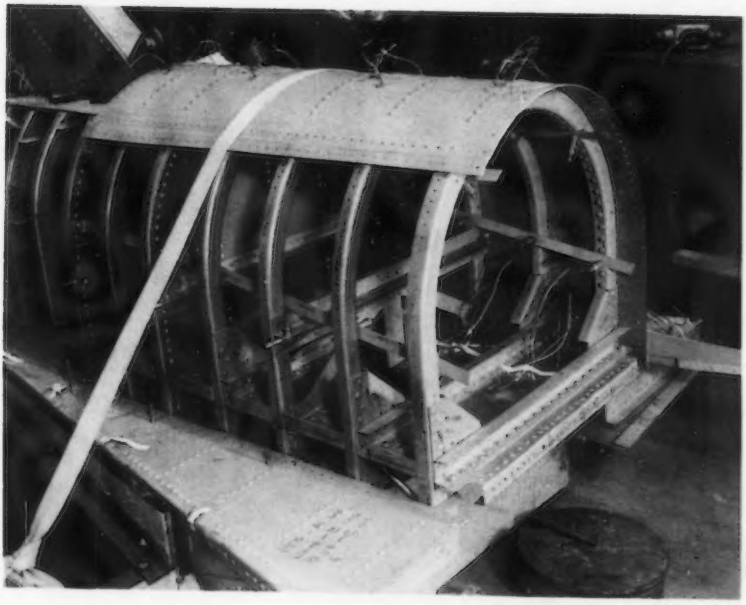

FIG. 8

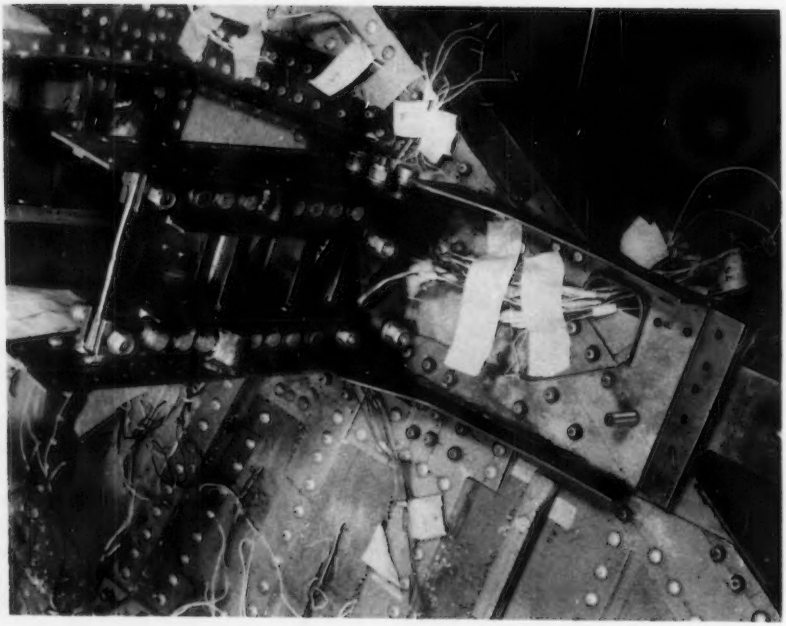

FIG. 10

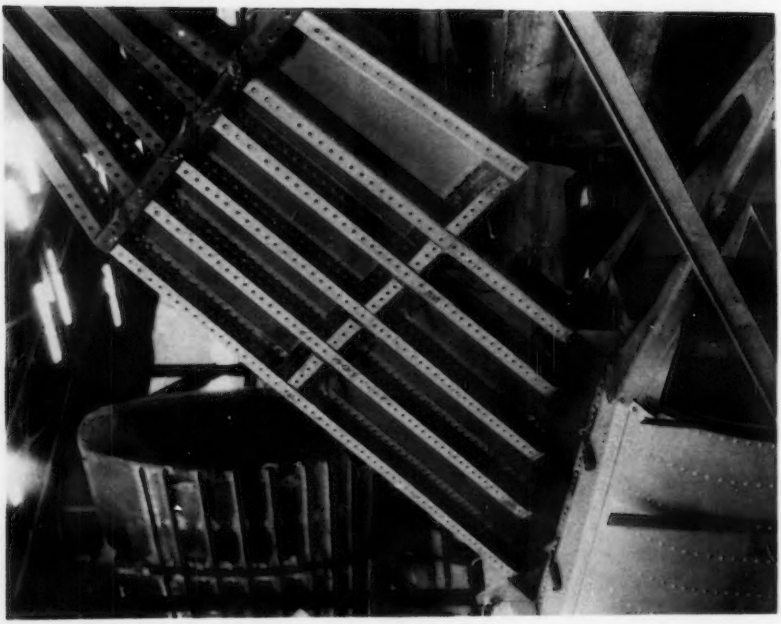

FIG. 9

their external loadings presents no difficulty, the unlumping of the resulting data to determine individual prototype member loads is next to impossible.

Load fittings are provided on the model to accommodate every major point of load introduction on the prototype such as pod hooks, landing gear fittings, and others. In addition, load points are provided at virtually every structural intersection for the application of needed loads and moments. This extensive load introduction system on the model permits application of scaled prototype distributed loadings with a minimum loss of accuracy due to lumping.

Representation Of Unconventional Prototype Structure.—A number of advanced manufacturing and design methods used in the prototype could not be incorporated in the model because of their unavailability at the time of model design or the excessive cost of tooling for a scaled representation. One of these was the corrugated spar and bulkhead webs in the wing substructure. These corrugations were designed to replace the conventional vertical stiffeners previously used in the prevention of web buckling. Because their exact representation was not feasible, it was decided to use conventional flat web stiffener combinations on the model (Fig. 11). However, the longer length of curved web per inch of spar on the airplane had to be considered in model flat-web design such that a correct representation of web shear deformation per inch of spar on the model would result.

This was done by substituting model webs having a thickness factor inversely proportional to the web length "growth factor" on the prototype. This resulted in a thinner web of shorter length operating at a higher stress than the longer airplane counterpart. The correct amount of web shear deformation per unit length of spar was obtained. Because this is one of the few cases where model stresses are not directly applicable to those on the airplane, the data obtained are presented in terms of equivalent airplane load in pounds. This is especially useful in the few cases where airplane webs have been replaced by diagonal trusses after the model design was completed.

A decision to simulate the structural sandwich of the airplane wing surfaces would have been entirely impossible in 1952 when the first model was designed, because bonded sandwich panels were still in the primitive stages of development. Even later a direct scaled representation on the model would have been prohibitive in both cost and time. Therefore, these surfaces were simulated by conventional flat skins and slugs (Fig. 11). The centroids of the skins on the model were located as closely as possible to the comparable surface panel centroid on the airplane. The simulation of the internal concentrated slug bending material in the airplane panels was included in spar and bulkhead caps and by external slugs where model cap areas became excessive.

Where feasible, exact airplane methods of construction are incorporated on the model. In the case of the outboard pylon plate, which provides attachment between the wing and nacelle, a welded steel structure is provided to simulate a similar steel forging used on the prototype (Fig. 12).

Instrumentation Installed On The Model.—In order to provide internal load distributions for its prototype, the model includes one of the most extensive installations of strain gages ever attempted (Fig. 13). These gages provide measurements of axial, shear, and combinations of axial strain at various locations on the model depending on the type gage and its installation. In spar and bulkhead flanges and fittings requiring only uniaxial stress determinations, approximately 550 axial gages are installed. In spar and bulkhead webs and

certain surface material for which only shearing stresses in one plane are required, 496 V-setts gages have been installed. The most refined strain determinations are obtained on model surface panels where 260 rosette gages are

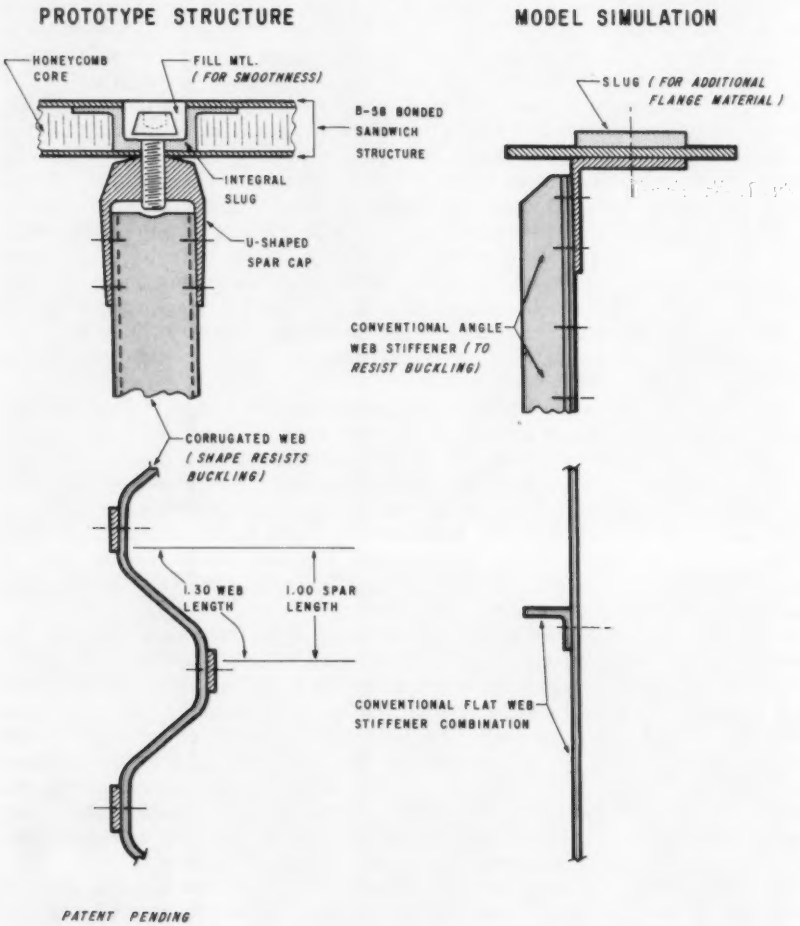

FIG. 11.—VIEW OF TYPICAL B-58 AND ELASTIC MODEL STRUCTURAL DETAILS FOR SURFACE PANEL AND SUBSTRUCTURE, INCLUDING MODEL REPRESENTATION OF BONDED SANDWICH PANELS AND CORRUGATED WEBS

mounted. The latter gages measure three values of strain at 45° to each other. These values of strain at a point are used to determine the complete state of stress using equations graphically represented by Mohr's Circle.

FIG. 12

FIG. 13

Wherever possible, each gage installed on the model is "backed" and wired into the recording instrument to eliminate the effect of local plate buckling from the recorded strains.

One of the most serious problems that has existed throughout the model program is the evaluation of long time drift due to temperature and other effects in the measured strain data. The temperature effects are not one of heat being applied as a part of the test, but rather a case of the model changing temperature due to its surroundings during the eight or more hours between the initial and final data recordings for a test.

Unfortunately, the unaided strain gage reflects total strain experienced by the part on which it is mounted and has no way of differentiating between strain produced by loading and that produced by thermal expansion. To avoid this, each active gage on the model is wired to a similar dummy gage mounted on an unloaded piece of identical material nearby. The wiring is such that the strain of the dummy gage (which is wholly thermal in nature) is subtracted from the total reading of the active gage (which is both thermal and loaded in nature) yielding only the strain produced by load. It is assumed that the material of the model and the material for the dummy gage will change temperature uniformly during the test.

The following additional provisions are made to either minimize, or help in evaluating these thermal effects:

1. The model is mounted in an air conditioned test laboratory where air temperature is held as constant as possible.
2. A high wooden wall has been built around the test area to protect it from the blasts of hot or cold air occasioned by opening doors to permit entrance of equipment or personnel to other areas of the test lab during a model test.
3. Both the initial and final readings for each gage are recorded with only tare load applied. Any difference between these readings indicates some sort of long time drift in the strain recording setup. Most of this is probably caused by temperature change in the model structure between these readings.

Data Recording Equipment On Model.—The strains and deflections on the elastic model are recorded by a number of different types of instruments depending on their locations and the accuracy required. Deflections near the root of the wing and along the centerline of the fuselage are measured by dial gages that can be read to the nearest 0.001 in. As these gages provide a maximum travel of only 1 in., deflections in the outer portion of the wing are measured by making observations with a surveyor's level to an accuracy of 0.01 in. (Fig. 13).

Indicated strains are measured by both manually read Brown Indicators and SADIC automatic recorders. Various switching techniques and patter box arrangements have been used to expand the capacity of the indicators to where approximately 1700 channels of instrumentation may be recorded using only two 100 channel SADIC's and 10 Brown recorders. Although the model has 1,826 channels of installed instrumentation, no condition yet tested has indicated a pre-test severity justifying the reading of more than 1500 channels. This elimination of strain readings in apparently non-critical areas has contributed greatly to the over-all economy of the program.

The validity of each recording instrument during a test is checked by reading at least one channel of strain data on each instrument from a calibrated load bar. At the end of the test, each recorded value of strain from the load

bar is compared against the known value as a check of the accuracy of each instrument. In a number of cases, faulty data from certain instruments have been corrected after the test and retests avoided by using correction factors derived from this check information.

LOAD PREPARATION AND TESTING

Load condition preparation for the model involves selecting the most critical conditions the airplane is required to sustain, determining the complete airplane loading for each, and converting these loads to model magnitude, keeping in mind both scale factors and model loading capabilities.

The B-58 bomber is designed to operate at all speeds up to twice the speed of sound at altitudes above 50,000 ft under a multiplicity of gross weight and weapons configurations. This array of possible conditions is so extensive that a criteria group is set up to determine the airplane's capability and to select the structurally significant conditions within the criteria approved by the Air Force. After its selection, a test condition is outlined by listing such items as its Mach number, gross weight, altitude, angular and scalar accelerations, attitude, control surface deflections, and weapons configuration.

This condition description is used by another group, charged with the responsibility of determining distributed loadings, as a guide to combining of unit data for the condition. This unit data consists of predicted pressure distribution over the airplane for certain types of situations such as unit change in angle of attack, elevator setting, yaw angle, and many others. After all necessary unit data have been combined as dictated by the condition description, a resulting pressure distribution for the entire airplane results. This is then combined with an inertia distribution consisting of each item of weight times its local acceleration, yielding a perfectly balanced airplane loading. For all conditions, total inertia loads exactly balance total applied loads. For flight conditions the applied loads result from pressure distributions, whereas those for ground conditions originate either from landing gear or drag chute loads.

After the airplane distributed loading for the condition has been obtained, it is lumped to model load introduction panel points and reduced in magnitude, through the use of model scale factors. This tabulation of "panel point loads" is released to the elastic model test group.

Pre-Test Condition Evaluation.—Because design stresses are urgently needed during the design stages of an airplane, efforts are made to restrict consideration to the more critical conditions for test on the model as a saving in both time and money. Therefore, as soon as a test condition has been received, its external load summaries are rigorously compared against those for previously tested critical conditions. Unless it appears to be comparatively critical, the condition is either omitted from testing or relegated to the latter stages of the test program. This severe scrutiny of external loads for a condition in comparison with others from the same airplane sometimes points up peculiarities that might indicate errors in some stage of the condition's preparation. Of course, similar checks of both severity and validity are performed in both the criteria and loads preparation groups while the condition is being prepared.

Preparation Of Pre-Test Data.—If the evaluation of a condition proves it to be both valid and significantly critical, it is released to the engineering test

lab for testing on the model. At that time, test lab personnel are notified of expected critical areas of the condition and its relative severity with respect to other conditions currently scheduled for testing. This information is used in determining what instrumented areas will be monitored during the test by the limited strain recording equipment.

While the actual rigging of load points, wiring of required strain gage channels, and pretest operations are continuing in the test lab, certain test facilitation data are being prepared by the elastic model group. The most important of these are the "load sequence cards" which indicate the order of loading panel points during a given test. Because of both personnel and equipment limitations it is impractical to load all 340 model points simultaneously. These load sequence cards provide a recommended order of loading that maintains a safe balance between up and down loads at all times. It was learned early in the program that any random loading of model panel points would soon result in disaster. In addition to maintaining an approximate vertical balance, the load sequence cards also keep side, roll, yaw, and pitch unbalances within safe limits.

Model Support Points.—The model is supported at only three points, which are instrumented to indicate any additional load carried by them during testing. Center line supports are located on the fuselage near the leading and trailing edges of the wing. They include a universal joint arrangement that prevents them from resisting either a roll or local pitching moment. The remaining support resists vertical load near the wing-leading edge at airplane span station 56.5. Because this point provides the model's only resistance to unbalanced roll, its load is carefully monitored throughout each test. No buildup of load assures the test engineer that only correct, properly sequenced loads are being applied during any load increment.

Preparation For Testing In Model Area.—After the panel point loads for a condition have been received by the test group, approximately four days are required to ready the model for testing. This time is consumed in checking electrical instrumentation and making provisions to load each panel point with its correct direction and magnitude of load.

The model is mounted in the inverted position (Figs. 14, 15, and 16) solely to reduce the number of panel points that must be rigged for upload application. For virtually all airplane flight situations, most of the airplane area has net up-loads applied. This would require up-rigging the majority of model panel points unless the model were inverted. However, by inverting the model, most points are simply down-loaded by applying weights to their load pans. This leaves a fewer number of up-points that must be rigged through an overhead truss and pulley arrangement.

For all ground handling conditions where the ratio of up-to-down loads on the airplane reverses, all the loads are applied in the reverse direction on the model and the signs of resulting strain and deflection data are changed during the manual data reduction operation. Because of the low stresses maintained on the model, the effects of compressive buckling may be disregarded.

After all rigging and other model setup is completed, a load card is attached to each panel point load pan indicating its correct incremental load for each phase of the planned test. These cards are used by both the mechanic loading the point and the engineer checking the point during the test.

Preload Of Model Condition.—In the early phases of the program it was found that a retest generally produced better, more linear data than the original test. After some study, it was decided that this result was caused by the earlier testing having removed the slack or "preloaded" the model in the direction

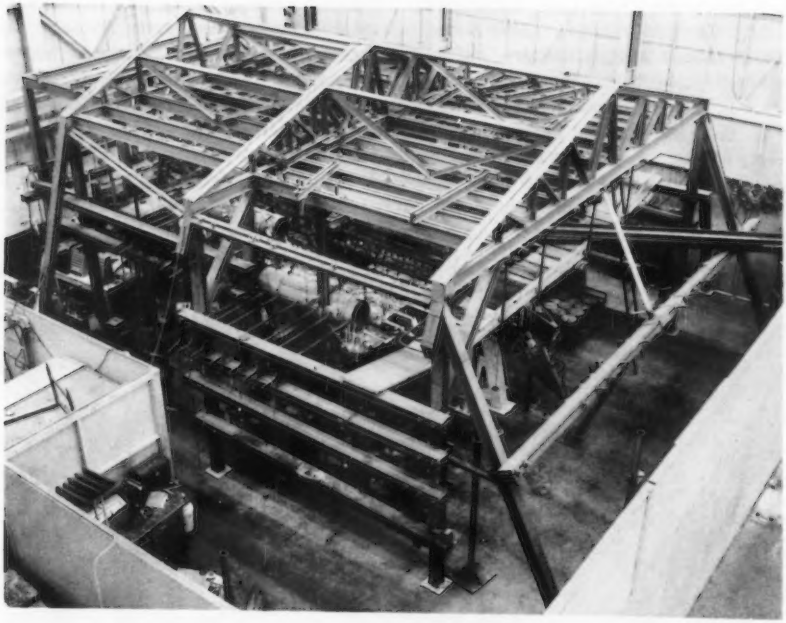

FIG. 14

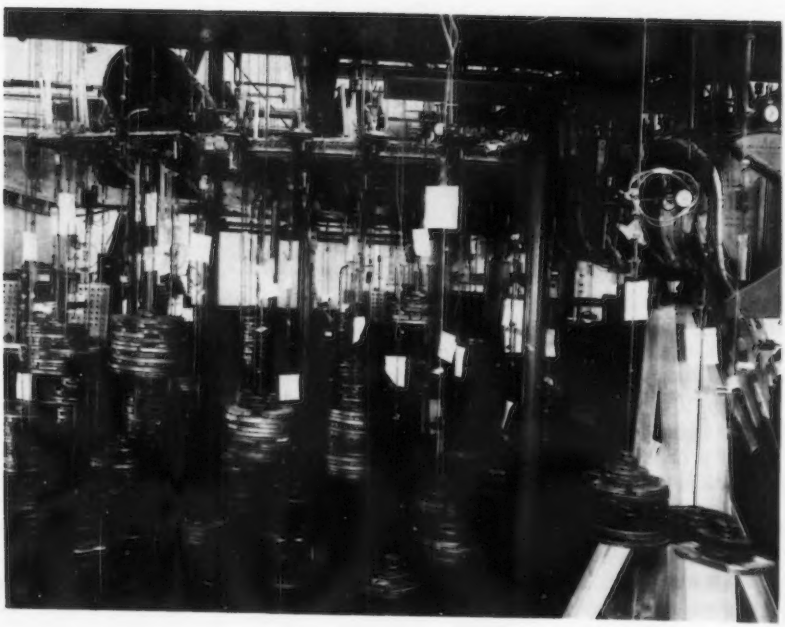

FIG. 15

of load for the given test. This prevented sudden unexplained jumps in the data during the latter test. After a number of tests were conducted to verify this assumption, a simplified preload was established as a preliminary to the testing each condition. Whereas the actual condition seldom has a loading above 35% equivalent airplane-magnitude, the preload generally is carried to only 25%. This is believed to provide a sufficient "stretch" and leaves a margin of safety so that only a few critical gages are monitored during preload. In addition, this loading serves to indicate possible points of trouble such as load cables binding on deflected model structure and others that could cause an expensive retest unless corrected prior to actual testing.

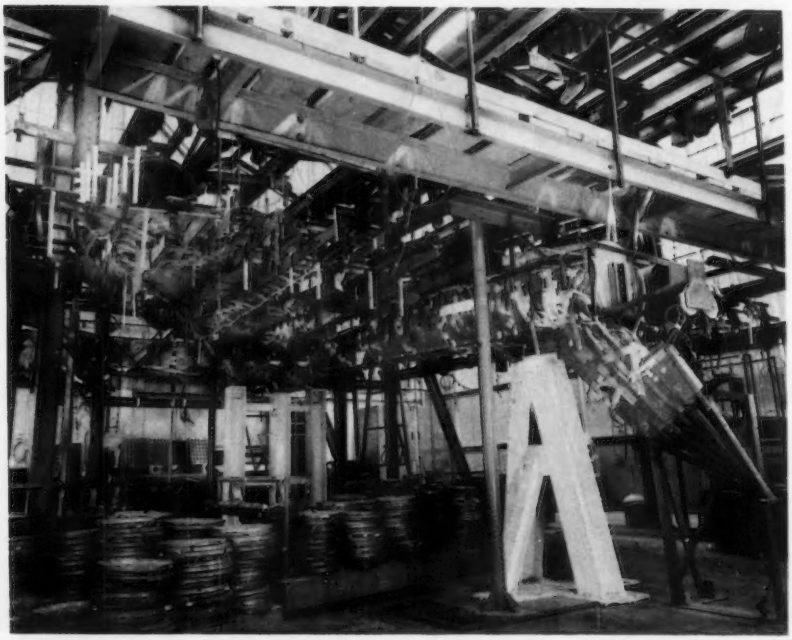

FIG. 16

Test Of A Model Condition.—The test of an elastic model condition is anticlimatic when compared with the time involved in both pre-test and post-test work for a condition, as it requires only one day out of the six weeks allocated for the complete processing of a condition.

Testing begins by applying a 5% tare load and recording all strain and deflection readings which, where possible, are then set at zero. The test continues with additional 10% loadings being applied and instrumentation again being read at each stage. Normally, after attaining 35% load and recording, the load is removed and again raised to 5%. This final tare reading is then

recorded and compared against the initial reading. Although these tare readings should theoretically be equal and all the intermediate readings perfectly linear, much of the comments on data reduction concerned with why they are not. The unloading to zero load and return to 5% for final readings consistently provides more linear data than a simple reduction from 35% to 5%.

DATA REDUCTION

The raw strain and deflection data measured during a test generally include five values (5, 15, 25, 35 and 5%) for each significant point. Manual data-reduction consists of establishing some logical sequence for these values so that an extrapolation to 100% may be obtained. In all cases other than rosette data, these extrapolated values are converted to airplane magnitude stresses, loads, or deflections, and are presented in a form suitable for use in stress analysis. In the case of rosette gages, most of the data reduction is accomplished by the use of high speed digital computers.

Computer Programmed Data Reduction.—Most of the extensive repetitive computations involved in elastic model data reduction are coded for solution by the digital computer. The first of these is the solution of the strains measured by the 45° rectangular rosettes on the model. Using the equations represented by Mohr's Circle, these strains are reduced so that the complete state of stress at the point is obtained. In a number of cases, this procedure produces as many as eleven values of stresses at a point for use in stress analysis of the area.

A part of this data reduction program provides the final measure of the validity of the test data by obtaining a comparison of internally measured versus externally applied loads at a number of "free bodies" taken at strategic points on the model (Fig. 17). In performing this comparison, the program uses virtually all of the strain data from the model for a condition and the model section properties in the region of each gage. In most cases, these comparisons indicate less than 10% error in locations such as a complete wing isolation outboard of airplane span-station 80.0. In practically all cases this comparison of internal to external loads indicates that the model stresses are slightly conservative. Later measurements on the B-58 static test program have verified this.

Presentation Of Model Data.—The entire elastic model program can be justified only if its results have made possible or simplified the stress analysis of the B-58 airplane. For this reason, all final model data from each test are presented in a manner that is convenient for use by the engineer performing stress analyses on each of the airplane components. In most cases, stress results are shown in exact location on scaled planforms of airplane structure (Figs. 18 and 19). This facilitates the stress analyst's becoming familiar with the over-all stress distribution for each condition and enables him to interpolate between instrumented points with ease. Extensive data for the wing include separate planforms for rosette principal stresses, spar and bulkhead flange axial stresses, and spar and bulkhead web shear loads. Similar, less extensive planforms are provided for fuselage and vertical tail structure with the remaining stress data being tabulated.

Most of the deflection data from the model is presented as chordwise plots of vertical deflection at a number of span stations from the airplane center line to the wing tip. The deflection of most points on the wing or fuselage can be obtained by interpolation within these basic curves.

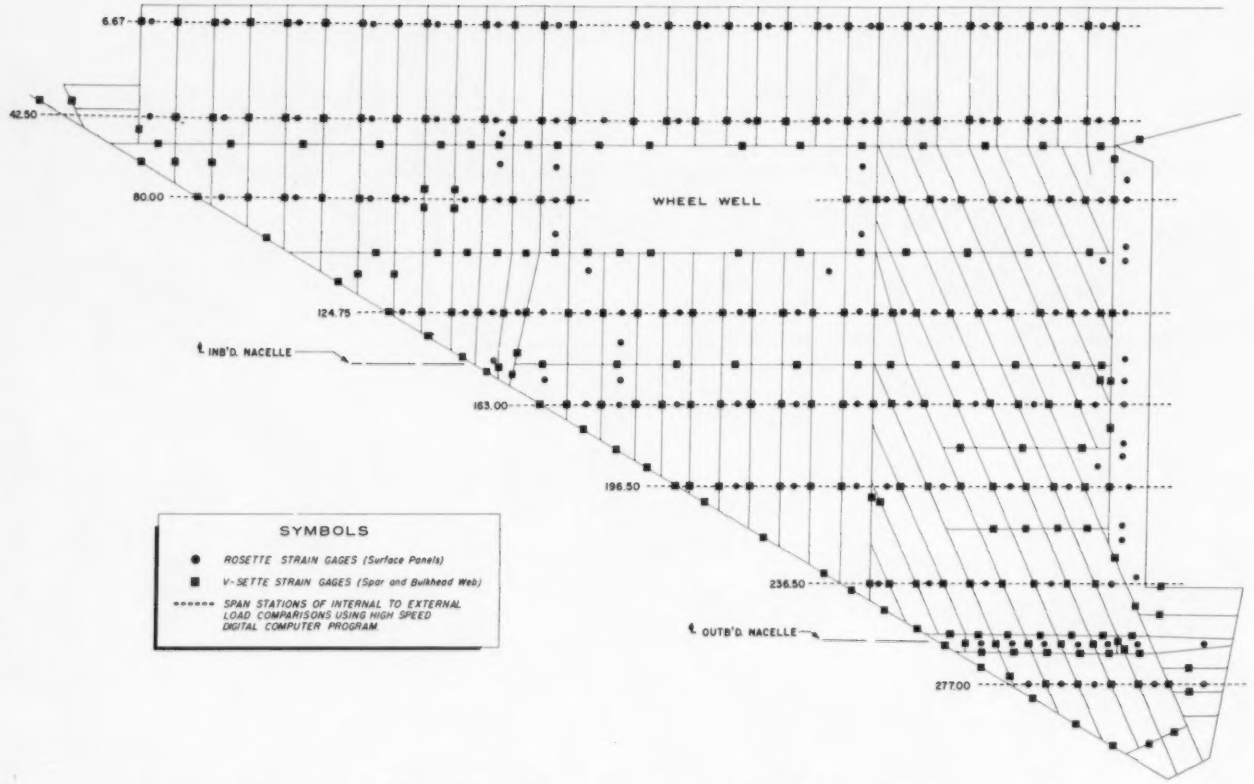

FIG. 17.—PLANFORM OF 3/8 SCALE ELASTIC MODEL WING SHOWING EXTENT OF INSTRUMENTATION AND LOCATIONS OF INTERNAL TO EXTERNAL LOAD COMPARISONS

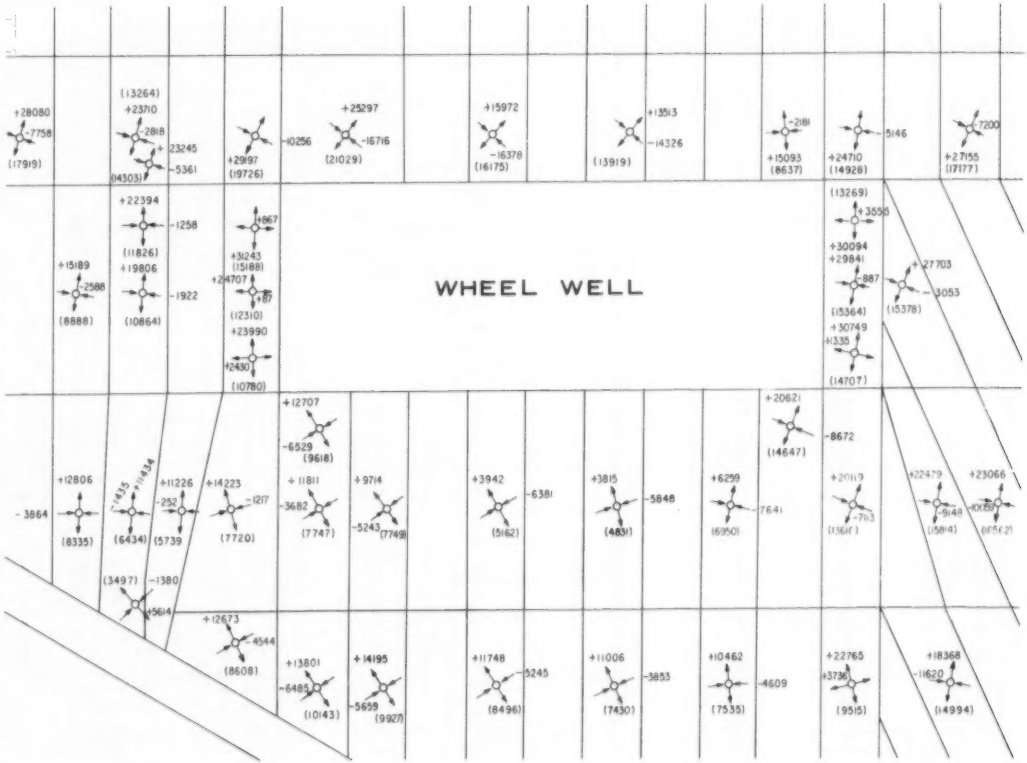

FIG. 18.—PARTIAL WING PLANFORM SHOWING METHOD OF PRESENTING ROSETTE, OR PRINCIPAL STRESS DATA FROM THE MODEL (NOTE ORIENTATION OF MAXIMUM PRINCIPAL STRESSES TO INDICATE FLOW OF LOAD AROUND WHEEL WELL)

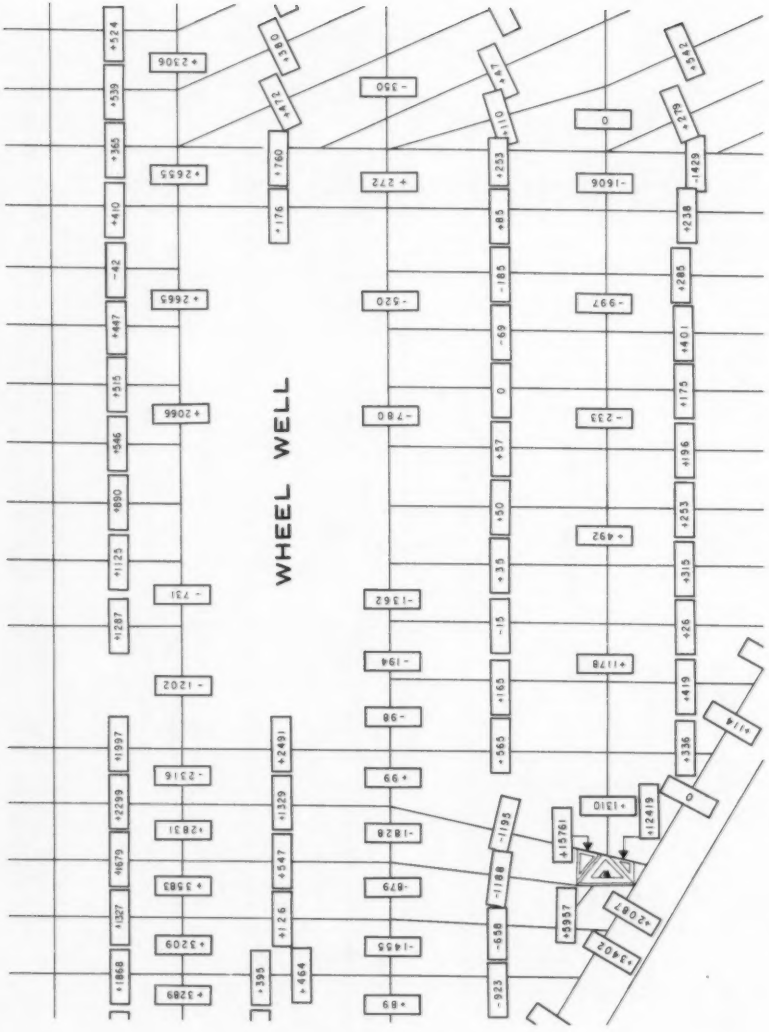

FIG. 19.—PARTIAL WING PLANFORM SHOWING METHOD OF PRESENTING PROTOTYPE MAGNITUDE SPAR AND BULKHEAD WEB SHEAR LOADS AS INDICATED BY THE MODEL

At the end of each major phase of model testing, composite wing planforms are prepared to indicate only the most significant value obtained at each point and the condition responsible. Because the B-58 airplane often experiences surface temperatures above 200°F due to aerodynamic heating, some consideration of reduced structural allowables at these elevated temperatures is necessary. Because the stress analyst must consider both stress magnitude and structural temperature, separate maximum surface stress planforms are prepared for "standard" and "elevated" temperature conditions. This simplification cannot be used on understructure, therefore only one maximum web shear load planform is presented. A complete list of maximum wing planforms is as follows:

Rosette Stress Data.—
Maximum Principal Stress (Hot and Cold Conditions Separately)
Minimum Principal Stress (Hot and Cold Conditions Separately)
Maximum Shearing Stress (Hot and Cold Conditions Separately)
Axial Stress Data.—
Maximum Spar and Bulkhead Flange Tension Stress (Hot and Cold Conditions Separately)
Maximum Spar and Bulkhead Flange Compression Stress (Hot and Cold Conditions Separately)
Web V-sette Data.—
Maximum Spar and Bulkhead Web Shear Loads (Irrespective of Sign With Hot and Cold Conditions Combined)

CONCLUSIONS

Remaining Direct Model Uses.—The 3/8 scale model is now fully occupied with determining stress distributions for the B-58 on certain final conditions that will enhance its use as a tactical weapon by the Air Force.

As a result of fatigue type failures found on a number of airplanes of varying types in its inventory, the Air Force has placed new emphasis on the determination of the service life and fatigue characteristics of all airplanes scheduled for future procurement.

This opens up an entirely new field of search for critical conditions because they now must be evaluated for both load magnitude and number of applications during the airplane service life. For static considerations, only magnitude of loading is considered. In the cyclic fatigue certification program for the B-58 now in progress, the elastic model is scheduled to have a major responsibility in refined stress determination for a number of conditions.

In addition to testing new conditions, the catalog of more than 100 conditions already tested will be used in the less refined stress predictions needed in the early phases of this program. Significant savings are realized since this preliminary work minimizes the total number of conditions tested on both the model and the full scale cyclic fatigue airplane.

Related Uses Of The Model.—Because the 3/8 scale elastic model is one of the largest, most extensively instrumented and consistently loaded redundant structures ever built, it is a natural source of information for the verification of proposed analytical methods of analyzing highly redundant structures.

Three distinct methods of analysis are under study. These are (1) a Direct Analogy Electric Analog Computer (DAEAC) solution, (2) a Consistent Distortion Solution (Q-07) and (3) a Stiffness Matrix Analysis of Structures (Q-01).

Although all three methods simulated either the B-58 or a hypothetical structure in their early stages, they now simulate the 3/8 scale elastic model. Where possible, they apply load distributions previously tested on the model and use its stress and deflection data in evaluating the accuracy of their solutions.

Elastic Model Contributions.—Through the use of elastic models in the design of the B-58 airplane, the time required for the final qualifications of its structure has been significantly shortened. Model stresses used in the design are being closely substantiated by the static test program how in progress. The almost complete absence of major structural failures during this static testing has validated the merits of this program and justified the many manhours involved. This means that inventory airplanes now in production will not be plagued with excessive retrofits and delays in the date of their combat readiness.

APPENDIX. MODEL SCALING FACTORS

The derivation of a complete set of scaling factors for loads, material sizes and material substitutions must be made at the beginning of any model program. These factors for a given model are dictated by such items as cost, ease of fabrication and versatility of the finished structure and its data. By proper adjustment of scale factors in the early phases of a model program, certain forms of output data are assured. In most cases, structural models are designed to have their strains equal to their prototype. Only this type model will be considered in the following examination.

Scaling factors will be derived in three stages. The simple "true scaled model," the adjustments required for dissimilar material substitutions, and special scaling factors necessitated by desired model deviations will be outlines, with special emphasis being shown for those used on the 3/8 scale elastic model.

True Scaled Models.—A true scaled model is one built to exact scale with direct substitution of prototype material and methods for construction. Although such a model design is generally impractical, the derivation of its scaling factors demonstrates the basic considerations required in a model design.

The following equation expresses the general scaling factor required for conversion of parameters from prototype to model magnitude.

$$(\text{Model Magnitude}) = (\text{Prototype Magnitude})\,(\text{Model Scale})^{n} \quad \ldots\ldots(1)$$

in which (n) represents the number of times the model scale factor (S) will be involved in the particular parameter. For example, the area (A) involves the square of a linear dimension; therefore, n = 2. In the case of a loading (P) which involves area in maintaining equal strains, n = 2. In the case of moment of inertia, involving both area and the square of a linear distance, n = 4.

Using these basic rules, the following geometric relationships between the model (subscript m) and its prototype (subscript p) can be stated.

$$\text{Width} \quad b_m = b_p\,(S) \quad \ldots\ldots\ldots\ldots\ldots\ldots(2a)$$

$$\text{Length} \quad l_m = l_p\,(S) \quad \ldots\ldots\ldots\ldots\ldots\ldots(2b)$$

Thickness $t_m = t_p\,(S)$ . . . . . (2c)

Since the area (A) is a function of width (b) times thickness (t),

$$A_m = b_m\, t_m \quad \text{. . . . . (3a)}$$

and

$$A_p = b_p\, t_p \quad \text{. . . . . (3b)}$$

therefore

$$A_m = b_p\, S\, t_p\, S = b_p\, t_p\, S^2 \quad \text{. . . . . (4a)}$$

or

$$A_m = A_p\, S^2 \quad \text{. . . . . (4b)}$$

Similarly the moment of inertia (I) and polar moment of inertia (J) are functions of an area times the square of a distance, therefore,

$$I_m = A_m\, l_m^2 \quad \text{. . . . . (5a)}$$

$$I_m = A_p\, S^2\, l_p^2\, S^2 \quad \text{. . . . . (5b)}$$

but

$$I_p = A_p\, l_p^2 \quad \text{. . . . . (6)}$$

so that

$$I_m = I_p\, S^4 \quad \text{. . . . . (7)}$$

Likewise,

$$J_m = J_p\, S^4 \quad \text{. . . . . (8)}$$

Applied loads (P) must be adjusted to maintain equal strains between the model and its prototype. Starting with this equality of strains,

$$\epsilon_m = \frac{P_m}{(A_m\, E_m)} \quad \text{. . . . . (9a)}$$

and

$$\epsilon_p = \frac{P_p}{(A_p\, E_p)} \quad \text{. . . . . (9b)}$$

Since for a true scaled model; $\epsilon_m = \epsilon_p$ and $E_m = E_p$

$$P_m = \frac{P_p\, A_m}{A_p} \quad \text{. . . . . (10)}$$

but since

$$A_m = A_p\, S^2 \quad \text{. . . . . (11)}$$

substitution yields

$$P_m = P_p\, S^2 \quad \text{. . . . . (12)}$$

Because moment (M) and torsion (T) involve load times a distance,

$$M_m = l_m\, P_p\, S^2 \quad \text{. . . . . (13a)}$$

since $l_m = l_p\, S$

$$M_m = l_p\, P_p\, S^3 \quad \text{. . . . . (13b)}$$

but $l_p\, P_p = M_p$

So

$$M_m = M_p\, S^3 \quad \text{. . . . . (13c)}$$

Likewise,

$$T_m = T_p\, S^3 \quad \text{. . . . . (14)}$$

These equations are equally true for external or internal loads.

The scale factor for deflection (δ) equivalence may be verified using a cantilever beam of length l and constant E I with a vertical load P at its free end.

$$\delta = \frac{P\, l^3}{3\, E\, I} \quad \text{. . . . . (15a)}$$

$$\delta_m = \frac{P_m l_m^3}{3 E_m I_m} \quad \ldots\ldots\ldots\ldots\ldots\ldots (15b)$$

$$\delta_p = \frac{P_p l_p^3}{3 E_p I_p} \quad \ldots\ldots\ldots\ldots\ldots\ldots (15c)$$

Substituting $P_m = P_p S^2$; $l_m = l_p S$; $I_m = I_p S^4$ and $E_m = E_p$ yields

$$\delta_m = \frac{P_p S^2 l_p^3 S^3}{3 E_p I_p S^4} = \frac{P_p l_p^3 S}{3 E_p I_p} \quad \ldots\ldots\ldots\ldots (16a)$$

or

$$\delta_m = \delta_p S \quad \ldots\ldots\ldots\ldots\ldots\ldots (16b)$$

In the same manner it can be shown that torsion applied at the free end yields,

$$\theta_m = \frac{T_m l_m}{G_m J_m} \quad \ldots\ldots\ldots\ldots\ldots\ldots (17a)$$

and

$$\theta_p = \frac{T_p l_p}{G_p J_p} \quad \ldots\ldots\ldots\ldots\ldots\ldots (17b)$$

Substituting $T_m = T_p S^3$; $l_m = l_p S$; $J_m = J_p S^4$ and $G_m = G_p$, yields

$$\theta_m = \frac{T_p S^3 l_p S}{G_p J_p S^4} = \frac{T_p l_p}{G_p J_p} \quad \ldots\ldots\ldots\ldots (18a)$$

or

$$\theta_m = \theta_p \quad \ldots\ldots\ldots\ldots\ldots\ldots (18b)$$

Scaled Models Of Dissimilar Materials.—In many cases during the development of a scaled model program it becomes apparent that use of some material other than that used on the prototype is either convenient or absolutely necessary. This concept is easily incorporated by applying certain adjustments to the true scale model factors.

Adjustments will only be required where a scale factor involves a consideration of thickness for either web or surface material. Geometric dimensions such as width, length and depth will not be affected. The general equation for equivalent thickness substitutions for dissimilar model materials is,

$$t_m E_m = S t_p E_p \quad \ldots\ldots\ldots\ldots\ldots\ldots (19a)$$

or

$$t_m = S t_p \left(\frac{E_p}{E_m}\right) \quad \ldots\ldots\ldots\ldots\ldots\ldots (19b)$$

Because the equations expressing area (A), moment of inertia (I), and polar moment of inertia (J) are functions of material thickness, their model magnitude may be obtained by multiplying their true scaled model values by the ratio of the modulus of elasticity of the prototype material to that of the model, or;

$$A_m = A_p \left(E_p/E_m\right) S^2 \quad \ldots\ldots\ldots\ldots\ldots\ldots (20a)$$

$$I_m = I_p \left(E_p/E_m\right) S^4 \quad \ldots\ldots\ldots\ldots\ldots\ldots (20b)$$

$$J_m = J_p \left(E_p/E_m\right) S^4 \quad \ldots\ldots\ldots\ldots\ldots\ldots \quad (20c)$$

The consistent application of these scale factors yields a model and prototype with equal strains. It is convenient in reducing strain data to determine prototype stress directly using only model strain and prototype moduli of elasticity or rigidity.

$$f_p = \epsilon_m E_p \quad \ldots\ldots\ldots\ldots\ldots\ldots \quad (21)$$

Special Scaling Requirements.—Often during the design of a model it is desirable to incorporate special features that are apparently inconsistent with

TABLE 1.—MODEL CONVERSION FACTORS FOR SIMILAR MATERIALS ON THE PROTOTYPE AND MODEL

Subject	Prototype Magnitude	(S)n	True Scale Model		Subject Independent Of "K"	3/8 Model Conversion Factor
			Magnitude	Conversion Factor		
Geometry						
Width	b	1	S b	S	Yes	S
Length	l	1	S l	S	Yes	S
Depth	d	1	S d	S	Yes	S
Material Thickness	t	1	S t	S	No[a]	S K
Material Properties						
Area	A	2	S^2 A	S^2	No[a]	S^2 K
Moment of Inertia	I	4	S^4 A d^2	S^4	No[a]	S^4 K
Polar Moment of Inertia	J	4	S^4 A r^2	S^4	No[a]	S^4 K
Data Reduction						
Load	P	2	S^2 P	S^2	No[a]	S^2 K
Moment	M	3	S^3 M	S^3	No[a]	S^3 K
Surface Strain	ϵ	0	ϵ	1.00	Yes[b]	1.00
Deflection	δ	1	S δ	S	Yes[b]	S
Twist	θ	0	θ	1.00	Yes[b]	1.00

[a] Apply "K" factor as a correction to the true scale model conversion factor.
[b] The "K" factor vanishes from these equations because it appears once in both the numerator and denominator.

both its prototype and a true scaled model. Two of these special features used in the 3/8 scale elastic model design were the substitution of flat webs on the model for comparable corrugated prototype webs and the substitution of equal thickness magnesium skins and webs for prototype aluminum structures (Fig. 11). In both cases, valid model data can be obtained if proper adjustments are made to scaling factors for both the model's structure and external loads.

The true scaled simulation of a rather thick prototype sandwich panel with a single flat skin on the model would yield a model surface which would obviously be much more critical in compressive buckling than the airplane. However, if the combined thickness of prototype aluminum skins is simulated with

an equal thickness of model magnesium skin, standard sheet stock may be used and the buckling problem is decreased. All that remains are adjustments to the affected scaling factors.

The substitution of magnesium flat webs on the model for equal thickness corrugated aluminum webs on the prototype requires no scale factor adjustment other than the "growth factor" reduction as explained in the paper. However, the original substitution of magnesium skins and webs directly for prototype aluminum counterparts requires the following scaling factor adjustments.

Since $t_m = t_p$ and $\epsilon_m = \epsilon_p$, where the first of these is specified, an additional adjustment (K) must be derived for the external loading (P) to make the second equation valid.

If $\epsilon_m = \epsilon_p$ and generally $\epsilon = \frac{P}{A\,E}$, then

$$\frac{K\,P_m}{A_m\,E_m} = \frac{P_p}{A_p\,E_p} \quad \ldots\ldots\ldots\ldots\ldots\ldots (22)$$

Substituting $A_m = b_m\,t_m$; and $P_m = P_p\,S^2$ yields

$$\frac{K\,S^2\,P_p}{b_m\,t_m\,E_m} = \frac{P_p}{A_p\,E_p} \quad \ldots\ldots\ldots\ldots\ldots\ldots (23)$$

However, $b_m = b_p\,S$, $t_m = t_p$ and $b_p\,t_p = A_p$. Substituting yields

$$\frac{K\,S^2\,P_p}{S\,A_p\,E_m} = \frac{P_p}{A_p\,E_p} \quad \ldots\ldots\ldots\ldots\ldots\ldots (24)$$

Therefore,

$$K = \frac{E_m}{E_p\,S} \quad \ldots\ldots\ldots\ldots\ldots\ldots (25)$$

In the specific case of the 3/8 scale model where magnesium versus aluminum substitutions are made, this becomes

$$K = \frac{6.5}{10.5 \times .375} = 1.651$$

Because the "K" factor is a function of the model load (P) all items that are a function of this load will require the same correction.

The scaling factors for the 3/8 scale model and a true scale model, using similar materials, are listed in Table 1 of this Appendix.

Symbols.—

Model Scale Ratio	S
Distance (inches)	b, l, d, r
Material Thickness (inches)	t
Material Area $(\text{inches})^2$	A
Moment of Inertia $(\text{inches})^4$	I
Polar Moment of Inertia $(\text{inches})^4$	J
Modulus of Elasticity (pounds/inch^2)	E
Modulus of Rigidity (pounds/inch^2)	G

Load (pounds)	P
Moment (inch-pounds)	M
Torsion (inch-pounds)	T
Axial Strain (inches/inch)	ϵ
Deflection (inches)	δ
Twist (radians)	θ
Subscript, pertaining to prototype	p
Subscript, pertaining to model	m

Journal of the
ENGINEERING MECHANICS DIVISION
Proceedings of the American Society of Civil Engineers

DISCUSSION

Note.—This paper is a part of the copyrighted Journal of the Engineering Mechanics Division, Proceedings of the American Society of Civil Engineers, Vol. 86, No. EM 4, August, 1960.

SHRINKAGE, SWELLING AND CREEP IN CEMENT[a]

Closure by A. Hrennikoff

A. HRENNIKOFF,[1] F. ASCE.—The writer wishes to acknowledge the private communications of Mr. T. C. Powers, Research Counsellor of the Portland Cement Association, on the subject of this paper.

Mr. Powers calls attention to the author's statement, "The presence of film (adsorbed) water in cement was demonstrated by several other investigators without, however, attributing to it the mechanical action (shrinkage-swelling) brought up in this paper." This statement is incorrect since Mr. Powers,[2] has clearly designated the adsorbed water as a cause of shrinkage-swelling phenomenon.

Although recognizing the priority of Mr. Powers in realizing the role played by the adsorbed water, the writer considers it only fair to point out that Mr. Powers' article, unlike the present paper, contains no detailed explanation of the mechanical action of film water. Furthermore, alongside of the adsorbed water theory, Mr. Powers devotes a comparable space to the exposition of the capillary action as another cause of shrinkage, an assertion with which the writer, as he explains at some length in his paper, strongly disagrees.

Mr. Powers also states that according to the recent observations with the electron microscope, the units of cement gel are not spherical, as reported by R. H. Bogue,[3] but have the shape of crumpled sheets and ribbons.

Leaving the final word on this subject to the specialists in electron microphotography, it may be said that the shape of the gel unit is not vital to the integrity of the author's theory, since the spherical shape vouched for at the time by a competent authority, was used by the author only for the sake of illustration. The significant remaining fact, irrespective of the gel elements being round, flat or elongated, is that they are distinct units surrounded by water, and the author's reasoning, leading to the conclusion of shrinkage-swelling and resulting from the attraction of the adsorbed water, is in no way affected by their shape. Also unaltered is the conclusion that shrinkage produced by drying is much smaller than the accompanying decrease in thickness of water films.

The disparity between the loss of water and the extent of shrinkage is discussed also by both Messrs. A. M. Neville and Keith Jones. Mr. Neville presents some figures referring to mortar cylinders illustrating this point. He correctly states that the rigid framework of the particles of sand and of unhydrated cement clinker accounts for the smallness of shrinkage in comparison with the loss of water. However, the writer wishes to add to this the point

[a] July, 1959, by A. Hrennikoff.

[1] Prof. of Civ. Engrg., Univ. of British Columbia, Vancouver, Canada.

[2] Bulletin 22, Portland Cement Assn., p. 582.

[3] "Chemistry of Portland Cement," by R. H. Bogue, 2nd Edition, Reinhold Publishing Corp., 1955, p. 627.

made by him on the basis of his theory. Every time the water film around the elements of cement gel decreases, the attraction between the latter brings them closer together, but the extent of this mutual approach, by the nature of the laws of attraction between the water and cement, is much smaller than the lost thickness of the water film.

Mr. Jones suggests the unequal size of gel units as a possible cause for the disparity between the amount of shrinkage and the corresponding water loss. He visualizes the gel units as belonging to two categories; the ones in contact with each other forming a framework giving rigidity to the whole mass, and the others occupying, more or less loosely, the empty spaces between the units of the first kind. The above mentioned information supplied by Mr. Powers with regard to the shape of the gel units suggests an irregularity even more far reaching than the one intimated by Mr. Jones. A diversity of conditions with respect to the available moisture at the grain contacts then becomes a strong probability. At the same time, the writer is doubtful of the presence of floating and loosely connected grains in the mass of hydrated cement. He feels that the units of cement gel either form in situ out of the grains of unhydrated cement, or they form by precipitation from the water solution. In both cases the units of gel, being under the action of strong chemical and physical forces, would form in a close contact with their neighbours and not in a loose aggregation.

The writer does not know to what inconsistency between the author's theory and his experimental results Mr. Jones refers in his discussion. If he means the disparity between the loss of water and the resultant shrinkage, then the writer considers this point not as an inconsistency but as a strong factor in favor of his theory.

The writer is grateful to all discussers for their constructive contributions to the subject of the paper. He regrets that the private communications of Mr. Powers had not been made part of the public discussion, but he considers it inappropriate to present here both Mr. Powers' and his views on a number of interesting points brought up in their correspondence.

COMPARATIVE STUDY OF A SEGMENTAL ARCH RING[a]

Discussion by J. A. Veltrop

J. A. VELTROP[6], M. ASCE.—Mr. Zienkiewicz has presented an interesting and valuable discussion of three of the most frequently used systems of shell equations for arch-dam design in comparing moments, thrusts, shears, and deflections along the arches for four values of the central angle: 90°, 120°, 180°, and 360°. The last two values are of little interest to arch-dam designers, but the last one serves the purpose of illustrating the limitations of Donnell's equations.

The comparison with the classical theory and especially with the corrected classical theory is most interesting, particularly the explanation of the physical meaning of the differences between Timoshenko's and Flügge's equations.

Since the purpose of the paper is primarily to compare various shell theories, the author has limited himself to constant radius and constant thickness arches. Numerical values are further limited to one set of arch dimensions with $R/t = 10$.

Mr. Zienkiewicz has also limited himself to arches with fixed abutments and with Poisson's ratio equal to zero. It should be noted that the author's conclusions are not limited to the specific numerical cases presented, but hold, generally, in the common range of R/t ratios and central angles.

The present discussion expands the original paper somewhat and adds a few observations which should be of particular interest to arch-dam designers. The computations covered in this discussion consist of:

Calculations for moments, thrusts, and deflections at abutment and crown for a number of R/t ratios: 0.025, 0.050, 0.075, 0.100, 0.150, and 0.200. These are limited to a central angle of 120°, which is representative for arch-dam design. These computations are performed first of all for three of the methods discussed by the author, namely Donnell, classical, and classical corrected (with $\mu = 0$). In addition, the following methods have been added: classical and classical corrected with $\mu = 0.2$, data from USBR tables which include abutment deformations, data from Parme's curves, and Donnell's equation with abutment deformations.

Like Mr. Zienkiewicz, the writer has limited these computations to constant thickness circular arches, as otherwise the amount of work would become prohibitive without adding to the basic purpose of the paper or to the discussion. For clarity of the ensuring discussion the writer has numbered and compiled the various methods and their limitations, as far as they are relevent to this discussion, in Table 2. Needless to say, all these methods include, of course,

[a] January, 1960, by O. C. Zienkiewicz.

[6] Head, Arch Dam Sect., Harza Engrg. Co., Chicago, Ill.

the so-called ribshortening effect and the usual assumption of the theory of elasticity.

The results of the writer's computations for methods 4 through 10 are presented in Table 3, together with the additional data computed for the author's method 1. The author's and writer's results both cover the case of half central angle $\phi = 60°$ and $t/R = 0.10$. These values are therefore tabulated separately in Table 4 for direct comparison of all ten methods of computation.

All formulas and numerical results have been adjusted to a pressure applied at the middle plane of the arch.

Explanation of Methods.—In order to facilitate comparison between the various methods used by the writer and the classical equation presented by Mr. Zienkiewicz, the various equations are written down and assumptions briefly discussed to illustrate pertinent differences.

Methods 4 and 6.—The classical theory of arch rings includes deformations due to axial forces, moments, and shears, while abutments are considered

TABLE 2.—COMPARISON OF METHODS

No.	Method	Shear Deflection	Abutment Deformation	Poisson's Ratio	Effect of Axial Force on Rotation
1	Donnell	No	No	0	No
2	Timoshenko	No	No	0	No
3	Flügge	No	No	0	Yes
4	Classical	Yes	No	0	No
5	Classical Corrected	Yes	No	0	Yes
6	Classical	Yes	No	0.2	No
7	Classical Corrected	Yes	No	0.2	Yes
8	USBR Tables	Yes	Yes	0.2	No
9	Parme's Curves	Yes	No	0.25	No
10	Donnell Revised	No	Yes	0	No

rigid. Using standard methods, one arrives at the following expressions (using the author's notation, for ease of comparison):

At crown

$$M_c = p\,R^2 \frac{\sin\phi}{\phi}\left(1 - \frac{\sin\phi}{\phi}\right) \quad \ldots\ldots\ldots\ldots \quad (11)$$

$$N_c = p\,R\left(1 - \frac{\sin\phi}{c}\right) \quad \ldots\ldots\ldots\ldots\ldots \quad (12)$$

and

$$w_c = \frac{p\,R^2}{E\,t}\left[\frac{\sin\phi}{C}\left\{\frac{R}{h}\left(\frac{\sin\phi}{\phi} - \frac{\sin\phi\,\cos\phi}{\phi} - \frac{\sin^2\phi}{2}\right)\right.\right.$$

$$\left.\left. + \left(\frac{k\,E}{G} - 1\right)\frac{\sin^2\phi}{2}\right\} + 1 - \cos\phi\right] \quad \ldots\ldots\ldots\ldots \quad (13)$$

At abutment

$$M_a = p\,R^2 \frac{\sin\phi}{C}\left(\cos\phi - \frac{\sin\phi}{\phi}\right) \quad \ldots\ldots\ldots\ldots \quad (14)$$

$$N_a = p\,R\left(1 - \frac{\sin\phi\,\cos\phi}{C}\right) \quad \ldots\ldots\ldots\ldots \quad (15)$$

TABLE 3

$2\phi = 120°$

t/R	0.025	0.050	0.075	0.100	0.150	0.200
Moment at Abutment						
1. Donnel	- .0007113	- .002829	- .006402	- .011058	- .02397	- .04055
4. Class. (μ=0)	- .0006149	- .002435	- .005393	- .009377	- .01986	- .03262
5. Class. corr. (μ=0)	- .0006690	- .002643	- .005857	- .010188	- .02167	- .03576
6. Class. (μ=.2)	- .0006147	- .002432	- .005377	- .009330	- .01965	- .03206
7. Class. corr.(μ=.2)	- .0006667	- .002640	- .005842	- .010 50	- .02146	- .03519
8. USBR Tables	- .0005946	- .002282	- .004905	- .008300	- .01675	- .02645
9. Parme's Curves		- .00247	- .00541	- .00931	- .0197	- .0320
10. Donnell Corr.	- .0007116	- .002833	- .006404	- .011111	- .02417	- .04090
Moment at Crown						
1. Donnell	.0003557	.001414	.003201	.005529	.01199	.02028
4. Class. (μ=0)	.0003253	.001288	.002853	.004961	.01051	.01726
5. Class. corr. (μ=0)	.0002733	.001082	.002392	.004151	.00874	.01424
6. Class. (μ=.2)	.0003252	.001287	.002845	.004936	.01040	.01696
7. Class. corr. (μ=.2)	.0002732	.001080	.002384	.004126	.00863	.01394
8. USBR Tables	.0003239	.001278	.002822	.004904	.01042	.01725
9. Parme's Curves		.00131	.00291	.00494	.0104	.0167
10. Donnell Corr.	.0003558	.001416	.003202	.005555	.01210	.02045
Thrust at Abutment						
1. Donnell	.9981	.9923	.9828	.9697	.9344	.8891
4. Class. (μ=0)	.9991	.9963	.9918	.9657	.9696	.9501
5. Class. corr. (μ=0)	.9991	.9963	.9918	.9857	.9696	.9500
6. Class. (μ=.2)	.9991	.9963	.9918	.9857	.9700	.9510
7. Class. corr. (μ=.2)	.9991	.9963	.9918	.9857	.9699	.9509
8. USBR Tables	.9995	.9961	.9918	.9867	.9730	.9564
9. Parme's Curves		.995	.991	.985	.976	.963
10. Donnell corr.	.9984	.9936	.9856	.9744	.9422	.8966
Thrust at Crown						
1. Donnell	.9981	.9923	.9828	.9697	.9344	.8891
4. Class (μ=0)	.9981	.9926	.9835	.9713	.9393	.9002
5. Class. corr. (μ=0)	.9981	.9926	.9835	.9713	.9392	.9000
6. Class. (μ=.2)	.9981	.9926	.9836	.9715	.9399	.9020
7. Class. corr. (μ=.2)	.9981	.9926	.9836	.9715	.9398	.9017
8. USBR Tables	.9985	.9932	.9841	.9733	.9461	.9127
9. Parme's Curves		.986	.984	.971	.939	.917
10. Donnell corr.	.9984	.9936	.9856	.9744	.9422	.8966
Deflection at Crown						
1. Donnell	1.8714	1.8605	1.8427	1.8182	1.7520	1.6670
4. Class. (μ=0)	1.8910	1.8805	1.8637	1.8410	1.7812	1.7084
5. Class. corr. (μ=0)	1.8909	1.8801	1.8628	1.8392	1.7776	1.7001
6. Class. (μ=.2)	1.8909	1.8802	1.8628	1.8396	1.7788	1.7058
7. Class, corr. (μ=.2)	1.8908	1.8798	1.8619	1.8380	1.7753	1.6995
8. USBR Tables	1.9395	1.9776	2.0111	2.0381	2.0805	2.1073
9. Parme's Curves		1.88	1.87	1.84	1.77	1.71
10. Donnell corr.	1.8720	1.8630	1.8480	1.8270	1.7665	1.6812

with

$$C = \frac{\sin 2\phi}{4}\left(\frac{R}{h} + 1 - \frac{k\,E}{G}\right) + \frac{\phi}{2}\left(\frac{R}{h} + 1 + \frac{k\,E}{G}\right) - \frac{R}{h}\,\frac{\sin^2\phi}{\phi} \quad \ldots\ldots\ldots \quad (16)$$

and where

$$\frac{R}{h} = 12\left(\frac{R}{t}\right)^2 \quad \ldots\ldots\ldots\ldots\ldots\ldots \quad (17)$$

in first approximation.

Eqs. 11 and 12 are identical to Eqs. 9a and 9b, when α is made equal to zero. The contribution of shear is included in the coefficient C with the term k E/G.

TABLE 4

$2\phi = 120°$ and $t/R = 0.1$

No.	Method	$M' = \frac{M}{P\,R^2}$		$N' = \frac{N}{P\,R}$		$W^1 = \frac{w\,E\,t}{P\,R^2}$	
		Abutment	Crown	Abutment	Crown	Abutment	Crown
1	Donnell	-0.01106	0.00553	-0.9698	-0.9698	0	1.8184
2	Timoshenko	-0.00962	0.00509	-0.9853	-0.9706	0	1.8483
3	Flügge	-0.01043	0.00428	-0.9853	-0.9706	0	1.8468
4	Class. (μ=0)	-0.00938	0.00496	-0.9857	-0.9713	0	1.8410
5	Class. Corr. (μ=0)	-0.01019	0.00415	-0.9857	-0.9713	0	1.8392
6	Class. (μ=.2)	-0.00933	0.00494	-0.9857	-0.9715	0	1.8396
7	Class. Corr. (μ=.2)	-0.01015	0.00413	-0.9857	-0.9715	0	1.8380
8	USBR Tables	-0.00830	0.00490	-0.9867	-0.9733	0.0041	2.0381
9	Parme's Curves	-0.931	0.00494	-0.985	-0.971	0	1.84
10	Donnell Corr.	-0.01111	0.00556	-0.9744	-0.9744	0	1.8270

From the theory of elasticity we have $E/G = 2(1 + \mu)$, so that the following numerical values are possible:

author: $\mu =$ 0, $k = 1.20$ gives $\frac{k\,E}{G} = 2\,K\,(1 + \mu) = 2.4$

writer: $\mu =$ 0, $k = 1.25$ $\frac{k\,E}{G} =$ $= 2.5$ (method 6)

writer: $\mu =$ 0.2, $k = 1.25$ $\frac{k\,E}{G} =$ $= 3.0$ (method 7)

The use of the values 2.5 and 3.0, therefore, illustrates the effect of Poisson's ratio. It should be noted that the author's value K is equal to 1/k of the writer.

Methods 5 and 7.—The classical corrected method includes all effects of classical methods 4 and 6, but is corrected for rotation due to axial forces and elongation by moment, as explained by A. J. S. Pippard and J. F. Baker (24). The equations for moments, thrusts, and deflection are:

At crown

$$M_c = p\,R^2\left[\frac{\sin\phi}{C^1}\left\{1 - \frac{\sin\phi}{\phi}\left(1 - \frac{h}{R}\right)\right\}\left(1 - \frac{h}{R}\right) - \frac{h}{R}\right] \quad \ldots\ldots\ldots \quad (18)$$

$$N_c = p\,R\left[1 - \frac{\sin\phi}{C^1}\left(1 - \frac{h}{R}\right)\right] \quad \ldots\ldots\ldots\ldots \quad (19)$$

and

$$w_c = \frac{p\,R^2}{E\,t}\left[\frac{\sin\phi}{C^1}\left(1 - \frac{h}{R}\right)\left\{\frac{R}{h}\left(\frac{\sin\phi}{\phi} - \frac{\sin\phi\,\cos\phi}{\phi} - \frac{\sin^2\phi}{2}\right)\right.\right.$$

$$\left.\left. - (1 - \cos\phi)\,\frac{\sin\phi}{\phi}\left(2 - \frac{h}{R}\right) + \frac{\sin^2\phi}{2}\left(1 + \frac{kE}{G}\right)\right\} + \left(1 - \frac{h}{R}\right)(1 - \cos\phi)\right] \ldots \quad (20)$$

At abutment

$$M_a = p\,R^2\left[\frac{\sin\phi}{C^1}\left\{\cos - \frac{\sin\phi}{\phi}\left(1 - \frac{h}{R}\right)\right\}\left(1 - \frac{h}{R}\right) - \frac{h}{R}\right] \ldots \quad (21)$$

$$N_a = p\,R\left[1 - \frac{\sin\phi\,\cos\phi}{C^1}\left(1 - \frac{h}{R}\right)\right] \ldots\ldots\ldots \quad (22)$$

with

$$C^1 = \frac{\sin 2\phi}{4}\left(\frac{R}{h} - 1 - \frac{k\,E}{G}\right) + \frac{\phi}{2}\left(\frac{R}{h} - 1 + \frac{k\,E}{G}\right) + \left(2 - \frac{h}{R} - \frac{R}{h}\right)\frac{\sin^2\phi}{\phi} \quad \ldots \quad (23)$$

where again Eq. 17 is applicable.

Several comments are in order. First, it should be noted that Eq. 16 for constant C cannot be derived directly from Eq. 23 for constant C^1. In going through the classical derivations for both by the energy method it can be seen that these differences are the direct result of a correction term for the work done by the axial force on rotation. However, expressions for moments and thrusts (Eqs. 11, 12, 14, and 15) can be derived directly from Eqs. 18, 19, 21, and 22 by replacing h/R with zero. In actual numerical calculations it appears that the term $\left(1 - \frac{h}{R}\right)$ is always very close to 1, however, the term - h/R cannot be neglected at the end of Eqs. 18 and 21. This verifies the author's statement that the main effect of the correction on the classical method is just the additional term h/R.

Comparison of crown deflection (Eqs. 13 and 20) shows that Eq. 20 has an extra term besides a few multipliers $\left(1 - \frac{h}{R}\right)$. The numerical importance will be elaborated upon subsequently in discussing the results.

Method 8.—The method used by the USBR (25) (26) is essentially the classical method, without the "correction" of methods 5 and 7 (25a). The important difference with methods 4 and 6 is inclusion of abutment deformations in the USBR method. The resulting equations are rather cumbersome and are not therefore worked out into a simple expression.

Method 9.—Parme's curves are based on the classical method for μ - 0.25, and for rigid abutments. Details of the derivation and equations for moments, thrusts, and crown deflection can be found (27).

Method 10.—Donnell's equations were corrected for abutment deformations, since these expressions are somewhat easier to handle than Timoshenko's and Flügge's. The writer derived moment, thrust, and deflection equations at crown and abutment including the effect of abutment rotations. This effect was introby using the following boundary conditions: w = v = 0 for y = 0 and y = 2 R ϕ and $w^o = w^{oo}$ L for y = 0 and y = 2 R ϕ with $L = \frac{K_1\,t}{12}$. Values of K_1 can be obtained (25b).

The equations for moment, thrust, and crown deflection are the same as Eqs. 7a through 7d, except that the coefficient Δ changes to

$$\Delta = \frac{1 + \frac{15}{4}\left(\frac{t}{R}\right)^2 \frac{1}{\phi 4} - \frac{15}{m^2 - 3}}{\frac{m^2 - 15}{m^2 - 3}} \quad \ldots\ldots\ldots\ldots (24)$$

with

$$m = \frac{12\,\phi}{K_1}\,\frac{R}{t} \quad \ldots\ldots\ldots\ldots\ldots\ldots\ldots\ldots (25)$$

Discussion of Results.—For convenience the subsequent material is divided into two categories. The first (A) compares moments, thrusts, and deflections due to different methods (No. 1 through 5 and 9), while the second (B) compares the effects of abutment deformation and of axial work on rotation again for moments, thrusts, and deflections.

A. Comparison of Methods.

1) As already indicated by the author in his conclusion (a), the deflections computed from the three shell theories show very good agreement. Table 4 shows that this also holds true for those computed by the classical methods (both with $\mu = 0$ and $\mu = 0.2$). The small differences between Donnell's results and the classical methods increase for thicker arches, as shown in Table 3. This is due to the effect of shear deflection which is included in the classical methods but not in Donnell's equations.

2) Substantially the same can be said about the thrust at abutments and crown, again Donnell's values are somewhat smaller. Moments show relatively larger differences than thrusts and deflections because of inclusion of the higher order terms in Flügge's equations and the work effect of axial force on rotation in the classical corrected method, as further discussed under B.

3) The differences between values obtained from Parme's curves (method 9) and methods 4 through 8 are generally somewhat larger than differences among methods 4 through 8. This may be due to the inaccuracies involved in the rather rough graphical interpolations from Parme's curves.

Conclusions.

a) Shell equations generally give satisfactory results but lead to substantial errors, which increase in magnitude when applied to arches, with $t/R > 0.1$, approximately, as indicated by Donnell's values in Table 3.

b) For the range of variables covered in this analysis there is practically no effect due to Poisson's ratio.

c) The suggestion of the author, made in his conclusion (d), to use the simple crown deflection formula derived from Donnell, is a useful one, but the error involved may be larger than he suggests, as can be seen from Table 3 by comparison with method 8.

B. Comparison of Basic Assumptions.

1) The greatest differences in moments, and deflections but not in thrusts are found between the USBR method which includes abutment deformations and the other methods, which do not include this effect. This follows directly by comparing the classical method 6 with the USBR method 8, the USBR being

based on exactly the same derivation throughout, except for the abutment deformation. This deformation decreases abutment moments considerably while hardly affecting crown moments. From Table 3, it can be seen that changes of abutment moments appear more consistent than those of crown moments, even though numerical values were computed with two more decimals than shown for methods 4, 5, 6, and 7. Perhaps the limited number of digits presented in the USBR tables accounts for the lack of consistency in data for method 8. Crown deflections also increase substantially.

This difference occurs for all values of t/R, but it can be seen from Table 3 that the significance of these differences increases for thicker arches. Table 3 also illustrates the large differences in crown deflection between the USBR method 8 and all other methods which overshadow the relatively small differences among the others. This leads to the conclusion that inclusion of abutment deformations in the arch computation is important for arch-dam analysis especially when cantilever deflections are to be equated with those of the arches.

2) The effect of abutment rotation was also added to method 1 and the results are shown as method 10. In comparing Eq. 24 with the expression of the author for the case of fixed abutments $\Delta = 1 + \frac{15}{4}\left(\frac{t}{R}\right)^2 \frac{1}{\phi 4}$ it can be seen that Eq. 24 should normally lead to smaller values of Δ and, therefore, larger values of deflection, thrust, and moment, as can be seen also from Table 3 by comparing results of method 1 with those of method 10. This is obviously contrary to expectations, as surely abutment moments should decrease, as confirmed by the classical methods and USBR data. The error seems inherent in Donnell's equations for moment and thrust (see author's Eq. 7c and 7d, respectively). No distinction is made there between abutment and crown thrust, and, furthermore, abutment moments are always twice crown moments, regardless of arch dimensions. Both the expressions for moment and thrust are apparently too oversimplified to reflect such refinements as abutment deformations. Consequently inclusion of abutment deformation does not lead to the correct effects.

3) Inclusion of the work of axial forces on rotation in the classical corrected method has a substantial effect on moments, but not on thrusts and crown deflection. One would expect this as the correction does not, in first instance at least, alter the static equilibrium, and that is what determines the order of magnitude of the thrust. (Note, for example, that for simple ring stresses from the cylinder formula, when ribshortening due to thrust is neglected, the coefficient for thrust at crown and at abutment would be 1.00). Then it also follows that the geometric pattern of radial deflections is not basically changed as illustrated by the small differences between deflection coefficients for classical and classical corrected methods.

One can see directly that with the effect of axial forces on rotation the moment at the crown needed to guarantee continuity is now smaller, as the coefficient shows. Subsequently, static equilibrium of half the arch will show that the abutment moment must then increase.

4) To compare the effects of abutment deformation with those of the work of axial forces on rotation reference is made to the coefficients in Table 4 for methods 4, 5, 6, 7, and 8. For thrusts and deflections inclusion of abutment deformations is significant, whereas the "correction" for work is not. For moments the results are quite different. Abutment deformation considerably decreases abutment moments, but the "correction" causes an almost equal

increase. This effect would seem to contradict the USBR statement (25a) and needs further investigation. Abutment deformation changes the crown moment only slightly, but the "correction" causes a considerable decrease.

Conclusions.

d) USBR data show that inclusion of abutment deformations in arch computations is important, especially for crown deflections and abutment moments.

e) It has been shown that Donnell's equations are not accurate enough to properly reflect the effect of abutment deformations.

f) The inclusion of work of axial forces on rotation, has a significant effect on moments at abutment and crown, but effects on thrust and deflection are negligible. This conclusion appears to contradict USBR practice of neglecting this effect.

Acknowledgments.—The writer would like to thank the several engineers of the arch dam section who have checked the numerical calculations, especially R. P. Wengler who checked all derivations and reviewed the entire discussion.

Bibliography.

25. "Trail Load Method of Analysing Arch Dams," U.S.B.R. Boulder Canyon Proj., Final Reports, Part V - Tech. Investigations, Bulletin 1, (a) p. 103. p. 48.

26. "Treatise on Dams," Chapter X, Arch Dams, U.S.B.R.

27. Arch Dams with Arches of Variable Thickness, by A. L. Parme, Modern developments in reinforced concrete, Portland Cement Assn.

WHITE NOISE REPRESENTATION OF EARTHQUAKES[a]

Discussion by D. E. Hudson,[8] G. W. Housner[9] and T. K. Caughey[10]

D. E. HUDSON,[8] G. W. HOUSNER,[9] and T. K. CAUGHEY.[10]—The author describes an interesting electrical experiment in which an artificial earthquake produced by a random (white noise) function generator is used to excite structures. In Fig. 1, the author compares the results of his experiment with average earthquake spectra and shows that there is close agreement except at the low period end where the earthquake spectra have a characteristic hump. The largest deviation is for the zero-damped spectrum curve, and here the author's points are, presumably, not too reliable as the zero-damped case is particularly difficult to handle accurately and larger samples would need to be averaged to give accurate results.

It is of interest to compare the author's spectrum points with the results of a simple approximate analysis based on an energy balance consideration.[11] If the excitation of an oscillator has a random characteristic, then, on the average, the total energy E of the system increases until the average rate of energy input is equal to the average rate of energy dissipation. For harmonic motion of a single degree of freedom viscous damped system, the average rate of energy loss is $\frac{2\pi\lambda}{T}E$, and, therefore, if the average power input is P;

$$\frac{dE}{dt} = P - \frac{2\pi\lambda}{T}E \quad \ldots\ldots\ldots\ldots\ldots\ldots (9)$$

The solution of this equation is

$$E = \frac{P\,T}{4\pi\lambda}\left(1 - e^{-\frac{4\pi\lambda}{T}t_o}\right) \quad \ldots\ldots\ldots\ldots\ldots\ldots (10)$$

in which t_o is the time at which E is evaluated. The energy E can also be written in terms of the relative velocity spectrum $V(\lambda, T)$ as

$$E = \frac{1}{2}m\,V^2(\lambda, T) \quad \ldots\ldots\ldots\ldots\ldots\ldots (11)$$

Combining Figs. 9 and 10 yields

$$V(\lambda, T) = \sqrt{\frac{2P \cdot t_o}{m}}\sqrt{\frac{1 - e^{-\frac{4\pi\lambda}{T}t_o}}{\frac{4\pi\lambda}{T}t_o}} \quad \ldots\ldots\ldots\ldots (12)$$

---

[a] April, 1960, by G. N. Bycroft.

[8] California Inst. of Tech., Pasadena, Calif.

[9] Prof. of Engrg., Calif. Inst. of Tech., Pasadena, Calif.

[10] Calif. Inst. of Tech., Pasadena, Calif.

[11] "Response Spectrum Techniques in Engineering Seismology," by D. E. Hudson, Proceedings, World Conf. on Earthquake Engrg., San Francisco, Calif., June, 1956.

Eq. 12 can be fitted to the scale used in Fig. 1 by setting $\frac{2 P t_o}{m} = 9$, and by choosing t_o in such a way that the best representation over the whole range of parameters is obtained. In Eq. 12, t_o is the time at which the average $V(\lambda, T)$ is computed, however, in the author's case the value of t_o is always chosen to give the largest value of $V(\lambda, T)$. The time t_o will, thus, be less than the 25 sec duration of the input. The value of t_o will also be influenced by the fact that the input is limited to a finite band width.

By putting $t_o = 6.5$ sec in Eq. 12 theoretical spectrum curves are obtained as shown in Fig. 17, which also shows the author's data points. The agreement of this simple analysis with the author's tests is very good. All of the author's points seem a bit high at the low period end and this presumably is an indication that the input was not a true white noise. It would, of course, be possible to accentuate this effect by the use of appropriate filters to modify the input so that it produces spectra virtually identical with earthquake spectra.

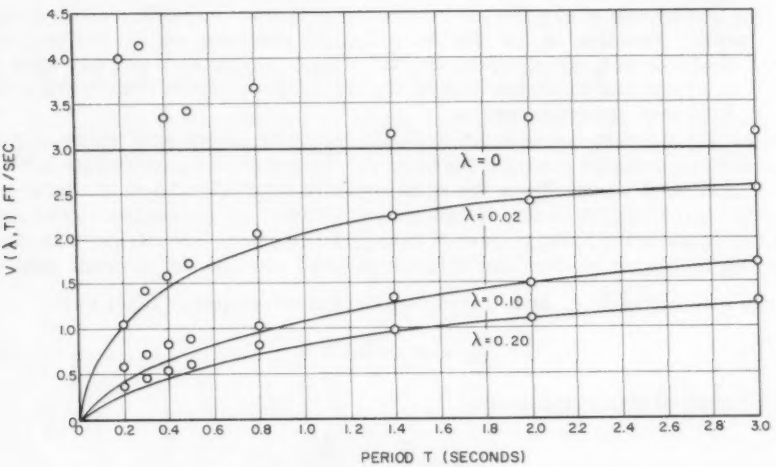

FIG. 17.—THEORETICAL AND EXPERIMENTAL SPECTRA

An actual earthquake record is not Gaussian and, of course, the author's input could not be truly Gaussian. It would be of interest to see some statistics on the frequency distribution of the experimentally determined $V(\lambda, T)$ values. If the range of these $V(\lambda, T)$ values were inconsistent with the range for actual earthquakes the input could be modified to correct for this. Another possibility would be to construct artificial earthquake records[12] whose average spectra agrees exactly with those of real earthquakes. Earthquake studies could then be made along the same lines that random shaking tests are used for missile reliability test studies.

The maximum yield displacements computed by Mr. Bycroft appear quite reasonable. It may be that some of the differences between the white noise

12 "Properties of Strong Ground Motion Earthquakes," by G. W. Housner, Bulletin, Seismol. Soc. of Amer., Vol. 44, July, 1954.

yield displacements and those computed in the previous paper are accounted for by inaccuracies in the earlier method of computation.

It is difficult to know exactly what interpretation to place on the computed maximum yield displacements since an ideal-plastic force-displacement relation was assumed for the oscillator. Similar computations made for elasto-plastic frames[13] also showed sizeable permanent displacements. In an actual building, of course, the force-displacement diagram would not have a flat plastic yielding but the diagram would be curved with slope greater than zero and as a result the maximum yield displacements would presumable be smaller.

Studies along the lines of the author's work are much needed, because one of the key questions regarding the behavior of structures during earthquakes is how much energy can be absorbed during the vibration without having the structure collapse.

13 "The Analysis of Structural Response to Earthquakes," by G. V. Berg, IP 291, Univ., of Michigan, May, 1958.

STRENGTH AND EFFICIENCY ASPECTS OF PLATE STRUCTURES[a]

Discussion by George Pincus and George Winter

GEORGE PINCUS,[15] A.M. ASCE and GEORGE WINTER,[16] F. ASCE.—The first part of Mr. Gerard's paper re-formulates well established relationships on the post-buckling strength of compressed plates. The supporting evidence consists of numerous tests in the field of largely non-ferrous aeronautical structures. It is gratifying to note that these relations are in strikingly close agreement with similar information developed some fifteen years ago by one of the present writers from tests on light-gage steel structural members of the civil engineering type.[17,18,19] The design code,[20] which has been in force nationally since 1946 for this widespread type of construction,[21] incorporates this information in explicit design formulation.[22] For this reason it may be of some interest to compare and correlate Mr. Gerard's presentation with this earlier information.

Th. von Karman was the first[23] to present a semi-intuitive equation for the post-buckling strength of plates, formulated in terms of the effective or equivalent width b_e rather than in terms of Mr. Gerard's average stress at failure, $\bar{\sigma}_f$. For rectangular plates with simply supported edges, this equation reads

$$\frac{b_e}{b} = 1.9 \frac{t}{b} \left(\frac{E}{\sigma_{cy}} \right)^{1/2} \quad \ldots\ldots\ldots\ldots\ldots\ldots (37)$$

---

[a] April, 1960, by George Gerard.

[15] Graduate Asst., School of Civ. Engrg., Cornell Univ., Ithaca, N. Y.

[16] Prof. and Head, Dept. of Structural Engrg., Cornell Univ., Ithaca, N. Y.

[17] "Strength of Thin Steel Compression Flange," by George Winter, Transactions, ASCE, Vol. 112, p. 527, 1947, reprinted with an added appendix as Cornell University Engrg. Experiment Sta. Reprint No. 32, 1947.

[18] "Performance of Thin Steel Compression Flanges," by George Winter, Third Congress Int. Assn. for Bridge and Structural Engrg., Liege, Prelim. Publ., p. 317, 1948; reprinted in Four Papers on the Performance of Thin Walled Steel Structures, Cornell Univ. Engrg. Experiment Sta. Reprint No. 33, 1950.

[19] "Performance of Compression Plates as Parts of Structural Members," by George Winter, Research Engrg. Structures Suppl., p. 49, London, 1949.

[20] "Specification for the Design of Light Gage Cold-Formed Steel Structural Members," Amer. Iron and Steel Inst., first issued in 1946, latest edition 1960.

[21] "Cold-Formed, Light Gage Steel Construction," by George Winter, Proceedings, ASCE, Vol. 85, No. ST 9, p. 151, 1959.

[22] "Commentary on the 1956 Edition of the Light Gage Cold-Formed Steel Design Manual," by George Winter, Amer. Iron and Steel Inst., 1958.

[23] "The Strength of Thin Plates in Compression," by Th. van Karman, E. E. Sechler, and L. H. Donnell, Transactions, ASME, vol. 54, 1932, p. 53.

Using Eq. 2, with k = 4, this can be re-written as

$$\frac{b_e}{b} = \left(\frac{\sigma_{cr}}{\sigma_{cy}}\right)^{1/2} \quad \ldots\ldots\ldots\ldots\ldots\ldots (38)$$

Since, by the definition of the effective width,

$$\bar{\sigma}_f \, b = \sigma_{cy} \, b_e \quad \ldots\ldots\ldots\ldots\ldots\ldots (39)$$

this can also be written as

$$\frac{\sigma_f}{\sigma_{cy}} = \left(\frac{\sigma_{cr}}{\sigma_{cy}}\right)^{1/2} \quad \ldots\ldots\ldots\ldots\ldots\ldots (40)$$

which is seen to be identical with Mr. Gerard's Eq. 3, with $\alpha_1 = 1.0$ and n = 0.5. In its alternate form the same relation can also be written (see Eq. 37) as

$$\frac{\sigma_f}{\sigma_{cy}} = 1.9 \, \frac{t}{b} \left(\frac{E}{\sigma_{cy}}\right)^{1/2} \quad \ldots\ldots\ldots\ldots\ldots\ldots (41)$$

which is identical with Mr. Gerard's Eq. 5, with $\beta = 1.9$, m = 1.

E. E. Sechler[24] was the first to note that the constant 1.9 in von Karman's equation needs adjusting to match test results. Further explorations of post-buckling strength were carried out during World War II. At that time security restrictions resulted in independent investigations in aeronautical engineering on the one hand, and in civil engineering on the other. On the basis of his tests, Winter[17,18] gave as an approximate lower bound, that is for simply supported edges,

$$\frac{b_e}{b} = 1.9 \, \frac{t}{b} \left(\frac{E}{\sigma_e}\right)^{1/2} \left[1 - 0.475 \, \frac{t}{b} \left(\frac{E}{\sigma_e}\right)^{1/2}\right] \ldots\ldots\ldots (42)$$

which, to include other edge conditions, can be written more generally as[19]

$$\frac{b_e}{b} = \left(\frac{\sigma_{cr}}{\sigma_e}\right)^{1/2} \left[1 - 0.25 \left(\frac{\sigma_{cr}}{\sigma_e}\right)^{1/2}\right] \ldots\ldots\ldots\ldots (43)$$

It is seen that the terms in the square bracketts of Eqs. 42 and 43 represent the experimental corrections to von Karman's original Eqs. 37 and 41.

Eqs. 42 and 43 are valid not only at failure, but for any edge stress σ_e larger than that causing initial buckling. The collapse load was found to be reached when this edge stress attained the yield point, $\sigma_e = \sigma_{cy}$, a finding which Mr. Gerard states to be in agreement with the later analyses of Stowell, Mayer and Budiansky.

It is important to note that Eqs. 42 and 43 are formulated in terms of the effective width b_e rather than the average collapse stress $\bar{\sigma}_f$. This permits conventional strength of materials methods to be applied to the design of members (such as beams) of which the particular compression plate is merely one of several components (such as the compression flange). In this case, the usual section properties apply, provided they are based on the effective, rather than the actual width. The fact that the effective width concept applies not only to

24 "The Ultimate Strength of Thin Flat Sheet in Compression," by E. E. Sechler, No. 27, Guggenheim Aeron. Lab., Calif. Inst. of Tech., 1933.

the edge stress at collapse, σ_{cy}, but also to edge stresses σ_e of smaller value, provides a more general tool of analysis and design. It permits one to analyze not only the case when the limiting load of the member is governed by the collapse of the compression plate, but also the frequent situations when it is determined by prior yielding of the tension flange, or by excessive deflection at design load.[22] For these reasons it is believed that the use of an effective width b_e is preferable to that of an average stress at collapse $\bar{\sigma}_f$ of the compressed plate.

It is interesting to compare numerically, the results of Eq. 5 with those of Eq. 42 (Fig. 10). The former was obtained primarily from tests on individual plates of non-ferrous metals while the latter was developed from tests on entire thin-walled steel members, of which the pertinent plate was merely one component. Correspondingly, in these latter tests some rotational edge restraint was always present, its amount depending on the configuration of the section. However, in many sections this restraint was small, and since Eq.

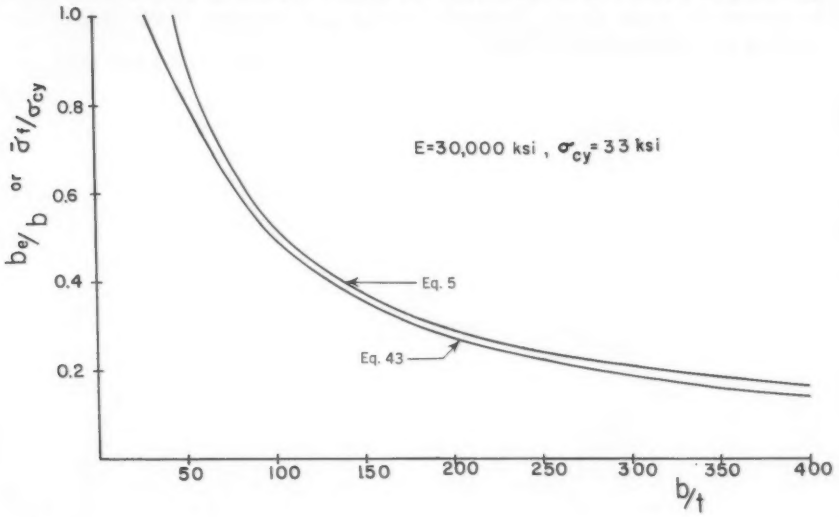

FIG. 10.—COMPARISON OF COLLAPSE CONDITIONS FOR SIMPLY SUPPORTED COMPRESSED STEEL PLATES.

42 was fitted closely to the lower bound of the scattering range, it represents substantially the conditions of simply supported edges.

For these conditions Mr. Gerard's Eq. 5, with m = 0.85 and β = 1.42 from Eq. 7, and using for mild structural steel σ_{cy} = 33 ksi and E = 30,000 ksi, becomes

$$\frac{b_e}{b} = \frac{\bar{\sigma}_f}{\sigma_{cy}} = 25.9\,(t/b)^{0.85} \quad \ldots\ldots\ldots\ldots\ldots (44)$$

On the other hand, for the same material's constants, Eq. 42 becomes

$$\frac{b_e}{b} = 57.3\,\frac{t}{b}\left(1 - 14.32\,\frac{t}{b}\right) \quad \ldots\ldots\ldots\ldots (45)$$

These two expressions have been plotted in Fig. 10.

It is seen that very close agreement is obtained over the entire relevant range. Eq. 42 is slightly more conservative, which is consistent with its character as a lower bound expression. Only in the region of low b/t-ratios, when the plate fails at an average stress in excess of about 85% of the yield strength, do the two expression deviate more strongly. In this range, however, buckling occurs in the plastic domain and the problem of post-buckling strength becomes largely meaningless. Also, performance in this range depends strongly on the detailed inelastic stress-strain characteristics of the particular material so that a single expression cannot be expected to apply equally well to all situations.

In view of the close agreement for this special case, there is little reason to doubt that similar agreement would exist between the more general expressions, Eq. 10 and the writers' Eq. 43.

To summarize, it is gratifying to note that the information on post-buckling strength of compressed plates, which for many years has been in widespread use in light-gage steel structures of the civil engineering type, is very satisfactorily confirmed by Mr. Gerard's recent data, obtained in the field of nonferrous aeronautical structures.

ERRATA

Journal of the Engineering Mechanics Division

Proceedings of the American Society of Civil Engineers

July, 1959

p. 129. At the beginning of the second full paragraph, change "The decrease" to "The decreases"

p. 131, line 17. Change $t_3 = 0.55R$ to $t_3 = 0.055R$

p. 134, line 8. Change A + G to A + C

PART 2

AUGUST 1960 — 24 NO. EM 4
VOLUME 86 PART 2

Your attention is invited

NEWS OF THE ENGINEERING MECHANICS DIVISION OF ASCE

JOURNAL OF THE ENGINEERING MECHANICS DIVISION
PROCEEDINGS OF THE AMERICAN SOCIETY OF CIVIL ENGINEERS

DIVISION ACTIVITIES
ENGINEERING MECHANICS DIVISION
Proceedings of the American Society of Civil Engineers

NEWS

August, 1960

UNDERGRADUATE PROGRAMS IN ENGINEERING MECHANICS

Dr. D. H. Pletta, Chairman Engineering Mechanics Division of ASCE and Head of Dept. of Engr. Mech. at V.P.I., submitted the following data on the growth of undergraduate engineering mechanics programs in the United States. The first was established at the U. of Mich. in 1928. It was followed by another at Purdue about 1940 which in 1954 was renamed engineering science. In 1957, one was established at V.P.I. and in 1959, another at Columbia. All of these are now approved by the ECPD. In addition Michigan, Northwestern and Penn State were awarded accreditation in engineering science in 1959. In engineering physics, Cornell (1951), Harvard (1951), Kansas (1949), Maine (1949), Michigan (1954), Oklahoma (1953), Toledo (1956), and the U. S. Naval Post Graduate School (1955) were accredited by ECPD. The growth of undergraduate curricula in these disciplines has been quite healthy, especially recently, and should in the future have considerable impact upon our division. There are at the moment other schools such as Manhattan College, University of Wisconsin, that are just starting programs but these are not yet eligible for accreditation because of the fact that they have not yet graduated any students.

The editor has noted that many regard the development of these separate programs as a sound evolution in engineering education, while others regard the apparent trend with apprehension. The second group prefers to regard engineering science and mechanics as an important part of the spectrum belonging to the professional depts. rather than as a separate discipline crowded between the professions and the sciences. Perhaps Purdue's recent action to combine the Engr. Science Dept. with a professional dept. (Aero) reflects this philosophy.

Concise reader comments are welcome and will be considered for presentation here.

Note.—No. 1960-24 is part of the copyrighted Journal of the Engineering Mechanics Division, Proceedings of the American Society of Civil Engineers, Vol. 86, No. EM 4, August, 1960.

Copyright 1960 by the American Society of Civil Engineers.

SECOND CONFERENCE ON ELECTRONIC COMPUTATION

As was announced previously, this conference will be held on September 8 and 9, 1960, at the Pittsburgh Hilton Hotel. It is planned to mail information on the program to 18,000 ASCE members. A list of the papers and authors follows:

Thursday morning, Sept. 8

Impact of Electronic Computation on Civil Engineers (Keynote Address), G. S. Richardson.
Computer Program Exchange: Myth and Reality, J. C. L. Chang.
Computer Design of Structural Steel for Buildings, M. Zar and C. Beck.
Computer Solutions to Linear Buckling Problems, R. J. Sylvester.
Error Analysis for Eigenvalue Problems, R. B. McCalley, Jr.
Optimum Design of Transmission Towers, G. P. Anaston.
Optimum Design of Reinforced Concrete Buildings, J. D. Graham.
A Vision of Our Automatic Future (Luncheon Address), N. J. Dean.

Thursday afternoon, Sept. 8

Computer Analysis of Structures, J. F. Borges.
Structural Idealization for Digital Computer Analysis, J. S. Archer and C. H. Samson, Jr.
Structural Design by Systematic Synthesis, L. A. Schmit, Jr.
Simultaneous Equations Solved by Over-Relaxation, F. G. Lehman.
The Electronic Computer as a Tool in Moment Distribution, J. E. Soehrens.
Multi-Story Frame Analysis by Digital Computer, M. F. Rubinstein.
Stiffness Method of Rigid Frame Analysis, M. L. Pei.
Computing Maximums Due to Moving Loads, J. N. Lingeman.
Some Fundamental Concepts and Their Use in Matrix Structural Analysis, F. R. Berman.
The Elements of Matrix Structural Analysis, S. Shore.
Dynamic Analysis of Circular Arches, R. T. Eppink, and A. S. Veletsos.
A Numerical Procedure for the Analysis of Continuous Plates, A. H. S. Ang, and N. M. Newmark.

Friday morning, Sept. 9

Sloping Surcharge Retaining Wall Design, M. A. Wadsworth.
Vessel Foundation Designs Using a Digital Computer, L. G. Horton, and E. S. Eichmann.
Stress Distribution Patterns and Settlement Characteristics of Structural Pile Foundations, E. P. Rausa.
Numerical Analysis of Laterally Loaded Piles, L. C. Reese, and H. Matlock.
A Computational Technique for Three-Dimensional Pin-Jointed Structures, C. E. Pearson.
The Finite Element Method in Plane Stress Analysis, R. W. Clough.
Numerical Analysis Applied to Beam Vibrations, E. N. Wilson.
Inversion of Band Matrices, S. O. Asplund.
The Use of Computers in Election Forecasting (Luncheon Address), M. A. Woodbury.

Friday afternoon, Sept. 9

Computer Analysis of Twin Box Culverts, J. S. Hoffman.
Computer Analysis of a Pier with Unlimited Shape, A. R. Barkocy.
Computer Design of Prestressed Concrete Beams for Deflection Control, F. Kulka.
Computer Methods for Dynamic Structural Response, V. H. Neubert.
Matrix Analysis of Non-Linear Structures, E. L. Wilson.
New Methods of Matrix Structural Analysis, B. Klein, and M. Chirico.

NATIONAL AMERICAN WELDING SOCIETY MEETING

According to a preliminary program printed in the June 1960 issue of WELDING JOURNAL, ASCE will participate in the sponsorship of four sessions at the AWS Fall Meeting to be held September 26-29, at the Hotel Penn-Sheraton, Pittsburgh, Pa. Titles and authors for these sessions are as follows:

Monday afternoon, Sept. 26

Welding of High-strength Low-alloy Structural Steels for Bridges, J. L. Beaton, and P. G. Jonas.
Behavior of Welded Built-up Beams Under Repeated Loads, J. E. Stallmeyer, L. R. Hall, and W. H. Munse.
The Flexural Fatigue Strength of Stiffened Beams, J. E. Stallmeyer, and W. H. Munse.

Tuesday morning, Sept. 27

Tests of Welded Plate Girders, B. T. Yen.
Design of Columns in Multi-story Frames, J. S. Ellis.
Welded Interior Beam-to-column Connections, J. D. Graham, A. N. Sherbourne, R. N. Khabbaz, and C. D. Jensen.

Tuesday afternoon, Sept. 27

Design Features for Welded Joints in Space Trusses for Retractable-roof Auditorium, E. Cohen.
Plastic Design of Fixed-base, Gabled Frames, S. P. Prawel, Jr. and R. L. Ketter.
Behavior of Haunched Connections, G. C. Lee, J. W. Fisher, and G. C. Driscoll.

Wednesday afternoon, Sept. 28

Strength of Welded Aluminum-alloy Box Beams, R. J. Brungraber.
Research and Development of Continuous Welded Rail, G. M. Magee.
Painting of Welds, J. D. Keane.

It is planned to publish a more detailed program in the September 1960 issue of WELDING JOURNAL.

WEST COAST COMMITTEE - MINUTES

The following are excerpts from a committee meeting held April 9, 1960, at the University of California, Berkeley:

1. The ASME Applied Mechanics Executive Committee has approved in principle that the national summer conference on Applied Mechanics should be held west of the Rockies every fourth year and in those years would be amalgamated with the West Coast Conference. The ASCE committee was in complete agreement with this proposal and expressed the desire to still be a participant in these particular meetings, although they would be primarily run by the ASME National Committee on Applied Mechanics.
2. Because of a larger number of papers, the ASME National committee would like to schedule more of their papers for presentation at the West Coast Conference. This means either longer meetings with more sessions, simultaneous sessions, or fewer ASCE papers.

   This committee feels there is no objection to simultaneous sections. (There were several in the 1959 West Coast conference.) There are definite advantages to retaining ASCE participation in this conference. In particular, this committee felt there are, at least in some years, already too many separate conferences and that applied mechanics is a binding area of joint,interest to both ASCE and ASME members.
3. The 1962 U. S. National Congress of Applied Mechanics is scheduled for Berkeley in 1962. The Committee agreed that it is probably desirable to not have a separate 1962 West Coast Conference.
4. It is desirable that the West Coast Committees of both ASCE and ASME have a representative on the committee from the school or area which is sponsoring a meeting.
5. ASCE participation in the West Coast conference should continue to grow. The West Coast Committee should request a budget for these conferences to help defray expenses, previously carried solely by ASME. This could be used for printing and mailing costs, losses on meals, Honorariums for General Lecturers, etc.
6. ASCE should investigate the possibility of furnishing preprints of ASCE papers at the meeting. There was also some discussion of length of ASCE papers in Engineering Mechanics, and it was felt they were too long. It is possible that the EM Division should have a shorter limit, due to the nature of the papers, than is the standard ASCE policy.
7. The West Coast Committee needs to be able to mail advance notices of West Coast Conferences to the EMD membership. This is necessary for publicity, as well as to insure ASCE sponsored papers at the conferences.
8. The West Coast Committee does not wish to review papers. It wishes only to screen papers that have been accepted for publication in the EM Journal and that may be available for presentation at the West Coast conference. The following steps are necessary for this screening process:

   A. Select from the Publications Committee list of accepted papers, a number that appear attractive for the West Coast conference. For this purpose, it is necessary that the chairman and secretary of the

West Coast Committee receive all reports of the EM Publications Committee indicating the status of all papers.

B. Obtain one or more copies of papers selected, to be screened by members of the West Coast Committee. It may be necessary to contact the program chairman, also, to determine if arrangements can be made for presentation of this paper at the West Coast meeting.

C. Have papers screened by members of the West Coast Committee and select those suitable for inclusion on the program.

D. Clear with Program Committee and write author inviting presentation at the West Coast conference.

PUBLICATIONS COMMITTEE - MINUTES

The following are the Minutes for a meeting held on May 7, 1960, at Purdue University:

1. Report of Secretary Wenk:
   a. Number of manuscripts submitted to EMD has increased from about 25 a year in 1955-1956 to about 60 a year. About 25 per cent of these have been rejected or withdrawn.
   b. Of the thirty papers submitted during the past six months, twenty-seven were about evenly divided among the fields of Elasticity, Mathematical Methods, Plasticity and Structural Dynamics. Two papers were concerned with Experimental Analysis and Analogs, one with Fluid Dynamics.
   c. About two thirds of the papers submitted are reviewed by Technical Committees within two months, few take more than four months.
   d. The present backlog of unpublished accepted papers is such that after acceptance a paper must wait from nine to twelve months before publication. This means that the time interval between submission of a manuscript and its publication in the Journal is usually 15-18 months with a minimum of 12 months. The change from four issues of the EMD Journal per year to six that is planned by the Society Publications Department should reduce the backlog and may allow reduction of the interval between submission and publication to as low as six months.
2. Reviewing Standards. The Division Secretary has authority to question and to reject reviews of manuscripts that do not meet Division standards. It was suggested that the form sent out by the Secretary requesting committee review of manuscripts be reworded to remove any vague or intermediate category of acceptability, e.g. "publish if space available" or the equivalent. Reviewers should take responsibility in terms of a flat yes or no. Doubtful cases should be rejected.
3. Short Technical Notes. This category of manuscript was originally proposed as a means of reducing processing time for short papers. In view of the short reviewing time for normal manuscripts, there appears no need for it.
4. Manuals in Preparation. The Commentary on Plastic Design, the last installment of which appeared in the April Journal, will be revised and ready for possible issue as a manual of practice by September, 1960.

The Protective Construction Manual is now being edited by the committee and the manuscript should be completed within a few weeks. Haltiwanger was requested to find out if its preliminary publication (for criticism by Society Membership) can be in a single issue of the Journal in order to avoid the separate printing with private funds as originally planned.

NEW EMD POLICY ON TECHNICAL PROGRAMS

In a memorandum dated May 31, 1960, M. P. White, Division Secretary, informed the Program Committees of a revision of the present EMD policy on technical programs. Until now technical sessions have been limited almost entirely to the annual meeting of the Society and to the programs co-sponsored by the West Coast Committee. Three factors leading to a revision of policy are: (1) Enough papers are received to fill ten to 15 technical sessions per year, (2) the division cannot count on more than six sessions at the annual meetings of the Society, (3) it has been shown that given the right conditions engineering mechanics meetings can be successful away from the annual meeting.

After a discussion of these factors, it was agreed at the 7 May EMD Executive Committee meeting that the division should in the future plan on technical sessions or meetings additional to the Annual Meeting. These might be (a) in connection with regional ASCE conventions, (b) jointly sponsored with some other society, or (c) pure EMD meetings preferably with help from a local ASCE group. Certain things were considered necessary for success: (a) At least two or three sessions having related themes, (b) a reasonable supply of potential attendance in the surrounding areas, (c) enthusiastic planning.

ITEMS FOR OCTOBER LETTER

News items and comments, to be considered for publication in a Newsletter for circulation with the Oct. 1960 EMD Journal, must be on your editor's desk by Wed., Sept. 28, 1960. Please note the change of address.

COMBINED INDEX TO ASCE PUBLICATIONS

For complete coverage of the Society's 1959 year in print, there is now a Combined Index covering the Division Journals, Transactions, and Civil Engineering. Also included are reprints of the Proceedings Abstracts that are published each month in Civil Engineering. The price of the Combined Index (ASCE publication 1960-10) is $2.00 with the usual 50% discount to members.

The coupon herewith will make ordering easy:

---------- CUT HERE----------

American Society of Civil Engineers
33 West 39th St.
New York 18, N. Y.

Please send me . . . . copy(s) of ASCE 1960-10. Enclosed is my remittance of $ . . . . My ASCE membership grade is . . . .

Print Name

Address

City Zone State

. . . of 1960-10

Donald L. Dean, Newsletter Editor, EMD
Department of Civil Engineering
University of Delaware
Newark, Delaware